University of Alberta

Behaviour of Steel Shear Connections for Assessing
Structural Vulnerability to Disproportionate Collapse

by

Steven A. Oosterhof

A thesis submitted to the Faculty of Graduate Studies and Research
in partial fulfillment of the requirements for the degree of

Doctor of Philosophy

in

Structural Engineering

Department of Civil and Environmental Engineering

For my wife and children,

who mean the world to me.

ABSTRACT

The performance of structures under the effects of extreme loads can be a critical consideration in their design. The potential for disproportionate collapse following localized damage to a column can be mitigated by the provision of sufficient strength and ductility throughout a structural system to allow for the establishment of a stable alternative load path. An understanding of the behaviour of shear connections in steel gravity frames under the unique combinations of moment, shear, and axial force relevant to column removal scenarios is necessary to assess the vulnerability of a structure to disproportionate collapse. However, such an understanding is currently limited by a deficiency of physical test data.

In order to investigate the inherent robustness of commonly-used steel shear connections, an experimental program consisting of 45 full-scale physical tests was completed. Specimens included shear tab, welded–bolted single angle, bolted–bolted single angle, bolted–bolted double angle, and seat and top angle connections combined with different types of shear connections at the beam web. A testing procedure was developed that imposes upon a connection the force and deformation demands that are expected following removal of the central column in a symmetric two-bay frame. Various geometric arrangements of each connection type were tested, and each arrangement was subjected to a range of loading histories representing different column removal scenarios.

The physical test results characterize the load development history, deformation mechanisms, and failure modes expected following column removal for each type

of connection. Connection stiffness, strength, and ductility limits under the effects of combined loading are quantified.

An approach to mechanical modelling that predicts connection response following column removal is presented and validated using the test results. The models are used to expand the database of results and study the effects of critical parameters on performance. Design recommendations based on the physical tests and mechanical modelling are presented, including connection detailing considerations and a simplified connection modelling technique that is suitable for whole-building column removal analysis.

ACKNOWLEDGEMENTS

TABLE OF CONTENTS

LIST OF TABLES

LIST OF FIGURES

LIST OF SYMBOLS

Latin Symbols

a	Deformation capacity parameter on the load-deformation curve (Figure 2.1); boundary condition coefficient (Equation 6.2)
A_{gv}	Gross shear area
A_{nv}	Net shear area
b	Deformation capacity parameter on the load-deformation curve (Figure 2.1)
c	Residual strength parameter on the load-deformation curve (Figure 2.1)
℄	Centreline
d	Bolt diameter
d_b	Depth of beam
d_{bg}	Depth of bolt group
e	Eccentricity between mechanical model spring and connection centre of rotation
e_{icr}	Vertical eccentricity between unrestrained instantaneous centres of rotation at opposite beam ends
E	Young's modulus of elasticity
F_{br}	Bearing force
F_R	Resultant applied force
F_t	Bolt tension force
F_v	Bolt shear force
G	Shear modulus
H	Horizontal load
H_r	Factored horizontal resistance
K_1	Initial stiffness of an angle segment in tension
K_2	Hardening stiffness of an angle segment in tension
K_b	Plate bending stiffness for a single bolt in bearing
K_{br}	Plate bearing stiffness for a single bolt in bearing
K_i	Initial stiffness of a single bolt in bearing
K_v	Plate shearing stiffness for a single bolt in bearing

L	Span length
L_e	Horizontal edge distance (from centre of bolt hole to edge of connecting element)
L_{eff}	Effective length of angle leg perpendicular to applied tension
M	Moment
n	Total number of rows of bolts
n_{eff}	Number of effective bolts at failure
P	Point load
Q	Uniformly distributed floor load
R_n	Nominal component resistance
$R_{n,angle}$	Nominal resistance of an angle segment in tension
$R_{n,br}$	Nominal bolt bearing and tear-out resistance
$R_{nt,bolt}$	Nominal bolt tensile resistance
$R_{nv,bolt}$	Nominal bolt shear resistance
$R_{y,angle}$	Nominal force to cause yielding in an angle segment in tension
s	Spacing of ties
S	Fillet weld leg length
t	Thickness of connecting element (plate or angle)
T	Thrust force
V	Vertical load
V_r	Factored vertical shear resistance
x, y, z	Cartesian coordinates

Greek Symbols

α   Angle of inclination of bolt tear-out shear planes

β   Angle of inclination of resultant force line of action in a bolted–
         bolted angle segment under tension

γ   Angle of inclination of resultant applied force, F_R

Δ   Deformation

Δ_3 Elongation demand in the direction of the rotated beam axis

Δ_{max} Localized deformation capacity at bolt locations

θ_c Beam chord rotation angle (with respect to the horizontal)

θ_{final} Beam chord rotation angle at final failure (at all bolt locations)

θ_u Beam chord rotation angle at ultimate load (i.e., maximum resultant
         applied force, corresponding to initial failure)

λ_D Dead load factor

λ_L Live load factor

μ_p Plastic hardening stiffness factor

σ_{ij} Normal stress on the plane perpendicular to the i-axis acting in the
         j-direction

σ_u Static ultimate strength

σ_y Static yield strength

τ_{ij} Shear stress on the plane perpendicular to the i-axis acting in the
         j-direction

ω   Uniformly distributed line load

1.   INTRODUCTION

1.1.   Background

1.1.1. *Extreme Loading and Disproportionate Collapse*

The public largely takes for granted the strength and stability of structures. This is both a testament to the sound state of current structural engineering practices and a mandate to continue to protect public safety. The consequences of structural collapse can be catastrophic, and are thus regarded as unacceptable by the public and the engineering community alike. Instances of structural collapse are relatively rare; however, when a building experiences an event that was unanticipated in design, localized failures can indeed occur. The demands exerted upon structures by abnormal events are classified as extreme loads, which consist of loads that are not normally prescribed in building codes or accounted for by designers (Burnett, 1975). Examples of events that may lead to such loads include accidental blasts, vehicular collisions, terrorist attacks, natural disasters, and human errors. It is often impractical (if not impossible) to design explicitly for events of this nature using the statistical approaches applied to the treatment of more conventional loads, yet it is generally considered good engineering practice to mitigate the potential for collapse under extreme loads by incorporating concepts of structural integrity and robustness into design.

Extreme loads on structures can lead to progressive collapse—that is, widespread structural failure initiated by localized damage, where one local failure leads to another. This is analogous to the domino effect, wherein a disturbance at some location propagates to cause extensive failure. The combination of insufficient redundancy and a substantial disturbance has resulted in numerous building collapses in the past. Progressive collapse famously occurred in the Murrah Federal Building as a result of the Oklahoma City bombing in 1995, a tragedy in which widespread structural failure resulted in mass casualties. Many other case studies exist and have been discussed in the literature, consisting of both well-known and less-publicized collapses.

In cases where the extent of structural failure is considered to be far more severe than the event that initiated it, it is termed "disproportionate collapse". The principal objective when designing against extreme loads is the mitigation of disproportionate collapse. (The terms "progressive collapse" and "disproportionate collapse" are typically used interchangeably in the literature; the latter is used herein to describe both phenomena.) The collapse resistance of buildings under extreme loads is a critical consideration in their design. Although enhancing structural integrity has long been accepted as good engineering practice, taking special measures specifically to mitigate disproportionate collapse is becoming an increasingly prevalent design objective.

A building can become vulnerable to disproportionate collapse when an extreme loading event causes severe localized damage to one or more major structural elements such as columns or transfer girders. Collapse resistance under a column removal scenario has been widely adopted as a metric for the quantification of structural integrity. For a structure to avoid collapse under column removal, it must be able to redistribute the loads from the compromised column to adjacent structural members. One significant mechanism that allows this to occur is known as catenary action, which is characterized by the formation of axial tension in the beams adjacent to the removed column and their connections. Tensile forces develop as a result of the deformed geometry of the system; namely, the substantial vertical deflection at the removed column location. Figure 1.1 shows two bays of a bare steel frame where a column has been removed and catenary action has been mobilized. At each storey, the beams act similarly to cables to support the vertical load, resulting in both horizontal and vertical forces at the remaining columns. If a structural system has both the ductility to sustain the required deformations and the strength to carry the unique combination of loads applied to it through the development of catenary action, a state of equilibrium can be achieved and widespread collapse avoided—a result that would provide an opportunity for the safe evacuation of building occupants. The performance of beam-to-column connections are of critical importance to the development of catenary action in the structural system as a whole.

1.1.2. Shear Connections

Steel-framed buildings commonly consist of lateral force resisting systems (such as shear walls, braced frames, or moment frames), with the remaining structure designed to resist vertical loads and transfer lateral loads to these components by leaning against them. Such "leaning" (or "gravity") frames are primarily designed to carry gravity loads, using shear connections to attach beams to columns. Structural designers typically assume that shear connections behave as rotationally-unrestrained pins that carry pure shear. This simplifying assumption has been shown to be appropriate under conventional gravity loading conditions if connections are detailed to ensure sufficient rotational flexibility. In practice, however, the beam-to-column connections used in steel construction lie on a spectrum between purely pinned and fixed conditions.

Several examples of commonly-used shear connections are shown schematically in Figure 1.2. The connection types included in the figure are representative of those tested in the experimental program described in Chapter 3. Shear tab connections (Figure 1.2(a)) consist of a single plate welded perpendicular to the column flange and bolted to the beam web. Welded–bolted angle connections (Figure 1.2(b)) consist of angles with one leg welded to the column flange and the perpendicular leg bolted to the beam web. Bolted–bolted angle connections (Figure 1.2(c)) have a similar overall geometry, but with the angle legs at both the column and the beam connected using bolts. Angle connections may consist of either a single angle or two symmetric angles (one on each side of the beam web). Seat and top angles can be combined with any of these web connection types (as shown in Figure 1.2(d) with a bolted–bolted web angle) to form what is commonly classified as a semi-rigid connection, rather than a shear connection, due to the increased bending resistance achieved by attaching the beam flanges to the column.

1.2. Statement of Problem

Because of their ubiquity in steel structures, it is of significant importance to assess the inherent robustness of commonly-used steel shear connections. Localized damage to a structural component caused by an extreme load can impose demands on a structural system that are substantially different from those typically considered in design. While the behaviour of shear connections under the effects of conventional gravity loading has been studied extensively, their strength and ductility under large rotations and the combined effects of moment, shear, and tension are generally not well understood. The performance of shear connections under these conditions is fundamental to the formation of catenary action, and thus to the overall integrity of a structural system in the event of a column being compromised by an extreme loading scenario. Although current design guidelines that explicitly address disproportionate collapse resistance place significant emphasis on beam-to-column connections, an improved understanding of shear connection behaviour under the unique demands caused by column removal is necessary to develop approaches to design that are both realistic and practical.

1.3. Scope and Objective

In order to investigate the performance of common steel shear connections under the strength and ductility demands resulting from column removal, an experimental program consisting of 45 full-scale physical tests was completed. Specimens included shear tab, welded–bolted single angle, bolted–bolted single angle, bolted–bolted double angle, and seat and top angle connections combined with different types of shear connections at the beam web.

An approach to mechanical modelling that predicts the progression of connection response and failure following column removal is developed and validated by the test results. The models are used to perform parametric studies that extend the dataset to include a wider range of connection geometries and loading conditions.

4

Simplified connection models based on the most critical parameters affecting behaviour are proposed as practical tools for use in whole-building analyses.

The principal objective of this research program is to contribute to the understanding of the robustness of steel shear connections under the demands of a column removal scenario by:

1. expanding the limited database of physical test results;
2. characterizing connection load development history, deformation mechanisms, and failure modes;
3. quantifying connection stiffness, strength, and ductility limits;
4. modelling connection behaviour following column loss accurately;
5. identifying critical parameters that affect performance; and
6. developing practical design recommendations for the assessment and improvement of structural integrity.

1.4.   Organization of Report

This document is organized into seven chapters, with tables and figures appearing at the end of each chapter. Supplementary details are presented in five appendices that follow the main body. Units of measure appearing in all figures are in millimetres, unless noted otherwise.

Chapter 2 provides an overview of the current design guidelines related to disproportionate collapse mitigation and reviews previous research programs that investigated the behaviour of steel shear connections under various loading conditions relevant to structural integrity. Details of the current experimental program—including the test set-up, testing procedure, specimen descriptions, and material properties—are described in Chapter 3. Chapter 4 reports the test results, with discussions on the observed deformation mechanisms, failure modes, and load development characteristics. Chapter 5 presents a detailed discussion and analysis of the research results for shear tab and welded–bolted angle connections, including details of the proposed mechanical models, parametric studies, and design recommendations. Chapter 6 contains a similar treatment to that of

Chapter 5, but for bolted–bolted angles. Chapter 7 summarizes the research program and its main conclusions, and includes suggestions for future work in this field of study.
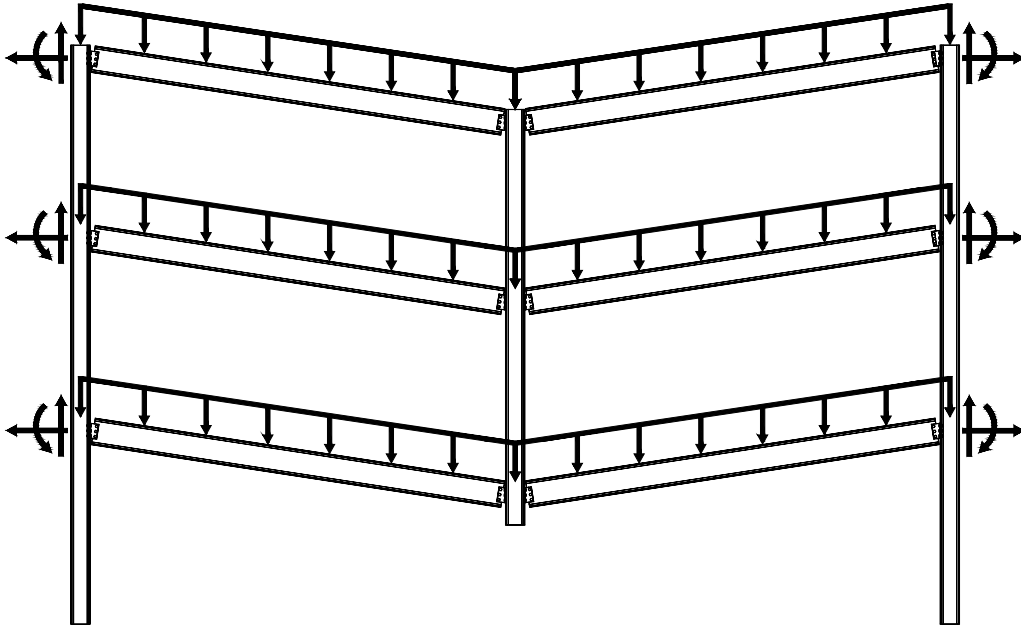
Figure 1.1. Catenary action in a gravity frame following column removal.

(a) (b)

(c) (d)
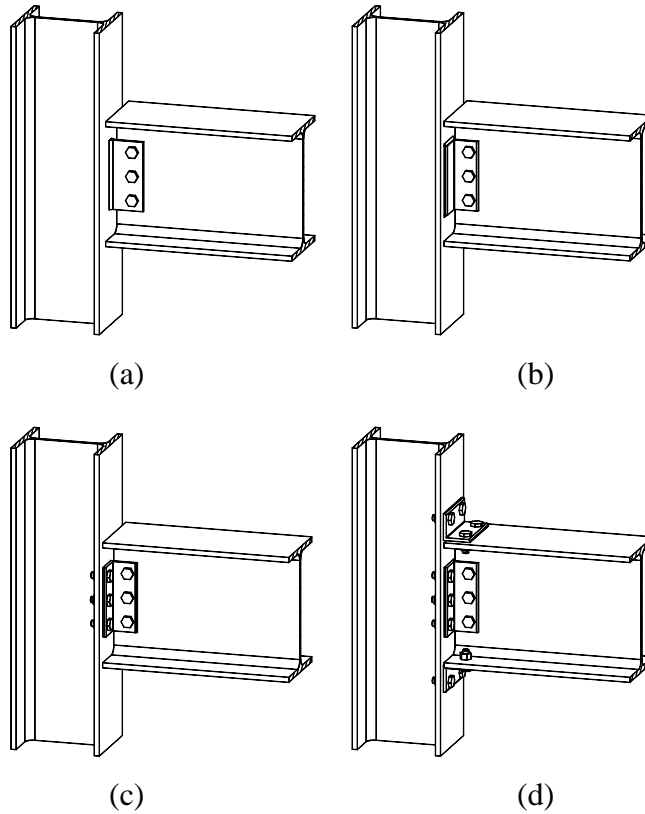
Figure 1.2. Common shear connection types: (a) shear tab, (b) welded–bolted angle, (c) bolted–bolted angle, and (d) combined seat and top angle with bolted–bolted web angle.

2. LITERATURE REVIEW

This chapter reviews the literature that provides relevant context to this research program. Current design guidelines that address disproportionate collapse mitigation are outlined. Previous physical testing programs and analytical studies that examined shear connection behaviour under loading conditions that are pertinent to connection robustness—particularly, loading that includes axial tension—are summarized and discussed.

2.1. Design Guidelines for Disproportionate Collapse Mitigation

This section provides an overview of the current design guidelines that specifically address disproportionate collapse mitigation, with an emphasis on details pertaining to steel shear connection design. Current guidelines include various approaches to the subject that range in detail, complexity, and impact on design. Most include, as a minimum, general statements about the importance of providing an adequate level of structural integrity, although many do not provide specific guidance or practical recommendations for achieving or improving it. The simplest approach to addressing the issue involves the implementation of indirect methods, wherein a set of prescriptive rules that improve member continuity and robustness is provided. More developed guidelines that address disproportionate collapse mitigation include procedures for direct design methods, which define specific extreme loading scenarios to design for. Table 2.1 describes the prominent direct and indirect methods that are employed by the various current design guidelines. The approach that is required for an individual building project is typically determined by the authority having jurisdiction, the building owner, and/or an assessed level of risk for disproportionate collapse. As a result of growing interest from the engineering community and a wide range of ongoing research on the topic, guidelines related to disproportionate collapse mitigation appearing in design guidelines continue to evolve rapidly.

2.1.1. GSA (2003)

The United States General Services Administration (GSA) released the most recent version of its *Progressive Collapse Analysis and Design Guidelines* (hereafter referred to as the GSA Guidelines) in 2003, outlining procedures for the assessment and reduction of the potential for disproportionate collapse. The guideline is mandatory for federal buildings, but has also been released to the public and adopted for other structures where disproportionate collapse mitigation is a design consideration.

The GSA Guidelines provide a method for the classification of buildings based on their risk for disproportionate collapse, which is used to determine the required design approach. Buildings determined to be at low risk are exempt from the special design requirements contained in the document. All other buildings are to be designed using the alternative path method. The approach presented for this method requires that the damage resulting from the instantaneous removal of a single column at various specified locations be confined to a limited area adjacent to the removed column. The guidelines include a detailed procedure for a linear static analysis to evaluate structural performance following column removal. Each component of the structure is to be assessed using a demand–capacity ratio (DCR), which is defined as the ratio of the demand acting on a component to the ultimate unfactored capacity. Members with a response that exceeds the provided DCR limits are considered to be severely damaged or collapsed. Table 2.2 lists the DCR limits given for the connection types included in this research program. Nonlinear analysis procedures are also permitted by the GSA Guidelines, although no details for their implementation are given. However, acceptance criteria for nonlinear analysis are provided. The performance of each member is to be assessed according to a specified deformation limit rather than a DCR; the plastic rotation limits for the connection types included in this research program are included in Table 2.3.

The GSA Guidelines also require that the rotational capacity of steel connections be proven by physical testing performed according to testing procedures outlined

in *Seismic Provisions for Structural Steel Buildings*, AISC 341-02 (AISC 2002). These tests apply cyclic demands representative of seismic events. The GSA Guidelines suggest that using this testing method for qualification "…is considered to be both practical and prudent…" until additional research, including physical testing that examines the specific condition of column removal, has been conducted. While the notion of accommodating significant plastic deformation without brittle failure is directly relevant to both seismic design and general structural integrity, the cyclic load histories prescribed by AISC 341-02 are significantly different from the load history that would result from a column removal scenario. Thus, adopting this testing procedure for connection qualification may not adequately permit assessment of performance for disproportionate collapse mitigation.

2.1.2. *UFC 4-023-03 (DoD, 2009)*

The United States Department of Defence (DoD) Unified Facilities Criteria has also developed a detailed design guideline to address disproportionate collapse: *Design of Buildings to Resist Progressive Collapse*, UFC 4-023-03 (DoD, 2009). The guideline is mandatory for DoD facilities, but has also been made available as a reference for other building owners and standards organizations considering disproportionate collapse mitigation.

Similar to the GSA Guidelines, UFC 4-023-03 provides a method for the classification of buildings to determine the required design approach based on its risk for disproportionate collapse, and buildings determined to be at the lowest risk level are exempt from the special design requirements contained in the guideline. For other structures, the guideline requires collapse mitigation measures involving various combinations of the tie force, enhanced local resistance, and alternative path methods, according to the assessed level of risk.

The tie force method presented in UFC 4-023-03 requires structural components to resist specified horizontal (for beams) or vertical (for columns) tensile forces. The magnitudes of the horizontal tie forces are calculated as a function of the

building's gravity loads and plan geometry, according to the equations shown in Table 2.4. Beams and their connections must be able to resist tie forces at a rotation of 0.20 radians, unless the forces are carried by an acceptably ductile floor or roof system. While these requirements contribute to the ductility and continuity of a structural system, the simplified approach considers horizontal tie forces independently of all other loads, thereby neglecting the combined effect of forces acting concurrently in other directions. Thus, the method does not directly assess connection performance under strength and ductility demands that are representative of those expected to result from a localized damage event leading to large deformations in a structure.

UFC 4-023-03 provides comprehensive guidance for implementing the alternative path method, including detailed procedures for the completion of linear static, nonlinear static, and nonlinear dynamic analyses. Structural members that contribute to collapse resistance in a column removal analysis are designated as primary, and are assigned stricter acceptance criteria than secondary structural components that do not contribute. UFC 4-023-03 references *Seismic Rehabilitation of Existing Buildings*, ASCE/SEI 41-06 (ASCE, 2007), for the acceptance criteria and modelling parameters to be used for column removal analysis. The values provided in ASCE/SEI 41-06 are stated in UFC 4-023-03 to be considered conservative for use with the alternative path method because they are based on cyclic testing, which applies a load history that is more severe (due primarily to the development of low cycle fatigue damage) than that expected following column removal. For specific connection types where research has shown the acceptance criteria in ASCE/SEI 41-06 to be overly conservative, modified values for analysis are included in UFC 4-023-03. The acceptance criteria and modelling parameters from these documents for the connection types included in this research program are listed in Table 2.2 (for linear static analysis) and Table 2.3 (for nonlinear analysis).

The linear static analysis procedure outlined in UFC 4-023-03 is principally similar to that presented in GSA (2003). The guideline requires the maximum

load effects obtained from a linear static model to be less than the factored resistance of each component increased by an element demand modifier, called an m-factor, which is similar to the approach using DCR limits from the GSA Guidelines.

For nonlinear analysis, the acceptance criteria to be used for steel connections for moment, shear, and axial load effects are dependent upon their demonstrated ductility under each type of load, as determined by the amount of deformation that can be accommodated after the onset of yielding, before capacity loss occurs. Actions having low ductility are classified as force-controlled, and affected components must be designed not to exceed their expected yield strength. More ductile actions are classified as deformation-controlled; affected components are allowed to yield and are limited by their ductility capacity. Deformation-controlled components are modelled using the characteristic load–deformation curve from ASCE/SEI 41-06, as shown in Figure 2.1, which can be defined for a specific action by the yield strength (normalized to a value of 1.0), rate of strain hardening, two deformation capacity parameters (a and b), and a residual strength parameter (c). Where plastic rotation limits are not specifically provided in UFC 4-023-03, they are to be taken from ASCE/SEI 41-06. The acceptance criteria for secondary members are based on the "collapse prevention" condition shown in Figure 2.1. For primary members, more conservative points to the left on the curve—representing the "life safety" condition—are used, defined in ASCE/SEI 41-06 as a state in which a structure has sustained some damage, but maintains a margin against collapse.

2.1.3. ASCE/SEI 7-10 (2010)

The American Society of Civil Engineers (ASCE) standard *Minimum Design Loads for Buildings and Other Structures*, ASCE/SEI 7-10 (2010), contains a brief section with disproportionate collapse mitigation guidelines, listing the enhanced local resistance and alternative path methods as potential design approaches. The standard does not include a classification system to determine when such considerations are required. Little guidance is provided for the

implementation of the alternative path method, beyond stating that the designer is responsible for the selection of elements to be notionally removed, and that stability analysis may be completed using any method that considers second-order effects.

2.1.4. *Eurocode 1 (CEN, 2006)*

The Eurocode provides disproportionate collapse mitigation guidelines in *Eurocode 1: Actions on Structures*, EN 1991-1-7:2006 (CEN, 2006). This European standard contains procedures for both indirect (including tie force and integrity detailing) and direct (including event control, enhanced local resistance, and alternative path) design methods. The approach to be used for a specific building is determined by a classification system based on building type and occupancy. Structures in the lowest risk category require no exceptional design efforts. The next classification tier requires structural components to resist prescribed horizontal tie forces, which are calculated as a function of a building's gravity load and plan geometry. As seen in Table 2.4, the tie force equations have a form that is similar to those in UFC 4-023-03, but include a minimum horizontal force value of 75 kN and have coefficients that generally result in lower horizontal tie forces. The Eurocode does not require tie forces to be carried at a specified minimum rotation; thus, it does not ensure that structural components will have the ductility to sustain any level of horizontal load following extreme events that cause significant levels of rotational deformation.

Buildings in the highest risk categories must be designed to resist both horizontal and vertical tie forces, or else be analyzed using the alternative path method. When using the alternative path method, the building is to be analyzed under cases considering the individual removal of each column and each beam supporting a column. Elements that cause widespread collapse when notionally removed are deemed "key elements", and must be designed for a prescribed accidental load (i.e., using the enhanced local resistance method). However, no procedure is given for the implementation of the alternative path analysis.

2.1.5. International Building Code (ICC, 2012)

The *International Building Code* (ICC, 2012) contains a brief section on structural integrity, the provisions of which are required for certain buildings depending on building type and occupancy. For steel construction, the code includes horizontal tie force requirements, which are shown in Table 2.4. Each beam end connection is required to resist a nominal horizontal tie force (in the absence of vertical load and rotation) equal to two-thirds of its required factored vertical shear strength. Similar to the requirements of UFC 4-023-03 and the Eurocode, the tie forces from the *International Building Code* are dependent upon a building's gravity load and plan geometry, although these parameters do not appear explicitly in the design equations. The minimum horizontal tie force value is specified as 45 kN.

2.1.6. CSA S850-12 (2012)

The Canadian Standards Association (CSA) has recently developed standard CSA S850-12: *Design and Assessment of Buildings Subjected to Blast Loads* (CSA, 2012), which specifically addresses structural integrity and the mitigation of disproportionate collapse. The standard requires that structural components be designed to resist specified blast effects. Components that fail to satisfy acceptance criteria under these effects must either be redesigned to resist the load (i.e., the enhanced local resistance method) or instantaneously removed in an analysis that demonstrates the ability of the structure to resist collapse in their absence (i.e., the alternative path method). Determining the elements to be removed for the alternative path method according to their performance under a specified blast event differentiates CSA S850-12 from UFC 4-023-03 and the GSA Guidelines, which both prescribe threat-independent locations for column removal. CSA S850-12 provides some direction for linear and nonlinear analysis procedures, although the majority of alternative path method guidelines, including acceptance criteria and modelling parameters for linear and nonlinear analyses, are taken directly from UFC 4-023-03 (as included in Tables 2.2 and 2.3).

2.1.7. *National Building Code of Canada (NRC, 2010)*

Commentary B of the *National Building Code of Canada* (NRC, 2010) discusses structural integrity requirements to resist disproportionate collapse. It is stated that structures designed according to CSA standards will usually have an adequate degree of structural integrity as a result of the standards' connection detailing requirements. Possible approaches to disproportionate collapse mitigation are listed, including the tie force, event control, enhanced local resistance, and alternative path methods. However, no classification system for determining when these measures should be taken is included, and no specific procedures for their implementation are provided.

2.1.8. *CSA S16-09 (2009)*

The CSA standard *Design of Steel Structures*, CSA S16-09 (CSA, 2009), explicitly requires that steel connections be designed to resist disproportionate collapse. It addresses this requirement simply by stating that the requirements contained in the standard "…generally provide a satisfactory level of structural integrity for steel structures…", and it provides no further guidance on the subject.

2.2. Previous Research on Shear Connections under Conventional Loading

Extensive research has been completed on the performance of commonly-used steel shear connections under conventional loading that is representative of the demands on connections in undamaged steel frames primarily designed to resist gravity loads. Physical testing of these connections typically included the application of a vertical load and a nominal rotation approximating a pin-ended condition. This body of research has culminated in the current design provisions presented in steel design standards throughout the world, including the Canadian standard CSA S16-09 (CSA, 2009) and the American standard AISC 360-10 (AISC, 2010). The loading scenario considered in this research program is distinctly different from the conventional loading case, as it includes much larger

connection rotations and the application of combined moment, shear, and tension. The determination of shear connection performance under these demands is beyond the scope of the requirements contained in most current design standards. However, the state of knowledge on shear connection behaviour, including the current understanding of the various potential failure modes and capacity prediction equations, will be applied in the discussion and analysis presented in subsequent chapters.

Unexpected beam-to-column connection failures caused by the 1994 Northridge earthquake prompted a surge in steel connection research that examined the effects of seismic loading. This research led to the publication of FEMA 355D: *State of the Art Report on Connection Performance* (FEMA, 2000). Although the document focusses on the performance of moment connections, it also provides empirically-determined moment–rotation relationships for a variety of shear connections. However, the predicted rotational stiffnesses and capacities presented in the document do not account for the effect of axial force on the development of connection moment.

2.3.   Previous Research on Shear Connections under Tension

The tie force method seeks to improve structural integrity by ensuring adequate connectivity between elements—particularly by designing beam-to-column connections to resist a nominal tensile force. Furthermore, structural stability following column removal depends on the development of significant axial tension (albeit in combination with large deflections and other forces) through catenary action. This section summarizes research that has investigated the performance of shear connections under pure axial tension. Although these studies are useful for the understanding of connection behaviour as it relates to structural integrity, the test results and proposed approaches to design summarized in this section are limited to the case where axial tension is considered independently from shear and rotation; therefore, conclusions cannot be directly applied to the more severe combination of load and deformation demands that are expected to result from a column removal scenario.

2.3.1. De Stefano and Astaneh (1991)

The results of four physical tests on welded–bolted double angle connections under pure tension were reported by De Stefano and Astaneh (1991). The two angles were connected to opposite sides of a thick plate (representing the beam web) using a single bolt, and welded along the toe of each perpendicular angle leg to a second thick plate (representing the column). The application of tension caused the angle heels to pull away from the column plate through the development of plastic hinges near the weld and near the angle heel. An approximately bilinear load versus displacement curve was recorded, exhibiting a high initial stiffness in the elastic region of behaviour followed by a decrease in stiffness as inelastic behaviour became dominant. The results were used to develop an analytical model of the connections using empirical stiffness values. Further research has been recommended for the determination of appropriate deformation limits for modelling.

2.3.2. Owens and Moore (1992)

Owens and Moore (1992) performed a series of physical tests on various shear connections loaded in pure tension. The testing program was motivated by a need for experimentally-verified approaches to designing for tie forces specified in the design standards of the time.

Eleven bolted–bolted double angle connections were tested, each having one, three, five, or seven bolts in a single vertical row on each of the angle legs. The load versus displacement curves for the connections were approximately bilinear, exhibiting relatively high initial stiffness, followed by a decrease in stiffness to about 10 % of the initial value. Measured axial displacements reached between 31 mm and 50 mm prior to failure. Significant prying forces were measured in the connection bolts at the column. Four failure modes were observed in the tests: bolt punching through the angle leg at the column (washers were not used), bolt tear-out in the angle at the beam web, bolt tear-out in the beam web, and tearing of the angle gross section near the heel.

Ten partial-depth end plate connections were also tested, each having one, three, five, or seven bolts in a single vertical row on each side of the beam web. The load−displacement relationship was similar to the bilinear behaviour observed for double angle connections. Displacements reached between 8 mm and 41 mm prior to failure. Failure occurred by tearing of the end plate near the weld toe in all of the specimens except for those with only one bolt on each side of the beam web, which failed by bolt punching through the plate (in these tests, a washer was installed against the plate).

A methodology to predict the resistance of the tested connection types loaded in axial tension using large displacement analysis was proposed. The approach calculates tensile capacity based on the forces that would develop when plastic hinges form at the critical sections, as observed during testing. The von Mises yield criterion was used to define the interaction between shear and normal stresses, and a limit on total axial deformation was proposed based on the test results. The resulting capacity predictions were shown to be reasonably consistent with those from the physical tests.

2.3.3. Roddis and Blass (2012)

In order to investigate the ability of single angle connections to resist specified horizontal tie forces, a finite element study of single angle connections in tension was completed by Roddis and Blass (2012). The study found that the method presented in AISC 360-10 (AISC, 2010) for calculating prying forces grossly underpredicts the capacity of single angles in tension due to the flexibility of the angle leg that generates the prying force. Future physical testing of single angle connections under high tensile loads was recommended in order to augment the limited data currently available on the topic.

2.4. Previous Physical Testing of Shear Connections under Combined Moment, Shear, and Tension

This section discusses physical testing programs that investigated the performance of shear connections under loading conditions that included a combination of moment, shear, and tension.

2.4.1. Girhammar (1980)

The first column removal tests reported in the literature were carried out by Girhammar, who completed physical tests under both static (Girhammar, 1980a) and dynamic (Girhammar, 1980b) loading conditions. The static and dynamic tests were performed on specimens with similar overall geometries; each represented a two-bay steel frame, consisting of two beams (with 5.0 m spans) connected to a common central column stub. The opposite ends of the beams were connected to rigidly-anchored column stubs. In the static tests, load was applied by a single actuator at the central column. Dynamic tests simulated sudden column removal by supporting the central column stub with a wire that was severed after the beams had been loaded with dead weight. Both studies showed the development of significant catenary action following column removal.

The first type of connection, which was tested only in the static test series, was a full-depth end plate connection. This connection type is considered semi-rigid, because it can develop significant moment as a result of the end plate being welded to the flanges of the beam. Early in these tests, compressive arching action was observed as a result of the vertical eccentricity between the centres of rotation of the connections on opposite ends of each beam (this phenomenon is discussed further in Chapter 6). However, all tests progressed beyond this phase and showed significant catenary (tensile) forces prior to the achievement of the ultimate load. Failure modes included successive bolt fracture, bolt punching through the end plate, plate tearing along the weld, and weld fracture.

The second connection type tested (under both static and dynamic loading conditions) was a bolted heel connection—a connection type that was commonly

used in Sweden at the time, but is rare in North American construction. This type of shear connection consists of an end plate (connected to the column by a single bolt on each side of the beam web) that extends beyond the bottom flange of the beam and sits on a thicker plate that is welded to the column flange. In both the static and dynamic tests, deformation prior to failure was accommodated primarily by yielding of the end plate. Ultimate loads in the static tests were reached prior to the observed failure mode of either bolt fracture in tension or bolt punching through the end plate. Both dynamic tests resisted collapse following column removal under the levels of dead weight applied, which were considered to be typical gravity loads for the structural system.

The test results showed bending action at the early stages of the tests, with catenary action becoming the dominant load-carrying mechanism as the tests progressed towards failure. An analytical investigation was performed to quantify deformations and forces resulting from column loss. Capacity prediction equations for various potential failure modes were developed for the two types of connections that were tested. Using connection parameters derived from the static tests, a rigid-body analysis of the system under dynamic effects was able to predict maximum deflections and reactions within 10 % of those recorded in the dynamic test.

2.4.2. *Astaneh and Ho (1993)*

Astaneh and Ho (1993) summarized the results of five physical tests performed on welded–bolted and bolted–bolted double angle connections under cyclic tension combined with moment and shear. Each specimen was connected to the beam web with five bolts arranged in a single vertical row. Angle legs were connected to the column flange by a similar row of five bolts or a weld along the angle toe. The first load cycle was completed under pure tension. Subsequent load cycles (until connection failure occurred) included axial tension in the presence of a constant shear and nominal rotation representative of typical gravity loading conditions. Axial deformations were accommodated by the formation of plastic hinges in the connection angles, which were observed at the bolt and weld

locations and near the angle heel. It was found that, under the applied load history, bolted–bolted double angles demonstrated greater ductility and strength than welded–bolted double angles with similar geometries, due to the tendency of the weld to fracture in the welded specimens as a result of the severe root opening action.

2.4.3. Astaneh et al. (2002)

Two column removal tests on a full-scale single storey steel structure with shear connections and a composite concrete slab were completed by Astaneh et al. (2002a, 2002b). The two tests used a similar set-up and testing procedure. The geometries of the two specimens were nominally identical, with the exception of the addition of reinforcing cables in the slab (parallel to the girder line) in the test described in Astaneh et al. (2002b), which were specifically intended to increase the system's resistance to collapse following column removal.

The test specimens were four bays long and one bay wide. The two main interior bays each had 6.1 m spans; the perpendicular bay had a 5.5 m span. Beam-to-column connections included two types of shear connections: shear tabs and seat angles combined with single angle web connections. Shear tabs were connected to the beam web with five bolts in a single vertical row; bolts were installed in long horizontally-slotted holes, which were included to allow the connection to undergo large rotations before developing bolt bearing forces. The single angle connections were bolted to the beam and column webs using three bolts in a single vertical row on each leg of the angle. The seat angle was attached to the bottom flange of the beam using two bolts and to the column using two rows of two bolts each.

Each specimen was loaded by removing the support at the central column and applying a predetermined value of vertical displacement. After the specified displacement was reached, the specimen was returned to its original position. The partially-damaged structure was then reloaded to a greater maximum vertical

displacement; this process was repeated for cycles with maximum vertical displacements between 500 mm and 900 mm.

Results showed that both specimens were able to resist the vertical load specified for column removal analysis in the GSA Guidelines through the effective development of catenary action. As expected, the cable-reinforced system had significantly greater capacity than the conventional composite system, resisting more than double the vertical load during the test. The difference between the loads carried by the two systems was marginal for mid-span deflections less than 300 mm; however, beyond this point, the resistances provided by the two systems diverged as catenary forces began to develop more rapidly in the reinforcing cable in the slab.

In both tests, similar deformation mechanisms and failure modes were observed in the shear connections. The shear tabs with slotted holes reached 0.14 radians of rotation without significant damage. Localized bearing deformations were observed at the extreme bolts, but the connections did not experience failure in either of the tests. The bolts connecting the seat angles to the columns failed abruptly in tension at the removed column location in both tests. Following the failure of the seat angles, the web angles were observed to tear along a plastic hinge that had formed near the angle heel. Local buckling of the beam web and flange were observed at some beam-to-column connection locations. Although the concrete slabs experienced extensive cracking and crushing in both tests, particularly around the columns, they were considered to have contributed to the total resistance achieved at the ultimate load condition.

The study recommended the use of slotted holes in shear tabs to improve their rotational ductility. It was also suggested that seat angles be proportioned to ensure that yielding of the angle leg governs over bolt tension failure, in order to avoid what was observed to be a brittle failure mode with an undesirable impact on the ability of the system to sustain catenary forces. For the specimen without cables, it was concluded that the ultimate capacity of the composite system was

limited by beam-to-column connection capacity, and that further research is required in order to characterize the behaviour of shear connections under large rotations and combined shear and tension for the development of appropriate design guidelines.

2.4.4. Guravich (2002)

Guravich (2002) performed 111 physical tests on various types of steel shear connections to determine the residual tensile capacity of connections loaded to specified shear and rotation values. The test set-up consisted of a cantilever beam (oriented vertically) connected to a perpendicular test column. Specimens that would be welded to the column flange in practice were instead welded to a 19 mm thick transfer plate, which was in turn bolted to the column flange. The use of a heavily-reinforced test beam and a very deep test column allowed these elements to be reused for many tests and served to isolate most of the deformation during testing to the connecting elements. Hydraulic actuators were used to apply load to the cantilever test beam at three locations. Two actuators were positioned horizontally: one at the column end of the beam (to apply mainly shear), and a second at the far end of the beam (to apply mainly rotation). A third actuator for applying tensile load was connected at the far end of the beam and was kept in alignment with the beam axis throughout each test.

The cantilever beams were rotated to 0.03 radians at the start of each test and held at this rotation throughout the subsequent application of shear and/or tension. A beam rotation of 0.03 radians was selected for all tests based on an analytical study performed by Astaneh (1989), which showed that this rotation value was appropriate for the testing of a wide range of shear connection assemblies under the effects of conventional gravity loading. The rotated beams were loaded to 50 % or 100 % of the nominal factored shear capacity, and then loaded in axial tension to failure. Additionally, several connection geometries were tested under either pure shear or pure tensile loads.

Eleven shear tab connections were tested, although two results were discounted due to inadequate lateral bracing during testing that led to premature failure. Each shear tab specimen was connected to the beam web with three bolts arranged in a single vertical row. The specimens demonstrated significant ductility in the direction of tensile loading through localized bolt bearing deformations. All specimens tested in tension or combined tension and shear failed in the plate, either by tearing of the net section along the line of bolts or bolt tear-out in the direction of the applied tension. The study showed that the tensile capacity of shear tab connections is inversely related to the level of applied shear, and it was suggested that edge distance is a critical parameter in determining capacity.

The twelve welded–bolted single angle connections included in the testing program were all loaded in combined shear and tension. Each specimen had three bolts arranged in a single vertical row connecting the angle to the beam web, and a fillet weld along the full length of three sides of the angle leg (the heel, top, and bottom) connecting it to the transfer plate. The governing failure mode for all tests in this series was either bolt shear or tearing of the net section of the angle along the line of bolts on the beam web. The results showed that, for the connection geometry and ratios of shear and tension loading applied, interaction between the forces did not affect capacity significantly. Additionally, it was found that the thinner angles achieved higher ultimate tensile loads. This observation was attributed to their increased ductility, which was primarily achieved through localized bolt bearing deformations.

Thirty-six welded–bolted double angle connections were tested. The angles were bolted to the beam web using two or three bolts in a single vertical row and were welded to the transfer plate. The weld configuration was different from that used for the single angle connections, with the weld being placed along the toes of the angles with partial return welds at the top and bottom of the angle. The governing failure mode observed in tests with combined shear and tension loading was weld fracture initiating at the toe of the return weld; this led to the recommendation that the connection arrangement is not appropriate when there is a tensile demand on a

connection. Two specimens were modified with the return weld extended along the full length of the top and bottom of the angle, which led to a decrease in ductility, but a considerable increase in strength.

Forty-nine bolted–bolted double angle specimens were tested. Each angle had two or three bolts in single vertical rows at both the beam web and the column flange. Ductility prior to failure was attributed to localized bolt bearing deformations, bolt slip, and separation of the angle heel from the column. Five unique failure modes were observed: bolt shear, bolt punching through the column bolt hole, tearing of the net section of the angle along the column bolt line, tearing of the net section of the angle along the beam web bolt line, and tearing of the gross section of the angle near the heel.

Three end plate connections were tested under combined shear and tension. Each plate had one vertical row of two bolts on each side of the beam web connecting the end plate to the column flange. The three tests used beams with different web thicknesses, which caused web tearing to be the governing failure mode for the test with the thinnest beam web, and plate tearing near the weld toe to govern for the other two tests.

While the test results reported by Guravich provide a significant contribution to the understanding of shear connection behaviour when tensile forces are present, the specified load history and applied level of rotation are not consistent with the significantly higher magnitude of rotation expected to develop at beam-to-column shear connections following the removal of a column.

2.4.5. Thompson (2009)

A series of nine column removal tests with shear tab connections was completed by Thompson (2009). The test set-up consisted of a partial two-bay frame, with two beams connected to each side of a central column stub. The beams were each approximately 2.0 m long and were pin-supported at the end away from the test connection, representing the inflection point under normal loading and support conditions. Vertical displacement was applied at a quasi-static rate by a single

actuator at the central column, representing a point load at the location of a removed column.

Shear tabs had three, four, or five bolts arranged in a single vertical row. The test results demonstrated the ability of these simple connections to develop catenary forces and sustain significant rotation (between 0.09 radians and 0.14 radians) following column removal. The connections developed vertical loads of only 7.5 % to 9 % of their predicted unfactored capacity under pure shear loading. Bolt bearing deformations were typically observed prior to the ultimate load condition. Observed failure modes included: bolt shear, bolt tear-out in the axial direction of the beam, and plate tearing along the net section at the line of bolts. The study suggested that future research should include further testing with varied shear tab geometry and the development of refined analysis methods for predicting the behaviour of shear tabs under combined moment, shear, and tension.

2.4.6. Friedman (2009)

Friedman (2009) conducted a research program that paralleled that of Thompson (2009), described above, applying the same test set-up, procedure, and analysis techniques to tee connections. Nine column removal tests were completed on tee connections with three, four, or five bolts arranged in a single vertical row in the tee stem. The test results demonstrated that tee connections are also able to develop catenary forces and sustain significant rotation (between 0.07 radians and 0.13 radians) following column removal. The connections developed vertical loads of 6.4 % to 7.7 % of their predicted unfactored capacity under pure shear loading. Deformations from bolt bearing and tee yielding were observed prior to the ultimate load condition. Bolt shear governed the failure of all specimens. The study suggested that future research should include similar testing of tee connections with varied geometry and column removal tests with different types of shear connections.

2.4.7. Baldassino et al. (2010)

Baldassino et al. (2010) subjected full-depth end plate connections to a simple loading history developed by a single inclined actuator at the end of a cantilever beam. This test set-up effectively applied moment, shear and tension simultaneously; however, it did not allow the variation of the relative proportions of these forces independently throughout testing.

The eleven end plates tested were connected to either a column stub or a rigid support using two vertical lines of two bolts each. Extensive plastic deformation of the end plate (and column flanges, for specimens with non-rigid supports) was observed prior to failure. In all tests, failure was caused by bolt fracture under combined tension and bending.

Results showed that end plate tensile capacity is inversely related to applied rotation and shear. Additionally, it was shown that the flexibility of the supporting column is an important parameter in determining performance, with the more flexible column stub leading to significantly lower ultimate loads.

2.4.8. Weigand et al. (2012)

Weigand et al. (2012) summarized the testing methodology and preliminary results for a study on the structural integrity of shear connections that is currently underway. The test set-up uses a single actuator perpendicular to a cantilever beam to apply rotation in combination with a second pin-mounted actuator assembly to apply axial load in the direction of the rotated beam. The resultant load history applied using this procedure is approximately equivalent to the "point load" case considered as part of this research program (as described in Chapter 3).

At the time that the referenced conference paper was published, only two tests had been completed on shear tabs. Both specimens failed by bolt shear and developed only 15 % and 20 % of their factored design shear capacities (as calculated in the absence of axial forces) before failure occurred under predominantly tensile forces.

2.4.9. Yang and Tan (2013)

Yang and Tan (2013a, 2013b) reported on a series of column removal experiments that included shear connections, semi-rigid connections, and composite connections. The test set-up consisted of two beams connected to a central column stub and pin-supported at their opposite ends 2.3 m away from the column face. A single point load was applied at the central column stub.

Seven tests were performed on bare steel connections (Yang and Tan, 2013b), which included the following connection types: bolted–bolted double angle, seat and top angle, shear tab, combined top and seat angle with double web angle, and full-depth end plate connections. All tests failed under predominantly tensile load developed through catenary action. Bolted–bolted double angle connections failed by tearing near the angle heel, and the shear tab connection experienced bolt shear failure with limited bearing deformations.

Five tests were performed on composite bolted–bolted double angle and end plate connections (Yang and Tan, 2013a). A comparison of the composite specimen test results and those for similar connections tested without a slab demonstrated an increased load-carrying capacity in the composite case, even without anchoring the perimeter of the slab to allow for the development of membrane action. The authors recorded a transition from bending to catenary action as the central column deflection increased. The test results, together with the finite element analyses (Yang and Tan, 2012), were used to show that the current rotation limits used as acceptance criteria in UFC 4-023-03 (DoD, 2009) may be overly conservative.

2.4.10. Column Removal Tests with Moment Connections

Physical tests that examined the response of steel frames with moment connections to a column removal scenario have been completed by Demonceau (2008), Karns et al. (2009), Sadek et al. (2010), and others. The performance of steel moment frames following column removal typically depends on the development of plastic hinges in the beams away from connection locations. In

contrast, the present study focusses on the deformation of shear connections, which is the primary mechanism for the development of catenary action in gravity frames.

2.5. Previous Analytical Studies of Shear Connections under Combined Moment, Shear, and Tension

This section summarizes research that investigated the behaviour of shear connections under combined moment, shear, and tension using analytical approaches. These studies employed methods including mechanical models and finite element analysis, either in lieu of or to complement data from physical tests.

2.5.1. Thornton (1997)

Using yield line theory, Thornton (1997) considered the effect of the interaction between shear and tension on bolted–bolted double angle, partial-depth end plate, and tee connections. The study found that the presence of axial force decreases the rotational flexibility of shear connections, which are typically assumed by designers to behave as true pins. To avoid connection failure under combined loads, Thornton developed practical design recommendations to ensure connection details that maintain acceptable levels of strength and ductility.

2.5.2. Yang (1997)

Yang (1997) performed finite element analyses to study the behaviour of double angle connections under combined moment, shear, and tension. Physical tests of double angles under pure tension were used to validate the finite element model. The modelled connections were bolted to the column using a single vertical line of bolts in each angle and welded to the beam web along three sides of the adjacent angle leg. The program only varied angle thickness, but was later expanded by Hong et al. (2001) to study the effects of bolt spacing. The finite element model included a column stub connected to a beam that was supported by a true pin at its far end. A uniformly distributed vertical load was applied to the beam in combination with a horizontal tension force of 50 % of the total vertical

load. This load history and the resulting rotations are significantly different from those expected in a column removal scenario.

It was concluded that connection stiffness increases as angle thickness increases and as bolt spacing decreases. Plastic hinges were shown to develop in the connection angles as they were pulled away from the column. An equivalent spring model was developed to predict connection behaviour, using spring stiffnesses that were derived from the finite element analysis results. For the proposed approach to be applied to other connection geometries, similar finite element analyses would need to be completed, since the complexity of connection behaviour under combined loading prevented the development of a generalized connection model.

2.5.3. *Byfield and Paramasavim (2007)*

To investigate the viability of catenary action development as a means of preventing collapse in structures with shear connections, Byfield and Paramasavim (2007) considered the forces expected to develop in a connection following column removal. The analysis examined both shear tab and bolted–bolted double angle connections, and assumed that connection failure would occur due to prying forces caused by bearing of the beam flange on the column flange at a rotation of 0.07 radians (which corresponds to 10 mm of local bearing deformation at the extreme bolt for the shear tab configuration considered). Based on these assumptions, it was suggested that typical shear connections would be incapable of developing sufficient catenary forces to prevent collapse following column removal.

2.5.4. *Izzuddin et al. (2008)*

Izzuddin et al. (2008) presented an energy-based approach for determining the collapse resistance of structures following column removal. The outlined procedure employs a nonlinear static analysis and calculates the maximum dynamic response using the energy absorbed in the static analysis (rather than using a dynamic load amplification factor, as recommended in UFC 4-023-03 and

the GSA Guidelines). The maximum deformations resulting from the analysis are then compared to empirically-derived ductility acceptance criteria. The current limitation of the proposed approach lies in the determination of these criteria, particularly for the often-critical beam-to-column connections. It was observed that "...there is currently a shortage of data on connection ductility supply, especially in relation to the combined influence of rotational and axial connection deformations, and more so for connections that are not considered within the context of seismic design", which led to the conclusion that "…there is still a considerable need for extensive experimental work to determine the ductility supply of various connection types".

2.5.5. *Sadek et al. (2008)*

Sadek et al. (2008) performed finite element analyses to study the behaviour of a steel frame with shear connections and a composite concrete slab under a column removal scenario, citing as motivations the prevalence of this framing system and the current lack of information on its resistance to collapse. It was noted that no experimental data were available to quantify the response of the connections under a column removal scenario. All beam-to-column connections in the model consisted of shear tabs with three bolts in a single vertical row. Column removal analysis was completed for two cases: the first including only the steel framing components, and the second with the addition of a composite slab. The importance of connection behaviour to the collapse resistance of the structure was demonstrated, as connection failure under the effects of catenary forces limited the ultimate load capacity in both cases (with and without the inclusion of the composite slab). Bolt tear-out in the web at the shear tab connection was observed as the governing connection failure mode. Plastic strains were monitored in the connection bolts and shear tab plate material, although neither reached the point of fracture. Beams remained elastic at the gross section. In a test of the steel gravity frame alone, the ultimate strength was achieved at 0.088 radians of connection rotation.

The system that included a metal deck and composite concrete slab was shown to provide increased resistance to collapse—resisting more than twice the vertical load of the model that did not include these elements—by preventing undamaged columns from being pulled towards the removed column and by carrying tensile forces through the slab reinforcement. However, even with the contribution of the slab, the system was not able to carry the specified vertical load required by the GSA Guidelines. This finding is different from that of Astaneh et al. (2002b), who showed experimentally that a steel framing system with shear connections and a composite slab (although it had different shear connection details and overall geometry) could resist the specified loads.

2.5.6. Karns et al. (2009)

The GSA completed a testing program to characterize the behaviour of steel frames under the effects of a blast load that compromises a column. The program has been summarized by Karns et al. (2009), although the full report on the testing program has not been made available to the public. The physical testing program only considered moment frames. For each test, the central column in a two-bay frame was damaged using explosives, followed by the application of vertical load at the damaged or removed column location. Finite element modelling of the tests was carried out and verified using the test data. The model was subsequently used to examine the behaviour of other types of connections under similar loading conditions, including bolted–bolted double angle and shear tab connections. Results from the finite element analysis suggested that the ultimate load carried by the shear tab under catenary action was much lower than that carried by a similarly-proportioned bolted–bolted double angle. It was recommended that connections be detailed to sustain large rotations in the presence of axial loads to improve resistance of a frame to disproportionate collapse. Results from the finite element models were an important source of information for the modelling and acceptance criteria included in UFC 4-023-03 (shown in Tables 2.2 and 2.3).

2.5.7. Liu (2010)

Liu (2010a) analyzed the development of catenary action using a mechanical model, and hypothesized that the strains imposed on shear tab connections following the removal of a column would cause them to fail. Retrofit schemes were suggested to improve their performance by adding reinforcing plates to carry horizontal tension through the columns. Using finite element analysis, Liu (2010b) confirmed that shear tab connections are the critical elements for a typical framing system under a column removal scenario and demonstrated the improvements achieved by the proposed retrofit details.

2.5.8. Gong (2010)

Gong (2010) developed a practical procedure to estimate the forces that would be experienced by shear connections following column removal. However, the approach does not account for any interaction between rotation and axial force; the limitation is attributed to a lack of physical tests designed to study their combined effects. It was suggested that the critical considerations for the design of resilient connections are strength in the axial direction and ductility supply. In order to design connections to resist these unique demands, it was recommended that the brittle failure modes of weld and bolt fracture should be avoided, and further, that "…experimental studies on ductility supply in connections are greatly needed in future endeavours".

2.5.9. Raebel (2011)

Using commercially-available structural analysis software, Raebel (2011) modelled a three-storey building subjected to the removal of an interior column in the first storey. This work built upon a similar exercise by Foley et al. (2007) that formed part of a report to the American Institute of Steel Construction on the robustness of structural steel framing systems, but focussed more extensively on the behaviour of shear connections. The beam-to-column connection arrangements that were modelled consisted of shear tabs, seat angles combined with shear tabs, and shear tabs with a composite concrete slab. Connection models

were defined using stiffnesses and rotation limits taken from moment–rotation relationships recorded in previous seismic tests that used cyclic load histories. The modelling results showed that the addition of a seat angle and concrete reinforcement acting in tension both increased the collapse resistance of a structural system, but that the concrete itself was detrimental due to the effect of its dead weight on the steel frame. The studies performed by Raebel and Foley et al. both demonstrated a quantified level of inherent robustness in structural framing systems with shear connections and a composite concrete deck, but also asserted their potential vulnerability to collapse in a column removal scenario.

2.5.10. Yim and Krauthammer (2012)

Yim and Krauthammer (2012) developed a detailed component model for shear tab connections, including individual springs to represent various actions on the plate, bolts, column, and beam; each spring must be defined using an empirically-determined force–deformation relationship. The component model was shown to accurately predict the results of previous physical tests that included a wide range of loading conditions including blast and seismic loads, and was proposed as a potentially useful tool for analyses related to disproportionate collapse mitigation.

2.5.11. Main and Sadek (2012)

The National Institute of Standards and Technology published a technical note (Main and Sadek, 2012) describing the use of analytical modelling to assess the performance of gravity framing systems with shear tab connections when subject to a column loss. The study assembled detailed finite element models and "reduced" models that replaced a high-density element mesh with a series of springs at bolt locations. The analytical models were validated against the physical testing data from the column removal tests performed by Thompson (2009), and the reduced model was shown to predict ultimate load within 21.3 % and ultimate rotation within 26.1 %. This discrepancy was justified by the high coefficient of variation of the physical test results. The initial stiffness

and ultimate displacement of the springs in the reduced model were both increased in proportion to the depth of the bolt group, based on the relationship between maximum rotation and depth of the bolt group contained in FEMA 355D (FEMA, 2000), which is based on seismic tests.

The reduced model by Main and Sadek (2012) was utilized to study a gravity frame following column removal under both quasi-static and dynamic loading conditions (the energy balance method of Izzuddin et al. (2008) was adopted for the dynamic case). The effects of span length, connection strength, connection failure mode, and the inclusion of a composite concrete slab were studied. Results were used to recommend a new horizontal tie force requirement for composite framing systems with shear tab connections, which is included in Table 2.4.

2.6. Conclusion

Several recently-developed design guidelines collectively provide extensive recommendations for achieving increased resistance against disproportionate collapse by using a variety of approaches, including the tie force and alternative path methods. Each of these methods aims to ensure that beam-to-column connections provide adequate strength and/or ductility under loading conditions that are significantly different from those considered in conventional design. However, in order to apply these methods, accurate connection models are needed and there is currently a limited amount of research that examines the behaviour of commonly-used shear connections under the combined effects of moment, shear, and tension. Previous research programs that have investigated this topic are summarized above. These provide significant insight into the development of catenary action in steel frames with shear connections; however, as repeatedly asserted in the literature, there remains a deficiency in the current state of knowledge. In particular, there is a need for an increased database of full-scale test results that extends the breadth of connection geometries, an improved understanding of the response of connections under the demands imposed by a column removal scenario, and the development of design tools for the prediction of connection performance under these demands. Therefore, it is the objective of

this research program to contribute to the understanding of commonly-used shear connection behaviour under the effects of combined moment, shear, and tension resulting from a column removal, for the purpose of developing practical design recommendations that yield improvements to the level of structural integrity achieved in steel buildings.

Table 2.1. Design approaches for disproportionate collapse mitigation.

Method	Description
Indirect	
Tie Force	Provision of minimum tensile resistances at member connections
Integrity Detailing	Detailing specifications that are required even when they are beyond what is necessary to resist the defined load cases
Direct	
Event Control	Protection of a building from experiencing an extreme load
Enhanced Local Resistance	Proportioning of members to resist specified extreme loads without sustaining extensive damage
Alternative Path	Establishment of a stable load path following specified localized damage events, such as the removal of a column

Table 2.2. Acceptance criteria for linear static analysis procedures.

Connection Type	Acceptance Criteria	
GSA (2003)	**DCR**	
Combined Seat and Top Angle		
a. Shear in Bolt	1.5	
b. Tension in Horizontal Leg of Angle	1.5	
c. Tension in Bolt	1.5	
d. Flexure in Angles	3	
Shear Connection without Slab	2	
UFC 4-023-03 (DoD, 2009)	**m-factor**	
	Primary	**Secondary**
Double Angle		
a. Shear in Bolt	$5.8 - 4.21 \times 10^{-3}d_{bg}$	$8.7 - 6.34 \times 10^{-3}d_{bg}$
b. Tension in Bolt	1.5	4
c. Flexure in Angles	$8.9 - 7.60 \times 10^{-3}d_{bg}$	$13.0 - 11.4 \times 10^{-3}d_{bg}$
Shear Tab	$5.8 - 4.21 \times 10^{-3}d_{bg}$	$8.7 - 6.34 \times 10^{-3}d_{bg}$
ASCE/SEI 41-06 (ASCE, 2007) - Referred to by UFC 4-023-03		
Combined Seat and Top Angle[†]		
a. Shear in Bolt	2	3
b. Tension in Horizontal Leg of Angle	1.5	1.5
c. Tension in Bolt	1.25	2
d. Flexure in Angles	5	7
Shear Connection without Slab	—	$13.0 - 11.4 \times 10^{-3}d_{bg}$

†If d_b>457 mm, multiply m-factor by $457/d_b$; values need not be less than 1.0.

d_b = depth of beam, mm

d_{bg} = depth of bolt group, mm

Table 2.3. Modelling parameters and acceptance criteria for nonlinear analysis procedures.

Connection Type	Modelling Parameters[†]			Acceptance Criteria	
	a	b	c	Plastic Rotation Angle (radians)	
GSA (2003)					
Shear Tab or Combined Seat and Top Angle					
a. Shear in Bolt	—	—	—	0.015	
b. Tension in Plate or Angles	—	—	—	0.015	
c. Tension in Bolt	—	—	—	0.015	
d. Flexure in Plate or Angles	—	—	—	0.025	
UFC 4-023-03 (DoD, 2009)				**Primary**	**Secondary**
Double Angle					
a. Shear in Bolt	$0.0502 - 59.1 \times 10^{-6}d_{bg}$	$0.072 - 86.6 \times 10^{-6}d_{bg}$	0.200	$0.0502 - 59.1 \times 10^{-6}d_{bg}$	$0.0503 - 43.3 \times 10^{-6}d_{bg}$
b. Tension in Bolt	$0.0502 - 59.1 \times 10^{-6}d_{bg}$	$0.072 - 86.6 \times 10^{-6}d_{bg}$	0.200	$0.0502 - 59.1 \times 10^{-6}d_{bg}$	$0.0503 - 43.3 \times 10^{-6}d_{bg}$
c. Flexure in Angles	$0.1125 - 0.106 \times 10^{-3}d_{bg}$	$0.150 - 0.142 \times 10^{-3}d_{bg}$	0.400	$0.1125 - 0.106 \times 10^{-3}d_{bg}$	$0.150 - 0.142 \times 10^{-3}d_{bg}$
Shear Tab	$0.0502 - 59.1 \times 10^{-6}d_{bg}$	$0.072 - 86.6 \times 10^{-6}d_{bg}$	0.200	$0.0502 - 59.1 \times 10^{-6}d_{bg}$	$0.1125 - 0.106 \times 10^{-3}d_{bg}$
ASCE/SEI 41-06 (ASCE, 2007) — Referred to by UFC 4-023-03					
Combined Seat and Top Angle					
a. Shear in Bolt	0.018	0.024	0.100	0.010	0.015
b. Tension in Horizontal Legs of Angles	0.012	0.018	0.800	0.008	0.010
c. Tension in Bolt	0.008	0.013	0.500	0.004	0.010
d. Flexure in Angles	0.042	0.084	0.200	0.025	0.035
Shear Connection without Slab	$0.150 - 0.142 \times 10^{-3}d_{bg}$	$0.150 - 0.142 \times 10^{-3}d_{bg}$	0.400	—	$0.1125 - 0.106 \times 10^{-3}d_{bg}$

[†]Refer to Figure 2.1. d_{bg} = depth of bolt group, mm

Table 2.4. Horizontal tie force requirements.

Member Location	Horizontal Tie Force[†]
UFC 4-023-03 (DoD, 2009)	
Interior	$3\,Q_f\,L\,s$
Perimeter	$6\,Q_f\,L\,s_p$
Eurocode 1 (CEN, 2006)	
Interior	$0.8\,Q_f\,L\,s \geq 75$ kN
Perimeter	$0.4\,Q_f\,L\,s \geq 75$ kN
International Building Code (ICC, 2012)	
Interior/Perimeter	$2/3\,V_r \geq 45$ kN
Main and Sadek (2012)	
Interior/Perimeter	$0.32\,(Q_f)^2$

†Some notation has been modified for consistency among guidelines.
Q_f = factored floor load (kN/m^2) = $\lambda_D Q_D + \lambda_L Q_L$
Q_D = dead load; Q_L = live load
λ_D = dead load factor; $\lambda_D = 1.2$ in UFC 4-023-03; $\lambda_D = 1.0$ in Eurocode 1
λ_L = live load factor; $\lambda_L = 0.5$ in UFC 4-023-03;
     λ_D varies from 0 to 0.9 in Eurocode 1, depending on the type of live load
L = span length of ties
s = spacing of ties (implied, but not explicitly defined, in UFC 4-023-03)
s_p = 0.91 m
V_r = factored vertical shear resistance of connection
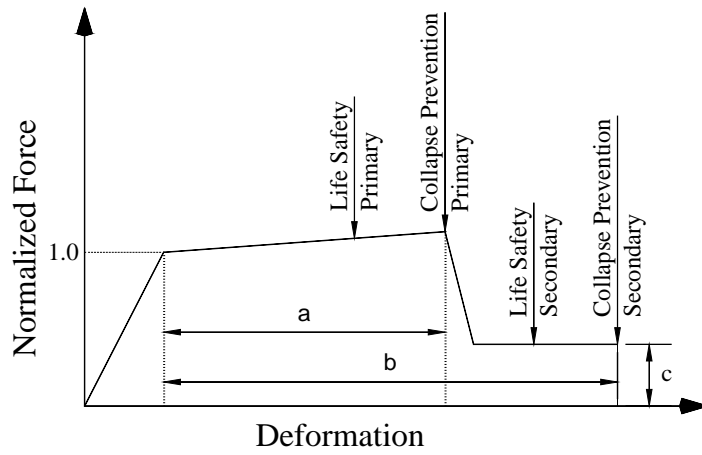
Figure 2.1. Generalized component force–deformation curve for nonlinear modelling and acceptance criteria (adapted from ASCE/SEI 41-06 (ASCE, 2007)).

3.   EXPERIMENTAL PROGRAM

In order to investigate the performance of common steel beam-to-column shear connections under the strength and ductility demands caused by column removal, an experimental program consisting of 45 full-scale physical tests was completed in the I.F. Morrison Structural Engineering Laboratory at the University of Alberta. The main parameters varied among the tests include connection type, connection geometry, and applied loading history. Material properties were determined using standard tension coupon testing. This chapter presents details of the experimental method, test specimens, and material properties; experimental results are reported in Chapter 4.

3.1.   Test Set-up

The test set-up shown in Figures 3.1 and 3.2 was designed to be capable of applying independent levels of moment, shear, and axial tension to beam-to-column connections. Hydraulic actuators at three locations were used to load a cantilever beam (test beam) connected to the flange of a column stub (test column) by the connection being studied. The use of two vertical actuators (Actuators 1 and 2) allows for the application of any desired combination of moment and shear to the connection. Since Actuator 1 was located near the test column, it was relatively ineffective for applying moment to the connection, but offered efficient control over the total applied shear. Conversely, load applied by Actuator 2 was significantly farther from the connection, and thus induced a much higher ratio of applied moment to applied shear, as well as being more efficient for applying connection rotation. The vertical actuators were pinned at each end, allowing them to rotate freely in the plane of the beam web as the beam underwent rotation and translation. Actuators 1 and 2 were each rated for a maximum load of 680 kN in compression and 550 kN in tension. The cantilevered end of the test beam was moved upwards in all tests.

Actuator 3 (actually a coupled pair of actuators in parallel) was pin-connected to the web of the test beam away from the test connection, and oriented to apply

42

primarily axial load along the centreline of the beam. Its initial inclination was selected such that the actuator and beam axes were approximately aligned at the rotation corresponding to the maximum applied axial load for that test. Actuator 3 was rated for a maximum load of 1360 kN in tension; since the assembly had three pins between its support at the reaction wall and the test beam, compressive forces could cause it to buckle. However, this limitation was inconsequential because, although small compressive forces were encountered during some loading regimes, all specimens failed under axial tension.

A rigid reaction frame was provided by a diagonally braced column at the test column end and a rigid shear wall adjacent to Actuator 3. All components of the reaction frame were connected to a concrete strong floor using pretensioned high-strength steel anchor rods. Polytetrafluoroethylene (commonly referred to by the proprietary name Teflon®) slide plates connected to each side of the test beam moved along rigid columns (not shown in Figure 3.1 for clarity) to provide lateral bracing to the beam near the test connection. Teflon was chosen for this application because of its exceptionally low coefficient of friction, provided by the manufacturer as 0.04 for the material grade used. The predicted vertical friction forces are considered sufficiently small to be neglected.

3.2. Instrumentation

Figure 3.3 shows the general arrangement of the electronic instrumentation used to measure forces, displacements, rotations, and strains imposed on the system during testing. Redundant measurements of critical parameters were taken to affirm the accuracy of recorded data.

Each actuator was instrumented with a load cell to measure the applied force, a clinometer to measure actuator rotation, and a cable transducer to measure actuator stroke. This allowed the magnitude, direction, and location of the force applied to the test beam by each actuator to be calculated explicitly throughout the test, which, in turn, permitted an accurate resolution of the three applied forces into their orthogonal components for the determination of the moment, shear, and

axial force demands to be applied to the connection. All three load cells were calibrated in tension and compression using an MTS6000 universal testing machine immediately prior to performing the first test. Pressure transducers were installed on the hydraulic lines connected to the actuators to allow a redundant calculation of each applied force.

A cable transducer mounted to the web of the test beam and attached to the face of the test column flange provided a direct measurement of the axial elongation of the system, with reference to the test column flange, along the centreline of the beam. Although the deformations were concentrated within the connection region (the beam was designed to remain elastic), to minimize the error that would result from the two fixed points of the cable transducer not being exactly aligned with the beam web, these points were separated by a distance of more than one metre. Vertical displacement at the bolt line of the connection was also measured using a cable transducer. Beam rotation was measured using a clinometer, which was also mounted along the centreline of the beam web. Four linear variable displacement transducers (LVDTs)—two on each side of the column web—were installed to monitor any horizontal displacement of the test column flange for the tests with unstiffened columns.

Measurement signals from the electronic instrumentation were processed using an HBM MGCplus data acquisition system and the software catmanAP Version 3.0. The software was programmed to perform real-time calculations based on regularly updated instrumentation data, which allowed the measured loads and deformations to be used as feedback for the determination of the applied load history, as per the procedure outlined in Section 3.3.3.

The initial geometry of each test, including as-built specimen dimensions and actuator locations, was measured and recorded. Manual distance measurements were also performed at regular intervals during testing to record relevant quantities not captured by the instrumentation discussed above, including tear

lengths, gap distances between the column face and beam flange, and separation between the column face and the heel of the connection angle.

A series of dial gauges was used to monitor whether any movement occurred in the steel baseplate or reaction column. No detectable movement of the baseplate was measured; horizontal displacement of the reaction column at the height of the test column was less than 3 mm for all tests, and did not affect the axial displacement measurements on the test specimen.

Surface strains in the test connection region were measured using a Vic-3D 2009 optical strain imaging system from Correlated Solutions Inc. This system performs digital image correlation, a technique that tracks the relative displacements of unique points within a speckled pattern using simultaneous pairs of digital images taken by two cameras focused on a common area of interest, as shown in Figure 3.4(a). Each specimen was speckled with an isotropic pattern of black dots on a white background to provide a field of high-contrast points for mapping surface strains, as seen in Figure 3.4(b).

3.3.   Load History

The key to evaluating the performance of connections experimentally under the effects of extreme loads is the selection of an appropriate load history. As discussed in Section 3.1, the test design allowed for the application of prescribed combinations of loads; this section outlines a rationale for the proportions of moment, shear, and tension—which change during the loading regime and are influenced by the connection response itself—that can be reasonably expected following severe damage to a supporting column.

3.3.1. Simplified Column Removal Analysis

The types of loads under consideration are highly variable by nature. The exact consequences of an extreme loading event are difficult, if not impossible, to predict. It is for this reason that column removal analysis has been adopted by design codes and an array of current research on the topic (as summarized in

Chapter 2) as being a consistent and reasonable approach for the improvement of collapse resistance following many different types of local damage. This loading scenario is not intended to represent a specific event; rather, it provides a general assessment of a structural system's robustness. Loading histories based on column removal analysis provide realistic combinations of strength and ductility demands concurrently. It is important to consider these demands together in testing and design, since successful collapse resistance by catenary action is achieved through the effective development of combined forces at large deflections.

3.3.1.1. Equilibrium of Forces

The series of free body diagrams shown in Figures 3.5, 3.6, and 3.7 is used to examine a range of potential strength and ductility demands that could be expected to develop in shear connections under a column removal scenario. In the derivations that follow, the forces in the connections, V and H, are taken as vertical and horizontal, respectively, rather than perpendicular and parallel to the axis of the rotated beam. Thus, a fixed Cartesian coordinate system is established in which the direction of gravity loading and the initial orientations of the beam and column are aligned with primary axes; forces can be resolved with respect to the axis of the beam using its rotation angle at any instant. The axial orientation of the connecting element itself is difficult to define, since the axis of the highly distorted connection will vary between the locations where the connecting element is attached to the beam web and where it is attached to the column flange.

The simple case of a symmetric three-hinged beam with a central point load, which was solved by Timoshenko (1955), is shown in Figure 3.5. Each hinge can be taken to represent a rotationally flexible connection in a two-bay frame, with the hinge at the centre corresponding to the location of a removed column below. It is necessary to consider the displaced system in order to formulate the equilibrium condition including catenary action. The resulting vertical force carried by each of the central and end connections, V_1 (subscripts of V distinguish the unique cases), in terms of the horizontal force, H, and the beam chord rotation angle, θ_c, is given by:

$$V_1 = \frac{P}{2} = H \tan \theta_c \qquad\qquad [3.1]$$

For this case, the resultant connection force (obtained from the vector addition of V_1 and H) acts at an angle θ_c; that is, it acts in the axial direction of the rotated beam.

A similar free body diagram with a uniformly distributed load, ω, is shown in Figure 3.6. For this case, the vertical force carried by the connections at the end supports, V_2, is different from that at the removed column, V_3. This produces two additional potential relationships between vertical force, horizontal force, and rotation at the connections:

$$V_2 = \omega L = 2H \tan \theta_c \qquad\qquad [3.2]$$

$$V_3 = 0 \qquad\qquad [3.3]$$

Comparing Equations 3.1 and 3.2 reveals that the vertical forces at the end connection required for equilibrium at equal rotation and horizontal force values are different by a factor of two for the cases of a point load and a uniformly distributed load. Equation 3.3, for the central connection and the uniformly distributed load, represents a third unique load combination (i.e., horizontal force only).

Timoshenko's three-hinged beam is modified further to consider the rotational and axial stiffnesses of the connections, represented in Figure 3.7 by axial and rotational springs at each connection location. Without the axial springs to account for the elongation of the four connections—which, in the case of shear connections, are typically much more flexible than the beams—the axial forces would be proportional to the elongation of the two beams. Astaneh (2007) used a similar model in a discussion of shear connection design for disproportionate collapse; however, a lack of information for the selection of an axial spring stiffness and failure criteria was noted, and the approach assumed that the moment resistance of the connection is negligible. Since shear connections are capable of developing moment, albeit typically small, it is included in the

47

equilibrium formulation below. For both the central and end connections (assuming an identical rotational stiffness), the vertical force is:

$$V_4 = \frac{P}{2} = H \tan \theta_c + \frac{2M}{L}$$ [3.4]

Replacing the point load shown in Figure 3.7 with a uniformly distributed load, a similar derivation gives (for the end and central connections, respectively):

$$V_5 = \omega L = 2\left(H \tan \theta_c + \frac{2M}{L}\right)$$ [3.5]

$$V_6 = 0$$ [3.6]

In the presence of a nonzero connection moment or a distributed load, the resultant connection force acts at an angle different from θ_c.

3.3.1.2. Compatibility of Displacements

For a symmetric two-bay frame, the central column is restrained to move vertically after the removal of a column below. Thus, if the end columns are prevented from moving inward, a right triangle is formed by the initial span length, the vertical deflection at the removed column, and the final distance between points of rotation. Using simple trigonometry, the change in total length of the beam and connections at any rotation can be calculated. This change in length will be an elongation, since the deformed geometry forms the hypotenuse of the triangle; it is this deformation that results in the development of a tensile catenary force. If the elastic elongation of the beam is neglected as being much smaller than the elongation of the axially-flexible shear connections, half of this total span elongation can be attributed to each of the two connections in the span. The elongation of each connection in the direction of the rotated beam axis, Δ_3, is thus related to the initial span length, L, and the chord rotation angle, θ_c, as follows:

$$\Delta_3 = \frac{L}{2}\left(\frac{1}{\cos \theta_c} - 1\right)$$ [3.7]

3.3.2. Selection of Load Histories

The column removal analysis outlined in Section 3.3.1 is used to establish a simple, yet reasonable, combination of strength and ductility demands to assess the robustness of shear connections. This section provides a rationale for the selection of the load histories applied in the testing program.

The three unique equilibrium conditions expressed in Equations 3.1, 3.2, and 3.3 represent the cases of a central point load (for either connection), a uniformly distributed load for the connection at the removed column, and a uniformly distributed load for the connection at the remaining column, respectively. Each defines a significantly different rate of vertical load development with respect to horizontal tension and connection rotation. Load histories satisfying the two nonzero vertical load conditions were applied using the test set-up outlined above, since the zero vertical force case at the removed column is always paired with a more severe load combination at the remaining column. Thus, a practical range of vertical loading proportions is established by the examination of the two load arrangements.

There are several other realistic load arrangements that are bounded by these two cases. For example, the case of a damaged column with some residual capacity and that of a series of point loads (such as those applied to a beam by a series of joists) would both fall within this envelope. Additionally, characteristics that control behaviour under the range of load histories selected can be used to examine situations that may fall outside of this range, such as an unsymmetrical load or span arrangement.

Equations 3.4 and 3.5 provide similar equilibrium formulations to those selected for use in the testing program, but include the contribution of connection moment to the development of total vertical load. Research on shear connections under conventional gravity and seismic loading conditions has concluded that the moments developed by typical shear connections are relatively small, which has led to their treatment as true pins in the design of the supported beams. The

moment resistance of shear connections becomes even smaller in the presence of the axial tension resulting from catenary action. The use of Equations 3.4 and 3.5 in place of Equations 3.1 and 3.2 would result in slightly greater total applied vertical loads at given rotations, and corresponding changes to the direction in which the resultant applied load acts; however, the proportion of applied vertical load is also varied by the inclusion of two different loading cases. While it is acknowledged that shear connections do not behave as true pins, their treatment as such in the formulation of a load history is considered a reasonable simplification that provides combinations of moment, shear, and axial forces representative of a column removal scenario. The total moment developed in each connection was measured throughout the tests (and is reported in Chapter 4), and the effect of including the moment term in the calculation of total vertical load is studied in Chapters 5 and 6.

In addition to providing the means for selecting loading protocols for the testing program, the column removal analysis discussed above requires the selection of an assumed span length to calculate the axial deformation demands imposed on the connection by compatibility using Equation 3.7. While the span length of a beam in a building is correlated with the shear capacity of its connections, many other factors impact this relationship (including design load level, tributary area, and deflection criteria). In practice, any specific connection design could be appropriate for a wide range of span lengths; thus a range of span length values was selected that is considered representative of common steel building layouts. For connections with three bolts, span lengths of 6 m and 9 m were considered; connections with five bolts were tested assuming span lengths of 8 m and 12 m.

Considering a range of span lengths affects the rate of axial deformation demand development with beam rotation. A similar effect occurs due to varying flexibilities of the structure surrounding the two-bay frame where the column has been removed. Thus, test results achieved by considering a range of span lengths could be used to examine collapse resistance in the case where non-rigid axial

restraints at the remaining column locations tend to decrease the rate of axial deformation demand development.

3.3.3. Load Application Procedure

This section discusses the procedure used to apply loads that satisfy the prescribed equilibrium and compatibility conditions discussed above using the test set-up shown in Figure 3.1. In general, this was achieved by controlling each of the three actuators independently through incremental load steps to achieve target load and displacement values calculated using real-time data output. Figure 3.8 illustrates this iterative process using a flowchart. Load steps are depicted using blue process rectangles with bold text; calculations of the target load history are shown in green process rectangles with regular text; measured data outputs are shown in red parallelograms; and decision steps are indicated using orange diamonds.

The target values of vertical load for the equilibrium condition (Equation 3.1 or 3.2 for an assumed point load or uniformly distributed load, respectively) and axial displacement for the compatibility condition (Equation 3.7) were calculated using continuously updated values of the measured loads and deformations. Complete details of the computations programmed into the data acquisition software appear in Appendix A.

Connections were tested under quasi-static loading conditions, with each load step representing a unique state of static equilibrium for a column removal scenario. Beam rotation was increased incrementally throughout the test, primarily by using Actuator 2 under displacement control. Rotation was advanced by the smallest practical interval (as limited by the precision of control of Actuator 2, which was able to advance rotation in increments of approximately 0.001 radians), in order to produce a smooth loading curve with minimal deviation from the target load and displacement values. At each rotation level, Actuators 1 and 3 were adjusted to approach the calculated load history targets. Although the flowchart shows the incremental application of load using Actuators 1 and 3 as sequential processes, the hydraulic controls operator was able to adjust load at these two locations at the

51

same time in order to approach the equilibrium and compatibility conditions for the current rotation step concurrently. The level of convergence achieved between the calculated and measured load histories is discussed in Chapter 4.

Loading for all tests proceeded until specimen failure, with failure defined as the point at which connection damage had eliminated any significant level of residual capacity.

3.4.   Description of Test Specimens

A total of 45 full-scale beam-to-column connections were tested to failure under loading conditions representative of a column removal scenario. The specimens consisted of shear connections and shear connections combined with seat and top angles. The critical geometric parameters of the test specimens are discussed in this section; a complete set of fabrication drawings is included in Appendix B.

Connections were generally designed with geometries considered typical for shear connections in gravity frames. The *Handbook of Steel Construction* (CISC, 2010) and *Steel Construction Manual* (AISC, 2011) were consulted for standard dimensions and general design requirements. Additionally, seven steel fabricators from across Canada provided information, based on their experience, to aid in the selection of test specimens that are representative of shear connections most commonly used in structural steel buildings. In so doing, this program seeks to examine connection arrangements already proven to be economical by their use in current practice.

Table 3.1 summarizes the composition of the experimental program in a specimen matrix, with the test specimens organized into three geometric classes. Class A consists of connections with the connecting element (plate or angle) thickness equal to 9.5 mm, and the bolt diameter equal to 22 mm. Class B comprises lighter connections than those in Class A, with similar overall geometries but thinner connecting elements (6.4 mm thick) and smaller bolts (19 mm diameter). Class C connections are geometrically similar to their corresponding Class B connections, but include the addition of 6.4 mm thick seat and top angles, also with 19 mm

52

diameter bolts. The value in the body of Table 3.1 indicates the number of tests performed under different load histories (as discussed in Section 3.3) for each connection geometry. Figure 3.9 describes the specimen naming convention used throughout this report, which includes information on the connection type, number of horizontal rows of bolts, and geometric classification.

All specimens were fabricated by Supreme Steel in Edmonton, Alberta. As-built measurements were found to be within normal fabrication tolerances for all specimens.

3.4.1. Test Columns

All connections were attached to the flange of a test column stub, fabricated from a W250×89 section. The test columns were designed not to fail during the tests, in order to isolate and study the ductility and strength of the connecting elements. The columns were extended a minimum of 250 mm (the cross-sectional depth of the column) beyond the top and bottom of the connecting elements.

Two reusable test columns were fabricated for the single and double angle specimens that were bolted to the column flange. One column was designed with holes for 22 mm diameter bolts to accommodate Class A specimens, and one with holes for 19 mm diameter bolts to accommodate Classes B and C specimens. Since these columns were reused for many tests and the angle connections loaded the flange away from the web centreline, transverse web stiffeners were installed to limit bending deformations of the column flange and web. In order to examine the effect of column deformation on the behaviour of single and double angle connections, two single angle and two double angle tests were repeated on both stiffened and unstiffened columns. Unstiffened test columns were fabricated for each test specimen where connecting elements were welded to the column near the web centreline (i.e., shear tabs and welded–bolted single angles).

3.4.2. Test Beams

Figure 3.10 shows the geometry of the cantilever beams used for the tests. All web connections were bolted to the test beam, with bolt holes centred about beam mid-depth. Similar to the test columns, the beams were designed not to fail during the tests, in order to study the ductility and strength of the connecting elements. Web doubler plates were added at the Actuator 3 pin connection location to prevent web failure.

A total of four test beams were fabricated and used for all of the tests. W310×143 sections were used for tests with three horizontal rows of bolts, and W530×165 sections for tests with five rows of bolts. Two test beams were fabricated from each cross-section, with similar overall geometries but different hole sizes to accommodate either 19 mm or 22 mm diameter connection bolts.

3.4.3. Shear Tab Connections

Shear tab connections consist of a single plate welded perpendicular to the column flange and bolted to the beam web. Figure 3.11 shows the typical geometry of the three- and five-bolt shear tab connections tested. The parameters that distinguish each of the nine shear tab specimens are summarized in Table 3.2. Shear tabs were designed following the recommendations of Astaneh et al. (1989), as presented in the *Handbook of Steel Construction* (CISC, 2010). A typical pitch (vertical distance between bolts) of 80 mm was used for all shear tab connections. Welds were sized to develop the full strength of the plate material in shear. All vertical and horizontal edge distances were 35 mm from the centre of the bolt holes. The initial gap distance between the column and beam flanges was 25 mm. Shear tabs were attached to the column flange at a slight horizontal offset to achieve alignment of the beam and column centrelines.

3.4.4. Single and Double Angle Connections

Figure 3.12 shows the typical geometry of the single and double angle connection specimens. All angle connections were bolted to the beam using either three or

54

five bolts in a single vertical line. Bolt lines were located at a gauge of 60 mm from the angle heel, resulting in an initial gap of 10 mm between the column and beam flanges and a horizontal edge distance of 29 mm. Vertical edge distances (at the top and bottom bolts) were 35 mm for all specimens. Angles were attached to the column flange at a slight horizontal offset to achieve alignment of the beam and column centrelines. Figure 3.13 (Section A-A from Figure 3.12, with the beam not shown for clarity) shows the distinguishing features of the three types of angle connections included in the experimental program. The figure only shows the geometry the three-bolt specimens; five-bolt specimens are similar.

3.4.4.1. Welded–Bolted Single Angle Connections

Welded–bolted single angle connections were bolted to the beam and welded to the column along three sides of the outstanding leg (with no weld along the toe), as shown in Figure 3.13(a). The parameters that distinguish each of the five welded–bolted single angle specimens are summarized in Table 3.3. Each welded–bolted single angle connection was welded to an unstiffened test column. Double angle connections welded at the column were not included in the testing program because this arrangement is not commonly used in practice.

3.4.4.2. Bolted–Bolted Single Angle Connections

Bolted–bolted single angle connections were geometrically similar to the welded–bolted specimens, but were bolted to the column as well as to the beam, as shown in Figure 3.13(b). The arrangement of bolts on each of the angle legs (attached to the column flange and beam web) was the same. Reusable stiffened test columns were typically used for this connection type; two tests were repeated using unstiffened columns to examine any effects that the presence of stiffeners imposed on connection response. The parameters that distinguish each of the fifteen bolted–bolted single angle specimens are summarized in Table 3.4.

3.4.4.3. Bolted–Bolted Double Angle Connections

Double angle connections consist of two similar angles, one on each side of the beam web, as shown in Figure 3.13(c). Contrary to all other connection types in

the experimental program, double angle connections are symmetric about the beam web centreline. Tests were performed using the same stiffened test columns that were used for the single angle connections, with the exception of two connections that were tested using unstiffened columns. The parameters that distinguish each of the six bolted–bolted double angle specimens are summarized in Table 3.5.

3.4.5. Combined Seat and Top Angle Connections

Seat and top angles were bolted to both the column and beam flanges, and were used in combination with web connections of various types, in order to examine their potential benefit as a retrofit option for existing shear connections. Figures 3.14 and 3.15 show the geometries of connections that were reinforced with a seat and top angle. Because the gap distance between the column and beam flanges was greater for shear tabs than for angle connections, seat and top angles used in combination with shear tabs had longer leg lengths. For each of these specimens, both the specified geometry of the web connection and applied load history were equivalent to a corresponding test specimen without the added angles, as shown in Table 3.6. This allows the test results for connections with and without seat and top angles to be directly compared.

3.4.6. Connection Bolts

New ASTM A325 high strength bolts without washers were used for each test specimen. In no cases were bolt threads intercepted by a shear plane. Bolt holes were drilled 1.6 mm larger than the specified bolt diameter.

All connection bolts were installed to the snug-tight condition, as is common practice for shear connections that are not expected to be loaded cyclically or in tension. The snug-tight condition induces a small clamping force compared to that achieved by the turn-of-nut method.

3.5. Material Properties

3.5.1. Specified Material Grades

Angles and plates used to fabricate the connections were specified as CAN/CSA-G40.21-04 (CSA, 2004) Grade 300W, which requires a minimum yield strength of 300 MPa and an ultimate strength between 450 MPa and 620 MPa. W-shapes used for the test columns and beams were specified as Grade 350W, which requires a minimum yield strength of 350 MPa and an ultimate strength between 450 MPa and 650 MPa. All plate of the same thickness and all W-shapes and angles of the same size were fabricated from the same piece in order to keep the material properties for each test as consistent as possible and to reduce the number of tension coupon tests required to define the material properties of the connection elements.

3.5.2. Tension Coupon Tests

A series of ancillary tests was performed to quantify material parameters relevant to connection behaviour, including: Young's modulus of elasticity, E; static yield strength, σ_y; and static ultimate strength, σ_u. Tension coupon tests were performed following the standard testing method described in ASTM A370-11 (ASTM, 2011). Load was applied at a rate of 0.6 mm/min until strain hardening began, at which time the rate was increased to 2.4 mm/min. During each test, loading was stopped three times when the stress had reached the yield plateau and one additional time prior to necking at the approximate maximum engineering stress, in order to obtain static values of σ_y and σ_u.

All coupons were water-jet cut with the profile shown in Figure 3.16. The locations from which coupons were extracted for each of the cross-sections tested are shown in Figure 3.17. Four coupons were tested for each plate and angle section, except for the L89×89×6.4 section, which only had three coupons extracted that were acceptable for testing. Six coupons were tested for the test column (W-shape) section — two from the web and two from each flange.

Tension coupons were not extracted from the test beams, as these were not loaded inelastically in the connection tests.

Figure 3.18 shows the stress–strain curves for the four coupons cut from the 9.5 mm plate. Similar curves were obtained for each set of coupons, and can be found in Appendix C. Linear regression was used to determine E from the slope of the stress–strain curve between zero stress and the proportional limit. Table 3.7 reports the mean values of E, σ_y, and σ_u for each set of coupons tested. For all specimens, the yield strain was near 0.20 %, strain hardening occurred between 1.6 % and 2.1 % strain, necking causing a decrease in engineering stress initiated between 17 % and 22 % strain, and the reduced cross-section ruptured between 23 % and 31 % strain (except for one L89x89x6.4 coupon, which was fabricated with a notch in the reduced cross section that caused premature rupture at 19 % strain).

Table 3.1. Specimen matrix.

# of Bolts, Class Connection Type	3A	3B	3C	5A	5B	5C
Shear Tab	3	2	2	2	2	2
Welded–Bolted Single Angle	3	—	—	—	2	—
Bolted–Bolted Single Angle	4	5	2	2	4	2
Bolted–Bolted Double Angle	—	3	2	—	3	—

Table 3.2. Shear tab specimen parameters.

	Specimen Geometry[†]				Load History Parameters[††]	
Specimen ID	Rows of Bolts	Plate Thickness t (mm)	Bolt Diameter d (mm)	Weld Size S (mm)	Load Arrangement P or ω	Span Length L (m)
ST3A-1	3	9.5	22	6	P	6.0
ST3A-2	3	9.5	22	6	ω	6.0
ST3A-3	3	9.5	22	6	ω	9.0
ST3B-1	3	6.4	19	5	ω	6.0
ST3B-2	3	6.4	19	5	ω	9.0
ST5A-1	5	9.5	22	6	ω	8.0
ST5A-2	5	9.5	22	6	ω	12.0
ST5B-1	5	6.4	19	5	ω	8.0
ST5B-2	5	6.4	19	5	ω	12.0

†*Refer to Figure 3.11.*   ††*Refer to Section 3.3.*

Table 3.3. Welded–bolted single angle specimen parameters.

	Specimen Geometry[†]				Load History Parameters[††]	
Specimen ID	Rows of Bolts	Angle Thickness t (mm)	Bolt Diameter d (mm)	Weld Size S (mm)	Load Arrangement P or ω	Span Length L (m)
WA3A-1	3	9.5	22	8	P	6.0
WA3A-2	3	9.5	22	8	ω	6.0
WA3A-3	3	9.5	22	8	ω	9.0
WA5B-1	5	6.4	19	6	ω	8.0
WA5B-2	5	6.4	19	6	ω	12.0

†*Refer to Figures 3.12 and 3.13(a).*   ††*Refer to Section 3.3.*

Table 3.4. Bolted–bolted single angle specimen parameters.

Specimen ID	Specimen Geometry[†]				Load History Parameters[††]	
	Rows of Bolts	Angle Thickness t (mm)	Bolt Diameter d (mm)	Stiffened Column	Load Arrangement P or ω	Span Length L (m)
SA3A-1	3	9.5	22	Yes	P	6.0
SA3A-2	3	9.5	22	Yes	ω	6.0
SA3A-3	3	9.5	22	Yes	ω	9.0
SA3A-4	3	9.5	22	Yes	ω	6.0
SA3B-1	3	6.4	19	Yes	P	9.0
SA3B-2	3	6.4	19	Yes	ω	6.0
SA3B-3	3	6.4	19	Yes	ω	9.0
SA3B-4	3	6.4	19	Yes	P	6.0
SA3B-5	3	6.4	19	No	ω	9.0
SA5A-1	5	9.5	22	Yes	ω	8.0
SA5A-2	5	9.5	22	Yes	ω	12.0
SA5B-1	5	6.4	19	Yes	P	8.0
SA5B-2	5	6.4	19	Yes	ω	8.0
SA5B-3	5	6.4	19	Yes	ω	12.0
SA5B-4	5	6.4	19	No	ω	12.0

†*Refer to Figures 3.12 and 3.13(b).*   ††*Refer to Section 3.3.*

Table 3.5. Bolted–bolted double angle specimen parameters.

Specimen ID	Specimen Geometry[†]				Load History Parameters[††]	
	Rows of Bolts	Angle Thickness t (mm)	Bolt Diameter d (mm)	Stiffened Column	Load Arrangement P or ω	Span Length L (m)
DA3B-1	3	6.4	19	Yes	ω	6.0
DA3B-2	3	6.4	19	Yes	ω	9.0
DA3B-3	3	6.4	19	No	ω	9.0
DA5B-1	5	6.4	19	Yes	ω	8.0
DA5B-2	5	6.4	19	Yes	ω	12.0
DA5B-3	5	6.4	19	No	ω	8.0

†*Refer to Figures 3.12 and 3.13(c).*   ††*Refer to Section 3.3.*

Table 3.6. Combined seat and top angle specimen parameters.

| Specimen ID | Specimen Geometry[†] | | Bolt Diameter d (mm) | Load History Parameters[††] | |
	Similar Web Connection	Seat and Top Angle Designation		Load Arrangement P or ω	Span Length L (m)
ST3C-1	ST3B-1	L102x102x6.4	19	ω	6.0
ST3C-2	ST3B-2	L102x102x6.4	19	ω	9.0
ST5C-1	ST5B-1	L102x102x6.4	19	ω	8.0
ST5C-2	ST5B-2	L102x102x6.4	19	ω	12.0
SA3C-1	SA3B-2	L89x89x6.4	19	ω	6.0
SA3C-2	SA3B-3	L89x89x6.4	19	ω	9.0
SA5C-1	SA5B-2	L89x89x6.4	19	ω	8.0
SA5C-2	SA5B-3	L89x89x6.4	19	ω	12.0
DA3C-1	DA3B-1	L89x89x6.4	19	ω	6.0
DA3C-2	DA3B-2	L89x89x6.4	19	ω	9.0

†*Refer to Figures 3.14 and 3.15.*   ††*Refer to Section 3.3.*

Table 3.7. Material properties.

Section	Young's Modulus E (MPa)	Static Yield Strength σ_y (MPa)	Static Ultimate Strength σ_u (MPa)
PL9.5	194 755	353	433
PL6.4	195 565	323	458
L89x89x9.5	190 380	351	501
L89x89x6.4	195 640	344	499
L102x102x6.4	193 755	362	502
W250x89 (flange)	199 110	352	472
W250x89 (web)	194 090	385	481
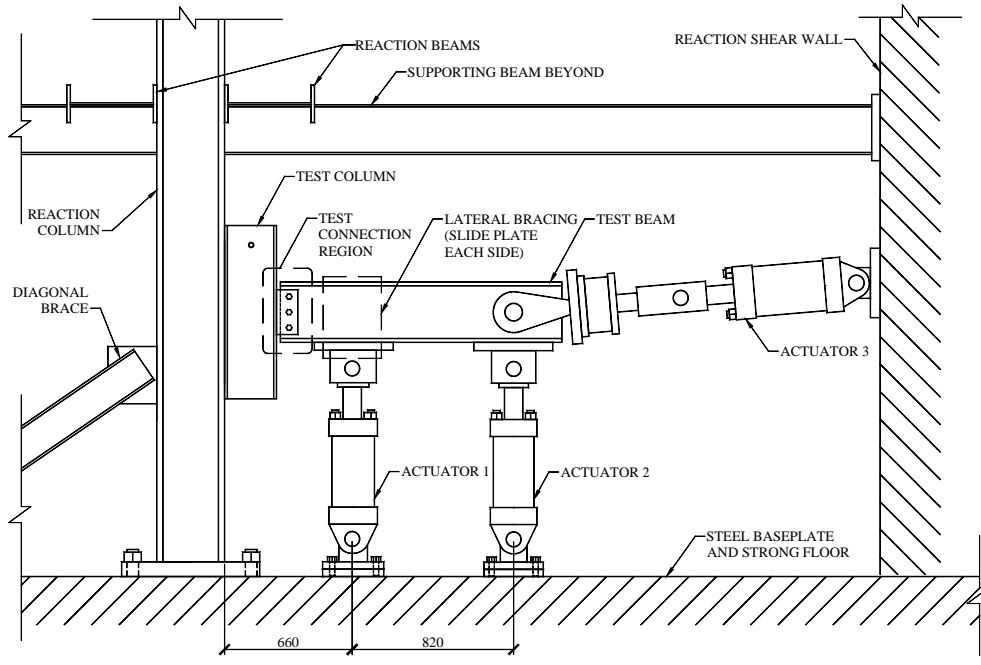
Figure 3.1. Schematic of test set-up.
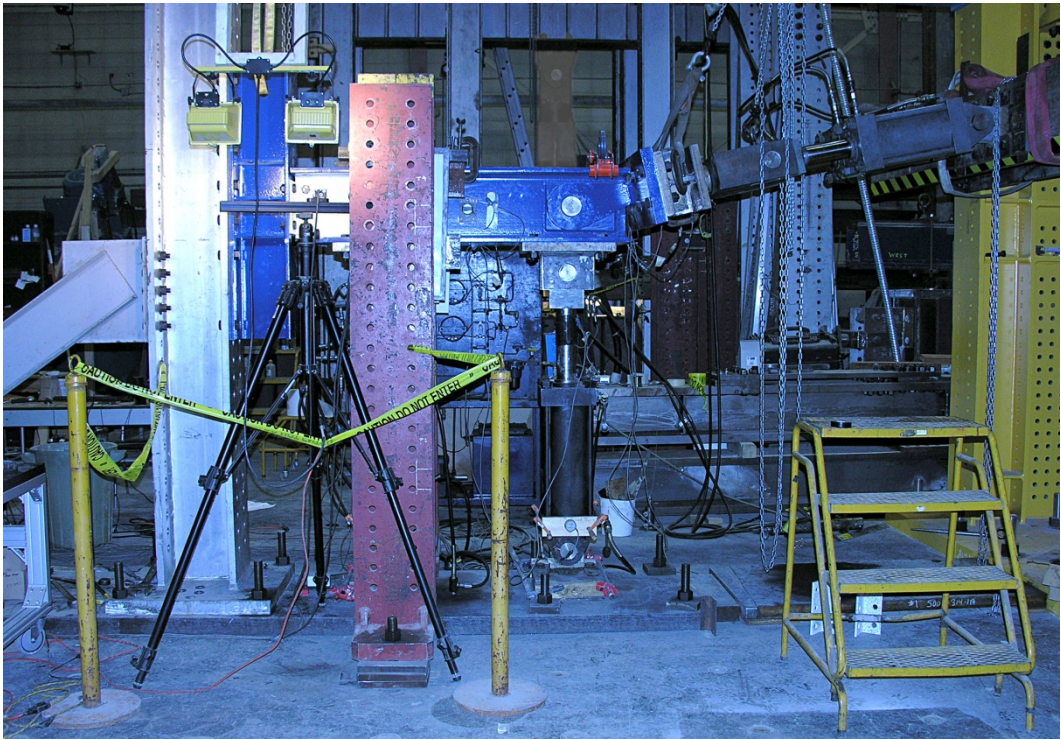
Figure 3.2. Typical test set-up.
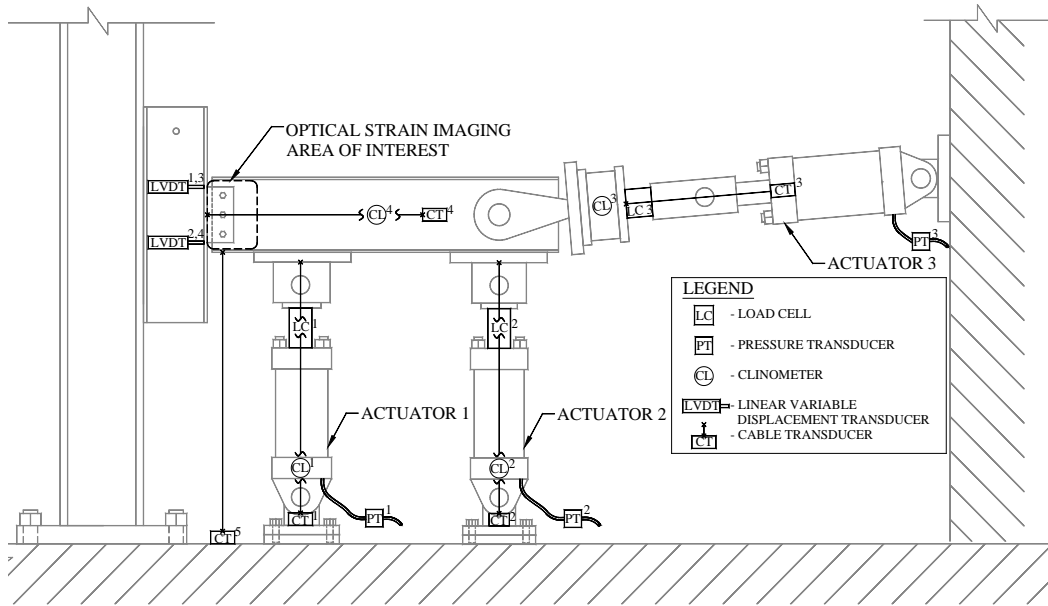
Figure 3.3. Instrumentation diagram.

(a)   (b)
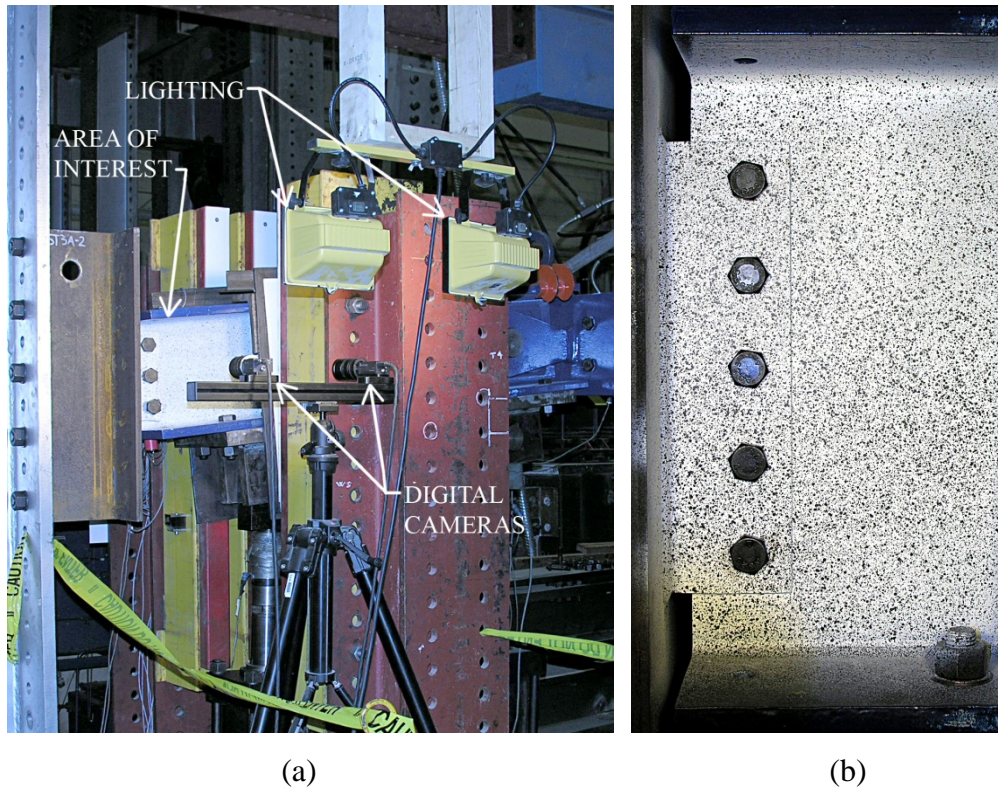
Figure 3.4. Optical strain imaging: (a) camera set-up, and (b) typical speckle pattern in area of interest.
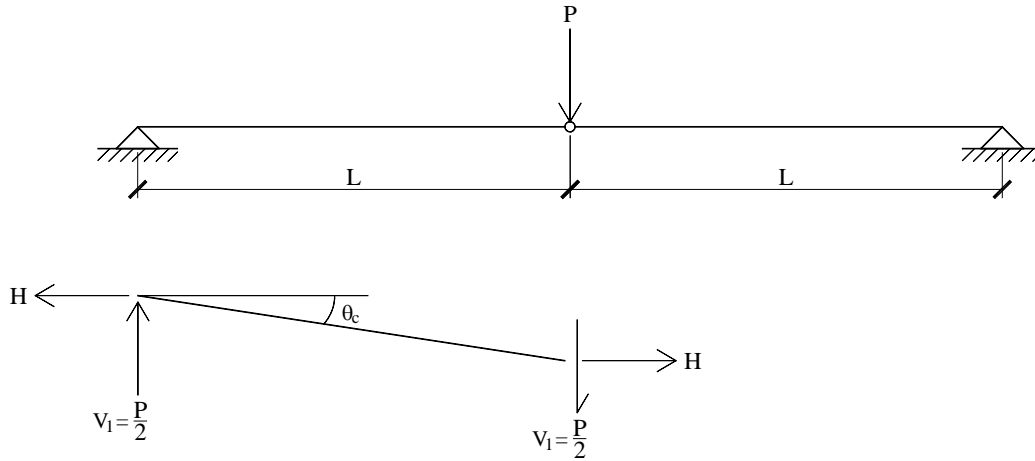
Figure 3.5. Three-hinged beam under point load (after Timoshenko, 1955).
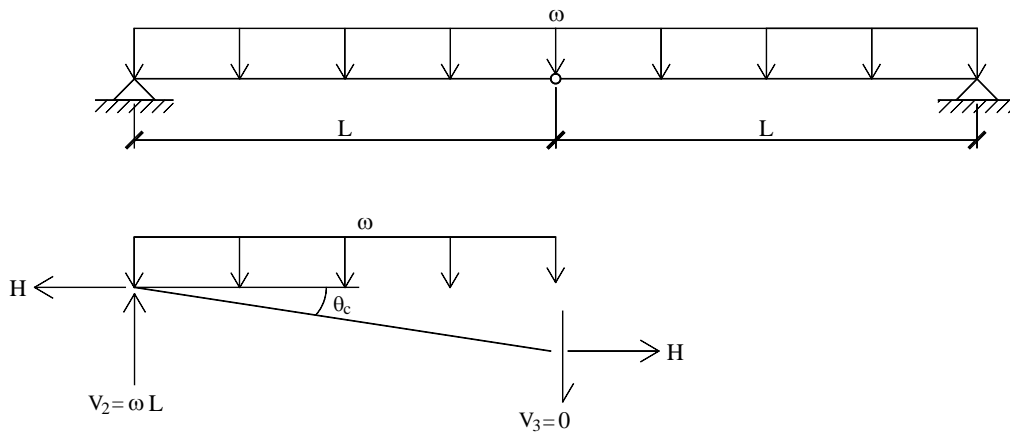
Figure 3.6. Three-hinged beam under uniformly distributed load.
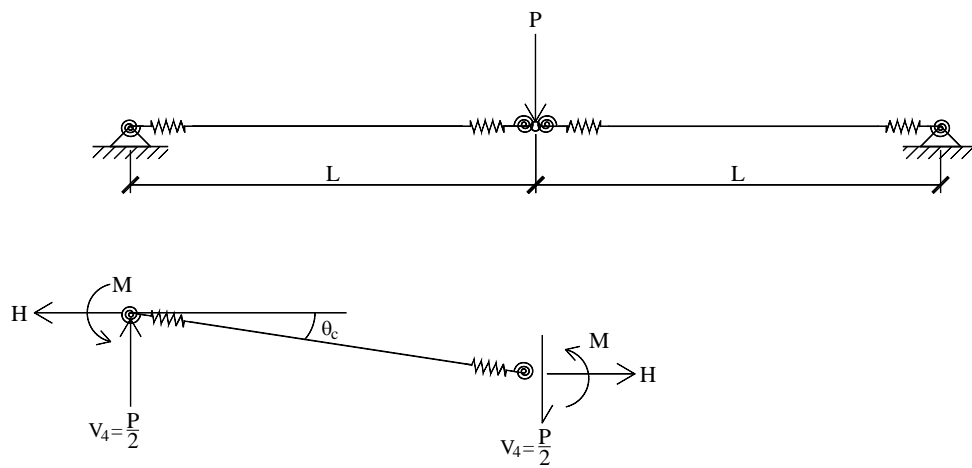
Figure 3.7. Modified three-hinged beam with connections represented by springs.
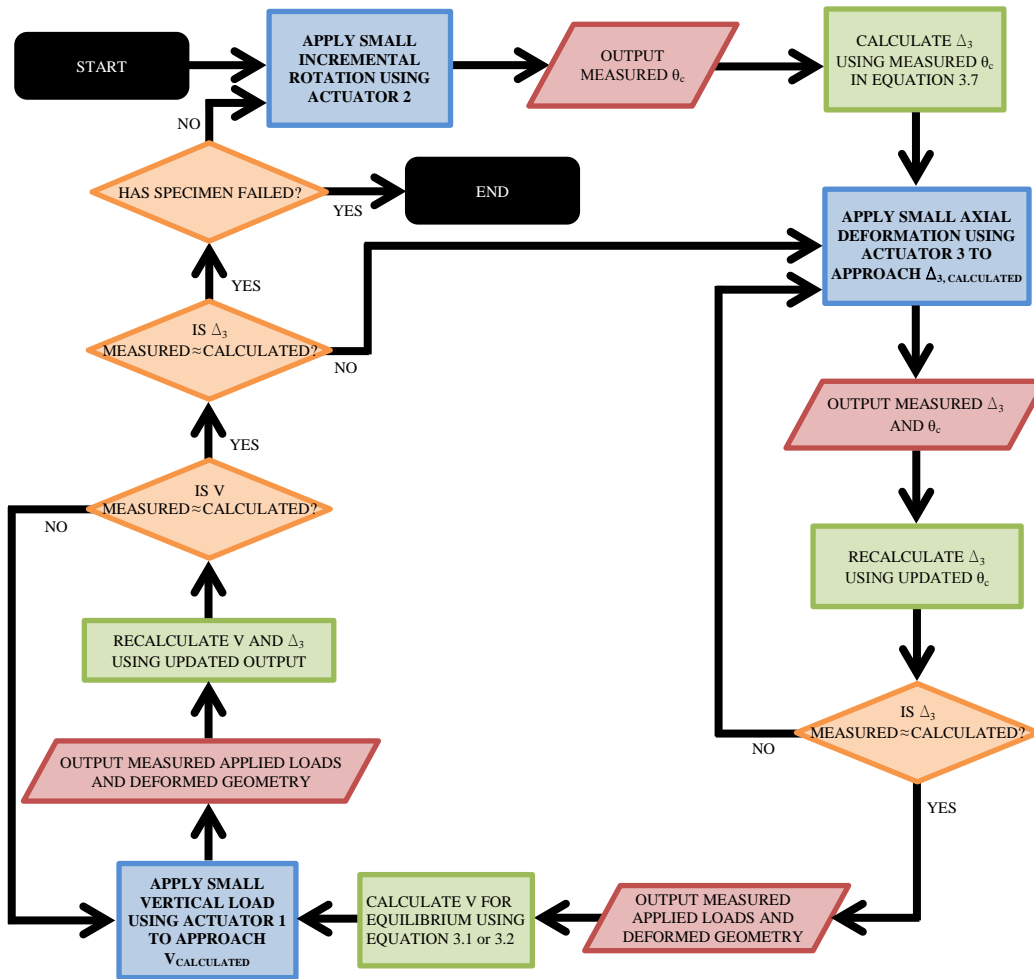
Figure 3.8. Load application flow chart.
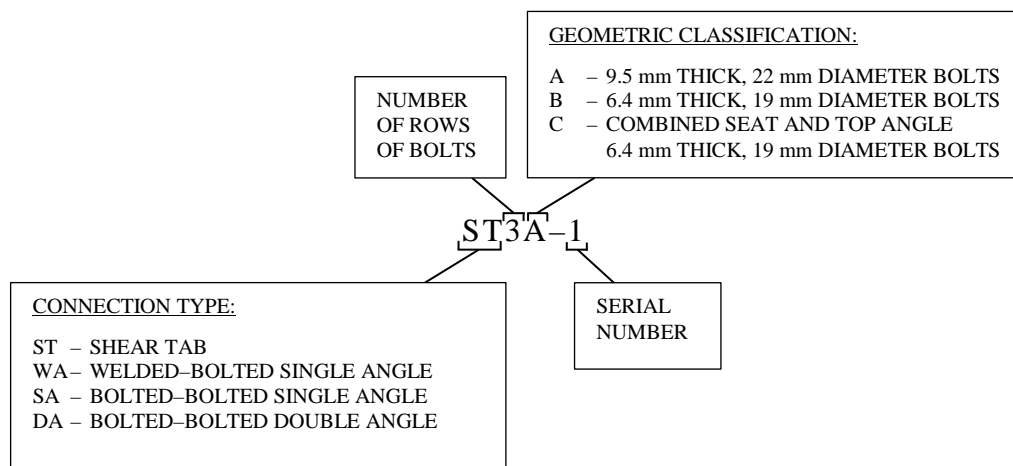
Figure 3.9. Specimen naming convention.
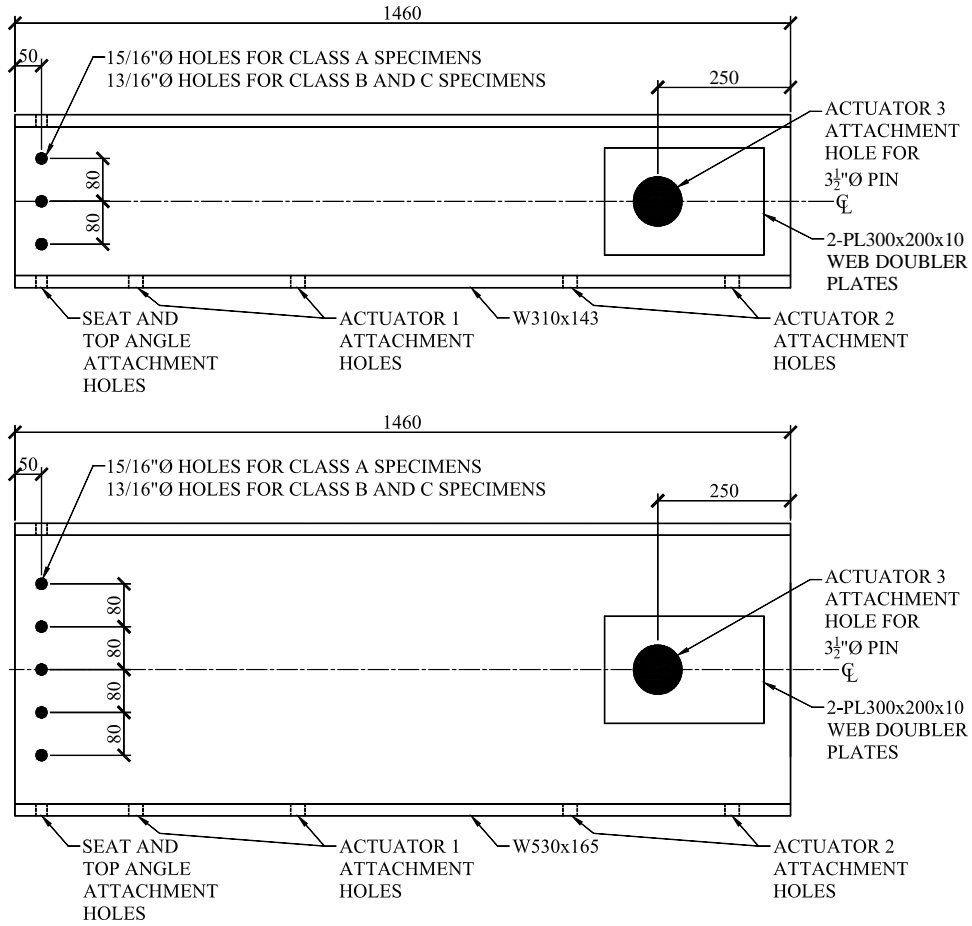
Figure 3.10. Test beam details.
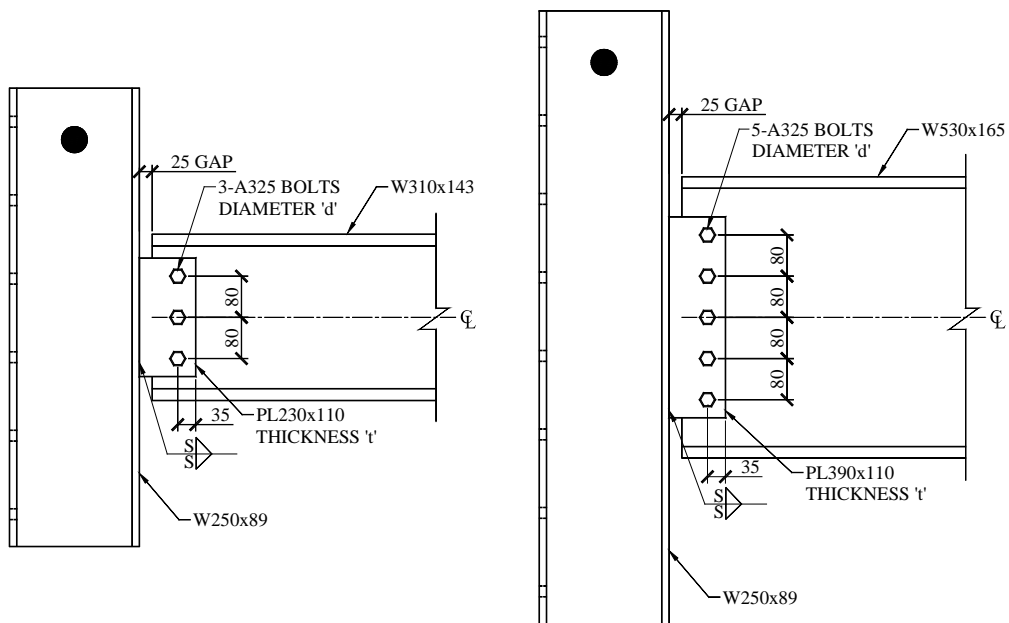
Figure 3.11. Shear tab details.

66
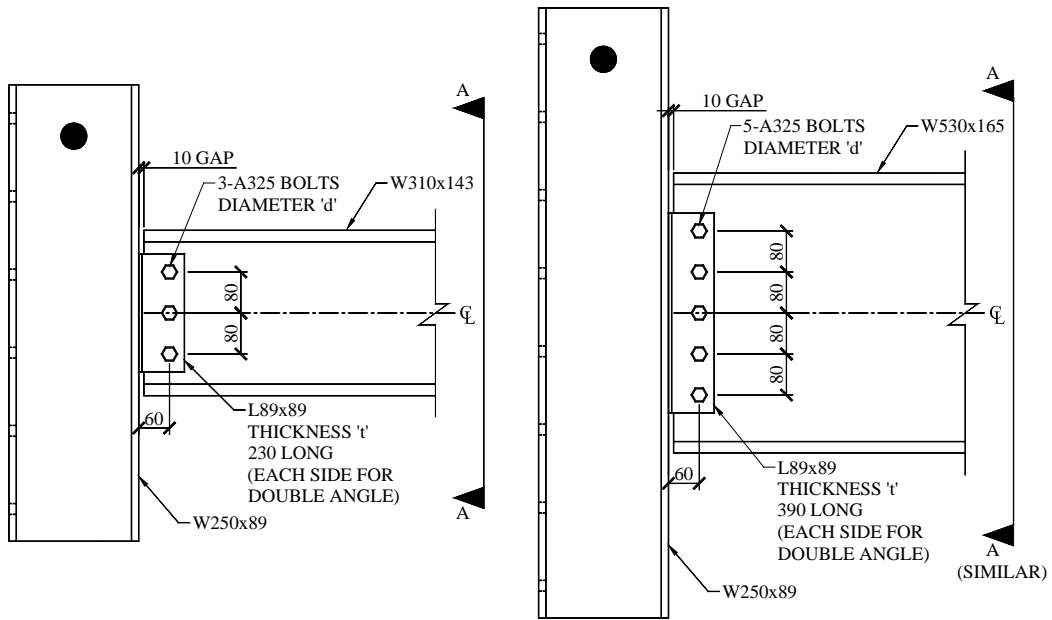
Figure 3.12. Single and double angle connection details.

(a)   (b)   (c)
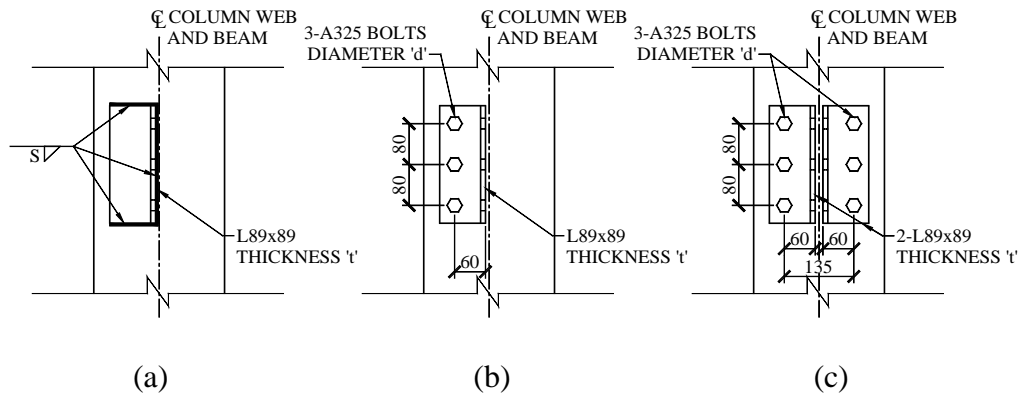
Figure 3.13. Section A-A from Figure 3.12 for: (a) welded–bolted single angle, (b) bolted–bolted single angle, and (c) bolted–bolted double angle.
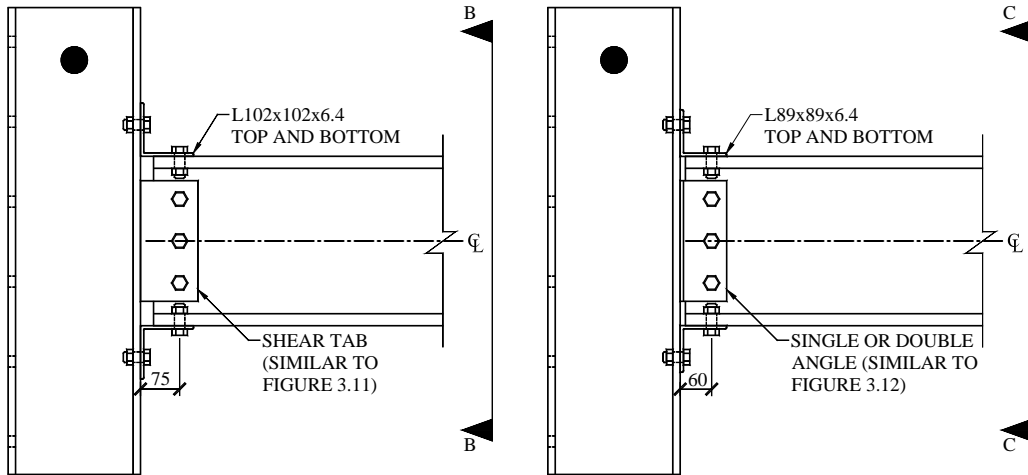
Figure 3.14. Combined seat and top angle connection details.

(a)

(b)
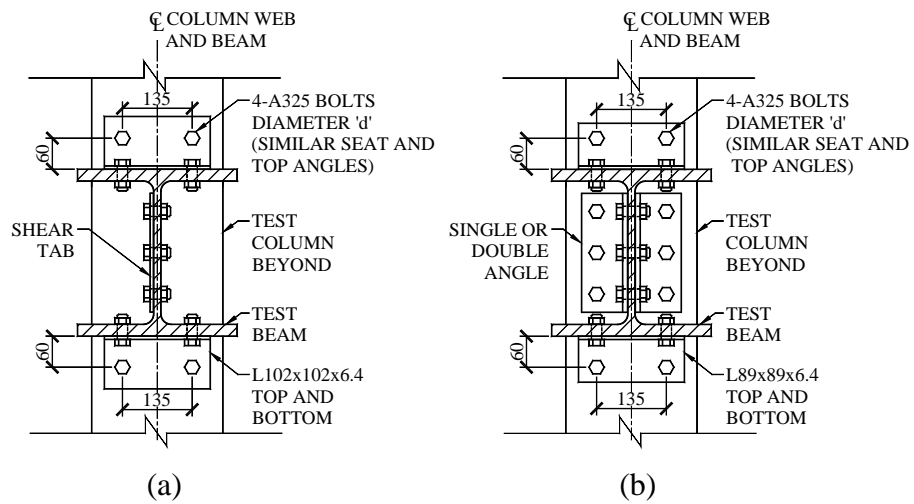
Figure 3.15. Sections from Figure 3.14 for seat and top angle combined with:

(a) shear tab (Section B-B), and (b) angle connections (Section C-C).
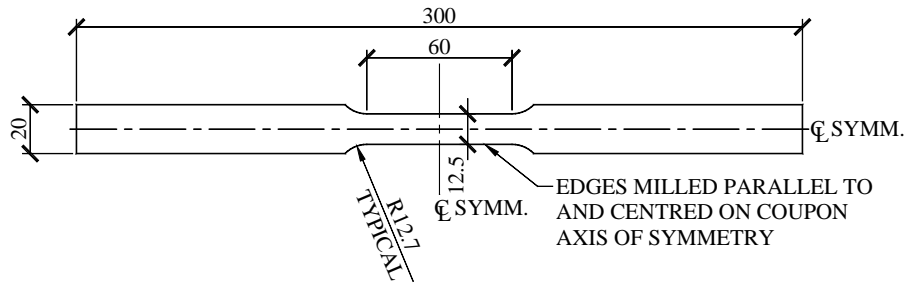
Figure 3.16. Tension coupon profile.
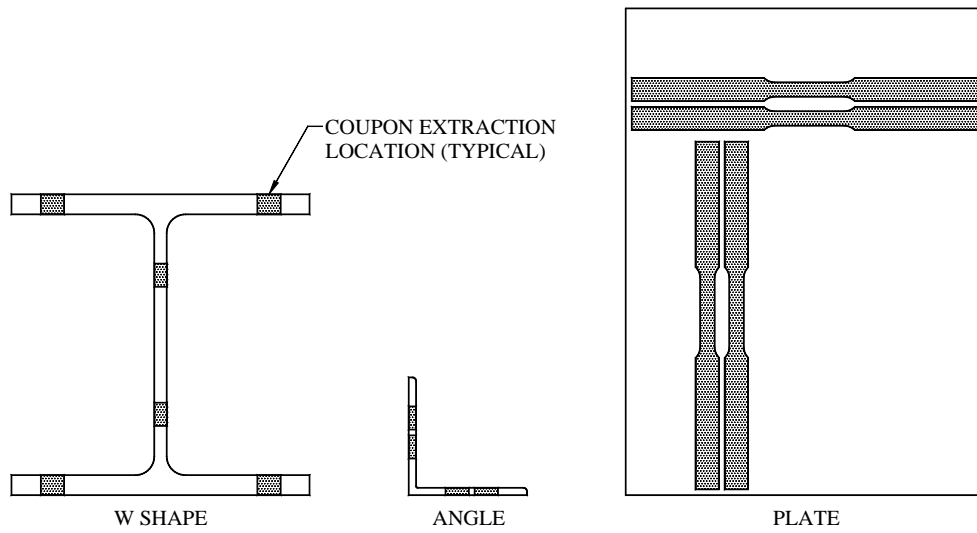
Figure 3.17. Tension coupon extraction locations.
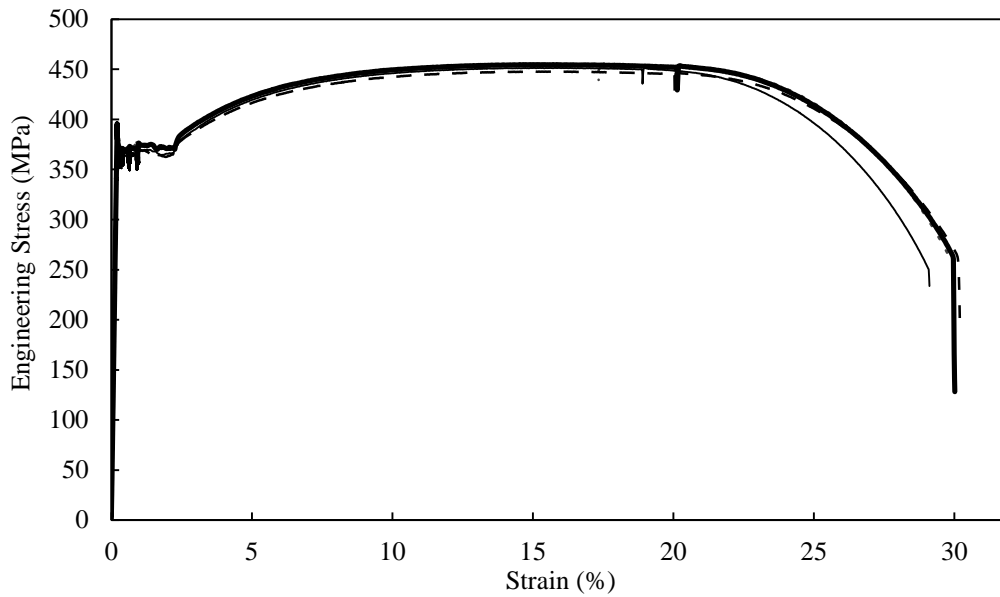
Figure 3.18. Stress–strain curves for tension coupons from 9.5 mm plate.

69

4.   TEST RESULTS

This chapter reports observations made during the laboratory tests described in Chapter 3. Qualitative observations that focus on the dominant deformation mechanisms and failure modes are presented for each connection type. Typical load versus rotation curves are included and their characteristics are discussed. The plots are annotated with observations that had significant effects on the connection behaviour, including deformation and fracture events. To facilitate the discussions, bolt locations are numbered sequentially from the top to the bottom of the connection (vertical loading was in the upward direction), beginning with the line of bolts on the beam web. For cases where the connection was also bolted to the column flange, the numbering is continued from the top to the bottom of the left side of the column flange (when facing the column from the test beam side), followed by the bolts on the right side of the column flange (where present). A complete collection of load versus rotation curves for all 45 test specimens, annotated with significant test events, form Appendix D.

Tables 4.1 through 4.5 summarize the maximum moment, loads, and deformations at the ultimate load condition, the failure mode, and the post-damage (i.e., following the ultimate load condition) response for each test. The ultimate load condition is defined as the point of maximum applied resultant force, which typically occurred immediately before the initiation of the first tear in the connection material. Where multiple failure modes were observed, they are listed in chronological order of their occurrence. Detailed discussions and analyses of the test results for each connection type are provided in Chapters 5 and 6.

4.1.   Results: Shear Tab Connections

Table 4.1 summarizes the test results for the shear tab specimens. In each shear tab test, the maximum moment reported occurred at a rotation smaller than that corresponding to the ultimate load condition.

4.1.1. Deformation Mechanism

Figure 4.1 illustrates the typical progression of deformation and failure observed during the shear tab tests. Extensive local yielding of the plate was visible at bolt bearing locations prior to tear initiation. This "plate bulging" mechanism was principally responsible for the overall ductility observed in the shear tab tests. The average measured total deformation at each bolt location immediately prior to tear initiation at that bolt was 35.4 mm for Series A specimens and 26.9 mm for Series B specimens.

No bearing of the top beam flange against the column flange was observed in any of the shear tab tests (all of which had an initial gap of 25 mm). While beam rotation initially caused the top flange to move towards the column, at higher rotations the axial deformation demands for the load history being considered caused this gap to increase before contact occurred.

4.1.2. Failure Modes

All shear tab specimens failed by bolt tear-out in the approximate direction of the beam axis as a result of the catenary force transferred to the plate material by bolt bearing. The first observed fracture always occurred at the extreme bolt, where axial demand was the greatest because of the applied rotation. In all cases, fracture was preceded by the extensive bearing deformations discussed in Section 4.1.1. All connection bolts were examined for damage following testing; no bolts failed and no significant permanent shear deformation was visible. Bearing deformation of the beam web was limited to less than 1 mm.

Tear initiation in the shear tab occurred by one of two modes: either along shear planes or by tensile splitting at the leading edge of the plate, as seen in Figure 4.2(a) and (b), respectively. Shear plane tears were characterised by failure surfaces approximately aligned with the direction of the resultant applied (dominantly axial) force—one extending from each of the top and bottom of the bolt hole to the edge of the plate. Tensile splitting tears were caused by the tensile strains imposed on the plate edge during bulging, and were only observed in

Series B specimens. These latter tears either connected with or were followed by the initiation of separate shear plane tears, leading to bolt tear-out. Figure 4.2(c) shows specimen ST5B-2 after the completion of the test with the bolts removed, which exposes the fracture paths of successive bolt tear-outs. The progression of failure at each successive bolt from bottom to top, caused by the increasing rotation and axial demand throughout the test, is termed "button-popping" herein.

4.1.3. Load Development Characteristics

Figure 4.3 shows the load development for specimen ST5A-1. The general shapes of the plots of vertical load, horizontal load, and moment are typical of the nine shear tab tests. Figure 4.4 shows photographs of specimen ST5A-1 at three points during the test: undeformed, extreme bolt (bolt 5) tear-out, and maximum vertical load (which was attained after damage had occurred at the extreme bolt).

The horizontal load reached a maximum immediately before the first tear initiated in the plate at the extreme bolt, and then decreased in a stepwise manner as failure in the plate occurred at successive bolt locations, as seen in Figure 4.3. Applied vertical load did not decrease in this same way after failure was initiated at the extreme bolt. Although the connection had already sustained damage at this stage, the increased rotation caused the catenary forces in the system to become more efficient at carrying load in the vertical direction. Thus, in some shear tab tests (including specimen ST5A-1, shown in Figure 4.3), the maximum vertical load was reached after rupture had occurred at the extreme bolt.

Shear tabs displayed a relatively high rotational stiffness at low rotations. Maximum moments were recorded shortly after significant catenary forces began to develop. Catenary tension eventually dominated the axial stresses in the connection, effectively decreasing the moment to zero. Following the tear-out of the lower bolts, the moment measured about a point at mid-height of the connection became negative, as the axial force was resisted at the undamaged bolt locations above mid-height. The resulting negative moment would be negligibly small if included in the calculation of the target vertical load (according to

Equation 3.4 or 3.5) in all cases where it was observed. The moment becomes positive (although still negligibly small) if it is calculated about the centre of the undamaged bolt group.

4.2.   Results: Welded–Bolted Single Angle Connections

Single angle connections that were welded to the column and bolted to the beam behaved similarly to shear tab connections. The behaviour of both connection types can be considered as the behaviour of a single plate (or angle leg) that is rigidly connected by a weld to a perpendicular column flange. Since the dominant deformation mechanism and failure mode in these connections were away from the weld, the presence of the angle leg welded to the column did not affect behaviour.

The horizontal edge distances (from the centre of the bolt hole to the edge of the plate) for welded–bolted single angle specimens were shorter than for the shear tab specimens in order to keep the standard gauge distance of 60 mm for the angles used, which caused them to have lower bolt tear-out resistances than shear tab specimens with otherwise similar geometry.

Table 4.2 summarizes the results for each welded–bolted single angle specimen.

4.2.1. Deformation Mechanism

Similar to the shear tab specimens, the dominant deformation mechanism was plate bulging (refer to Figure 4.1). The average measured total deformation at each bolt location immediately prior to tear initiation at that bolt was 21.3 mm for Series A specimens, and 18.6 mm for Series B specimens. Bearing of the top beam flange against the column was not observed for any of the welded–bolted single angle tests (all of which had an initial gap of 10 mm).

4.2.2. Failure Mode

The governing failure mode was bolt tear-out (refer to Figure 4.2) for all welded–bolted single angle specimens. Although tear initiation by tensile splitting was not

observed for any of the specimens tested, it is expected that certain connection geometries could cause this phenomenon to occur. All connection bolts were examined for damage following testing; no bolts failed and no significant permanent shear deformation was visible. Bearing deformation of the beam web was limited to less than 1 mm.

4.2.3. Load Development Characteristics

Figure 4.5 shows the load development of specimen WA3A-2. The characteristics of this curve are representative of the welded–bolted single angle test results, and are similar to those discussed for shear tab tests in Section 4.1.3. Figure 4.6 shows photographs of specimen WA3A-2 at three points during the test: undeformed, extreme bolt (bolt 3) tear-out, and maximum vertical load (which was attained after damage had occurred at the extreme bolt).

4.3.   Results: Bolted–Bolted Single Angle Connections

Table 4.3 summarizes the test results for each bolted–bolted single angle specimen. Compressive arching action (which is discussed in Section 4.3.1.1) occurred during the early stages of the tests. The resulting local maximum moment during arching action is presented in the table, as well as the maximum moment developed following the onset of tensile catenary forces. Since the compressive forces and coincident moments developed were well below the connection capacity, they are not considered to have influenced the ultimate failure mode or loads.

4.3.1. Deformation Mechanism

Single angle connections that were bolted to the column exhibited behaviour that was significantly different from the welded case presented in Section 4.2. Because the angle was not connected at the heel, a different mechanism dominated deformations in the axial direction of the beam. The application of moment and tension caused the angle to form plastic hinges near the bolt lines and the angle heel. Figure 4.7 shows the development of this mechanism under combined moment, shear, and tension. During the bending-dominant stage of each test, the

74

connection tended to rotate about a point near the top of the angle, as a portion of the angle remained in contact with the column flange. At later stages, the increased axial elongation demand caused the entire length of the angle heel to pull away from the column surface. This "unfolding" mechanism gave these connections significantly lower axial and rotational stiffnesses and higher ultimate rotation values than shear tabs and welded–bolted single angles with similar overall geometries. The measured displacement of the extreme bolt connected to the beam web prior to tear initiation was between 35 and 60 mm for bolted–bolted single angle specimens. Plastic hinges typically formed first at locations 1 and 3 (shown in Figure 4.7), and in some Series A specimens, were the only hinge locations evident prior to failure.

A limited amount of bolt bearing deformation (as discussed in Section 4.1.1) was visible on the angle leg connected to the beam web. However, this mechanism never progressed to a bolt tear-out failure mode. Bearing deformation at the extreme bolt was measured to be less than 5 mm for all Series A specimens and less than 3 mm for all Series B specimens—a relatively small contribution to the overall ductility when compared to the displacements attributed to the angle unfolding mechanism.

Bearing of the top beam flange against the column was not observed for any of the bolted–bolted single angle tests (all of which had an initial gap of 10 mm). While beam rotation initially caused the top flange to move towards the column, at higher rotations the axial deformation demands for the load history being considered caused this gap to increase before contact occurred.

4.3.1.1. Compressive Arching Action

Compressive axial forces were recorded at low rotations in the bolted–bolted single angle tests. This resulted from the presence of a vertical eccentricity between the connection's instantaneous centre of rotation (if horizontally unrestrained) and the centreline of the test beam caused by a significantly higher stiffness in the compressive direction than in the tensile direction (which does not

occur when the element bolted to the beam web is welded directly to the column, as was the case for shear tab and welded–bolted single angle connections). The derivation of Equation 3.7 includes the assumption that the connections rotate about their mid-height. However, at early stages of testing (during the bending-dominant phase depicted in Figure 4.7), bolted–bolted single angle connections tended to rotate about a point near the top of the angle heel. In some cases, this caused the centreline of the connection to be pried away from the column flange at a rate greater than the development of calculated axial elongation demand, resulting in a compressive reaction.

The test set-up used a three-pinned arrangement for Actuator 3, which limited the level of axial compressive force that could be developed dependably during the tests. Although measurable compressive forces were achieved by locking the displacement of the actuator and maintaining alignment between the pins, the test specimens were not actively loaded in compression. Thus, the full compressive reactions required to restrain the axial movement of the connections during arching action were not achieved. The compressive axial forces developed at low rotations during the tests are not considered to be an accurate representation of the equilibrium state in a column removal scenario, and thus are not included in the results—axial forces are only reported for the range of rotations beyond which compressive arching action would have developed.

For all tests, the presence of compressive arching action was found to exist only during early stages in the loading history; tensile demands invariably dominated behaviour and governed failure as the large rotations and catenary action associated with column removal were developed. It is expected that the presence of compressive arching action had a negligible effect on the performance of the connections reported herein.

Further discussion of the phenomenon of compressive arching action following column removal—including details of its cause, analysis, and implications—is included in Chapter 6.

4.3.1.2. Unstiffened Test Column

The 67.5 mm horizontal eccentricity between the column web centreline (where the horizontal force was effectively resisted by the column) and the line of bolts connecting the single angle to the column flange (where the horizontal force was applied to the column) resulted in a torque in the column. Two bolted–bolted single angle tests were conducted using unstiffened test columns (specimens SA3B-5 and SA5B-4). Figure 4.8(a) shows the deformation mechanism observed in the unstiffened column. Deformation for the single angle case was dominated by bending of the 10.7 mm thick column web, which caused the column flange to rotate. The bending of the 17.3 mm thick flange connected to the angle, (acting as a cantilever extending from the column web) also contributed to the total deformation, but was negligible compared to the bending of the thinner web.

Although the flange displacement (shown as $\Delta_{\text{COLUMN FLANGE}}$ in Figure 4.8) decreased the axial displacement demand on the angle (shown as $\Delta_{\text{CONNECTION}}$), the inclined flange also increased the angle through which the plastic hinges needed to rotate to accommodate axial displacement. The two counteractive effects were approximately balanced, as the specimens tested using unstiffened columns failed at beam rotations and loads similar to those with similar geometries tested on stiffened columns. The maximum flange displacement at the column bolt line for specimen SA3B-5 was 3.0 mm, and for specimen SA5B-4 was 3.8 mm (compared to a total centreline axial displacement of approximately 37 mm for both specimens). Since these displacements are mainly attributed to web bending in the tested stub column, they are expected to be much lower in a continuous column, where flange bending (as described for double angles in Section 4.4.1.2) would be expected to dominate over the effects of the applied column torque.

4.3.2. Failure Modes

All angle connections failed by the propagation of a tear that formed at the bottom of the angle. Tears developed along one of the plastic hinges that formed due to

the unfolding deformation mechanism shown in Figure 4.7, either near the angle heel (as shown in Figure 4.9(a)) or on the beam web side of the line of column bolts (as shown in Figure 4.9(b)). The ensuing upward tear propagation, caused by the increasing rotational and axial demand throughout the test, is termed "unzipping" (versus "button-popping", which is discussed in Section 4.1.2 for shear tab connections).

Tearing of the gross section near the angle heel was more commonly observed in Series A specimens than in Series B specimens. These tears were found to be unstable; that is, any increase in rotation caused the tear to propagate and the applied load to decrease. This failure mode occasionally developed suddenly, with immediate tear propagation across the full depth of the angle accompanied by a loud noise, resulting in complete and brittle connection fracture. Tears formed at the hinge on the beam side of the angle heel (hinge 3 in Figure 4.7) in all specimens where the failure mode was observed except for SA5A-1, which failed along hinge 2.

Tears that formed along the column bolt line (more commonly observed in Series B specimens) typically initiated at the column bolt hole locations, as shown in Figure 4.9(c). These tears propagated along jagged paths between bolts, but were arrested when they reached each subsequent bolt hole, which allowed the connections to establish new, stable load paths.

All connection bolts were examined for damage following testing; no bolts failed and no significant permanent shear deformation was visible. Bearing deformation of the beam web was limited to less than 1 mm.

4.3.3. Load Development Characteristics

This section discusses the typical load versus rotation curves for each of the two failure modes observed to govern the behaviour of bolted–bolted single angle connections: failure by tearing near the angle heel, and tearing near the column bolt line.

4.3.3.1. Failure by Tearing near the Angle Heel

Figure 4.10 shows the load development for specimen SA5A-1. The general shapes of the plots of vertical load, horizontal load, and moment are typical of the bolted–bolted single angle tests that failed along the plastic hinge near the angle heel. Figure 4.11 shows photographs of this specimen at three points during the test: undeformed, tear initiation at the angle heel, and unstable tear propagation. For specimen SA5A-1, 0.14 mm excess axial elongation applied early in the test may have prevented the development of compressive arching action at small rotations, which was observed for all other bolted–bolted single angle tests.

Horizontal load reached a maximum immediately before a tear was initiated on the front surface of the angle at the bottom of the plastic hinge that had formed near the angle heel. After a small increase in rotation, the surface tear became a through-thickness tear that propagated upwards. This stage was characterized by the continuous degradation of horizontal load, vertical load, and moment as any additional demand caused the progression of unzipping along the angle heel.

The applied moment recorded for bolted–bolted single angle connections displayed two local maxima (the minor peak in Figure 4.10 at 0.006 radians of rotation is neglected)—one at low rotation and horizontal force, and a second prior to damage initiation. At low rotations (during the bending-dominant phase shown in Figure 4.7), the plastic hinges associated with the unfolding mechanism were only developed along a partial depth of the connection. As rotation was increased, the applied axial elongation led to the development of tensile axial stresses that decreased the total moment in the connection, similar to the behaviour observed in the shear tab connection specimens. However, at the instant that the full depth of the angle heel separated from the column flange, the moment began to increase again. This corresponds to the tension-dominant phase shown in Figure 4.7, where the plastic hinges have developed across the full depth of the angle; the higher rotational stiffness observed at this stage is primarily attributed to the increasing alignment between the resultant force and the unfolding angle.

4.3.3.2. Failure by Tearing near the Column Bolt Line

Figure 4.12 shows the load development for specimen SA3B-2. The general shapes of the plots of vertical load, horizontal load, and moment are typical of bolted–bolted single angle tests that failed along the plastic hinge near the column bolt line. Figure 4.13 shows photographs of this specimen at three points during in the test: undeformed, tear initiation at the extreme column bolt (bolt 6) location, and the propagation of a jagged tear across the full depth of the angle.

Compressive arching action was observed at the early stages of the test, as rotation about the top of the angle heel pried the connection centreline away from the column flange. Horizontal tension was developed at larger rotations, as the axial elongation demand exceeded the deformation caused by the prying action. Prior to the initiation of the first tear near the line of column bolts, the development of forces was similar to the cases governed by angle heel tearing.

In the test shown, tear propagation progressed upwards along a jagged path connecting the bolt holes at the column flange (as seen in Figure 4.13(c)). The maximum horizontal load was measured immediately before a tear initiated below the bottom column bolt hole. A stepwise decrease of horizontal load was observed as tears formed between subsequent bolt holes. The residual capacity of this connection after the tears were arrested at the bolt holes was sufficient to lead to the achievement of a maximum vertical load after damage was initiated.

4.4.   Results: Bolted–Bolted Double Angle Connections

Bolted–bolted double angle connections behaved similarly to bolted–bolted single angle connections, with the exception of the increased overall strength and stiffness attributed to the addition of a second connecting angle. Table 4.4 summarizes the test results for each bolted–bolted double angle specimen. For cases where compressive arching action occurred, the local maximum moments are reported during the stages of arching action and following the onset of catenary forces.

4.4.1. Deformation Mechanism

Similar to the bolted–bolted single angle specimens, deformations were dominated by the unfolding mechanism (refer to Figure 4.7), which developed symmetrically in both angles. The measured displacement of the extreme bolt connected to the beam web prior to tear initiation (in the direction of the beam axis) was between 42 and 47 mm for all bolted–bolted double angle specimens. Bearing deformations in the angles at the bolts connecting them to the beam web were less than 3 mm for all tests. Bearing of the top beam flange against the column was not observed for any of the bolted–bolted double angle tests (all of which had an initial gap of 10 mm).

4.4.1.1. Compressive Arching Action

Compressive arching action was observed at low rotations during the five bolt bolted–bolted double angle tests; however, no significant compressive arching occurred while testing the three-bolt double angle connections, which have a smaller vertical eccentricity between the their instantaneous centre of rotation (if horizontally unrestrained) and the centreline of the test beam than the five bolt connections. While arching action did develop for three bolt single angle tests with similar connection geometry, it is postulated that the addition of a second angle tends to increase the connection stiffness in tension more than in compression, resulting in decreased compressive axial deformation demands that could be accommodated by flexibility of the test set up and bolt slippage.

4.4.1.2. Unstiffened Test Column

Specimens DA3B-3 and DA5B-3 were tested using unstiffened columns. Double angle connections loaded the test columns symmetrically on each side of the column web, which prevented the flange rotation in unstiffened columns with single angle connections (shown in Figure 4.8(a)). Column deformation for the double angle case was dominated by bending of the flanges, which acted as a pair of cantilevers extending from the column web, as shown in Figure 4.8(b). The

maximum flange displacement at the column bolt lines for specimen DA3B-3 was 0.9 mm, and for specimen DA5B-3 was 1.3 mm.

4.4.2. Failure Modes

The governing failure modes for the bolted–bolted double angle specimens were similar to those discussed in Section 4.3.2 for the single angle specimens. Tearing of the net section along the plastic hinge formed on the beam-web side of the column bolt line occurred in all but one of the specimens, which failed by tearing of the gross section near the angle heel, along plastic hinge 3 in Figure 4.7. (All double angle specimens were Series B, which more commonly failed along the column bolt line in the single angle tests.) Tearing was initiated and propagated in both angles in an approximately symmetric manner, although minor inherent geometric and loading asymmetries occasionally caused the failure of one angle slightly before the other. All connection bolts were examined for damage following testing; no bolts failed and no significant permanent shear deformation was visible. Bearing deformation of the beam web was limited to less than 1 mm.

4.4.3. Load Development Characteristics

Figure 4.14 shows the load development for specimen DA3B-1. The characteristics of this curve are representative of the bolted–bolted double angle test results, and are similar to those discussed in Section 4.3.3 for bolted–bolted single angle connections. Figure 4.15 shows photographs of specimen DA3B-1 at two points during the test: tear propagation from the extreme bolt to the bottom of the angle leg, and a bottom view of the unfolded angles with a well-developed tear near the end of the test.

4.5.   Results: Combined Seat and Top Angle Connections

Table 4.5 summarizes the test results for each combined seat and top angle (Series C) specimen.

4.5.1. Deformation Mechanism

Figure 4.16 illustrates the deformation of a shear tab combined with seat and top angles under combined moment, shear, and tension. During the bending-dominant phase, the top angle remained in contact with the column flange and underwent minimal bending deformation. The seat angle, however, deformed extensively by the unfolding mechanism observed in other bolted–bolted angle connections. At this stage, a moderate amount of deformation was observed in the web connecting element, by mechanisms similar to those discussed above for specimens without the seat and top angle added. The tension-dominant phase was characterised by the separation of the top angle heel from the column flange as it began to unfold under tension. In the seat angle, deformation demands in the axial direction of the beam were so severe at the rotation levels required to develop tension in the top angle that they typically led to complete fracture of the seat angle.

4.5.1.1. Compressive Arching Action

The presence of the top angle caused the centre of rotation for the connection to shift upwards during the bending dominant phase of deformation, which increased the rate at which the connection centreline was pried away from the column at low beam rotations. Consequently, the resulting compressive arching action (discussed in Section 4.3.1.1) was more pronounced for Series C specimens than for Series B specimens with similar web connections.

4.5.2. Failure Modes

The first element to fail in all of the Series C tests except for specimen ST3C-2 was the seat angle. (Specimen ST3C-2 failed by extreme-bolt tear-out in the web connection slightly before seat angle failure.) Seat angles failed by the propagation of a tear that formed along a plastic hinge either near the angle heel (shown in Figure 4.17(a)) or on the top side of the line of column bolts (shown in Figure 4.17(b)). Tearing near the angle heel was more commonly observed in specimens with shear tab web connections, and tearing along the column bolt line was typical of bolted–bolted web angle connections (which had seat and top

angles with shorter leg lengths than those used with the shear tabs because of the smaller gap between the beam and the column flange). Tear propagation in both failure modes was often rapid due to the approximately uniform plastic hinge deformation along the entire length of the seat angle (compared to the gradient of deformation present in web angles due to the applied rotation).

Failure of the web connection was governed by the same failure modes as for the case without an added seat and top angle, which were discussed in Sections 4.1 through 4.4. In all tests, the capacity degradation caused by the failure of the seat angle and web connection was sufficient to deem the connection failed and end the test before any tearing was observed in the top angle. All connection bolts were examined for damage following testing; no bolts failed and no significant permanent shear deformation was visible. Bearing deformation of the beam web was limited to less than 1 mm.

4.5.3.   Load Development Characteristics

Figure 4.18 shows the load development for specimen ST5C-1. Figure 4.19 shows photographs of this specimen at three points during the test: maximum moment, seat angle failure, and peak post-damage response.

Connecting the beam flanges to the column resulted in the development of a much higher moment at low rotations for Series C connections than those recorded for Series B connections with identical web connections. Seat angle fracture, seen in Figure 4.19(b), led to a precipitous drop in the applied moment. This failure, however, typically occurred prior to the ultimate load condition, as the undamaged connection elements continued to develop higher catenary forces. The seat angle did not demonstrate sufficient ductility to accommodate the deformations necessary to develop ultimate forces in the other connection elements.

Following the failure of the seat angle, the characteristics of load development were similar to the unreinforced Series B case (with the exception of an increase

in capacity recognized due to the presence of the remaining top angle), as behaviour was largely controlled by the web connection.

4.6. Consistency between Target and Measured Load Histories

The nature of the load application procedure outlined in Chapter 4 requires that target values of both vertical load and axial displacement be achieved simultaneously in order to emulate the demands of a column removal scenario on the connection being tested. The precision of this iterative process depends on both operator skill and the practical limitation on the load increment that can be applied by the actuators. This section reports the level of consistency achieved between the target and measured load histories during the tests.

4.6.1. Equilibrium Condition

Vertical load was applied to meet the target value calculated using Equation 3.1 or 3.2 (depending on the selected load arrangement). The applied vertical load was typically within 2 kN of the target value at the ultimate load condition. Considering all tests, the maximum deviation between the measured and calculated loads at the ultimate load condition was 5 kN. The difference between the target and measured vertical loads was highest for bolted–bolted single angle connections as a consequence of their low rotational and axial stiffnesses.

Damage events caused sudden changes in connection resistance, which created discontinuities in the target and applied loads. Following such an event, the total applied vertical load was returned to the target value before rotation was advanced.

Instances where the vertical load target value was missed by more than 10 kN are noted on the load versus rotation curves in Appendix D. In no tests did a difference of this magnitude occur at or near the ultimate load condition.

4.6.2. Compatibility Condition

Axial elongation was applied to meet the target value calculated using Equation 3.7. The measured axial displacement was typically within 0.25 mm of the target value during the tests. Before damage initiation, the maximum recorded deviation from the target value was 1 mm for all tests (except for SA5B-4, where the target axial displacement demand was 4 mm greater than the applied displacement at an early stage in the test due to operator error, as noted in Appendix D). Following damage events that caused a severe, instantaneous decrease in connection stiffness, the maximum deviation between the measured and target displacement values was 5 mm (although agreement within 1 mm was typically maintained after damage occurred, and any discrepancy was corrected before rotation was advanced). During the compressive arching stage (when present), excess axial displacement at the centreline of the connection caused by the prying of the connection away from the column flange was between 0 and 4 mm for all tests.

4.7. Repeatability

The repeatability of test results was demonstrated by the inclusion of a replicate bolted–bolted single angle test. Specimens SA3A-2 and SA3A-4 were designed with the same nominal geometry and equivalent prescribed loading history parameters. The two tests showed similar load development characteristics, with maximum moment, vertical loads, and horizontal loads that all differed by less than 2.3 %, and the specimens failed in the same mode (tearing of the gross section along a plastic hinge near the angle heel). Failure was initiated at similar rotations (within 0.004 radians), although the fracture propagated more quickly in specimen SA3A-2 than in SA3A-4. Overall, a comparison of the results confirms that acceptable repeatability of the tests was achieved. Although no other tests were replicated, comparisons of tests within each series of geometrically similar test specimens also suggest repeatability, as recorded differences between the behaviour of tests within each series are consistent with the differences expected as a result of their varied loading histories.

Table 4.1. Summary of results: shear tab specimens.

| Specimen ID | Maximum Moment (kN·m) | Ultimate Load Condition | | | | Failure Mode[†] | Peak Post-damage Response | |
		Horizontal Load (kN)	Vertical Load (kN)	Beam Rotation (radians)	₵ Axial Displacement (mm)		Vertical Load (kN)	Beam Rotation (radians)
ST3A-1	17.8	514.2	62.2	0.115	19.9	TO	55.4	0.148
ST3A-2	16.1	505.1	124.1	0.118	21.0	TO	106.5	0.152
ST3A-3	13.2	520.6	105.9	0.101	23.1	TO	87.8	0.117
ST3B-1	9.6	331.1	65.7[*]	0.098	14.5	TS, TO	71.0	0.125
ST3B-2	12.1	335.2	58.0	0.086	16.7	TS, TO	54.9	0.100
ST5A-1	53.6	715.6	133.0[*]	0.094	17.7	TO	151.9	0.110
ST5A-2	51.1	822.4	138.6	0.083	20.7	TO	128.2	0.096
ST5B-1	48.5	471.3	74.5[*]	0.079	12.5	TO	82.2	0.107
ST5B-2	34.5	510.7	66.3[*]	0.068	13.9	TS, TO	69.4	0.083

†Failure modes: TO – Tear-out of extreme bolt

                TS – Tensile splitting at plate edge near extreme bolt

*Exceeded by post-damage vertical load

Table 4.2. Summary of results: welded–bolted single angle specimens.

Specimen ID	Maximum Moment (kN·m)	Ultimate Load Condition				Failure Mode[†]	Peak Post-damage Response	
		Horizontal Load (kN)	Vertical Load (kN)	Beam Rotation (radians)	₵ Axial Displacement (mm)		Vertical Load (kN)	Beam Rotation (radians)
WA3A-1	11.7	419.2	40.8	0.097	14.2	TO	35.9	0.117
WA3A-2	11.6	430.9	78.7*	0.089	11.9	TO	82.6	0.118
WA3A-3	14.2	492.4	74.2	0.076	13.0	TO	66.9	0.086
WA5B-1	46.5	318.3	46.8*	0.072	10.4	TO	49.3	0.112
WA5B-2	29.4	391.9	40.0*	0.051	7.8	TO	44.6	0.061

†Failure modes: TO – Tear-out of extreme bolt

*Exceeded by post-damage vertical load

Table 4.3. Summary of results: bolted–bolted single angle specimens.

Specimen ID	Maximum Moment		Ultimate Load Condition				Failure Mode†	Peak Post-damage Response	
	Arching Action (kN·m)	Catenary Action (kN·m)	Horizontal Load (kN)	Vertical Load (kN)	Beam Rotation (radians)	℄ Axial Displacement (mm)		Vertical Load (kN)	Beam Rotation (radians)
SA3A-1	11.0	12.4	328.5	55.1	0.166	41.8	TG	N/A	N/A
SA3A-2	9.9	4.9	238.9	61.9	0.129	25.1	TG	N/A	N/A
SA3A-3	10.3	9.8	349.0	94.9	0.135	41.3	TG	N/A	N/A
SA3A-4	9.3	5.0	235.1	63.3*	0.133	26.7	TG	65.9	0.148
SA3B-1	7.9	4.1	166.9	23.6	0.140	44.5	TN	21.7	0.154
SA3B-2	6.8	3.1	131.1	38.1*	0.152	35.0	TN	47.2	0.194
SA3B-3	6.9	4.1	145.8	37.9*	0.130	38.3	TN, TG	42.3	0.160
SA3B-4	8.2	3.0	153.0	25.8*	0.167	42.3	TN	26.6	0.194
SA3B-5	8.4	4.1	126.2	37.8	0.129	37.7	TG	20.5	0.139
SA5A-1	41.9	34.1	517.0	139.9	0.133	35.6	TG	N/A	N/A
SA5A-2	27.1	21.1	414.6	78.4	0.094	26.6	TG	N/A	N/A
SA5B-1	29.9	21.0	258.1	33.0	0.133	35.6	TN	30.6	0.146
SA5B-2	28.6	17.8	246.0	60.0	0.122	30.0	TN, TG	58.4	0.144
SA5B-3	25.7	12.7	240.2	52.7*	0.108	35.2	TN	53.5	0.149
SA5B-4	25.1	7.7	194.2	43.1*	0.110	36.5	TN	48.1	0.130

†Failure modes:　　TG – Tearing of gross section along plastic hinge near angle heel

TN – Tearing of net section along plastic hinge near column bolt line

*Exceeded by post-damage vertical load

Table 4.4. Summary of results: bolted–bolted double angle specimens.

Specimen ID	Maximum Moment		Ultimate Load Condition				Failure Mode[†]	Peak Post-damage Response	
	Arching Action (kN·m)	Catenary Action (kN·m)	Horizontal Load (kN)	Vertical Load (kN)	Beam Rotation (radians)	℄ Axial Displacement (mm)		Vertical Load (kN)	Beam Rotation (radians)
DA3B-1	10.5[**]	10.3	345.1	98.8	0.149	33.6	TN	89.4	0.194
DA3B-2	9.6[**]	7.4	308.1	72.0	0.123	34.3	TG	52.7	0.138
DA3B-3	10.4[**]	8.8	352.6	82.2	0.120	32.6	TN	79.0	0.152
DA5B-1	47.1	30.6	522.5	120.2[*]	0.108	23.4	TN	127.8	0.134
DA5B-2	36.2	24.6	547.8	106.2[*]	0.097	28.3	TN	108.7	0.112
DA5B-3	59.4	31.6	528.3	124.6	0.118	28.0	TN	128.3	0.133

†Failure modes: TG – Tearing of gross section along plastic hinge near angle heel

TN – Tearing of net section along plastic hinge near column bolt line

*Exceeded by post-damage vertical load

**Specimen did not develop compressive forces; value given is peak moment prior to the development of significant catenary forces

Table 4.5. Summary of results: combined seat and top angle specimens.

Specimen ID	Maximum Moment		Ultimate Load Condition				Failure Mode[†]	Peak Post-damage Response	
	Arching Action (kN·m)	Catenary Action (kN·m)	Horizontal Load (kN)	Vertical Load (kN)	Beam Rotation (radians)	℄ Axial Displacement (mm)		Vertical Load (kN)	Beam Rotation (radians)
ST3C-1	68.6	34.0	504.4	102.4	0.106	16.9	SG, TO	94.6	0.130
ST3C-2	45.0	30.2	492.2	73.5[*]	0.075	12.7	TO, SG	79.8	0.093
ST5C-1	176.8	11.7	419.9	87.9	0.104	21.7	SG, TO	87.4	0.114
ST5C-2	136.1	67.2	610.1	82.4[*]	0.067	13.5	SG, TO	85.5	0.087
SA3C-1	56.6	30.7	304.3	67.3[*]	0.115	19.9	SN, TN	78.8	0.192
SA3C-2	34.0	29.0	350.7	71.1[*]	0.100	22.6	SN, TN	73.2	0.138
SA5C-1	162.0	18.3	301.3	76.4	0.126	32.0	SN, TN	75.5	0.141
SA5C-2	128.6	61.8	393.0	80.7	0.100	30.1	SG, SN, TN	78.5	0.124
DA3C-1	59.0	34.5	435.9	122.8	0.138	28.8	SG, TG	119.5	0.152
DA3C-2	39.2	34.1	482.8	113.8[*]	0.117	31.0	SN, TN	114.8	0.127

†Failure modes: TO – Tear-out of extreme bolt

TG – Tearing of gross section along plastic hinge near angle heel

TN – Tearing of net section along plastic hinge near column bolt line

SG – Tearing of gross section along plastic hinge near seat angle heel

SN – Tearing of net section along plastic hinge near seat angle column bolt line

*Exceeded by post-damage vertical load
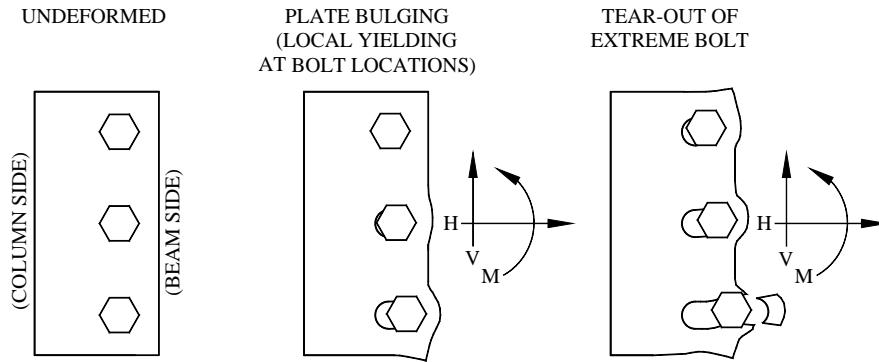
Figure 4.1. Deformation of shear tab connections under combined loading.
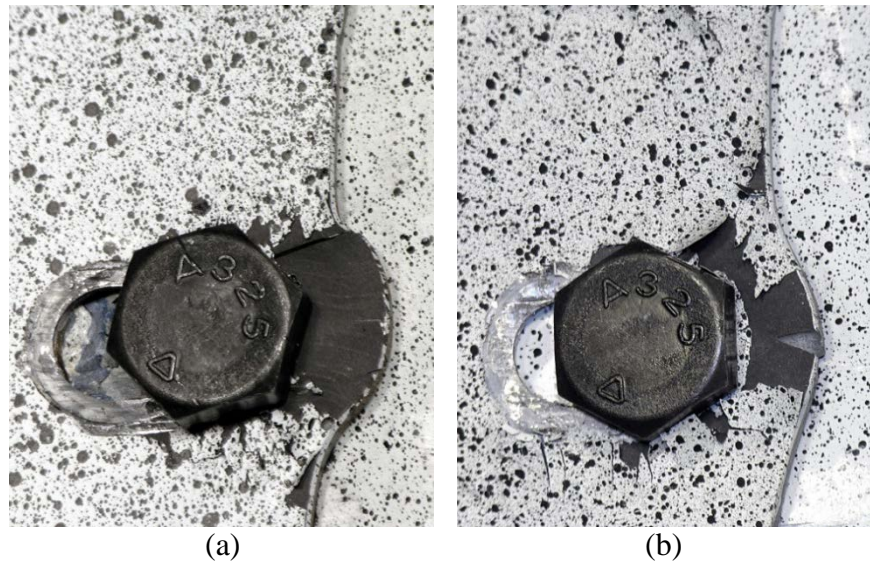
(a)

(b)

(c)

Figure 4.2. Shear tab failure modes: (a) shear plane tear, (b) tensile splitting, and (c) successive bolt tear-out ("button-popping").
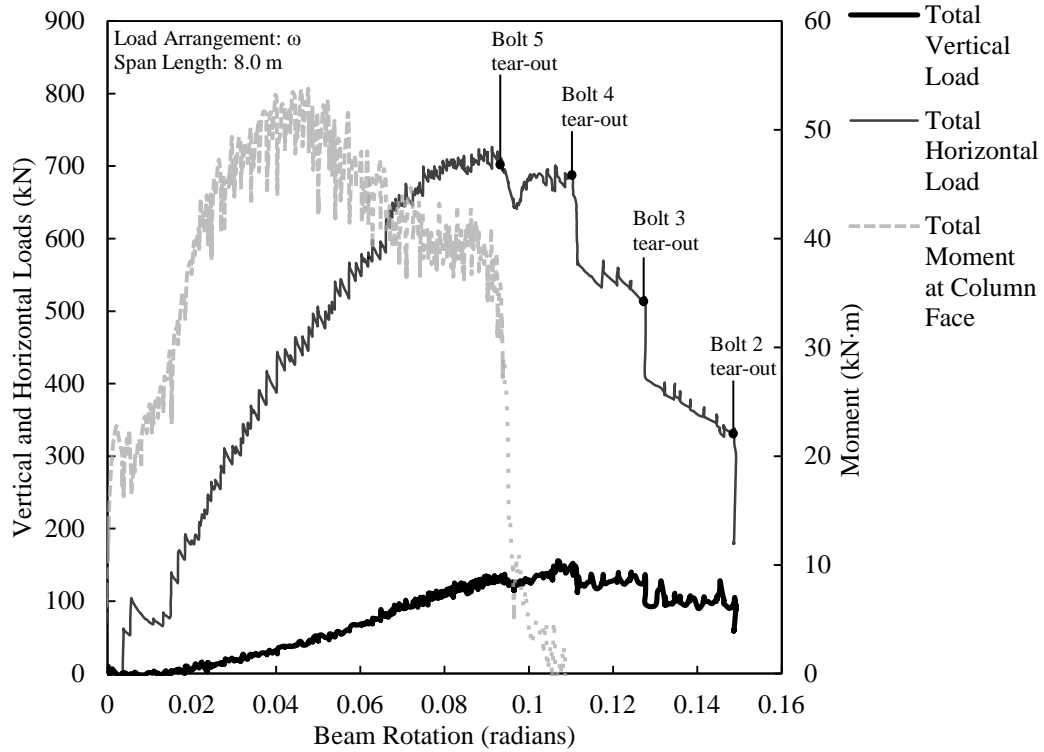
Figure 4.3. Load versus rotation for ST5A-1.

(a)   (b)   (c)
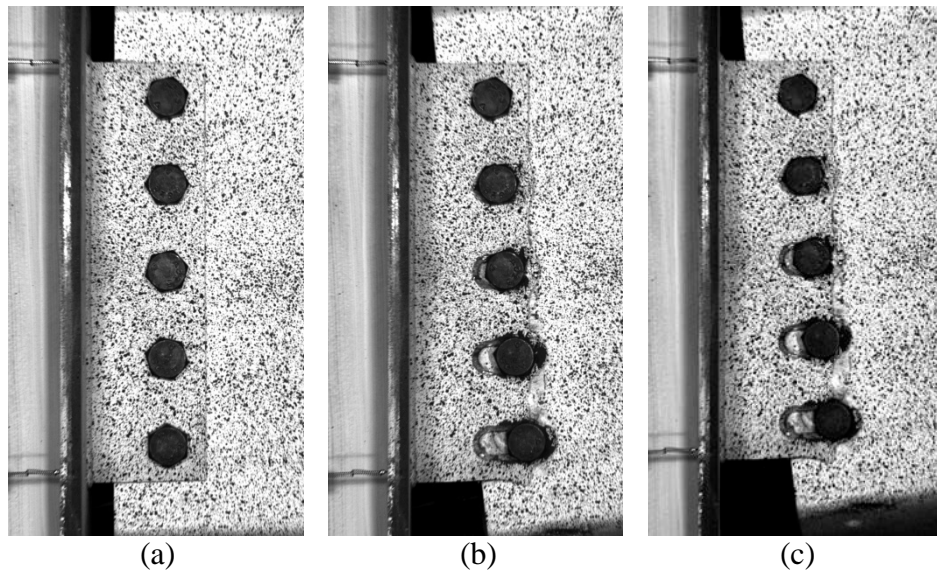
Figure 4.4. Specimen ST5A-1 at: (a) 0 radians (undeformed),

(b) 0.094 radians (extreme bolt tear-out), and (b) 0.110 radians (bolt 4

tear-out, peak post-damage response).
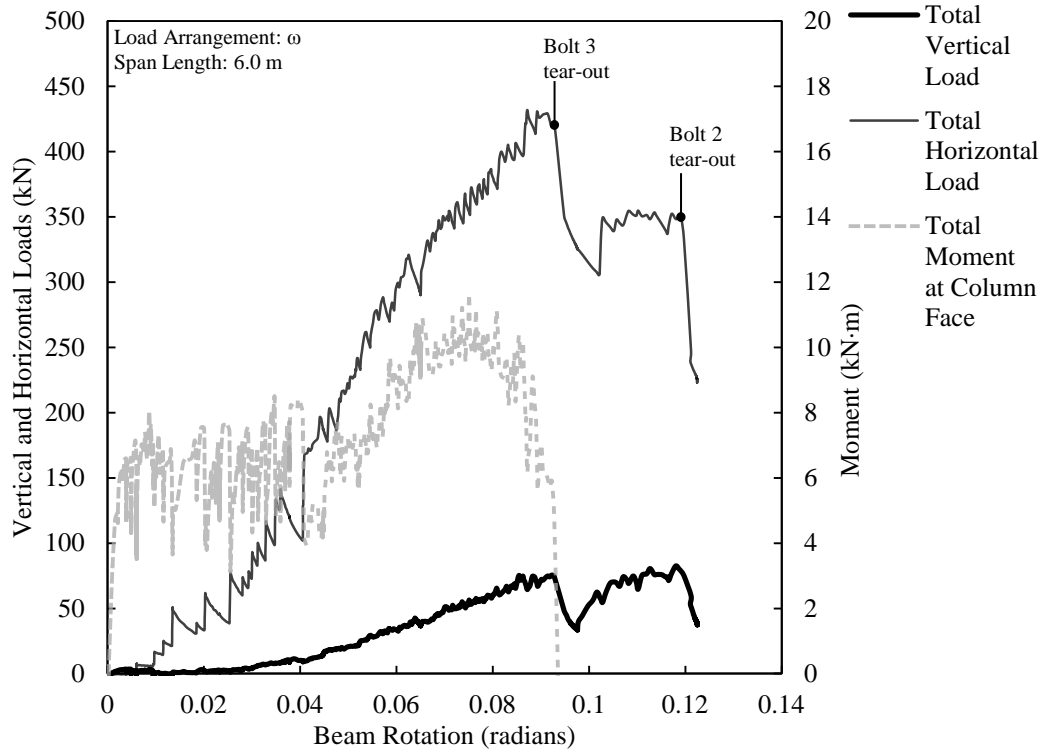
Figure 4.5. Load versus rotation for WA3A-2.

| (a) | (b) | (c) |
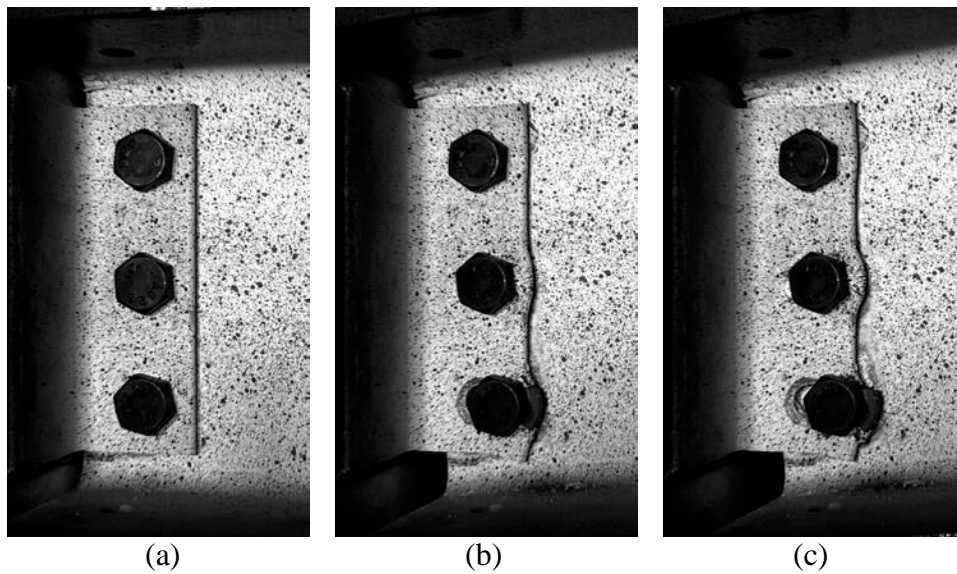
**Figure 4.6. Specimen WA3A-2 at: (a) 0 radians (undeformed),
(b) 0.089 radians (extreme bolt tear-out), and (c) 0.118 radians (bolt 2
tear-out, peak post-damage response).**

94

UNDEFORMED   BENDING DOMINANT   TENSION DOMINANT

TOP VIEW

SIDE VIEW

(COLUMN SIDE)   (BEAM SIDE)

BOTTOM VIEW

● PLASTIC HINGE
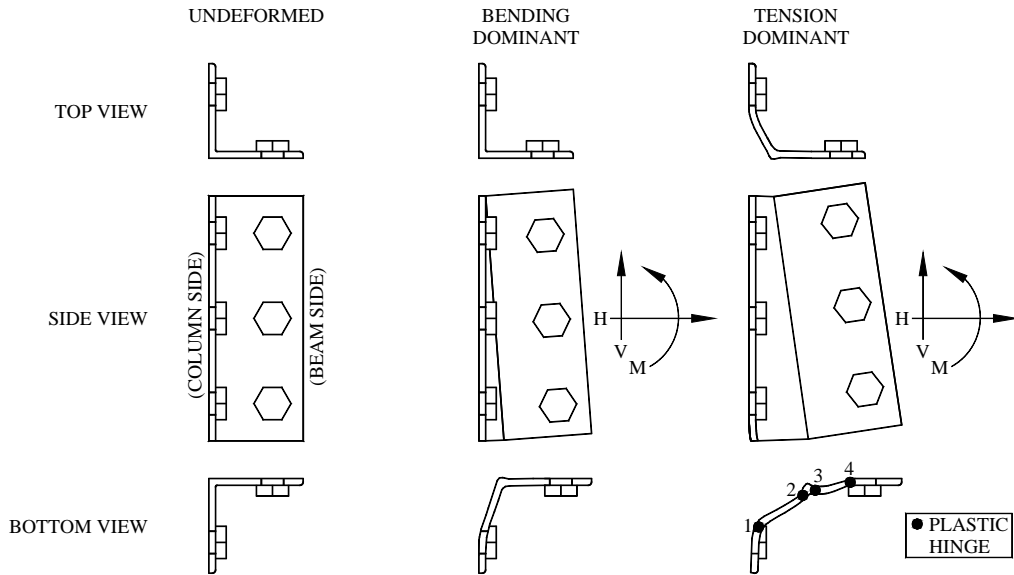
Figure 4.7. Deformation of bolted–bolted angle connections under combined loading.

INITIAL COLUMN FLANGE POSITION

BEAM WEB (FLANGES NOT SHOWN FOR CLARITY)

$\Delta_{\text{COLUMN FLANGE}}$

$\Delta_{\text{CONNECTION}}$

(a)

(b)
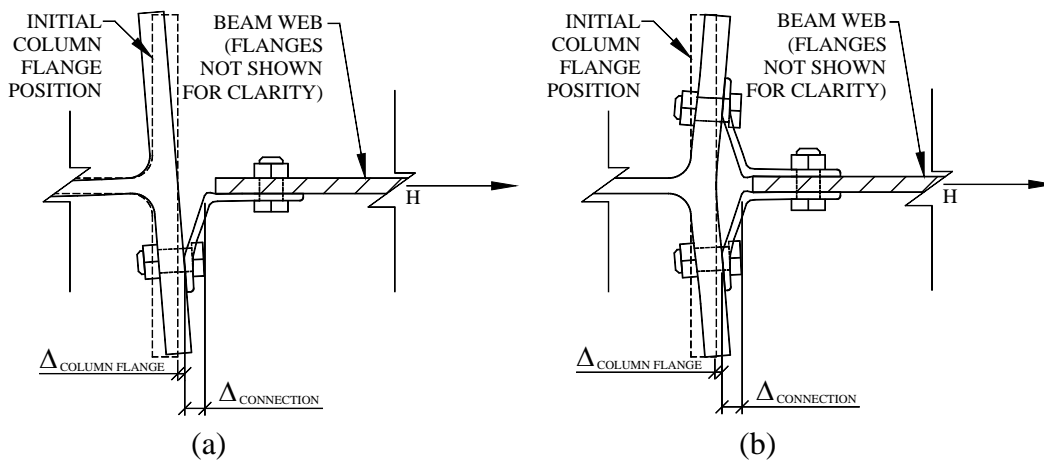
Figure 4.8. Deformation of unstiffened column for: (a) bolted–bolted single angle connection, and (b) bolted–bolted double angle connection.

95
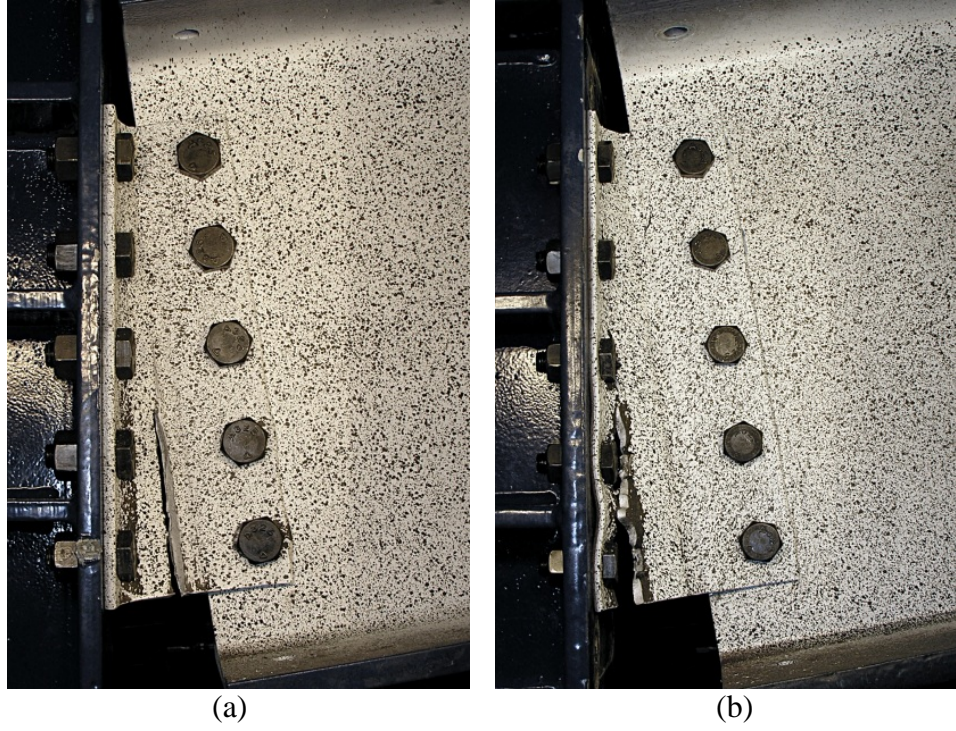
Figure 4.9. Bolted–bolted angle failure modes: (a) tearing along plastic hinge near angle heel, (b) tearing along plastic hinge near column bolt line, and (c) tear initiation at column bolt hole locations (angle connected to far side of beam web).
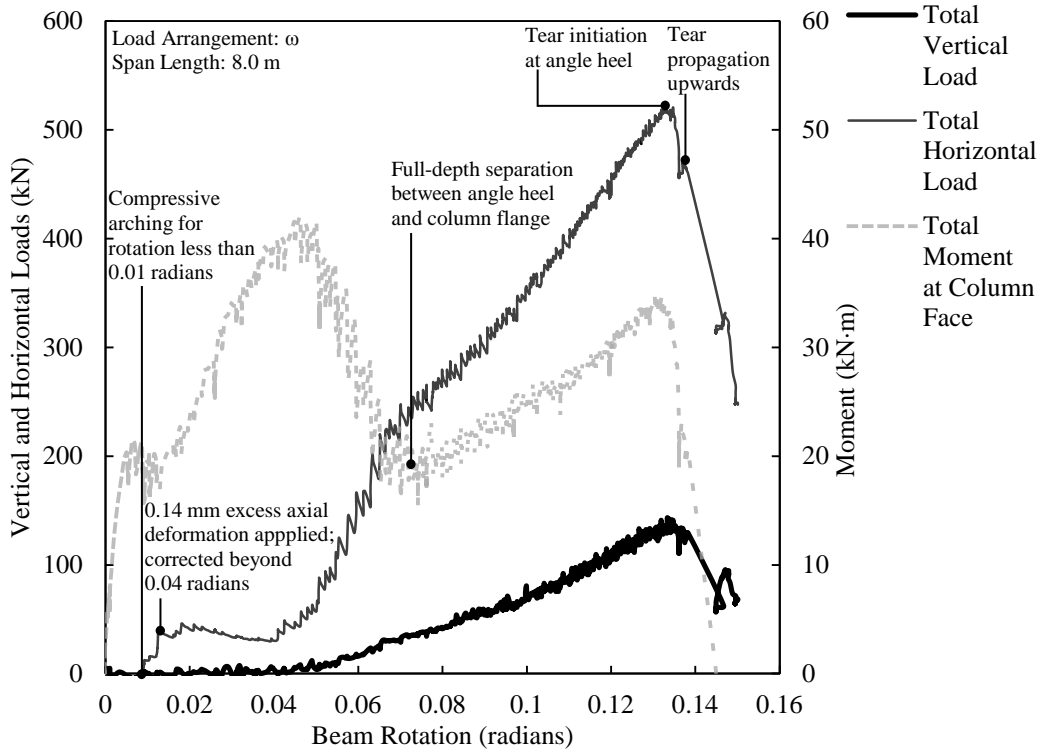
Figure 4.10. Load versus rotation for SA5A-1.
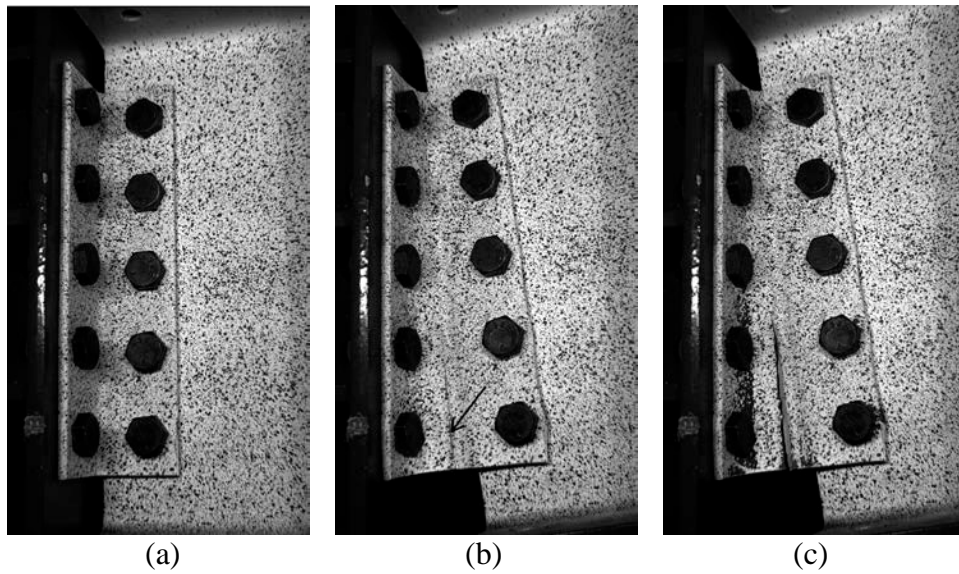
Figure 4.11. Specimen SA5A-1 at: (a) 0 radians (undeformed),

(b) 0.133 radians (tear initiation at angle heel), and (c) 0.147 radians (tear

propagation upwards).

97
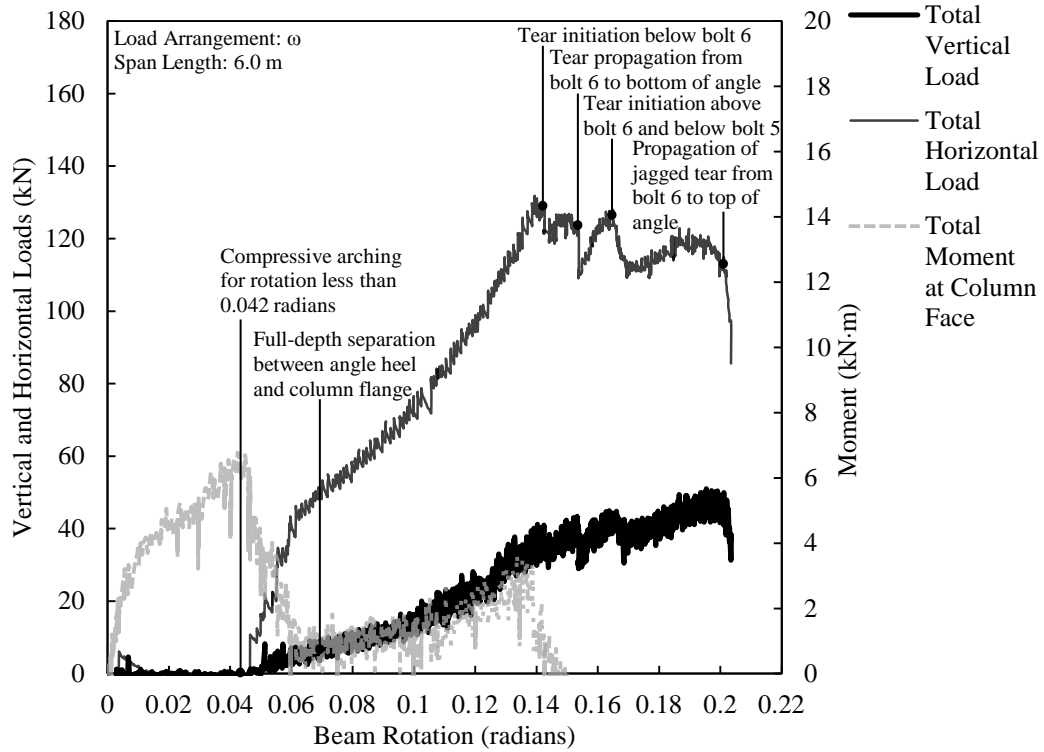
Figure 4.12. Load versus rotation for SA3B-2.

| (a) | (b) | (c) |
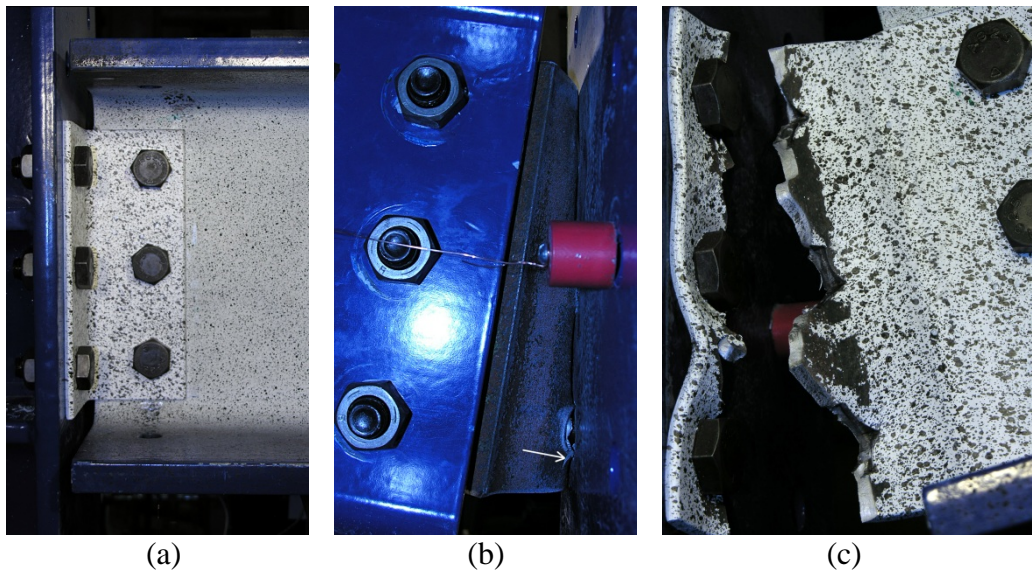
Figure 4.13. Specimen SA3B-2 at: (a) 0 radians (undeformed),

(b) 0.142 radians (tear initiation), and (c) 0.202 radians (tear propagation).
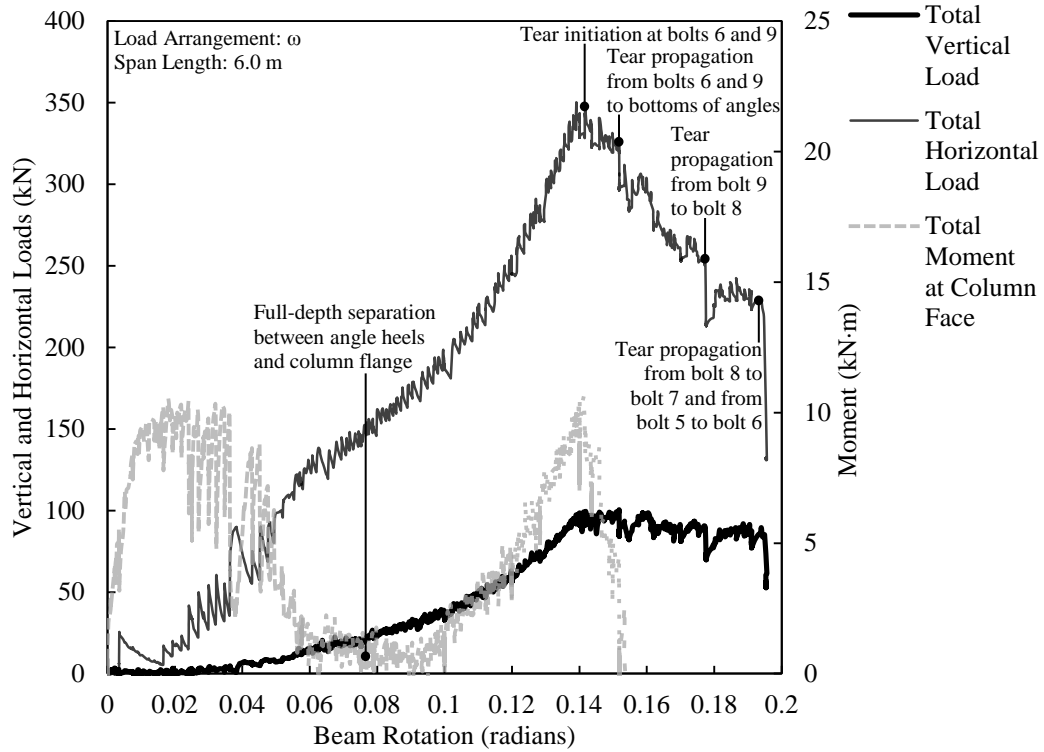
Figure 4.14. Load versus rotation for DA3B-1.

(a)   (b)
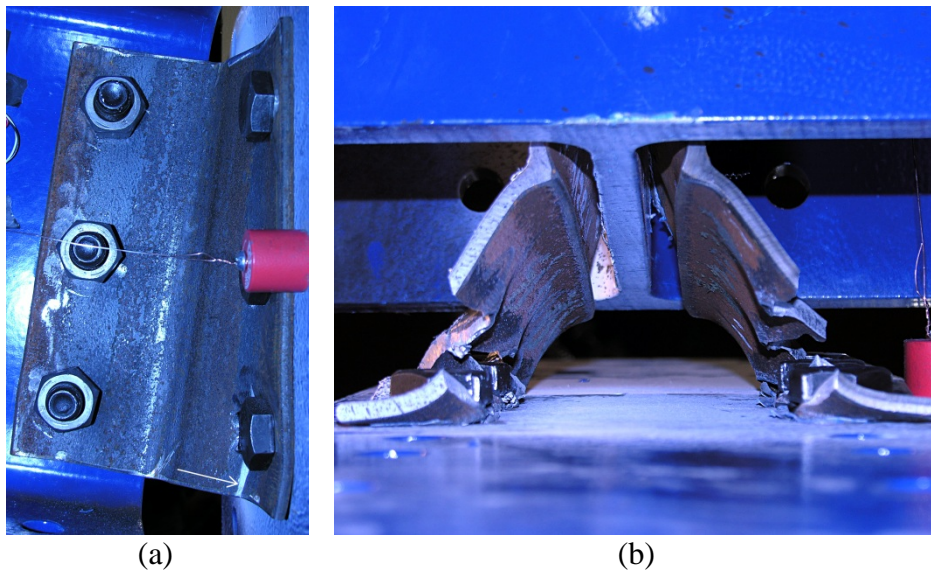
Figure 4.15. Double angle specimen DA3B-1 at: (a) 0.149 radians (tear to angle bottom), and (b) 0.194 radians (bottom view).
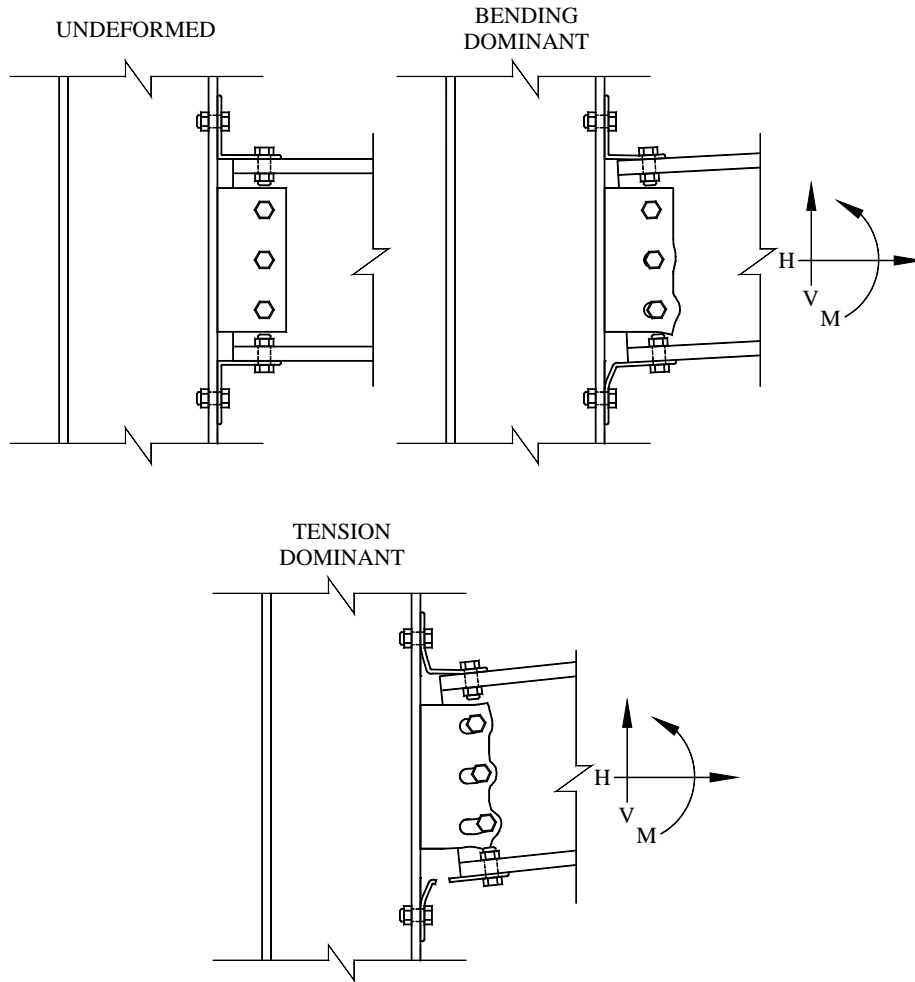
Figure 4.16. Deformation of combined seat and top angle connections (with shear tab) under combined loading.

Figure 4.17. Seat angle failure modes (viewed from below): (a) tearing along plastic hinge near angle heel, and (b) tearing along plastic hinges near column bolt line.
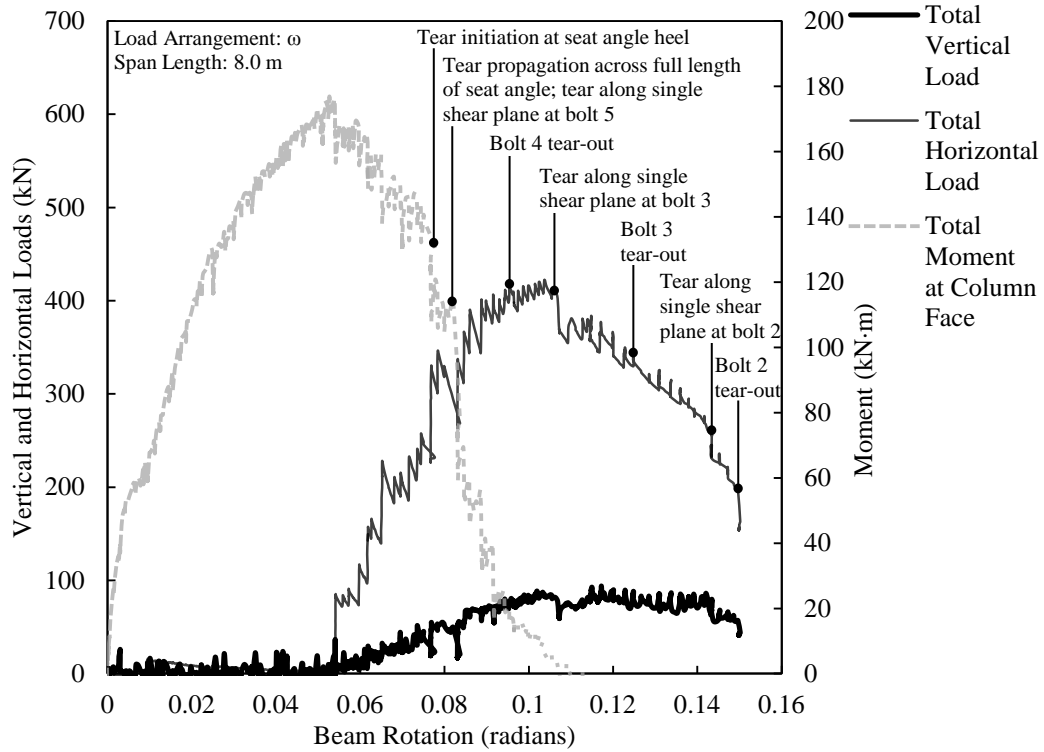
Figure 4.18. Load versus rotation for ST5C-1.

(a)	(b)	(c)
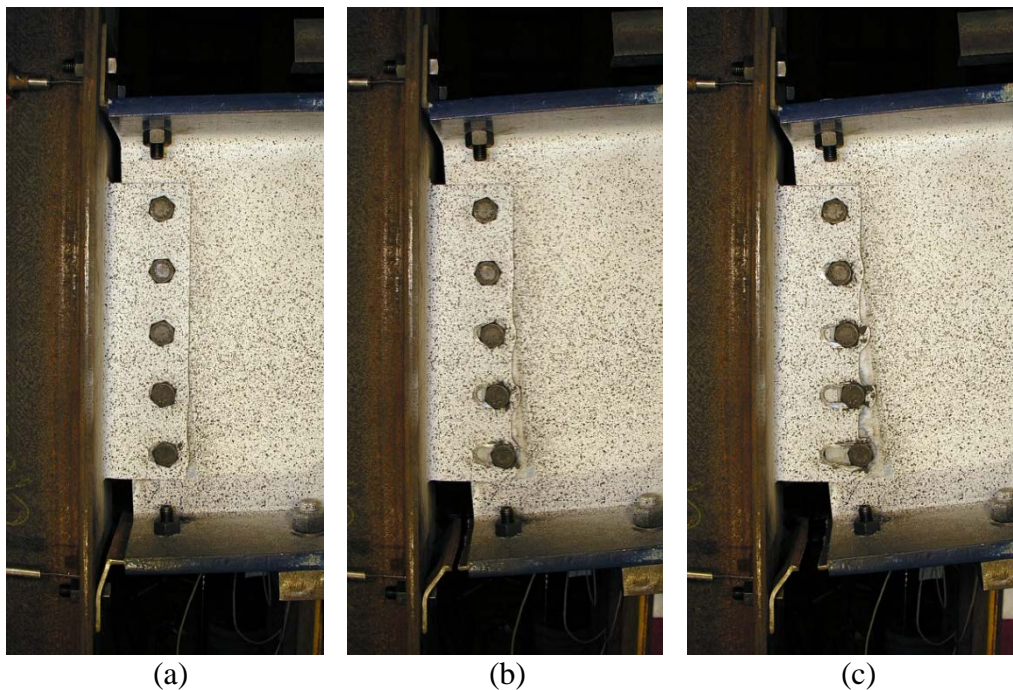
Figure 4.19. Shear tab with seat and top angles specimen ST5C-1 at:
(a) 0.05 radians (maximum moment), (b) 0.083 radians (seat angle failure),
and (c) 0.114 radians (peak post-damage response).

5. DISCUSSION AND ANALYSIS: SHEAR TAB AND WELDED–BOLTED ANGLE CONNECTIONS

The behaviour of both shear tab and welded–bolted single angle connections was observed to be dominated by deformation mechanisms and failure modes related to bolt bearing and tear-out, as reported in Chapter 4. Thus, for the sake of the discussion and analysis contained in this chapter, they are categorized together, and descriptions referring to "shear tab connections" generally refer to both connection types. The term "shear tab", therefore, applies to either the shear tab plate or the outstanding angle leg bolted to the beam web.

A mechanical model has been developed to predict shear tab connection behaviour under a column removal scenario. The details of this model are described, its results are validated using physical tests, and a parametric study is conducted to examine the impact of several variables on connection robustness. The effects of adding seat and top angles to shear tab connections are also discussed. Finally, design recommendations are given based on the test results and mechanical modelling. A similar approach is presented for bolted–bolted angle connections in Chapter 6.

5.1. Mechanical Model Definitions

Figure 5.1 shows the von Mises strains recorded by the optical strain imaging system during a shear tab connection test. (Von Mises strain is an invariant scalar quantity representing a combination of the principal strains at a point, and is defined for strain using an equation of the same form as the more commonly-used von Mises stress equation.) Strains are clearly concentrated at bolt bearing locations and are relatively low at all other locations. The top bolt in the five-bolt shear tab specimen shown is engaged in bearing in the compressive direction, and the development of shear tear-out planes in the tensile direction is evident ahead of each of the two bolts closest to the bottom of the connection. The dominance of localized stresses at bolt locations allows the behaviour of the entire connection to be accurately simulated by modelling a series of discrete spring elements at bolt

locations. Such a mechanical model, consisting of identical zero-length springs at bolt locations, is shown schematically in Figure 5.2. The rigid element on the column side is fixed, since deformations of the column and gross section of the shear tab did not actively contribute to the overall deformations that were measured during the physical tests. The rigid element on the beam side of the connection is roller-supported at the centreline of the connection, allowing rotation of the element about the centre of the bolt group and translation in the axial direction of the beam, which changes its orientation continuously during loading. The position of this rigid element, and the corresponding deformation of each spring, are determined by the compatibility conditions for a column removal scenario, as shown in Figure 5.2 and discussed further in Section 5.1.6. The vertical displacement of the system is exaggerated in the figure because the springs are illustrated with a nonzero initial length. The mechanical properties of the individual springs at bolt locations are defined by a force versus displacement curve that includes the effects of all components actively contributing to deformation. Force–displacement relationships for these components are taken from studies presented in the existing literature. The overall connection force and moment are calculated by summing the effects of the individual springs.

The mechanical model is used to predict the load development and ultimate capacities of shear tab connections. Using the software MATLAB Version 7.5.0, a program has been written that incrementally increases the model deformation calculated for a column removal scenario and solves for the corresponding force development in the individual spring elements at each step. The output is validated by comparing the predicted load versus rotation data to physical test results. An overview of the pertinent modelling details is included below.

5.1. Bolt Bearing

5.1.1.1. Bolt Tear-out Capacity Prediction

Nominal bolt bearing and tear-out resistance, $R_{n,br}$, is calculated according to the provisions of CSA S16-09 (CSA, 2009), reproduced in Equation 5.1. (In order to

determine expected resistance values, resistance factors are omitted in all capacity equations and measured values of σ_y and σ_u are used.) It is explicitly stated in the standard that the shear term of the block shear equation can be used to calculate bolt tear-out capacity, where the gross shear area, A_{gv}, is calculated along two parallel shear planes with length equal to the edge distance, L_e (shown in Figure 5.3), extending from the top and bottom of the bolt hole to the edge of the plate. All other variables in the equation have been defined previously. The effect of an inclined force on bolt tear-out capacity is discussed in Section 5.1.1.2. The upper limit in Equation 5.1 accounts for geometries with relatively large edge distances, which are governed by bearing failure rather than bolt tear-out, as would typically be the case for bolts bearing in the compressive direction for shear tab connections. The block shear capacity prediction equation given in AISC 360-10 (AISC, 2010) has a similar form to that appearing in CSA S16-09 and produces similar results; however, the American standard specifies the use of Equation 5.2 for the bolt bearing and tear-out failure modes.

$$R_{n,br} = 0.6\,A_{gv}\,\frac{\sigma_y + \sigma_u}{2} \leq 3\,t\,d\,\sigma_u$$
$$A_{gv} = 2\,L_e\,t$$

[5.1]

$$R_{n,br} = 1.5\left(L_e - \frac{d}{2}\right)t\,\sigma_u \leq 3\,t\,d\,\sigma_u$$

[5.2]

Equations 5.1 and 5.2 are evaluated using a compilation of 55 single-bolt bearing test results reported in the literature (taken from Lewis and Zwerneman (1996), Rex (1996), Kim (1996), and Aalberg and Larsen (2001)). Equation 5.1 produces a test-to-predicted ratio of 1.029 and a coefficient of variation of 0.104 when applied to these tests; comparatively, Equation 5.2 has a test-to-predicted ratio farther from 1.0 (1.189) and a significantly higher coefficient of variation (0.302) when applied to the same test results. Thus Equation 5.1 (from CSA S16-09) is used for bolt tear-out capacity prediction herein.

The 55 test results examined had edge-distance-to-bolt-diameter ratios that ranged from 0.6 to 4.8. A subset of 14 physical test results from the testing programs listed above that had ratios between 1.3 and 2.0 were examined separately, since this range is considered typical of fabrication practices for shear connections, and it envelopes the specimens tested in the current research program. These specimens had tear-out capacities that consistently exceeded those predicted by Equation 5.1, with an average test-to-predicted ratio of 1.086.

For the purpose of predicting the behaviour of the shear tab test specimens using the mechanical model, the expected tear-out resistance was taken as the value calculated using Equation 5.1, multiplied by the average test-to-predicted ratio from the physical tests of 1.086. For design purposes, however, it is considered reasonable and slightly conservative to use the capacity prediction equation without this increase factor.

5.1.1.2. Bolt Tear-out Capacity under Inclined Force

Bolt tear-out capacity has traditionally been considered under a force acting in a direction perpendicular to the edge of the element on which the bolt is bearing, which leads to the calculation of the gross shear area as given in Equation 5.1. However, the resultant direction of the applied force following column removal, F_R, is inclined with respect to the horizontal direction (perpendicular to the plate edge), as shown in Figure 5.3. This angle of inclination, γ, is dependent upon the loading arrangement. Vector addition of the horizontal and vertical forces (which are defined according to Equation 3.1 for a point load and Equation 3.2 for a uniformly distributed load, as discussed in Section 3.3.1.1) is used to determine the magnitude and direction of the resultant applied force (F_R and γ, respectively). For the point-load case, γ is equal to the beam chord rotation, θ_c. Under a uniformly distributed load, F_R acts horizontally at the removed column and at approximately double the beam rotation angle at the remaining column (the direction of γ is found by solving $\tan\gamma = 2\tan\theta_c$; thus, $\gamma \approx 2\theta_c$ for small values of θ_c). The application of the small-angle assumption to this case leads to an error of less than 2 % for beam rotation angles less than 0.22 radians, and is thus

considered appropriate for the modelling of shear connections under a column removal scenario.

As a consequence of the inclined resultant force, the critical shear plane is not in the horizontal direction, nor is it aligned with the resultant force. Increasing the angle of inclination of the assumed bolt tear-out shear planes (α, also included in Figure 5.3) from zero increases the length of the material engaged along the shear planes (and thus the resistance to bolt tear-out); however, the component of the resultant force that acts along those shear planes also increases. Equation 5.3 is an adaptation of Equation 5.1 to include the effects of an inclined failure plane on the applied force and tear-out resistance. In order to solve for the angle of the lower-bound critical failure path with respect to the horizontal direction, the angle α resulting in a minimum value for F_R in Equation 5.3 is found by solving the partial differential equation shown in Equation 5.4 within the domain $0 \leq \alpha \leq \gamma$, which reveals a critical shear plane angle equal to one-half of the angle between the horizontal and the resultant force direction ($\alpha = \gamma/2$). This derivation assumes that the component has sufficient capacity perpendicular to the critical shear planes to carry the portion of the inclined force that acts in this direction (which is clearly the case for the connections being considered).

$$F_R \cos(\gamma - \alpha) = 0.6 \left(\frac{A_{gv}}{\cos \alpha} \right) \frac{\sigma_y + \sigma_u}{2} \qquad [5.3]$$

$$0 = \frac{\partial}{\partial \alpha} \left(\frac{1}{\cos(\gamma - \alpha) \cos \alpha} \right)$$
$$\alpha = \frac{\gamma}{2} \qquad [5.4]$$

Considering failure in either the horizontal direction or in the direction of the applied load, versus assuming failure along shear planes at the critical angle, α, results in approximately a 2 % difference in load capacity for the specimens included in the testing program. Since the effect is small within the range of load inclinations recorded for the test specimens, the problem can be simplified by

requiring that the full magnitude of the inclined force be carried along the shortest (horizontal) shear planes. However, the inclination of the applied load becomes slightly more significant for connections with higher rotational capacities, as may be achieved for relatively short spans or connections with horizontally slotted holes. Since these cases are both included in the parametric study (Section 5.3), the force calculations in the mechanical model consider the inclined critical shear plane for completeness.

5.1.1.3. Force–Displacement Relationship

Rex and Easterling (2003) proposed Equation 5.5 to model the nonlinear relationship between bearing force, F_{br}, and bearing displacement, Δ, for single bolts bearing on a single plate toward a free edge. The initial stiffness, K_i, is calculated as a function of the bearing stiffness, K_{br}, bending stiffness of the segment of plate directly in front of the bolt hole towards the free edge, K_b, and shearing stiffness of the same plate segment, K_v, according to Equation 5.6 (where G is the shear modulus and all other variables have been defined previously).

$$
\begin{aligned}
F_{br} &= R_{n,br} \frac{1.74\,\overline{\Delta}}{(1+\overline{\Delta}^{0.5})^2} - 0.009\,\overline{\Delta} \\
\overline{\Delta} &= \frac{\Delta\,K_i}{R_{n,br}}
\end{aligned}
\tag{5.5}
$$

$$
\begin{aligned}
K_i &= \frac{1}{{}^{1}\!/\!{}_{K_{br}} + {}^{1}\!/\!{}_{K_b} + {}^{1}\!/\!{}_{K_v}} \\
K_{br} &= 120\,t\left(\frac{d}{25.4}\right)^{0.8}\sigma_y \\
K_b &= 32\,E\,t\left(\frac{L_e}{d} - \frac{1}{2}\right)^3 \\
K_v &= 6.67\,G\,t\left(\frac{L_e}{d} - \frac{1}{2}\right)
\end{aligned}
\tag{5.6}
$$

This equation was developed using regression techniques on the results of 48 tests of single bolts in bearing. Due to limitations of the test set-up, however, only one of these tests progressed to the stage of complete bolt tear-out. As a result, the derivation of the proposed relationship focussed on the initial stiffness and the increasing portion of the force versus displacement curve, and not the larger bolt displacements associated with the bolt tear-out failure mode. The force versus displacement curve generated by Equation 5.5 decreases after reaching a maximum force slightly less than $R_{n,br}$, as shown in Figure 5.4. However, there is insufficient experimental evidence to support this softening behaviour. On the contrary, single bolt tear-out tests performed by Kim (1996) and Aalberg and Larsen (2002), as well as the results of the current research program, suggest that single bolts in bearing that fail by bolt tear-out exhibit a ductile load plateau once the nominal tear-out resistance has been achieved. Thus, Equation 5.5 is modified by replacing the descending portion of the curve with a horizontal load plateau, as shown in Figure 5.4, until the maximum bearing displacement, $\Delta_{max,br}$, has been reached. Additionally, force values calculated using the equation have been increased by 1.6 % to achieve a peak force value equal to the nominal resistance, $R_{n,br}$.

This force–displacement relationship is used for bolt bearing on the shear tab and on the beam web. In the current testing program, the beam web had a much larger bearing resistance than the shear tab, which resulted in relatively small predictions of bearing deformation in the beam web. This is consistent with visual inspections of the beams following testing.

5.1.2. Bolt Shear

5.1.2.1. Bolt Shear Capacity Prediction

For bolts with threads excluded from the shear plane (as was the case for all connection bolts in the current testing program), the nominal bolt shear resistance, $R_{nv,bolt}$, is calculated according to the provisions of CSA S16-09 (CSA, 2009), reproduced in Equation 5.7, where the nominal value for static ultimate strength

of the bolt, σ_u, is used (a similar capacity equation is presented in AISC 360-10 (AISC, 2010)). In a report to the Research Council on Structural Connections, Moore et al. (2008) presented the results of 1018 bolts tested in single shear to failure (512 with threads excluded from the shear plane, and 506 with threads included in the shear plane). The results showed that the capacities of bolts in single shear consistently exceed their nominal values, with an average test-to-predicted ratio of approximately 1.25. Thus, for the purpose of predicting the behaviour of the test specimens, the expected bolt capacity, $R_{nv,bolt}$, is taken as that given by Equation 5.7 multiplied by 1.25.

$$R_{nv,bolt} = 0.60 \frac{\pi d^2}{4} \sigma_u \qquad\qquad [5.7]$$

5.1.2.2. Force–Displacement Relationship

The test set-up for bolts loaded in shear used by Moore et al. (2008) isolated bolt shear deformation from bearing deformation by using rigid elements to apply load to the bolts, which makes the test results useful for obtaining a force–displacement relationship for bolts in shear. Using regression techniques on the experimental results for ASTM A325 bolts tested in single shear with threads excluded from the shear plane, and removing bolt displacements attributed to apparent bolt slippage, the generalized trilinear force versus displacement curve shown in Figure 5.5 has been developed for use in the current study. The average shear displacement at failure, $\Delta_{max,bolt}$, was found to be approximately equal to 0.23 times the bolt diameter, with a coefficient of variation equal to 0.118. The same generalized curve can be applied when the bolt threads are included in the shear plane by application of the capacity reduction factor of 0.7 suggested by CSA S16-09 (CSA, 2009); however, there is higher variability associated with the test data reported by Moore et al. (2008) for this case.

5.1.3. Bolt Slippage

In the current testing program, bolt holes were fabricated with a diameter 1.6 mm larger than that of the bolts, which is consistent with typical industry practice. As

a result, there is the potential for bolts to undergo translation, known as slippage, before bolt bearing is initiated at the edge of the bolt hole. The average amount of bolt slippage that can occur is found by assuming that each bolt begins in the centre of its hole, which results in a potential slippage in any direction equal to one-half of the difference between the bolt and hole diameters in each of the two holes (shear tab and beam web). In the case of the test specimens in the current program, the average potential slippage is therefore 1.6 mm; the actual value could vary from zero to 3.2 mm, depending on the initial position of the bolt and the relative locations of the two hole centres.

In shear connections, bolts are typically installed to the snug-tight condition, which exerts a nonzero clamping force between connected components. Thus, a certain shear force threshold must be achieved to overcome the friction between the mating surfaces and initiate bolt slippage. Although the applied clamping force resulting from snug-tight bolt installation is known to vary considerably, modelling a threshold force of 30 kN at each bolt location results in load development behaviour that is consistent with the test results reported herein. The magnitude of the assumed threshold force has a noticeable impact on moment development at low rotations; however, the ultimate horizontal and vertical loads are not typically sensitive to this parameter for a threshold force of 30 kN ± 30 kN.

The characteristic behaviour of the bolt slippage function included in the mechanical model is illustrated for two cases. Figure 5.6 shows the development of bolt slippage and spring force with beam rotation for the bottom bolt of a five-bolt connection loaded as in the testing program, and Figure 5.7 illustrates the more complex case of a top bolt in the same connection, which includes a change in the direction of loading (the cause of this direction change is discussed in Section 5.1.6).

5.1.4. Failure Criteria

The total localized deformation at each bolt location at the instant bolt tear-out occurred was measured during the physical tests. This value includes bolt shear, bolt slippage, bolt bearing deformation in the shear tab and in the beam web, axial elongation of the beam, and column deformations. For the tests completed as part of the current program, the contribution of the latter two to the total measured deformations is negligible (estimated to be less than 0.5 mm in all cases) and thus is not included in the mechanical model. Table 5.1 lists the average total deformation at bolt tear-out, Δ_{max}, including all bolt locations where tear-out occurred, and the corresponding coefficient of variation, for each group of specimens with similar material properties, thicknesses, bolt diameters, and edge distances. This measurement provides a consistent and predictable failure criterion within each group. For elements governed by bolt tear-out, a ductile (deformation-controlled) failure criterion is used in the mechanical model that deletes a spring element when Δ_{max} has been exceeded.

Currently, there are insufficient experimental data available in the literature to propose an equation that accurately predicts bearing deformation at bolt tear-out as a function of material properties and geometry. In the mechanical model, the average values measured during the physical tests and reported in Table 5.1 are used as failure criteria, which are shown in Section 5.2 to result in accurate predictions of failure initiation. No measureable correlation was observed between the critical deformation value and either the depth of the connection or the distance of an individual bolt from the connection centreline.

Further research is recommended for the determination of the deformation limit parameter as a function of connection geometry and material properties; in the interim, for connections governed by bolt tear-out that are generally similar to those included in the current testing program, the values in Table 5.1 are recommended for modelling purposes. Based on the limited data available, Δ_{max} can be approximated as 70 % of the edge distance, L_e, where bolt tear-out is the

governing failure mode (which was not the case for the tests by Thompson (2009), shown in Table 5.1).

Although bolt shear failure was not observed in any of the tests performed in the current program, it is a potential failure mode for shear tab connections loaded under tension. Thus, a failure criterion for bolt shear is defined in the mechanical model. Elements governed by bolt shear failure are assigned a brittle (load-controlled) failure criterion that stipulates element removal if the nominal resistance of the bolt in shear, $R_{nv,bolt}$, is exceeded.

5.1.5. Numerical Construction of Composite Spring

The component force–displacement relationships and failure criteria discussed above are used to define a single composite spring that represents the behaviour of all active component springs arranged in series. Because explicit inverse functions of nonlinear force–displacement relationships do not always exist, this is accomplished numerically as part of the MATLAB script. The force–displacement relationships discussed above are used to populate matrices of displacements and corresponding forces for each active component spring. Nonlinear curves are discretized into 100 segments, with horizontal curve segments given a negligibly small positive slope to ensure a stable numerical solution. A composite spring is constructed as a new matrix of 100 force intervals from zero to the governing nominal resistance, R_n, and corresponding displacements are obtained by summing the displacements of the individual components at each force level using linear interpolation on the component matrices.

When the connection bolts act in bearing in the compressive direction, there is no free edge in the direction of the applied force. The edge distance effectively becomes infinite, and the initial stiffness of the component springs in the compressive direction is equal to the bearing stiffness, K_{br} (from Equation 5.6). Thus, component springs have unique force versus displacement curves in the compressive and tensile directions. In some cases, the direction of loading

changes as rotation increases. It is assumed that the component springs unload along the same path as they were loaded. The ultimate load condition typically occurs after the unloading is complete (i.e., the bolt is engaged in bearing in the direction of catenary tension); thus, the assumed unloading path has minimal impact on ultimate capacity predictions and a more convoluted scheme is not considered justified.

5.1.6. Column Removal Deformation Demand

In order to calculate the force in each composite spring in the mechanical model, the displacement and rotation of the roller-supported rigid element on the beam side of the component springs must be defined. The centreline axial deformation demand for a symmetric two-bay frame with shear connections following the removal of the central column, Δ_3, is given as a function of span length, L, and beam rotation, θ_c, in Equation 3.7. As shown in Figure 5.2, the change in length of each individual spring, Δ_{spring}, is related to the centreline axial deformation demand in proportion to the beam rotation angle and the eccentricity between the spring and the connection's centre of rotation, e, as given in the following equation:

$$
\begin{aligned}
\Delta_{spring} &= \Delta_3 + e\tan\theta_c \\
&= \frac{L}{2}\left(\frac{1}{\cos\theta_c} - 1\right) + e\tan\theta_c
\end{aligned}
\tag{5.8}
$$

This equation assumes that the entire line of bolts rotates about the centre of the bolt group and that this centre moves in the direction of the beam axis. The validity of these assumptions is evaluated by comparing the predicted location of each bolt in the connection assembly to the position of the bolt head measured using the optical strain imaging system, as shown in Figure 5.8 for specimen ST5A-1, which is representative of all shear tab connection tests. Equation 5.8 represents the total deformation demand at the connection, which must be satisfied by the sum of the shear tab bearing deformation, beam web bearing deformation, bolt shear deformation, and bolt slippage. Since the displacement

measured by the optical strain imaging system captures displacement of the bolt head, the predicted values reported in Figure 5.8 subtract component deformations predicted by the mechanical model that would not be visible on the bolt head (i.e., bolt shear deformation, beam web bearing deformation, and half of the bolt slippage). The results shown in the figure verify that the assumptions defined for the mechanical model result in accurate predictions of bolt displacement throughout the progression of the physical test, including stages after failure has occurred at some of the bolt locations (as suggested by the two sets of points farthest to the right in the figure, wherein the bolt symbols are omitted at the failed locations). The most noticeable discrepancies among the predicted and measured bolt displacement values exist at low rotations. This is attributed to the uncertainty associated with the initial positions of the bolts and the threshold at which bolt slippage occurs, and has only a marginal effect on the accuracy of the predicted displacements at the ultimate load condition. In all cases, the bolt displacements predicted by the mechanical model at rotations corresponding to the ultimate loads were within 2.0 mm of the displacements measured in the physical tests.

During the initial stages of some physical tests, the top bolt was observed to bear on the connection plate in the compressive direction, as seen for the five-bolt specimen shown in Figure 5.1. This behaviour is expected when the second term of Equation 5.8 is negative and is greater than the first term—a condition which may exist for bolts above the connection centreline at small rotations.

5.1.7. *Scope of Applicability*

The mechanical model is only applicable in cases where failure criteria are defined for the governing failure modes. For example, failure of the fillet weld between the shear tab and the column flange is not included in the model. Since this brittle failure mode is not desirable for collapse prevention, it was avoided by design in the physical tests.

114

Bearing of the top beam flange against the column flange as a result of beam rotation was not observed in any of the physical tests. Thus, a contact spring is not included at this location in the mechanical model. Connections with an initial gap distance of less than 10 mm and/or less severe tensile deformation demands than those imposed in the current testing program may lead to flange bearing, and would require the addition of a contact spring with an initial gap to the mechanical model.

The mechanical model focusses on behaviour in the connection region (similarly to the physical tests). In cases where external structural components (such as a non-rigid boundary condition at the column) may actively contribute to the overall deformation of the system, they should be included in the model as additional component springs. Furthermore, the model does not include the effects of a concrete floor slab, which would alter the demands and resistance of a structural system following column removal. Although a concrete slab was not included in the physical tests, the understanding of connection behaviour that has been developed herein can be applied directly to studies that include its effects. Detailed analyses including these effects are beyond the scope of the current program.

The mechanical model has been designed to predict the performance of shear connections under quasi-static loading conditions; thus, results cannot be directly applied to dynamic loading scenarios, including the instantaneous column removal that is recommended in current design guidelines for disproportionate collapse mitigation. However, the capacity predictions and force versus displacement results that are generated by the mechanical model provide information that can be used in conjunction with a range of analysis techniques, including the energy-based approach proposed by Izzuddin et al. (2008), in order to assess collapse resistance under the effects of dynamic loading scenarios.

5.2. Load Development and Capacity Prediction Results

The validity of the mechanical model discussed above is evaluated by simulating all 14 of the shear tab and welded–bolted single angle connection tests described in Chapters 3 and 4, as well as the three series of column removal experiments with shear tab connections performed by Thompson (2009). This section compares the load development and ultimate capacity predicted by the mechanical model to physical test results.

5.2.1. Load Development Prediction

Figure 5.9 shows the load versus rotation relationships for the five-bolt shear tab specimen ST5A-2, overlain with the mechanical model results (in blue). A similar plot is provided for the three-bolt welded–bolted single angle specimen WA3A-2 in Figure 5.10. Both figures demonstrate general agreement between the mechanical model and physical test results. Connection stiffness is effectively captured throughout the test by the series of component springs, and the bolt tear-out failure criterion leads to element removal at appropriate rotations. After initial failure occurs in specimen WA3A-2, the predicted horizontal load drops approximately 16 % below the value recorded in the test. This difference is attributed to the residual capacity at the extreme bolt following damage initiation in the test, compared to the complete removal of failed elements in the mechanical model. Although the difference between the physical test and the mechanical model increases following damage initiation in some cases, the model is generally able to predict loads effectively even after failure has occurred in some of the elements.

Bolt slippage results in a lag in moment development at low rotations, as indicated in Figure 5.10. This lag is more pronounced in the three-bolt specimens because all of the bolts in the connection tend to slip simultaneously. In some of the models, including the two cases demonstrated in Figures 5.9 and 5.10, the prediction of moment does not produce the same level of agreement with test results as the prediction of vertical and horizontal loads. Moment prediction is the

most sensitive to the modelling parameters with the greatest known variability—namely, maximum bolt slippage, force threshold to initiate slippage, and initial spring stiffness. Additionally, because the moment measured during the physical tests is relatively small, the measurements are expected to have a greater degree of measurement error than the recorded horizontal and vertical forces. The deviation between the measured and predicted moments is sufficiently small to have a negligible effect on predictions of ultimate capacity.

5.2.2. Ultimate Capacity Prediction

Figure 5.11 plots the maximum vertical load predicted by the mechanical model against that measured during the physical tests for the various connection geometries and loading conditions included in the physical testing program, demonstrating the accuracy and consistency of the mechanical model. Table 5.2 lists the maximum moment (M_{max}), maximum horizontal and vertical loads (H_{max} and V_{max}, respectively), and rotation at the ultimate load condition corresponding to tear-out of the extreme bolt (θ_u) predicted by the model, as well as the test-to-predicted ratios for each. The average test-to-predicted ratios for the critical parameters of maximum vertical force and maximum rotation are 0.986 and 0.964, respectively, and the corresponding coefficients of variation are 0.040 and 0.032. The reported statistics suggest that the model predicts both connection strength and ductility accurately and consistently.

5.2.3. Comparison to Physical Testing Data from Thompson (2009)

The mechanical model is also verified using data from the column removal experiments with shear tab connections performed by Thompson (2009). The following assumptions and alterations to the model described in Section 5.1 have been implemented to represent to the testing conditions specific to that program:

1. No tension coupon testing data was reported for the materials from which the test specimens were fabricated. Therefore, the material yield stress and ultimate strength are assumed as the expected values for the material grades used, which are obtained by multiplying the specified minimum

117

values by the expected-strength factors given in GSA (2003). The modulus of elasticity is assumed to be 200 000 MPa.

2. The physical tests were pin-supported by a single 32 mm diameter bolt in a standard hole at the opposite end of the beam from the removed column location. The model assumes that this "pin" slips 1.6 mm without developing any force, and includes a spring that simulates the bolt shear and bearing deformations at the pin location. The slippage and deformation at the pin support decrease the axial deformation demand exerted on the connection.

3. The test set-up introduced a vertical eccentricity between the centres of rotation at the two ends of the beam (i.e., the mid-depth of the connection and the pin support) for three- and four-bolt specimens. This decreases the axial elongation demand exerted on the connection, and is included in the model. (Further discussion on the effects of such an eccentricity is included in Section 6.1.4)

4. The effect of moment on the calculation of the vertical force required for equilibrium is included using Equation 3.4.

5. An effective span length of 3864 mm (twice the distance from the column face to the point of inflection represented by the pin support) is assumed for the calculation of axial deformation demand using Equation 5.8.

6. The average total deformation at the extreme bolt at failure (after adjusting for the expected deformation and slippage at the supporting pin)—determined empirically from the reported test results—is 15 mm for all tests (as included in Table 5.1). This value is much smaller than the average total deformation at failure of 35 mm, reported for the 9.5 mm thick plates tested in the current program. The difference is attributed primarily to the occurrence of brittle failure modes, such as bolt shear and net section tension failure, that were not observed in the current testing program.

7. The model analyses are terminated when damage progresses to the stage at which the physical tests were stopped.

Figure 5.12 shows the load development for the three nominally-identical four-bolt tests performed by Thompson (2009), overlain with the mechanical model results (in blue). Similar agreement was achieved for the three- and five-bolt test series. The predicted pattern of load development versus rotation demonstrates general consistency with the physical test results, and yields confidence in the versatility of the mechanical model to predict the behaviour of connection geometries and loading conditions beyond the scope of the physical testing performed as part of the current program. The impact of residual capacity at a damaged element is examined by specifying a residual resistance equal to one-half of the maximum resistance at the damaged element (shown as dotted blue lines for the horizontal and vertical loads). This improves agreement after failure for the one test result where significant horizontal load development following initial failure was recorded, but does not affect the rotations or loads achieved prior to that point. Because the presence of this residual capacity is not dependable, complete element removal is used for the parametric study presented in the next section. It is included in the figure only for the sake of comparison to the physical test results, in order to provide a possible explanation for the major differences between post-damage responses in repeated physical tests.

A summary of the loads and rotations predicted by the model for the tests of Thompson (2009) is presented in Table 5.3. These results are compared to the physical tests using test-to-predicted ratios that are based on the averages of each series of repeated physical tests. The model demonstrates the ability to predict maximum loads and rotations for the data set, but does not achieve the same level of accuracy as for the current testing program (summarized in Table 5.2). The mechanical model is sensitive to the assumed material properties and to the slippage and deformation characteristics of the pin support. Additionally, several different failure modes were observed in the tests—including the less ductile modes of bolt shear failure and net section tension failure—which decreases the consistency of the ultimate load-carrying capacity and ductility of the connections. Many of the component springs in models of specimens in the

current testing program reach a ductile yield plateau prior to failure, which causes the total load capacity to be less sensitive to the prescribed deformation limits.

The axial demands placed on the three- and four-bolt specimens tested by Thompson (2009) were significantly reduced by the vertical eccentricity between the centre of the connection bolt group and the pin support at the opposite end of the test beam. In cases where the connections at the ends of the beam are vertically aligned (which is common in practice), the maximum beam rotations at failure for connections that are otherwise identical to those tested by Thompson (2009) are expected to be significantly smaller than those achieved in the tests; thus, the maximum rotations reported cannot be used directly to determine general-purpose rotational ductility limits for analysis and design.

5.3.   Parametric Study

The validated mechanical model has been used to perform a parametric study that examines the effects of several variables on the strength and ductility of shear tab connections following column removal. Figures 5.13 through 5.17 show the maximum vertical load and corresponding beam rotation predicted by the model for specimens that are identical to the reference test specimens shown in the figure, except for the parameter being studied. In cases where the maximum vertical load is achieved following initial failure at the extreme bolt, the loads and rotations at both instances are included in the figures.

5.3.1.   Number of Bolts

Figure 5.13 shows the effect of the number of bolts (and concomitant connection depth) in a single vertical row (spaced at 80 mm) on the vertical load-carrying capacity and rotational ductility of shear tab connections. Increasing the number of bolts from two to five results in significant increases in vertical load-carrying capacity, which is consistent with the capacity increases seen between the physical test results for three- and five-bolt connections (although these results cannot be compared directly due to the differences in assumed span lengths). However, further increases in connection depth are not expected to provide

120

similar increases in strength, as the maximum vertical load shown in the figure plateaus for connections with more than five bolts. This is a result of the increased axial deformation demand on the extreme bolt (caused by its large eccentricity, e, in Equation 5.8), which leads to tear-out at relatively low rotations, while bolts on the opposite side of the bolt group are not yet effectively engaged in catenary tension. The maximum vertical load for the deeper connections is not reached until after tear-out failure has occurred at the extreme bolt (or, in some cases, multiple bolts). If the first bolt tear-out were to be adopted as the limit state, the design capacity of the deeper connections would actually decrease precipitously.

Table 5.4 reports the number of bolts effectively engaged in catenary tension at failure, n_{eff}, calculated as the sum of the spring forces divided by their total nominal resistance in tension. The efficiency of the bolt group is evaluated by the ratio of the number of effective bolts at failure to the total number of bolts in the connection (n_{eff}/n). Every bolt in the shallower connections has reached (or nearly reached) its tear-out capacity in tension prior to tear-out failure at the extreme bolt. However, as the number of bolts is increased, this efficiency is shown to decrease rapidly.

5.3.2. *Span Length*

The axial deformation demand imposed on a connection following column removal is a function of the span length of the beam. The deformation demand at each bolt location (i.e., at each spring in the mechanical model) is similarly affected by span length, according to Equation 5.8. Longer spans impose greater deformation demands in the direction of catenary tension than shorter spans at equivalent rotations. The effects of the rate of development of axial deformation demand are demonstrated by the physical test results reported in Chapter 4 for connections where the only varied parameter was the span length (as was the case for the following pairs of specimens: ST3A-2 and ST3A-3, ST3B-1 and ST3B-2, ST5A-1 and ST5A-2; ST5B-1 and ST5B-2; WA3A-2 and WA3A-3; and WA5B-1 and WA5B-2). Comparison of the load versus rotation curves for these pairs of tests (from Appendix D) shows that increasing the span length shifts the load

121

development curves to the left. Accordingly, tensile force development and bolt tear-out failure occur at lower rotations, and thus the vertical load-carrying capacity of the connection is reduced.

The mechanical model is used to examine the effect of varying span length beyond the values considered in the physical tests. The results of this study are shown in Figure 5.14 for a series of three-bolt connections and in Figure 5.15 for a series of five-bolt connections. As established by the physical test results, the figures clearly demonstrate decreased strength and ductility for longer span lengths. For relatively short spans, particularly in the case of the deeper five-bolt connections, the maximum vertical load tends to occur after tear-out of the extreme bolt. The small span length causes spring deformations to be dominated by the second term of Equation 5.8; thus, top bolts and bottom bolts tend to act in opposing directions at rotations corresponding to initial failure. However, these connections still outperform longer span lengths, as the remaining bolts effectively develop catenary tension at relatively large post-damage rotations.

5.3.3. Beam Web Tear-out Resistance

In the physical tests, the beam web had a significantly greater tensile tear-out resistance than the shear tab, in order to isolate and study the strength and ductility of the connection. For all test specimens, the beam web bearing deformations measured during the physical tests and the mechanical model simulations were less than 1 mm, and thus did not contribute significantly to the rotational ductility of the connections. In practical applications, the beam web could be more similar to the connection in thickness and tear-out resistance. In such cases, bearing deformations of both the beam web and the connecting element are available to accommodate axial deformation demands, which may increase the total rotational ductility of the connection following column removal.

The effect of the ratio of the tear-out resistances of the beam web and the shear tab is shown in Figure 5.16 (the result shown is typical of all shear tab arrangements included in the physical testing program). The vertical dashed line

represents a balanced condition, where the tear-out resistances of the two components are equal. In this theoretical case, both elements are able to deform plastically along the ductile force–displacement plateau shown in Figure 5.4, which significantly increases the predicted beam rotation at failure and the corresponding maximum vertical load. However, in practical applications, it is impossible to ensure that these designs are balanced, even if they are nominally designed to be so. Several uncertainties, including variability in as-built geometry and material properties, are likely to cause web-to-connection resistance ratios different from 1.0. As shown in Figure 5.16, there is a rapid decrease in maximum vertical load and rotational ductility for ratios deviating even slightly from 1.0; thus, it should not be assumed that using a beam with a lower tear-out resistance than that used in the current testing program will offer significant improvement to the overall strength and ductility of the connection assembly. Furthermore, the assumption of a balanced condition in practical design situations may lead to a gross overestimation of the assembly's rotational ductility and vertical load-carrying capacity.

5.3.4. *Horizontally Slotted Holes*

The specimens tested in the current program use standard holes that are 1.6 mm larger than the bolt diameter; however, the use of horizontally slotted holes could improve the rotational ductility of the connections by allowing greater bolt displacement prior to the initiation of bearing. This modification was shown by Astaneh et al. (2002a, 2002b) to provide adequate flexibility following column removal to avoid significant damage in a shear tab connection at a beam rotation of approximately 0.14 radians.

The use of horizontally slotted holes at bolt locations is modelled by increasing the maximum slippage that is permitted. A series of connections with a constant horizontal edge distance is modelled, which implies that the horizontal dimension of the shear tab is increased in proportion to the slot length. Maximum slippage is calculated assuming that the bolt begins in the centre of the horizontal slot, and that the beam web contains standard holes.

123

The effect of maximum slippage on connection strength and ductility following column removal is shown for a series of three-bolt connections in Figure 5.17. A similar trend occurs for deeper connections. The slippages associated with the maximum length of "short slots" and "long slots", as defined in CSA S16-09 (CSA, 2009), are indicated on the plots for reference. Although the connections all have similar tear-out capacities, the connections with slotted holes engage bolts in bearing at greater rotations, causing a greater portion of the resultant force to occur in the vertical direction. The benefit of the slotted holes is limited by the increased rate of axial deformation demand at large rotations (according to Equation 5.8). For the three-bolt connections shown in Figure 5.17, the use of long slotted holes increases the vertical load-carrying capacity following column removal by 31 %, and the beam rotation at failure by 37 %, when compared to a similar connection with standard holes. However, at low rotations (prior to initial failure) the connection forces are relatively low due to limited force development at each bolt location prior to the initiation of bearing. While this is not important to the maximum vertical loads shown in the figure, it may reduce the contribution of these connections to vertical load resistance following column removal if deflection is controlled by another (primary) element in the structure.

5.3.5. Shear Tab Thickness

The physical test results suggest that the thickness of the shear tab affects both the strength and ductility of the connections. Bolt tear-out resistance increases with the thickness of the plate (according to Equation 5.1), and the total deformation at failure measured during the physical tests also increases with thickness (as suggested by the data in Table 5.1, although bolt size and material properties also varied for the two plate thicknesses). The improved tear-out strength and ductility combine to cause significant improvements in the performance of 9.5 mm thick connections (compared to 6.4 mm thick connections).

5.3.6. Edge Distance

Horizontal edge distance, L_e (shown in Figure 5.3), is critical to the performance of shear tab connections under catenary tension. Bolt tear-out capacity is directly proportional to edge distance (according to Equation 5.1). Connection ductility is also affected by edge distance, as suggested by the data reported in Table 5.1 for specimens with similar thicknesses but different edge distances—total deformation at tear-out failure is significantly smaller for connections with shorter edge distances. However, it must be borne in mind that designing shear tab connections with greater horizontal edge distances than those tested may not improve performance under the demands of column removal. Rather, a greater edge distance may cause a failure mode that is more brittle than bolt tear-out to govern failure, such as bolt shear or net section tension failure. Although the nominal resistance at individual bolt locations may benefit from an increased edge distance, the decreased ductility associated with brittle failure modes could cause connection failure at lower rotations and decrease its vertical load-carrying capacity.

5.3.7. Loading Arrangement

The physical test results suggest that the maximum rotation at failure is not significantly affected by changing the simulated loading arrangement from a central point load to a uniformly distributed load, although the ratio of vertical to horizontal load is different by a factor of two for these cases. This suggests that, in the case of shear tab connections governed by bolt tear-out failure, the load-carrying mechanisms in the vertical and horizontal directions are predominantly independent. Furthermore, it suggests that the mechanical model can be used to predict the effects of including the contribution of connection moment to the vertical load (i.e., the second term in Equations 3.4 and 3.5), since this results in a comparatively small increase to the proportion of vertical to horizontal load. Figure 5.18 compares the development of vertical load with rotation under a central point load and a uniformly distributed load, and the modified predicted load development when the contribution of moment to the

125

vertical load is included for each loading arrangement. Consideration of the contribution of moment results in a marginal increase in the vertical load-carrying capacity. The relative increase in vertical load is more significant at low rotations than at failure, due to the initially-high moment and low axial force. In all of the physical tests performed, tensile catenary forces dominated behaviour at the ultimate state, and neglecting the moment is a conservative simplifying assumption that produces reasonable results. However, certain connection arrangements that could lead to bearing of the beam flange against the column flange, or the presence of a concrete slab, have the potential to cause significant increases to the moment developed at low rotations, which may cause its contribution to vertical load resistance to become significant.

5.4.   Combined Seat and Top Angle Connections

Connections with shear tabs (connected to the beam web) combined with seat and top angles (connected to the beam flanges) were included in the physical testing program to compare the performance of this type of semi-rigid connection to rotationally-flexible shear connections and to explore the option as a potential retrofit for existing structures. Four physical tests of shear tab connections combined with seat and top angles were completed: two connections with three bolts at the beam web (ST3C-1 and ST3C-2), and two with five bolts at the web (ST5C-1 and ST5C-2); details of the geometry of these specimens and individual test results are reported in Chapters 3 and 4, respectively.

Joining the beam flanges directly to the column using bolted–bolted angles significantly increases the rotational stiffness and moment capacity of a connection, as compared to connecting only the beam web. These connections— commonly classified as semi-rigid—developed maximum moments following column removal that were approximately four to seven times higher than those developed by the similar shear tab connections alone. Compressive arching action, which was not recorded for any shear tab connections, was developed in some cases where seat and top angles were added because of the large vertical eccentricity between the angles and their much higher stiffness in the compressive

126

direction than in the tensile direction. (The phenomenon of compressive arching action is discussed in more detail in Section 6.1.4). As a consequence of the limited ability of the test set-up to apply compression and the exclusion of the moment term in the determination of the vertical load required for equilibrium, the expected vertical load during arching action cannot be directly extracted from the test data. However, using the moment data recorded during the tests, it appears that the maximum vertical load that was eventually achieved under catenary action may be approached during arching action if the contribution of moment at low rotations is considered, but it is not likely to be exceeded by a substantial amount because the effective depth of the compressive strut is still relatively small compared to typical span lengths. Although the vertical load capacity under static loading conditions is not expected to be impacted extensively, the development of greater vertical load at low rotations is significant to the total energy absorbed by the connection under a dynamic loading scenario. It is thus considered more important to capture the moment developed at low rotations for the modelling of semi-rigid connections than for shear connections.

At later stages in the load history following column removal, the forces in the combined seat and top angle connections transitioned to a state where all elements acted in tension. Before the peak tensile load was reached, the bottom angle typically tore across its entire width either along the heel or the bolt line at the column, and thus no longer contributed to the total load being carried. (The bottom angle experienced the greatest axial deformation demand of all the components in the connection, due to its large eccentricity, e, in Equation 5.8.) Failure of the bottom angle caused the connection moment to drop drastically. The remaining top angle, however, did contribute to an increase in the maximum vertical load compared to Series B specimens with similar connections at the beam web. While only one of the seat/top angles appears to improve the load-carrying capacity of the connection during the catenary action phase, in a two-bay system with the central column removed the rotation and loading directions are opposite at the removed and remaining columns. Therefore, to

allow for the potential loss of any column, the addition of both angles is necessary to achieve this benefit even though one will likely fail prematurely.

Bolt tear-out in the shear tab occurred at similar localized deformations at each bolt location in test specimens with and without seat and top angle connections. Three-bolt shear tab connections combined with seat and top angles displayed increases to the maximum vertical load capacity of 44 % (ST3C-1) and 38 % (ST3C-2), and five-bolt connection capacities were increased by 7 % (ST5C-1) and 23 % (ST5C-2), when compared to connections with the same geometry and applied loading history, but without connection to the beam flange. The benefit to the shallower connections is greater (as a percentage) because the resistance added by the angles is larger in proportion to the capacity of the three-bolt shear tab connections alone. The capacity of specimen ST5C-2 was more substantially affected by the addition of seat and top angles than ST5C-1 because of the increased rate of axial elongation demand applied associated with its greater span length; in this case, the ratio of rotational-to-axial demands were not severe enough to cause premature fracture of the seat angle. For the deeper connections—particularly ST5C-1—the benefit of the added angles to the maximum static vertical load achieved following column removal is small. However, under a dynamic loading scenario, the additional energy absorbed at low rotations due to the increased extent of compressive arching action introduced by the seat and top angles may significantly improve collapse resistance.

5.5. Design Recommendations

5.5.1. Connection Detailing

The robustness of shear tab connections is directly related to their ability to accommodate localized bolt bearing in a ductile manner. Favourable performance can be achieved by proportioning connections such that the ductile bolt tear-out failure mode governs in the horizontal direction at each bolt location—as was the case for the connections included in the current testing program—rather than failure modes that are more brittle. Failure modes that should be avoided by

design include: weld failure, bolt shear failure, and net section tension failure. This objective can typically be achieved without significant (if any) deviation from typical connection arrangements meeting the minimum detailing requirements already prescribed by current North American steel design standards. The ductility demonstrated by the welded–bolted angle test specimens can be improved by increasing the horizontal edge distance from 29 mm (which meets the minimum edge distance requirements specified by CSA S16-09 (CSA, 2009) and AISC 360-10 (AISC, 2010) for shear connections with rolled edges, but not the CSA S16-09 requirement for members loaded directly towards a free edge with only a single bolt in the direction of the force). The use of horizontally slotted holes can improve robustness through an increase in rotational capacity, as discussed in Section 5.3.4.

5.5.2. Retrofit Options

It is increasingly common for a building owner to assess an existing building's resistance to disproportionate collapse, in order to ensure levels of safety that are appropriate for its current function. The results of the physical tests and mechanical modelling support several retrofit options to achieve improved robustness.

If it is found that an existing shear tab connection is expected to be governed by the brittle failure modes of bolt shear or weld failure under the effects of catenary tension, it may be possible to improve connection robustness significantly through the strengthening of the critical component to shift the governing failure mode to a more ductile one (for example, by replacing bolts with higher strength or larger ones, or by reinforcing the existing weld).

Increasing the strength of a connection by adding a second plate on the opposite side of the web that is similar to the first can also improve its robustness. This retrofit would have the potential to double the vertical load-carrying capacity of the connection acting in catenary tension (putting the bolts into double shear). However, in cases where the existing shear tab and beam web have similar

129

tear-out resistances, reinforcing the connection in this way will cause tensile failure of the beam web to govern, and thus limit the improvements offered by the retrofit. In such a case, reinforcement of the beam web by the addition of a doubler plate in the connection region may be required.

The potential benefit of adding seat and top angles to an existing shear tab connection is discussed in Section 5.4.

5.5.3. Tie Force Evaluation

The only tie force requirement of those summarized in Table 2.4 that can be evaluated without knowledge of building geometry or specified gravity loading is that from the *International Building Code* (ICC, 2012), which recommends that a connection be designed to carry a horizontal tie force equal to two-thirds of its required factored vertical shear resistance, independently from any other loads or rotations. Table 5.5 lists the factored shear resistance, V_r, of each test specimen (calculated according to CSA S16-09 (CSA, 2009), using specified minimum material strengths), and compares the factored horizontal resistance (H_r) and the maximum horizontal load measured during the test (H_{max}) to the *International Building Code* tie force requirement of $2/3\ V_r$. The calculated horizontal resistance is governed by bolt tear-out in all cases, which is consistent with the physical test results. Both the nominal and measured maximum horizontal loads exceed the tie force requirement for all specimens. Although the horizontal loads measured during the physical tests occurred in combination with vertical loads and large rotations, they exceeded the nominal horizontal resistances under pure tension in all cases because the calculated resistances include a resistance factor and use specified minimum material strength parameters. As demonstrated in Section 5.3.1, the calculated horizontal resistance of shear tab connections under tension accurately predicts the maximum horizontal load under combined loading following column removal for shallow connections, as indicated by the ratio n_{eff}/n being close to 1.0, but the increased demands imposed by rotation in deeper connections causes failure at much lower horizontal loads than expected under pure tension. (The resistances used to calculate n_{eff}/n include the small increase in

130

capacity for tear-out under an inclined force discussed in Section 5.1.1.2; however, since this increase is only about 2 %, similar results are achieved when examining the resistance to a purely horizontal load, as prescribed by the *International Building Code*.)

Table 5.5 also includes the maximum vertical load measured during each test, V_{max}, normalized as a fraction of the factored vertical shear resistance in order to compare the relative performance of the connections under column removal demands. Specimens tested under the effects of a central point load are indicated with an asterisk, since this condition decreases the proportion of vertical to horizontal load by a factor of one-half compared to the case of a uniformly distributed load. The total vertical load achieved during the physical tests represents a small fraction of the nominal shear capacity under conventional gravity loading, which suggests the limited ability of shear connections to prevent collapse following complete column removal without contributions from other structural components.

The results shown in Table 5.5 are used to evaluate how effectively tie force requirements improve shear tab connection robustness. The tie force approach captures only one parameter—horizontal resistance—that affects connection performance under a column removal scenario. The positive correlation between tie force resistance and vertical load-carrying performance following column removal is demonstrated by comparing the ST5B and WA5B test series. The 18 % higher horizontal tie force resistance ratio in the ST5B test series (as controlled by their respective horizontal edge distances) resulted in an increase to the vertical load-carrying performance of more than 50 %.

However, the tie force approach is a simplification that does not consider the many other factors that are shown in the parametric study (Section 5.3) to have direct effects on the strength and ductility of shear tab connections following column removal. The first nine (ST) specimens listed in Table 5.5 demonstrated very similar horizontal tie force resistance ratios (between 1.37 and 1.42);

however, the corresponding normalized vertical load capacity following column removal varied from 0.17 to 0.35—a difference of more than 100 %. This illustrates the importance of parameters not captured by the tie force approach (including depth of connection, span length, and loading arrangement) to the robustness of shear connections. Thus, the implementation of tie force provisions alone may result in inconsistent improvements to robustness. Furthermore, because such requirements ignore connection ductility, they may mislead designers into increasing horizontal resistance at the expense of ductility, which may be detrimental to connection performance following column removal (for example, increasing horizontal edge distances to improve tie force resistance may cause more brittle failure modes, such as bolt shear failure, to govern the connection behaviour).

5.5.4. *Simplified Connection Modelling for Column Removal Analysis*

5.5.4.1. Moment–Rotation Relationship

UFC 4-023-03 (DoD, 2009) provides modelling parameters for steel shear connections, including shear tabs, that define moment versus rotation curves (with the form discussed in Chapter 2). These curves are adapted from seismic design recommendations found in ASCE/SEI 41-06 (ASCE, 2007). Column removal has the potential to introduce very large tensile forces through the development of catenary action, which decreases the rotational stiffness and moment capacity of a connection; however, the current guidelines do not include this effect when defining the curves. Furthermore, the recommended rotation limits are much lower than those recorded in the physical tests. These discrepancies are demonstrated in Figure 5.19, which compares the curve generated by the modelling guidelines from UFC 4-023-03 to the moment expected following column removal, as measured during the physical testing of specimen ST5A-2. Two model curves are shown: the solid line represents the case where the maximum moment for the modelling curve is defined according to that measured during the test (thus including the effects of axial tension on moment development), and the dashed line represents the case where the moment capacity

is calculated under pure bending, which leads to the gross overestimation of the moment developed following column removal. Although the initial stiffness is effectively approximated by the recommended curve, the characteristics of moment development following the introduction of significant axial tension are not representative of the actual behaviour. Similar discrepancies exist for all specimens included in the current testing program.

Although the moment–rotation behaviour of moment connections is critical to energy absorption through plastic hinging in seismic design, the behaviour of shear connections following column removal is significantly different from this case. As discussed in Section 5.3.7, the moment contributes little to collapse prevention following column loss. Thus, modelling shear tab connections as rotationally pinned is expected to result in reasonable approximations of collapse resistance. If a rotational spring is included to represent connection bending resistance in column removal analysis, it must include the interaction of axial forces and moment. A more relevant force–deformation relationship for the modelling of shear tab connections under a column removal scenario captures the formation of catenary tension, as discussed below.

5.5.4.2. Force–Deformation Relationship

The general approach to modelling shear tab connections described in Section 5.1 is adapted to provide a simplified procedure to model the resultant force versus beam rotation using a single bilinear spring, which eliminates the need for computer programming by providing an approach that can be implemented using hand-calculations or with the aid of a spreadsheet. The relationship between connection force and rotation prior to initial failure is approximately linear as a result of the counteraction of the decreasing connection stiffness and increasing rate of axial deformation demand with rotation. Although using a single spring does not capture moment development, Section 5.5.1 proposes that the moment is reasonably negligible in the case of modelling shear tab connections under a column removal scenario. The form of the proposed bilinear force–deformation curve is illustrated schematically in Figure 5.20, and can be defined completely by

establishing two points: one representing initial failure (corresponding to the maximum resultant force), and a second representing final failure (corresponding to failure at all bolt locations). The connection forces and rotations corresponding to these two points can be approximated using the following procedure:

1. Estimate the localized deformation capacity at bolt locations, Δ_{max}. For specimens governed by bolt tear-out that are similar to those included in the current program, Δ_{max} can be taken from Table 5.1, or estimated as 70 % of the horizontal edge distance, L_e. (Refer to Section 5.1.4 for further discussion of this failure criterion.)

2. Calculate the rotation at initial failure, θ_u, by solving Equation 5.8 for θ_c, setting Δ_{spring} equal to Δ_{max} and e equal to the vertical eccentricity between the connection centreline and the extreme bolt. Calculate the rotation at final failure, θ_{final}, by solving Equation 5.8 with e equal to the vertical eccentricity between the connection centreline and the last bolt to fail.

3. Calculate the axial deformation at each bolt location in the connection at initial failure using Equation 5.8, setting θ_c equal to θ_u.

4. Determine the number of bolts effectively engaged in catenary tension at initial failure, n_{eff}, using the deformations calculated in Step 3, where the term "effective" refers to the proportion of the nominal capacity being utilized, F_{br}/R_n. For shear tab connections similar to those included in the current program, the force versus displacement curve at each bolt location (including all components actively contributing to deformation, as discussed in Section 5.1) can be approximated as elastic–perfectly plastic using Equation 5.9, where a suitable fit with the force versus displacement curves for all of the specimens tested and modelled is achieved using a value of displacement at yield, $\Delta_{yield\ point}$, equal to 5 mm plus the expected slippage distance (1.6 mm for standard holes). Alternatively, a more accurate force–displacement relationship can be defined using the approach outlined in Section 5.1.5.

$$\frac{F_{br}}{R_n} = \frac{\Delta_{bolt}}{\Delta_{yield\,point}} \le 1.0$$

$$n_{eff} = \sum \frac{F_{br}}{R_n}$$

[5.9]

5. Determine the governing nominal resistance at a single bolt location, R_n, in the horizontal direction (using Equation 5.1 for connections governed by bolt tear-out). Calculate the maximum resultant force in the connection, $F_{R,max}$, by multiplying n_{eff} by R_n.

6. Plot the resultant force versus rotation curve as shown in Figure 5.20. This curve defines the behaviour of the connection as a single spring that acts in the direction of the resultant force, γ. (As discussed in Section 5.1.1.2, $\gamma = \theta_c$ for point loads and $\gamma \approx 2\theta_c$ for uniformly distributed loads.) The curve can be manipulated to generate horizontal and vertical load versus rotation curves, and load versus displacement curves.

A worked example demonstrating the application of this procedure is given in Appendix E. The load development curves generated using this approach for four representative shear tab specimens are compared to the associated physical test results in Figure 5.21. For the sake of comparison with the physical tests, the nominal resistances (R_n, calculated in Step 5) were replaced by the expected values (according to the procedure discussed in Section 5.1.1). The dashed lines show the conservative results achieved by approximating Δ_{max} as 70 % of L_e, rather than using the (larger) average values reported in Table 5.1.

The simplified connection model described above could be directly applied within the column removal analysis framework described by Izzuddin et al. (2008). This framework includes an approach to account for dynamic effects that requires (as an input) a reasonable prediction of the nonlinear static response of beam-to-column connections following column removal—which is provided by the physical test results and validated modelling techniques presented herein—in order to facilitate an assessment of collapse resistance in the context of a three-dimensional frame with multiple beams, columns, and connections.

135

Table 5.1. Localized deformation at bolt tear-out.

Specimen Properties			Bolt Tear-out Statistics		
Connection Type	Connection Thickness	Horizontal Edge Distance	Average Total Deformation	Sample Size	Coefficient of Variation
	t (mm)	L_e (mm)	Δ_{max} (mm)		
ST	9.5	35	35	22	0.063
ST	6.4	35	27	16	0.116
WA	9.5	29	21	6	0.071
WA	6.4	29	18	8	0.122
ST*	9.5	38	15	9	0.103

*Specimens tested by Thompson (2009)

Table 5.2. Comparison of mechanical model and physical test results.

Specimen ID	Mechanical Model Results				Test-to-Predicted Ratio			
	M_{max}	H_{max}	V_{max}	θ_u	M_{max}	H_{max}	V_{max}	θ_u
	(kN·m)	(kN)	(kN)	(radians)				
ST3A-1	13.0	508.3	65.2	0.128	1.368	1.012	0.955	0.965
ST3A-2	14.9	502.0	130.9	0.128	1.078	1.006	0.948	0.957
ST3A-3	13.4	505.6	110.3	0.108	0.981	1.030	0.961	0.949
ST3B-1	9.3	330.1	73.5	0.110	1.027	1.003	0.966	0.913
ST3B-2	8.2	336.4	63.3	0.093	1.472	0.996	0.916	0.968
ST5A-1	53.5	757.6	150.1	0.098	1.002	0.945	1.012	0.964
ST5A-2	39.9	827.1	140.3	0.084	1.281	0.994	0.991	0.988
ST5B-1	35.7	467.2	78.2	0.083	1.358	1.008	1.051	0.970
ST5B-2	27.4	515.7	74.2	0.072	1.258	0.991	0.935	0.951
WA3A-1	11.2	429.4	40.5	0.094	1.042	0.976	1.008	1.032
WA3A-2	12.6	426.5	81.1	0.094	0.921	1.010	1.018	1.011
WA3A-3	11.4	444.3	71.7	0.080	1.247	1.108	1.035	0.950
WA5B-1	33.8	316.0	48.7	0.077	1.374	1.007	1.012	0.954
WA5B-2	25.5	406.9	44.9	0.055	1.153	0.963	0.992	0.927
Average					1.183	1.004	0.986	0.964
Maximum					1.472	1.108	1.051	1.032
Minimum					0.921	0.945	0.916	0.913
Standard Deviation					0.176	0.037	0.040	0.030
Coefficient of Variation					0.149	0.037	0.040	0.032

Table 5.3. Comparison of mechanical model and physical test results reported by Thompson (2009).

Number of Bolts	Mechanical Model Results				Test-to-Predicted Ratio			
	M_{max} (kN·m)	H_{max} (kN)	V_{max} (kN)	θ_u (radians)	M_{max}	H_{max}	V_{max}	θ_u
3	19.4	182.0	32.6	0.125	0.979	1.105	0.900	1.061
4	38.8	165.2	35.4	0.092	0.931	0.913	0.921	1.022
5	56.7	207.6	44.0	0.070	1.172	0.802	1.095	1.090
				Average	1.052	0.940	0.972	1.058
				Standard Deviation	0.170	0.153	0.107	0.034
				Coefficient of Variation	0.162	0.163	0.110	0.032

Table 5.4. Effective number of bolts engaged in catenary tension at failure.

Number of Bolts, n	Initial Failure		Maximum Vertical Load	
	n_{eff}	n_{eff}/n	n_{eff}	n_{eff}/n
2	2.00	1.00	—	—
3	3.00	1.00	—	—
4	3.90	0.98	—	—
5	4.45	0.89	—	—
6	4.72	0.79	3.70	0.62
7	4.00	0.57	2.89	0.41
8	3.52	0.44	2.83	0.35

Table 5.5. Tie force evaluation.

| Specimen ID | Factored Shear Resistance V_r (kN) | Horizontal-Resistance-to-Tie-Force-Requirement Ratio | | Measured-to-Factored Shear Resistance Ratio V_{max}/V_r |
		Factored $H_r/(2/3\ V_r)$	Measured $H_{max}/(2/3\ V_r)$	
ST3A-1	355	1.42	2.17	0.18[*]
ST3A-2	355	1.42	2.13	0.35
ST3A-3	355	1.42	2.20	0.30
ST3B-1	241	1.41	2.06	0.29
ST3B-2	241	1.41	2.09	0.24
ST5A-1	612	1.38	1.75	0.25
ST5A-2	612	1.38	2.01	0.23
ST5B-1	414	1.37	1.71	0.20
ST5B-2	414	1.37	1.85	0.17
WA3A-1	344	1.22	1.83	0.12[*]
WA3A-2	344	1.22	1.88	0.24
WA3A-3	344	1.22	2.15	0.22
WA5B-1	406	1.16	1.18	0.12
WA5B-2	406	1.16	1.45	0.11

*Tests performed under central point load.
 (All other specimens tested under uniformly distributed load.)
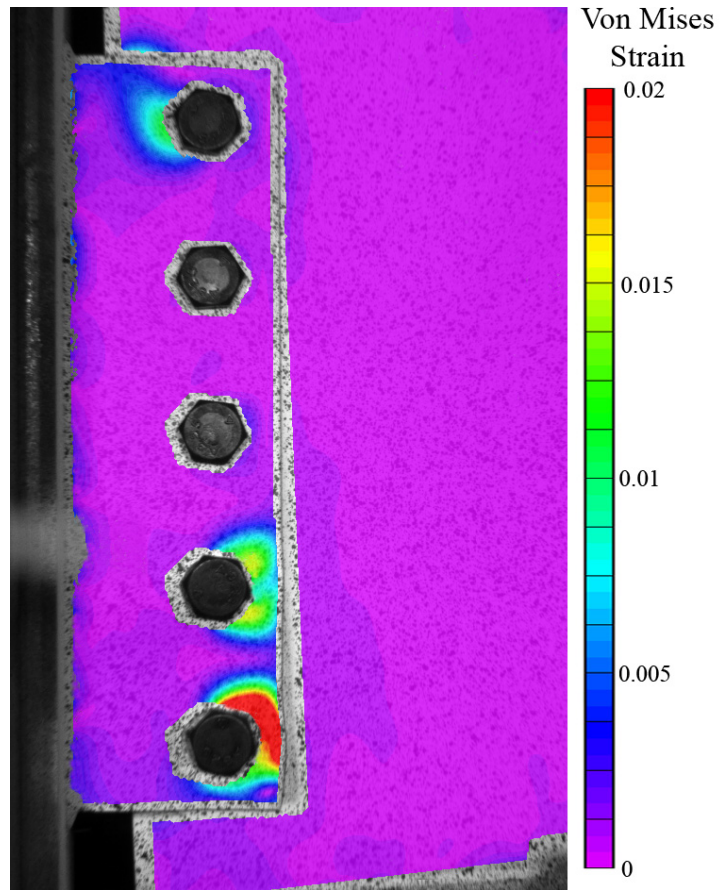
Figure 5.1. Von Mises strain showing localized bearing effects at bolt locations.
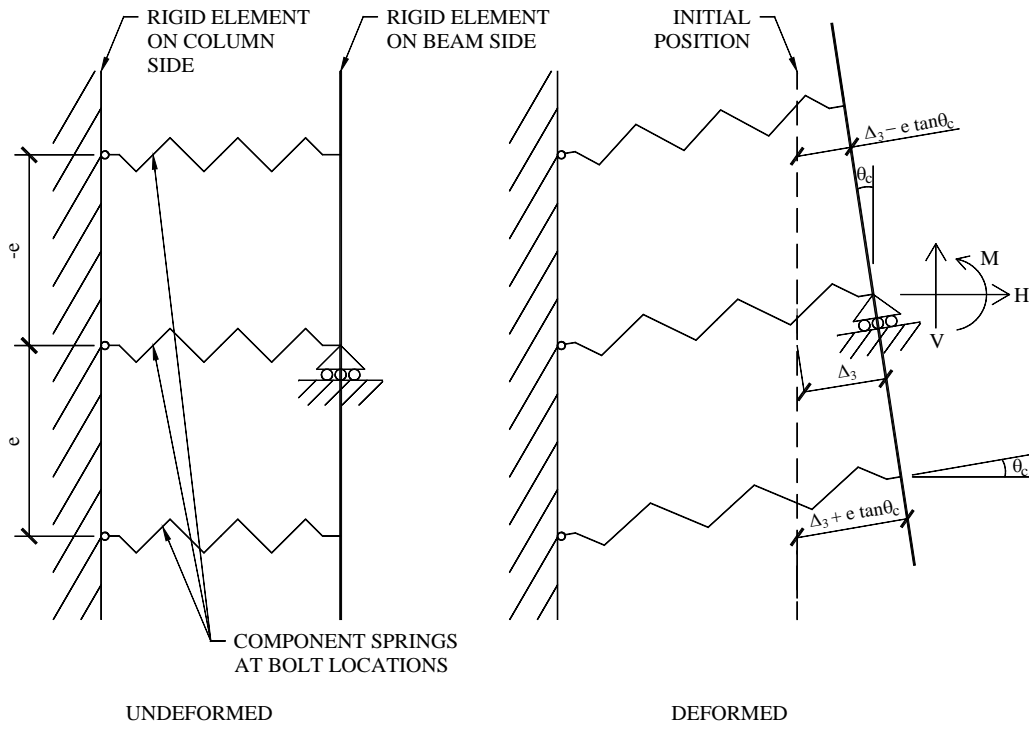
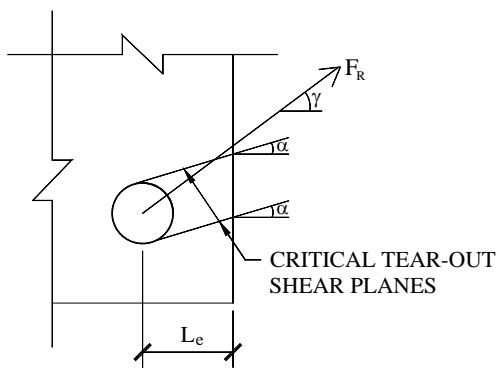**Figure 5.2. Mechanical model of shear tab connections.**

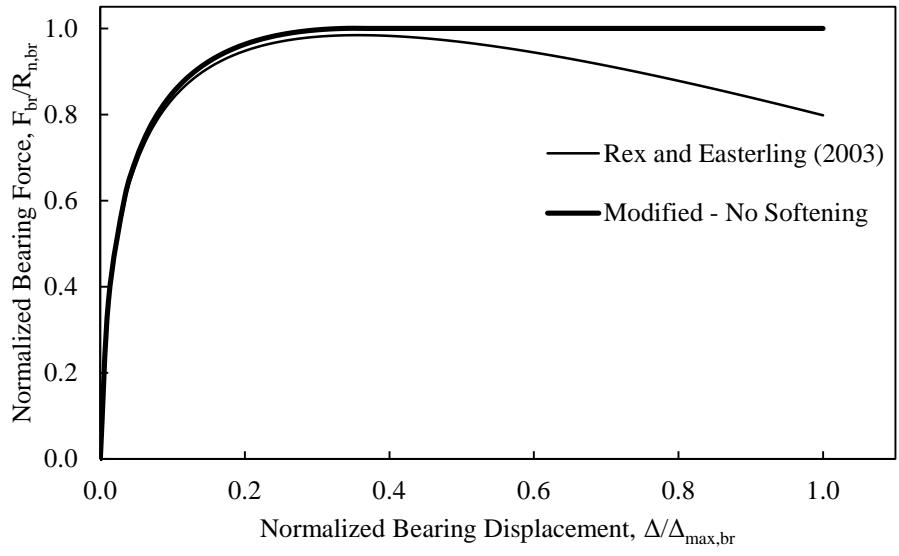**Figure 5.3. Bolt tear-out under an inclined force.**

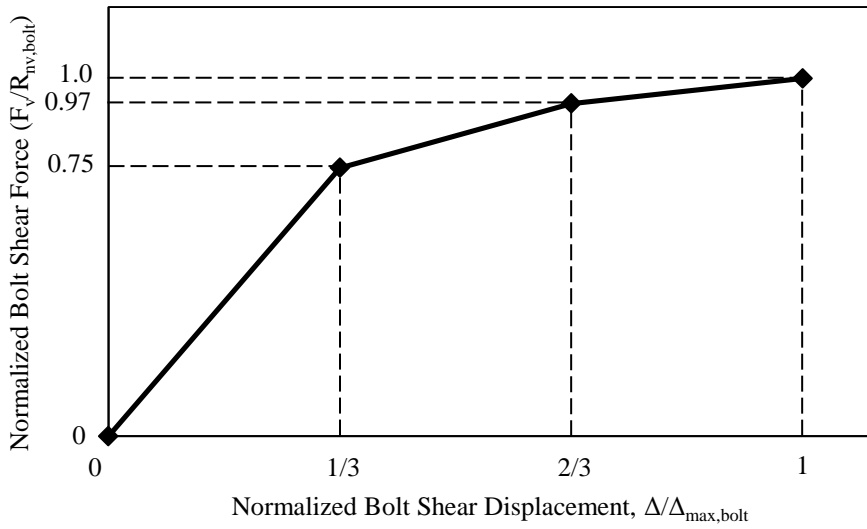**Figure 5.4. Force versus displacement for bearing deformations.**

Figure 5.5. Force versus displacement for bolts in single shear.
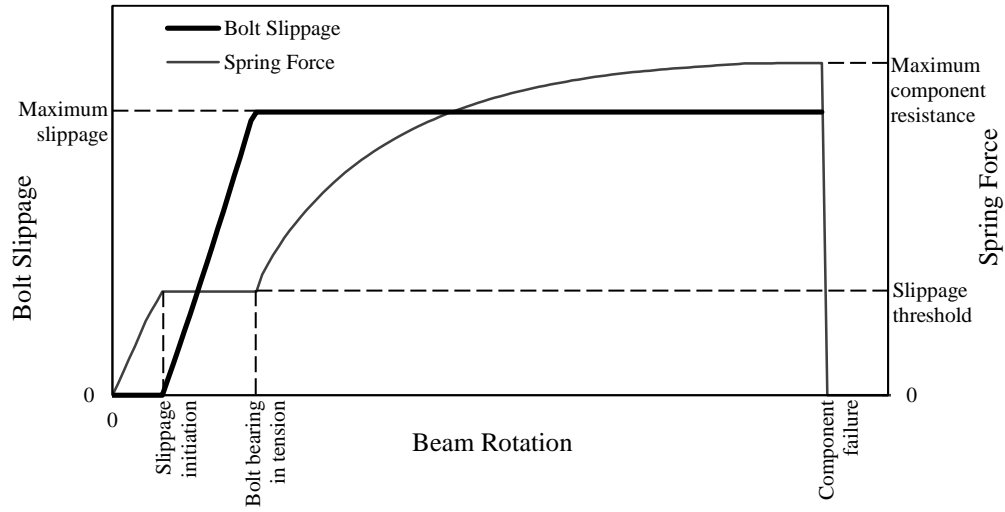
Figure 5.6. Representative behaviour of the bolt slippage function for a bottom bolt.
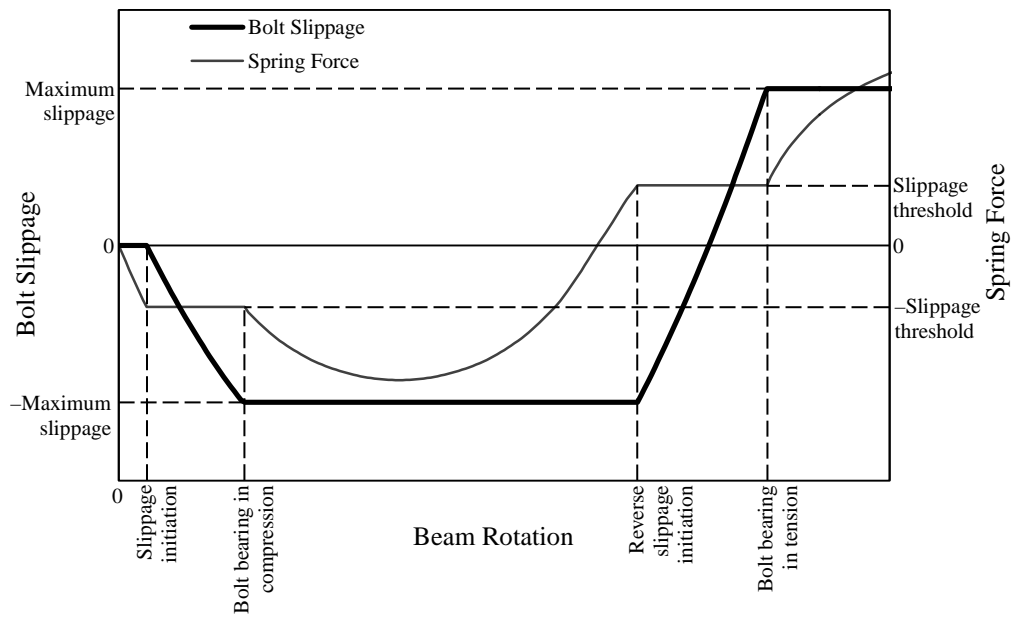
Figure 5.7. Representative behaviour of the bolt slippage function for a top bolt (including force direction change).
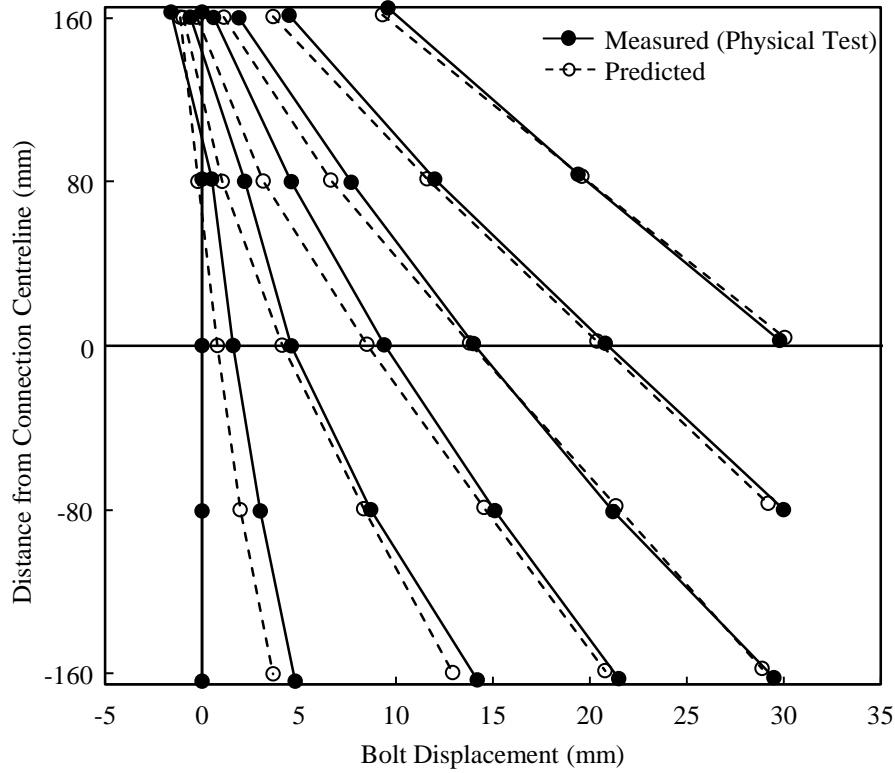
Figure 5.8. Prediction of bolt displacements.
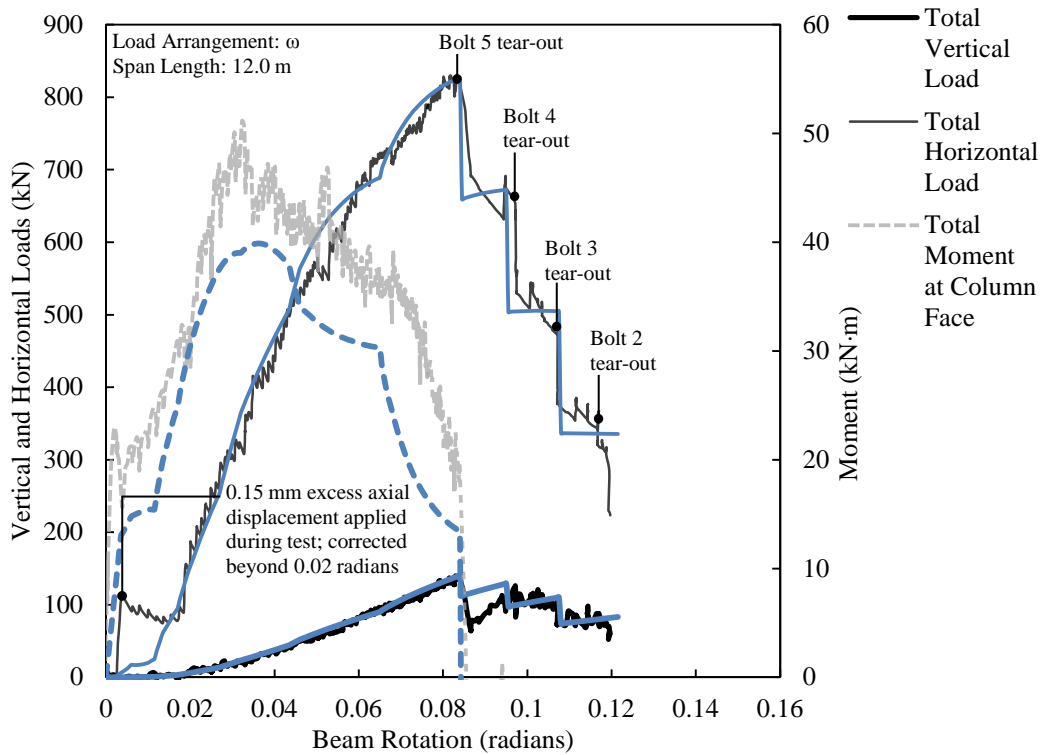
Figure 5.9. Comparison of mechanical model and test results for ST5A-2.

143
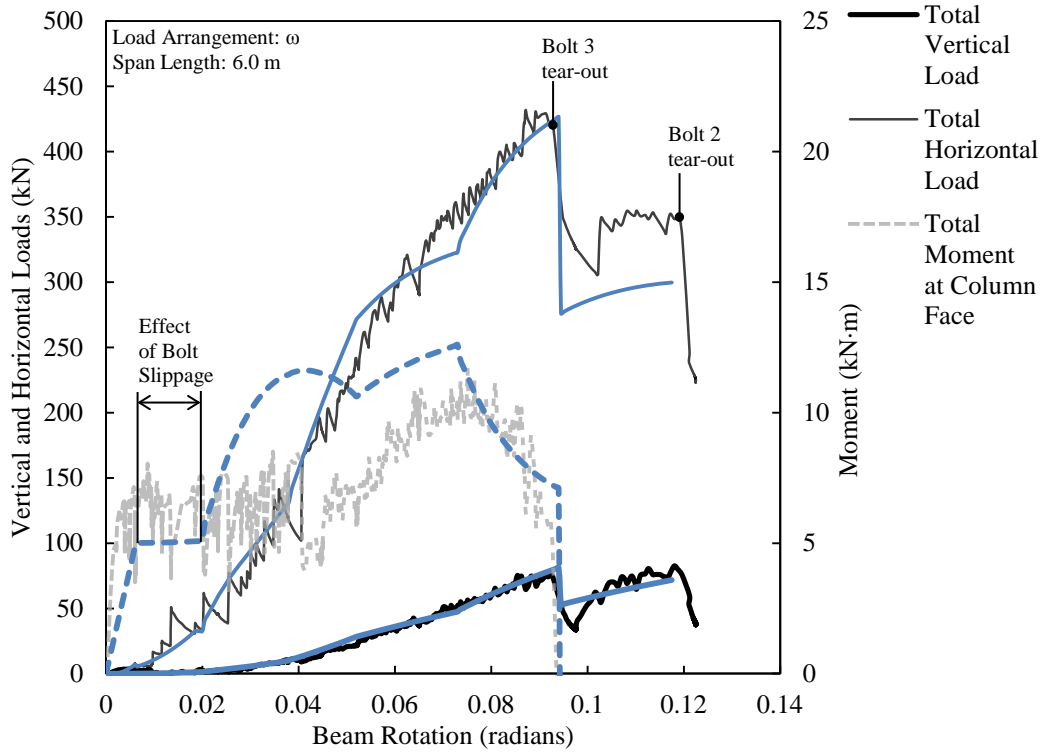
Figure 5.10. Comparison of mechanical model and test results for WA3A-2.
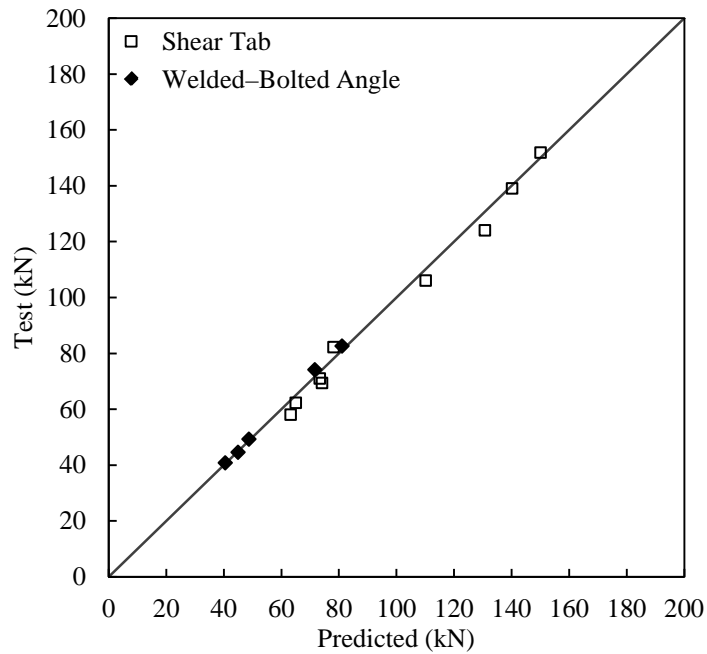
Figure 5.11. Comparison of mechanical model and test results for maximum vertical load.
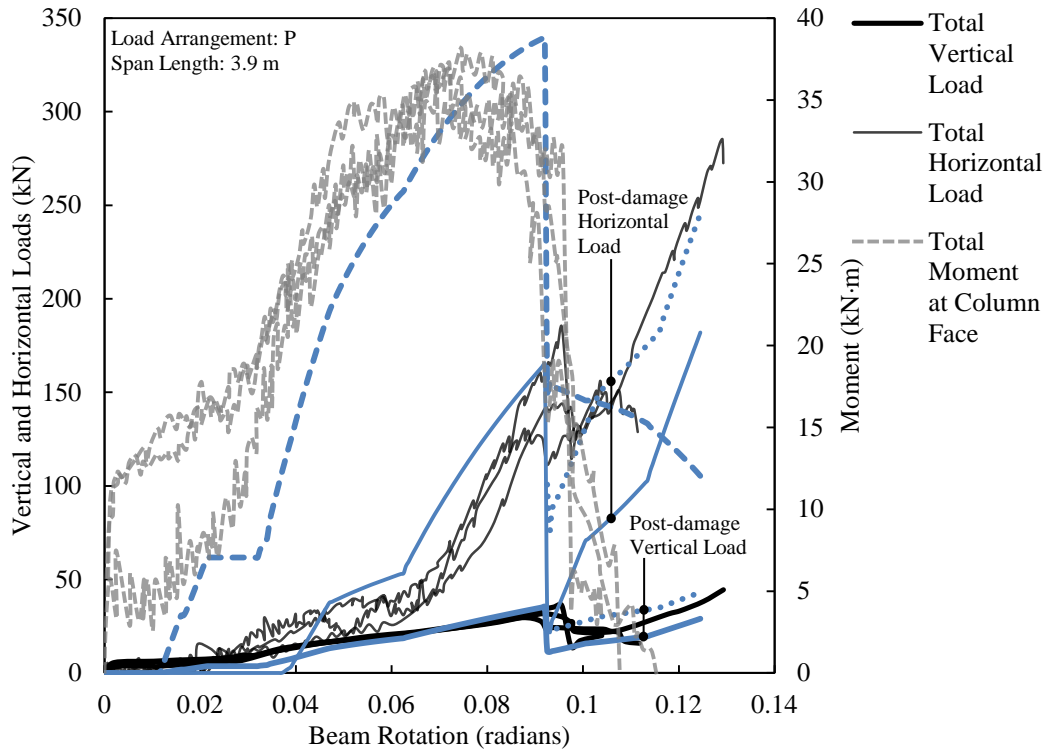
Figure 5.12. Comparison of mechanical model and test results for four-bolt column removal tests by Thompson (2009).
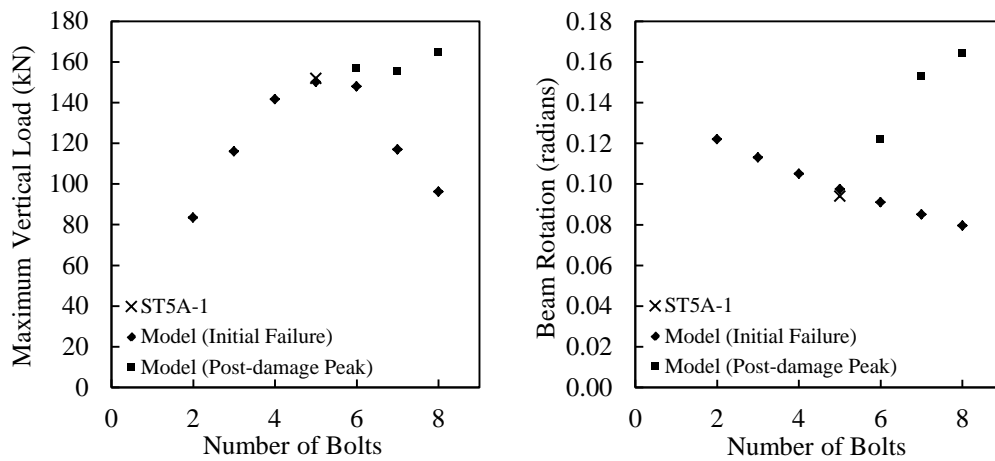
Figure 5.13. Parametric study: number of bolts.
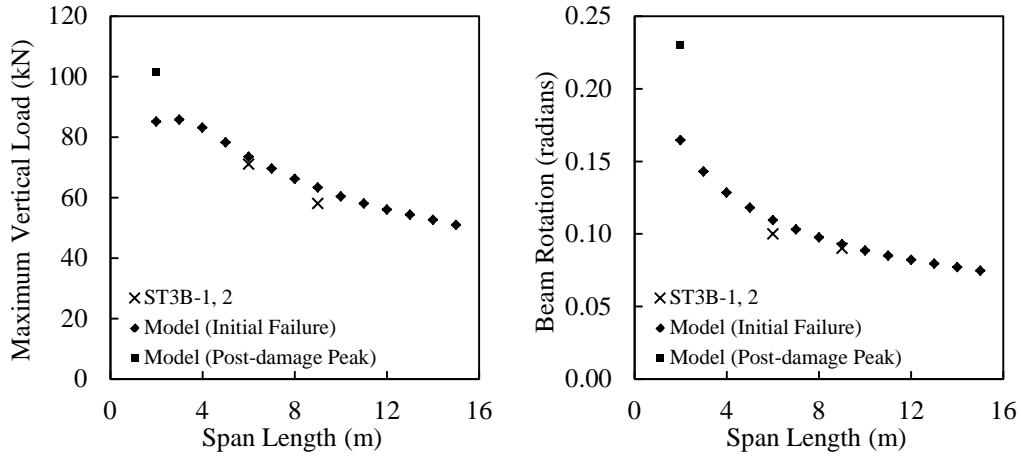
Figure 5.14. Parametric study: span length (three-bolt connections).
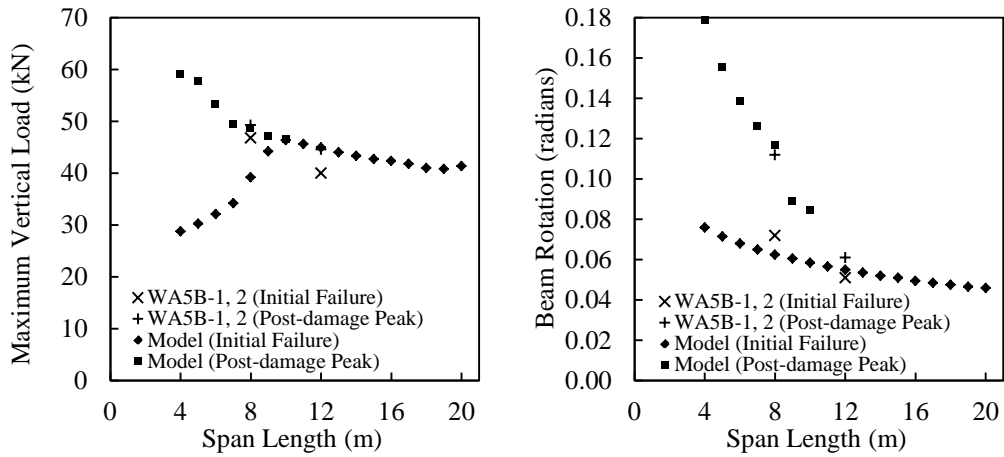
Figure 5.15. Parametric study: span length (five-bolt connections).
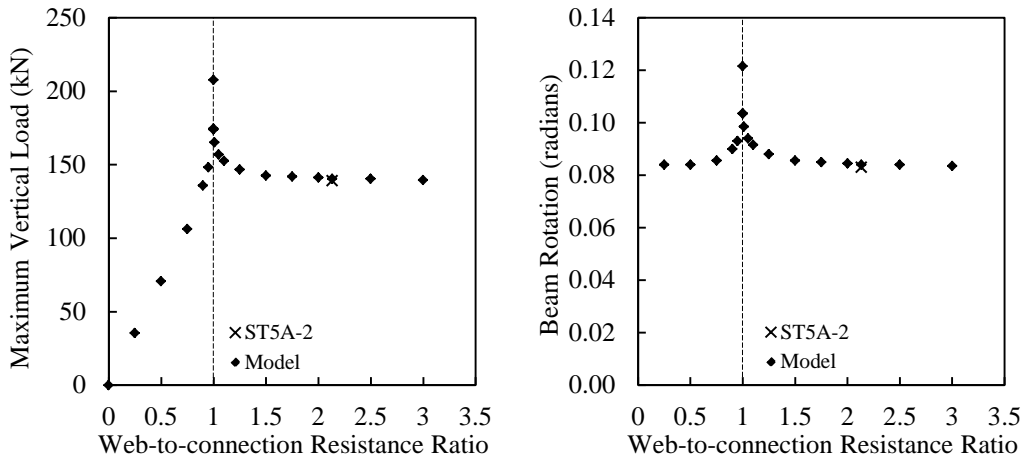
Figure 5.16. Parametric study: beam web tear-out resistance.

146
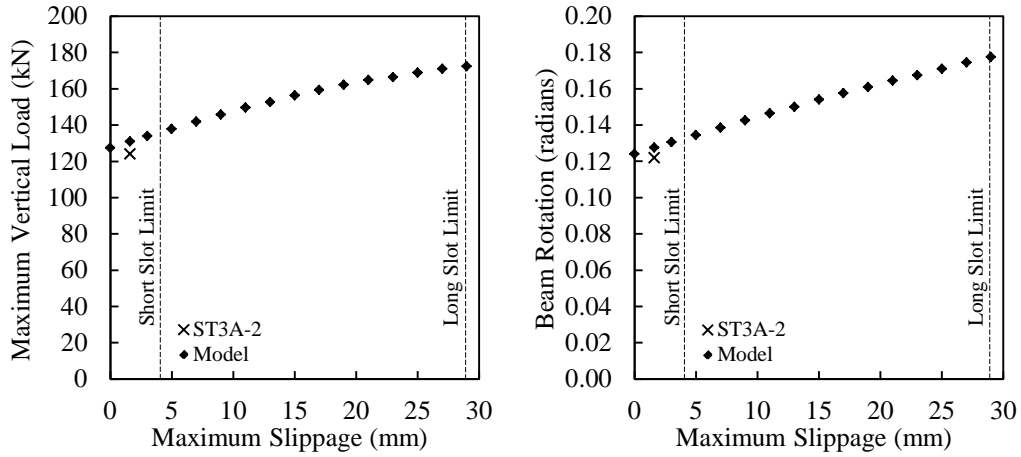
Figure 5.17. Parametric study: maximum bolt slippage.
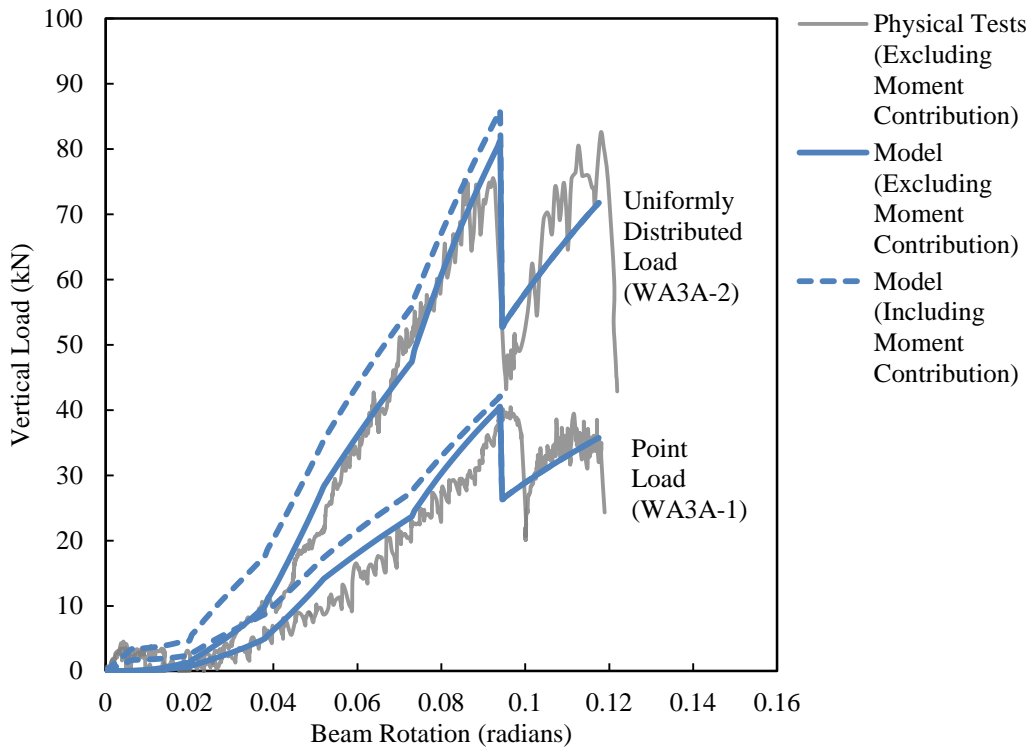
Figure 5.18. Parametric study: loading arrangement (proportion of vertical to horizontal load).
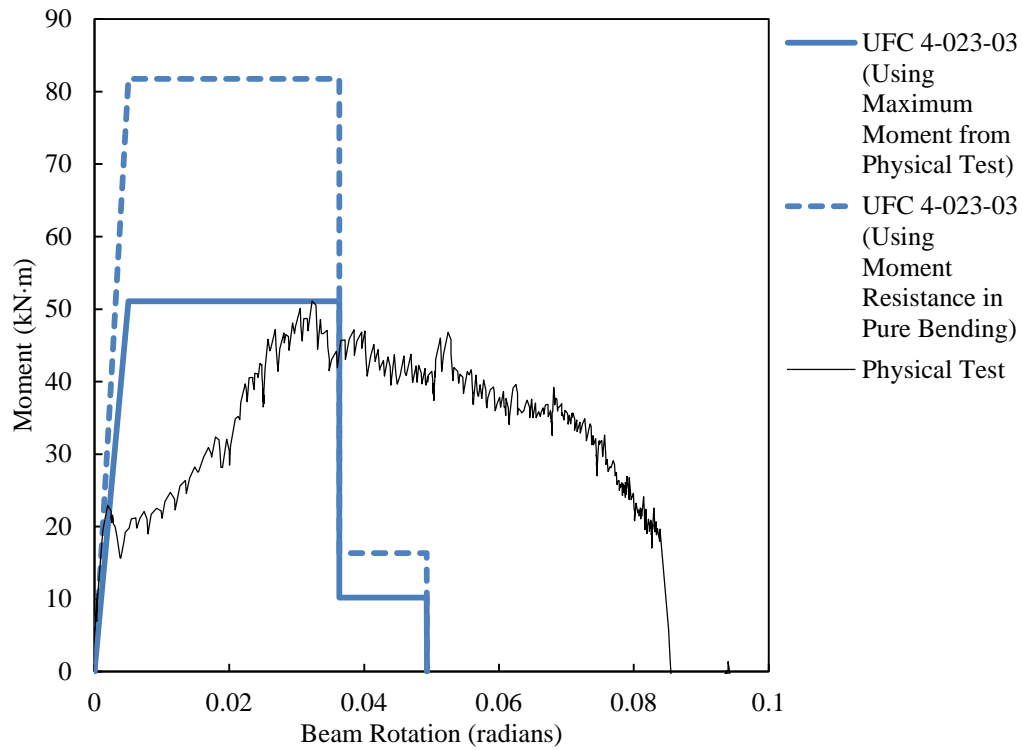
Figure 5.19. Comparison of moment versus rotation from UFC 4-023-03 (DoD, 2009) and test results for ST5A-2.
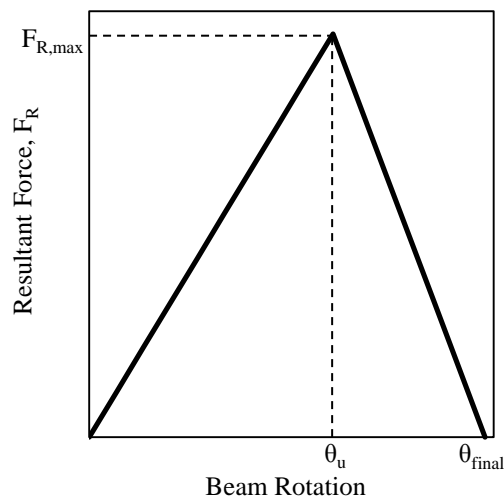
Figure 5.20. Generalized bilinear force versus rotation relationship.
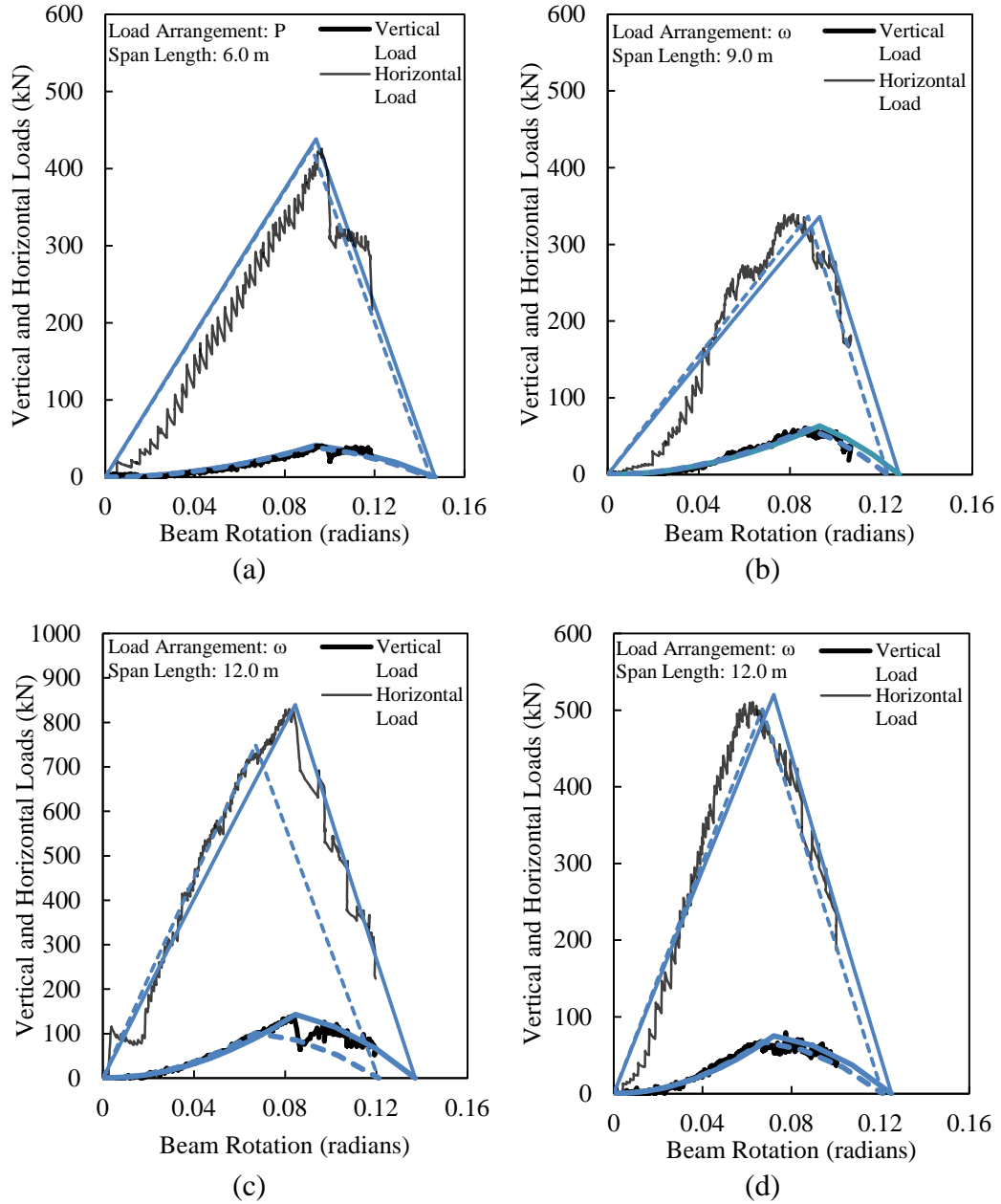
Figure 5.21. Simplified connection modelling results for: (a) WA3A-1, (b) ST3B-2, (c) ST5A-2, and (d) ST5B-2.

6. DISCUSSION AND ANALYSIS: BOLTED–BOLTED ANGLE CONNECTIONS

The behaviour of both single and double angle connections bolted to the beam web and to the column flange ("bolted–bolted") was observed to be dominated by the unfolding of the angles under catenary tension through the formation of plastic hinges, and the eventual tearing along one of these plastic hinges, as reported in Chapter 4. Thus, for the sake of the discussion and analysis contained in this chapter, bolted–bolted single and double angle connections are considered together.

The mechanical model for shear tab connections (discussed in Chapter 5) has been adapted to predict the behaviour of bolted–bolted angle connections under a column removal scenario. Modelling definitions that are unique to this connection type are described in Section 6.1, and the model results are validated by comparison to physical tests. The mechanical model is then used to perform a parametric study that examines the effects of several variables on connection robustness. The effects of adding seat and top angles to bolted–bolted angle connections are also discussed. Design recommendations based on the results of the physical tests and mechanical modelling are presented, and the performance of bolted–bolted angle connections is compared to that of shear tab and welded–bolted angle connections.

6.1. Mechanical Model Definitions

Figure 6.1 shows the von Mises strains recorded by the optical strain imaging system during a bolted–bolted single angle test, which are highest at plastic hinges that have formed along a partial depth of the angle heel and column bolt line. (The area to the immediate right of the column bolts—where there is no strain contour overlaying the black and white speckle pattern—is out of the field of view of the second camera, and thus strain data could not be generated there.) The partial-depth hinges shown in the figure correspond to a state of relatively high rotational and axial stiffnesses at a low beam rotation (and associated low

150

tensile demands). Connection stiffness decreases when rotational and axial demands cause the plastic hinges to develop along the full depth of the angle. Relatively high strains are also visible in Figure 6.1 on the beam web near the top bolt, as a result of the top of the angle bearing (in compression) against the column flange. The von Mises strains recorded on the compressive side of the angle hinge at the column bolt line are lower than those that would be expected on the tensile side (abutting the column flange, not visible in the figure), due to the net axial tension that is carried by the angle.

The mechanical model discretizes the angle into segments representing the tributary area surrounding each bolt, using individual component springs at each bolt location. However, the strain concentrations shown in Figure 6.1 are not discretized at bolt locations, as was the case for the shear tab connections (as shown in Figure 5.1); rather, a strain gradient that increases from the top of the angle to the bottom is evident. While bolts represent discrete points of force transfer in both connection types, the inclusion of component springs only at bolt locations is recognized as a rougher approximation of behaviour for bolted–bolted angle connections.

6.1.1. Angle Bending under Tension

6.1.1.1. Force–Displacement Relationship

The dominant deformation mechanism in bolted–bolted angles in tension is described in Chapter 4 as "unfolding" due to the development of plastic hinges in the angle. As a result of the horizontal eccentricity (perpendicular to the beam web) between bolts at the beam web and at the column flange, the catenary tension imposed by column removal places severe bending demands on the angle legs, even at relatively small tensile loads. Previous research programs that included the physical testing of angle connections under tension only (De Stefano and Astaneh (1991), Owens and Moore (1992), and Yang (1997)) have characterized the tensile force versus displacement curve as bilinear, as shown schematically in Figure 6.2. This simplified relationship can be defined

151

completely by four parameters: initial stiffness, K_1; yield force, $R_{y,angle}$; hardening stiffness, K_2; and nominal resistance, $R_{n,angle}$. The first three of these parameters are defined below; the determination of $R_{n,angle}$ is discussed in Section 6.1.1.2. Using these definitions, the yield displacement, $\Delta_{y,angle}$, and maximum displacement, $\Delta_{max,angle}$, can also be determined.

Figure 6.3 shows the free body diagram of a bolted–bolted angle segment under applied horizontal tension, H, and vertical load, V. The eccentricity between the force H at the two bolts introduces a perpendicular thrust force, T, resulting in the inclination of the line of action of the resultant force, F, at the angle β. This angle is a function of the initial position of the bolts, the unfolding deformation of the angle, and the moments resisted in the angle at the bolts. The moment at point 1 (Figure 6.3) is expected to be greater than the moment at point 4 through small deformations because of the greater rotational demand there; this difference decreases the angle β and the corresponding magnitude of the thrust force. However, if the state is considered where plastic hinges are fully formed at these points and strain-hardening is neglected, the line of action of force F acts in a straight line between the bolts, as shown. For the calculation of the thrust force acting on the bolts, the conservative simplifying assumption that the internal moments are equal at the bolts is used.

Four potential plastic hinge locations are indicated in Figure 6.3. The hinges labelled 1 and 3 were typically the first to form during the physical tests. In three tests (SA3A-2, SA3A-4, and SA3B-5) these hinges were the only two that were visible before failure. Hinge 1 was not consistently located at the discrete position shown in the figure (at the edge of the bolt hole). In Series B specimens (which had thinner angles), the angle deformed severely around the bolt head on the compressive side of the hinge; on the tensile side, the hinge line (and the eventual tear) tended to meander between the edge of the bolt hole at bolt locations and the centreline of the bolt line between bolts. Because the angles used for Series A specimens were thicker, localized deformations around the bolt heads were less

severe, and hinge 1 formed along a straighter vertical line near the edges of the bolt holes.

Pucinotti (2001) proposed the use of a bilinear force–displacement relationship (similar to that shown in Figure 6.2) to define discrete component springs at bolt locations for the mechanical modelling of bolted–bolted angle segments under tension. Before developing plastic hinges, bolted–bolted angles display a relatively high initial stiffness. Pucinotti (2001) recommended Equations 6.1 and 6.2 for the calculation of yield force and initial stiffness, respectively. Equation 6.1 determines the horizontal force to initiate yielding as that required to form plastic hinges at each end of a rigid bar with an effective length, L_{eff}, which is taken as the distance from the centreline of the perpendicular angle leg to the edge of the column bolt hole, as shown in Figure 6.3. A tributary width spanning half of the vertical distance between the centres of the bolts (or, for edge bolts, the distance from the centre of the bolt to the free edge of the angle) on each side of the bolt is used to determine the width, b. In Equation 6.2, the boundary condition at the bolt (assuming a fixed condition at the angle heel) is accounted for by the coefficient a, where the value is taken between 3 (for rotationally pinned) and 12 (for rotationally fixed). Pucinotti (2001) recommended a value of $a = 6$ for the partially-fixed condition expected at the bolt. All other variables in Equations 6.1 and 6.2 have been defined previously. The bilinear force–displacement relationship assumes that the initial stiffness, K_1, remains in effect until two fully-plastic hinges have formed. Although this neglects the gradual softening that is expected as partial plastic hinges develop, the physical test results for angles in pure tension suggest that this occurs over a negligible displacement range.

The stiffness of the angle following plastic hinge formation, K_2, is much lower than the initial stiffness, although it is still positive due to material hardening and the increasing efficiency of the deformed section as a tension membrane. Therefore, the slope of the force versus displacement curve during hardening is a function of both material properties and connection geometry. The literature suggests that this stiffness can be approximated as linear and determined

153

empirically as a fraction of the initial stiffness, expressed herein as the product of K_1 and a plastic hardening stiffness factor, μ_p, as shown in Equation 6.3. The reported value of μ_p varies significantly among testing programs. De Stefano and Astaneh (1991) demonstrated good agreement with test results using a value of $\mu_p = 0.026$; Owens and Moore (1992) observed that test results suggested $\mu_p \approx 0.10$ (although the referenced initial stiffness was lower than that calculated using Equation 6.2 because it included bolt deformation and slippage); and Pucinotti (2001) proposed the use of $\mu_p = 0.020$ for mechanical modelling. Good agreement with the hardening stiffnesses recorded in the current testing program is achieved using $\mu_p = 0.035$ for all Series A specimens, and $\mu_p = 0.075$ for all Series B specimens.

$$R_{y,angle} = \frac{b\,t^2\,\sigma_y}{2\,L_{eff}} \qquad\qquad [6.1]$$

$$K_1 = \frac{a\,E\,b\,t^3}{12\,L_{eff}^{\,3}} \qquad\qquad [6.2]$$

$$K_2 = \mu_p K_1 \qquad\qquad [6.3]$$

6.1.1.2. Failure Criterion

As reported in Chapter 4, all bolted–bolted angle specimens failed by one of two failure modes: tearing of the gross section along the plastic hinge near the angle heel (typical of Series A specimens), or tearing of the net section along the plastic hinge near the column bolt line (typical of Series B specimens). The failure criterion adopted for angle tearing in the mechanical model considers the combined stress state at the plastic hinge locations. The assumed average stress state on an element at the column bolt line is shown in Figure 6.4. In a recent study of double angle connections under combined moment and shear, Gong (2013) extended the von Mises yield criterion to predict the ultimate load condition by suggesting that tear initiation occurs when the von Mises stress at a plastic hinge exceeds the uniaxial ultimate tensile strength of the material. The von Mises stress is calculated by assuming that the normal stress at the location of a plastic hinge is equal to the uniaxial material yield strength and the shear stress

154

is averaged over the cross-sectional area of the angle. The resulting capacity predictions demonstrate excellent consistency with the test results reported by Gong (2013), achieving an average test-to-predicted ratio of 1.00 and a coefficient of variation of 0.047 for the seven tests completed.

The failure criterion proposed by Gong (2013) is used in the current mechanical model. The stress element shown in Figure 6.4 is located at the plastic hinge near the column bolt line, where the angle leg becomes parallel to the column flange. On this element, the horizontal force, H, acts perpendicular to the angle leg and induces the shear stress shown as τ_{xy}. The vertical force, V, induces shear stress on the same face of the element, but in the perpendicular direction (shown as τ_{xz}). Normal stress, σ_{xx}, results from the bending of the plastic hinge and the thrust force, and is assumed to be equal to the material yield strength, as shown in Equation 6.4. Average shear stresses, τ_{xy} and τ_{xz}, are calculated by dividing the total force transferred at an individual bolt by the net area, A_{nv}, of the angle cross-section attributed to it, as shown in Equations 6.5 and 6.6, where $A_{nv} = t(b-d)$. The failure criterion, shown in Equation 6.7, compares the resulting von Mises stress to the ultimate strength of the material. Solving Equations 6.4 through 6.7 gives Equation 6.8, which provides an expression for the nominal resistance (in the direction of the resultant applied load), $R_{n,angle}$, of an angle segment under combined moment, shear, and tension.

$$\sigma_{xx} \approx \sigma_y \qquad [6.4]$$

$$\tau_{xy} = \tau_{yx} \approx \frac{H}{A_{nv}} \qquad [6.5]$$

$$\tau_{xz} = \tau_{zx} \approx \frac{V}{A_{nv}} \qquad [6.6]$$

$$\sigma_u = \sqrt{\sigma_{xx}^2 + 3(\tau_{xy}^2 + \tau_{xz}^2)} \qquad [6.7]$$

$$R_{n,angle} = A_{nv}\sqrt{\frac{\sigma_u^2 - \sigma_y^2}{3}} \qquad [6.8]$$

The combined stress state at the plastic hinges near the angle heel under the same set of assumptions is less critical than at the column bolt line, primarily because

the cross-sectional area at the heel is not reduced by the presence of bolt holes. The critical shear stress that causes failure (according to Equation 6.7) is further reduced at the heel because the deformed shape of the angle causes the resultant forces to become more aligned with the normal-stress direction of the angle legs (e.g., the x–x direction shown in Figure 6.4 for the angle leg at the column face). However, in the case of the thicker Series A specimens, angle tearing at this location governed failure. There are several possible explanations for this shift in failure location that are not captured by the failure criterion described in this section. Tears at the column bolt line were observed to initiate at bolt hole locations, where localized stress concentrations were induced by the bolt head through the thickness of the deformed angle forced to bend around it. These stress concentrations are more severe in thinner material. Furthermore, normal strains at the extreme fibre at a plastic hinge in a thicker angle are greater than those at the same location in a thinner angle for plastic hinges that have rotated the same amount. Thus, normal stresses may become more critical to the initiation of tearing, and the assumption that the normal stress is approximately equal to the material yield strength throughout hinge rotation may not be valid in these cases. An additional factor that may have contributed to the shift in failure location is the possibility of lower fracture toughness in the region near the angle heel (similar changes in material properties in the so-called "k-areas" near the flange-to-web fillets of W-sections leading to fracture at these locations were reported by Tide (2000)). Based on the current data and modelling approach, a failure criterion that predicts the change in tear location with confidence could not be developed. However, performing an analysis that considers the critical stress state at the net section along the column bolt line provides a failure criterion that consistently underpredicts the ultimate capacity of the connection when tearing at the gross section occurs, and is therefore considered useful for a discussion of bolted–bolted angle robustness. The extent of the effect of this limitation on the accuracy of the mechanical model is discussed further in Section 6.2.

6.1.2. Bolt Shear and Tension

The force–displacement relationship and nominal resistance for bolts in single shear have been defined in Chapter 5. For double angle connections, the bolts at the beam web act in double shear. According to the capacity equation given in CSA S16-09 (CSA, 2009), bolts in double shear have twice the nominal resistance of bolts in single shear. For simplicity, the force–displacement relationship given for bolts in single shear is applied to bolts in double shear. The double shear condition is more complex and is expected to result in a slightly different deformation rate; however, the difference is assumed to be negligible compared to the deformation of the angle in tension, and thus does not warrant further refinement of the model.

The nominal resistance of a bolt loaded in tension, $R_{nt,bolt}$, is calculated according to the provisions of CSA S16-09 (CSA, 2009), reproduced in Equation 6.9, where the nominal value of the static ultimate strength of the bolt, σ_u, is used (a similar capacity equation is presented in AISC 360-10 (AISC, 2010)). Moore et al. (2008) showed that the expected capacity of bolts in tension exceeds this nominal value, with an average test-to-predicted ratio of approximately 1.22. Thus, for the purpose of predicting the behaviour of the test specimens, the expected bolt capacity is taken as that given by Equation 6.9 multiplied by 1.22. The failure criterion used for bolts in combined shear and tension is shown in Equation 6.10 (also from CSA S16-09), where F_v and F_t are the shear and tension loads applied to the bolt, respectively. The tensile deformation of the bolt is not included in the mechanical model; it is negligible compared to other sources of deformation because of the high axial stiffness of bolts in tension and the clamping force applied under the snug-tight condition. Prying force is calculated according to the procedure outlined in the *Handbook of Steel Construction* (CISC, 2010), which results in typical maximum prying forces in the column bolt equal to 20 kN for Series A specimens and 10 kN for Series B specimens. This force amplification is accounted for when Equation 6.10 is applied.

$$R_{nt,bolt} = 0.75 \frac{\pi d^2}{4} \sigma_u \tag{6.9}$$

$$1 = \left(\frac{F_v}{R_{nv,bolt}} \right)^2 + \left(\frac{F_t}{R_{nt,bolt}} \right)^2 \tag{6.10}$$

6.1.3. Unstiffened Column Deformations

For tests where the column did not have web stiffeners, column deformations attributed to web bending (as described in Section 4.3.1.2 for single angle connections) and flange bending (as described in Section 4.4.1.2 for double angle connections) are included in the model. For single angle connections, the column torque introduced due to the horizontal eccentricity between the column web and the column line of bolts caused the column web to bend. In the mechanical model, a component spring is added to simulate the resulting contribution to the total axial deformation. The stiffness of this spring is based on the treatment of the web as an elastic cantilever beam fixed at the end away from the connection, with a concentrated moment applied by the flange on the connection side. Flange bending for double angle connections is treated similarly, assuming the flange acts as an elastic cantilever beam that is fixed at the centreline of the column web (due to symmetry) with a point load applied at the column bolts.

6.1.4. Compressive Arching Action

The overall geometry of a symmetric two-bay frame with the central column removed is shown in Figure 6.5. Connections that are significantly stiffer in compression than in tension—as is typical of bolted–bolted angle connections—tend to rotate about points at different elevations at the two beam ends, separated by a vertical eccentricity between instantaneous centres of rotation, e_{icr}. This eccentricity is more severe for deeper connections, and is particularly pronounced for seat and top angle connections. The "unrestrained path of motion" in the figure shows that if rotation were to occur about the points at the remaining columns, the points at the removed column (if horizontally unrestrained) would initially move towards each other at small beam rotations because of the eccentricity. Since the condition of symmetry restrains the central column to

158

move vertically, a compressive "arch" (two compressive struts) forms. At larger beam rotations, catenary tension is developed as the unrestrained paths of motion of the two beams diverge. In connections where the compressive and tensile stiffnesses are approximately equal, the eccentricity between the instantaneous centres of rotation at the two beam ends is small, and catenary tension begins to develop at very low rotations.

In a real structure, the axial shortening demand during compressive arching action may be substantially accommodated by bolt slippage and the flexibility of the surrounding structure. Further research is recommended to identify structural systems in which the compressive arching mechanism can be mobilized for effective collapse prevention following column removal; for bolted–bolted angle connections similar to those included in the current study, such performance is not expected.

6.2. Load Development and Capacity Prediction Results

The validity of the mechanical model discussed above is evaluated by simulating all 21 bolted–bolted angle connection tests described in Chapters 3 and 4, and six pure tension tests performed by Owens and Moore (1992). This section compares the load development and ultimate capacity predicted by the mechanical model to the physical test results.

6.2.1. Load Development Prediction

Figure 6.6 shows the load versus rotation relationships for the five-bolt single angle specimen SA5B-1, overlain with the mechanical model results (in blue). A similar plot is provided for the three-bolt double angle specimen DA3B-1 in Figure 6.7. Both plots, which are representative of the agreement achieved for Series B tests, demonstrate consistency between the mechanical model and physical test results. (Series A results are discussed separately, following the discussion of Series B results.)

The bilinear force–displacement curve defined in the model for angles in tension results in the overall connection displaying high initial stiffness, followed by decreased stiffness once plastic hinging has occurred across the full depth of the angle. This behaviour is consistent with the stiffness evolution observed during the physical tests.

Compressive arching action is predicted by the mechanical model during the initial stages of all tests, although the predicted compressive forces and range of rotations during which they are present are smaller for three-bolt connections (due to the smaller dimension of e_{icr}—shown in Figure 6.5—than for deeper connections) and Series A specimens (which have compressive and tensile stiffnesses that are more similar than do Series B specimens). In cases where compressive arching action was observed during the physical tests, the mechanical model demonstrates similar behaviour, and transitions to the catenary tension phase occur at appropriate beam rotations (as seen for specimen SA5B-1 in Figure 6.6). Some of the physical tests did not exhibit compressive arching action (including specimen DA3B-1, shown in Figure 6.7); the relatively small compressive deformation demands generated by the model for these cases were likely accommodated in the test by bolt slippage and flexibility of the test set-up. This discrepancy is not considered significant during later stages of the test, where the model accurately predicts the development of the catenary action that causes failure.

The general pattern of moment development is also consistent between the model and the physical tests. The high initial stiffness of connection components in tension and compression results in the development of relatively high moment at low beam rotations. As the extent of plastic hinging increases, moment decreases from the initial peak. Finally, as rotation increases (along with tensile component forces), the moment again increases until failure occurs. The moment predicted by the mechanical model is less accurate (as a percentage) than the vertical and horizontal load predictions throughout the tests; however, the magnitude of

moment throughout testing is exceptionally low, and the discrepancies are considered to be inconsequential to the understanding of connection behaviour.

Component failure in the mechanical model is governed by tearing of the angle at the net section, which is consistent with the typical test results for Series B specimens. The complete instantaneous element removal at failure that is implemented by the mechanical model causes load decreases that are more abrupt and severe than those recorded during the gradual tear propagation in the physical tests. Although this tends to cause the underprediction of post-damage loads, the mechanical model is still considered to provide a reasonable approximation of damage evolution.

Figures 6.8 and 6.9 show the load versus rotation curves for specimens SA3A-3 and SA3A-4, respectively, overlain with the mechanical model results (in blue). The model produces slightly more accurate predictions of overall connection stiffness for Series A specimens than for Series B specimens, resulting in predicted loads and moments with less variability from the physical test results before failure. However, while damage initiation is predicted with reasonable accuracy for specimen SA3A-4 (Figure 6.9), the model fails prematurely for specimen SA3A-3 (Figure 6.8). These two specimens had identical nominal geometries, with the only unique variable between the two tests being the assumed span length. With a 9.0 m span, specimen SA3A-3 had a higher rate of axial elongation demand than the 6.0 m span assumed for SA3A-4 (as prescribed by Equation 3.7). Under otherwise similar conditions, specimen SA3A-3 failed at much higher loads and at a slightly greater rotation. This irregularity also exists between specimens SA5A-1 and SA5A-2, although the opposite (and more intuitive) correlation is recorded for Series B specimens with different span lengths (that is, specimens with longer spans failed at lower loads and rotations).

While the stress-based failure criterion defined herein produces reasonably consistent failure predictions for the Series B specimens, it fails to predict this increased capacity of some Series A specimens. Series A specimens exhibited

gross section failure near the angle heel, rather than the net section failure near the column bolt line observed in Series B specimens. In all cases where failure was governed by tearing of the gross section near the angle heel, the deformations at failure (and corresponding loads) are bounded below by mechanical model results employing the failure criterion adopted for the current study (i.e., failure on the net section), and above by results assuming a similar failure criterion on the gross section. Hence, it seems that both explanations for the discrepancy between the mechanical model and the test results (discussed in Section 6.1.1.2) may be acting concomitantly; that is, for Series A specimens, the critical stresses at the net section are reduced by the shift of the plastic hinge location away from the centreline of the bolt holes, and the strength and/or toughness of the cross-section near the angle heel are lower than at the bolts. Nevertheless, the adopted failure criterion does not predict the shift in failure location for the specimens fabricated from thicker angles. For all the Series A specimens tested, it consistently results in conservative ultimate load predictions.

6.2.2. Ultimate Capacity Prediction

Figure 6.10 compares the maximum vertical load recorded in the physical tests with the values predicted by the mechanical model. The model demonstrates accuracy and consistency when predicting maximum vertical load for Series B specimens. Results for Series A specimens all plot above the diagonal line that represents a test-to-predicted ratio of unity, exemplifying both the inaccuracy and the conservatism of the failure criterion when connections fail along the angle heel. The horizontal line to the right of each Series A result extends to the predicted capacity if failure along the gross section (rather than the net section) is assumed in the mechanical model to demonstrate that test specimens failed at loads bounded by predictions under these two assumptions (as discussed in Section 6.2.1). Table 6.1 (for Series B specimens) and Table 6.2 (for Series A specimens) list the maximum moment (M_{max}), maximum horizontal and vertical loads (H_{max} and V_{max}, respectively), and rotation at initial failure of the angle at the extreme bolt (θ_u) predicted by the model, as well as the test-to-predicted ratios

for each. Due to uncertainties associated with the prediction of angle tearing under combined loading, the mechanical model is less accurate for bolted–bolted angle connections than for shear tab connections (as reported in Chapter 5). However, acceptable levels of accuracy and consistency for the prediction of connection strength and ductility are achieved for Series B specimens, and the model provides conservative results for Series A specimens.

6.2.3.   Comparison to Pure Tension Tests by Owens and Moore (1992)

A series of tests on bolted–bolted double angles in pure tension was performed by Owens and Moore (1992) to investigate their ability to carry prescribed tie forces independently of other demands. Six of these tests have been simulated using the mechanical model to further validate its suitability for predicting bolted–bolted angle behaviour under tension. Two tests were completed on each of three connection geometries. Four five-bolt connections with two different angle thicknesses (8 mm and 10 mm) were tested, as well as two seven-bolt connections with 10 mm thick angles. (An additional five tests were not included because they either had multiple vertical lines of bolts at the beam web or failed by bolt tear-out in the beam web.) The pure tension tests are modelled using empirically-determined plastic hardening stiffness factor values (μ_p, from Equation 6.3) that generate good agreement with the test results and are consistent with the values used for the models of connections from the current testing program. The value of $\mu_p = 0.035$ used for the 9.5 mm thick angles tested in the current program also provides good agreement between the hardening stiffnesses of the mechanical model and the physical tests for the 10 mm thick angles tested by Owens and Moore (1992). A value of $\mu_p = 0.070$—which is between the values adopted for the 9.5 mm and 6.4 mm thick specimens in the current program—generates good results for the 8 mm thick angle specimen.

Figure 6.11 shows the force versus displacement curves for these tests, overlain with the mechanical model results (shown as dashed blue lines). The mechanical model results demonstrate that the force–displacement relationship defined for the component springs, which is dominated by the unfolding of the angles under

163

tension, is representative of actual connection behaviour. The use of Equations 6.1 and 6.2 to calculate yield force and initial stiffness of the angles approximates the initial connection response. The horizontal portion of the curves generated by the mechanical model at the initial stage of the test are caused by discrete bolt slippage (initiated at a 30 kN threshold at each bolt location), which appears to occur as a more gradual process in the physical tests. Hardening stiffness values that are consistent with those used for the models of the current testing program provide good agreement between the curves after yielding has occurred.

Independently from the empirically-determined plastic hardening stiffness factor, μ_p, the nominal resistance predicted by Equation 6.8 is accurate when applied to the case of pure tension for all three geometries tested. Thus, the failure criterion has been shown to provide good results for three different loading conditions: combined moment and shear (by Gong (2013), who proposed the criterion); pure tension (for physical tests by Owens and Moore (1992)); and combined moment, shear, and tension (for Series B connections in the current program).

Two other research programs that included the physical testing of angles under tension are summarized in Chapter 2. Pure tension tests by De Stefano and Astaneh (1991) were not modelled because the angles were welded to the column; tests by Yang (1997) were not included because the loading ceased prior to failure, at relatively small displacements.

6.3.   Parametric Study

The validated mechanical model has been used to perform a parametric study that examines the effects of several variables on the strength and ductility of bolted–bolted angle connections following column removal. Figures 6.12 through 6.16 show the maximum vertical load and corresponding beam rotation predicted by the model for specimens that are identical to the reference test specimens shown in the figure, except for the parameter being studied.

6.3.1. Number of Bolts

The physical test results demonstrate that the higher connection strength achieved when the number of bolts (and concomitant connection depth) in a single vertical row (spaced at 80 mm) is increased from three to five directly results in improved maximum vertical load following column removal. However, similarly to the parametric study results reported for shear tab connections in Chapter 5, this trend is not expected to continue for connections with more than five bolts. As shown in Figure 6.12, the maximum vertical load increases significantly as the number of bolts increases from two to five, but it plateaus for deeper connections because of the increased axial demands at the extreme bolt location (caused by the large eccentricity between the connection centreline and the extreme bolt, e, in Equation 5.8).

Although the deepest connections shown in Figure 6.12 experience initial failure at lower beam rotations and do not achieve significant benefits to the maximum vertical load, the plots do not depict the increased duration of the post-damage vertical load plateau that is achieved if the tear propagation is along the column bolt line and progresses in a stepwise manner between bolt holes. For a specimen with eight bolts that is otherwise similar to SA5B-3, the mechanical model predicts that the connection maintains 75 % of the maximum vertical load through a rotation of 0.16 radians, even though initial failure occurs at 0.09 radians. The high post-damage ductility (due to the inherent redundancy of connections with many bolts) is favourable for energy absorption following column removal, even though the increase in maximum vertical load following column removal is not proportional to the number of bolts. Additionally, deep connections increase the prominence of compressive arching action as a vertical load-carrying mechanism.

6.3.2. Span Length

The effect of span length on connection performance can be examined by directly comparing physical test results reported in Chapter 4 for connections where the only varied parameter was the span length (as was the case for the following pairs

of specimens: SA3A-2/SA3A-4 (repeated test) and SA3A-3, SA3B-1 and SA3B-4, SA3B-2 and SA3B-3, SA5A-1 and SA5A-2, SA5B-2 and SA5B-3, DA3B-1 and DA3B-2, and DA5B-1 and DA5B-2). In general, for Series B specimens, longer span lengths are correlated with lower maximum vertical loads and rotations. The mechanical model predicts that this trend continues for span lengths outside of the range considered in the physical tests, as shown in Figure 6.13 (for a series of three-bolt connections) and Figure 6.14 (for a series of five-bolt connections). Figure 6.15 shows a similar trend predicted by the mechanical model for Series A specimens, although the opposite correlation between strength and span length is present in the physical testing data—an irregularity discussed in Section 6.2.1.

Compressive arching action becomes more pronounced for short span lengths, as the vertical component of the line of arching action (i.e., the compressive strut) shown in Figure 6.5 becomes larger in proportion to the horizontal component. However, vertical loads resisted during the tensile catenary action phase still govern capacity in all cases modelled (even for very short span lengths).

6.3.3. *Horizontally Slotted Holes*

Figure 6.16 shows the potential benefit achieved by increasing the rotational ductility of a bolted–bolted angle connection through the introduction of horizontally-slotted holes to the angle leg connected to the beam web. Controlling all variables except for maximum slippage implies that the angle leg length would need to increase in proportion to slot length to provide a constant horizontal edge distance. Many of the resulting specimen geometries that have been modelled do not use standard angle sizes, and thus, would not be practical; however, the modelling exercise allows a detailed examination of the parameter for the full range of potential slot lengths. The maximum vertical load predicted by the mechanical model for the specimen shown was improved by 15 % when a long slotted hole was used in place of a standard hole. The addition of slotted holes provides less benefit for bolted–bolted angle connections than for shear tab connections for two reasons: first, bolted–bolted angle connections are able to

166

accommodate very large axial deformations through plastic hinge formation even without slotted holes and, second, the maximum usable localized deformation after bolt slippage occurs decreases for bolted–bolted angle connections with slotted holes because of the contribution of the increased proportion of applied vertical load at large rotations to the stress-based failure criterion (which wasn't the case for the shear tab connections, as these were controlled by a deformation-based failure criterion).

6.3.4. Angle Thickness

Test specimens were fabricated from one of two different angle sizes with different thicknesses: L89×89×9.5 (Series A) or L89×89×6.4 (Series B). The behaviour of bolted–bolted angle connections under the demands of column removal is significantly affected by the thickness of the angle. Series A connections have higher strength and stiffness than Series B specimens with similar geometries. Connections fabricated from each type of section typically failed at similar rotations; therefore, the stiffer Series A specimens consistently resisted significantly higher maximum vertical loads than the thinner connections. However, as a result of the change in failure location between the two series, tear propagation in Series A specimens was unstable, and the post-damage behaviour was much less ductile than for Series B specimens.

6.3.5. Number of Angles

A comparison of test results for single and double angle connections reveals that the deformation mechanisms and failure modes of each were similar, as were the measured rotation at failure and load capacity (per angle). The test set-up included lateral bracing near the connection, which prevented the asymmetry of a single angle from resulting in lateral beam displacement that may have led to a differentiation in behaviour from the symmetric double angle case.

6.3.6. Column Stiffness

The mechanical model predicts maximum flange displacement at the connection bolts for the single angle tests with unstiffened columns equal to 2.5 mm for SA3B-5 (compared to 3.0 mm recorded during the physical test) and 3.0 mm for SA5B-4 (compared to 3.8 mm recorded during the physical test). For a single angle connected to a full-length column (rather than the column stub used in the tests), the increased length of the column web in bending and restraint provided by the continuous column flange are expected to significantly reduce the magnitude of this displacement to the point that it is typically negligible compared to other sources of deformation.

For double angle connections with an unstiffened column, both the predicted values of maximum flange displacement and those recorded during the physical tests were much less than for the single angle case (caused by column web bending), because the column flange was much thicker than the column web, and the cantilevered segment in bending was shorter. The resulting predicted maximum displacement at the connection bolts is 0.5 mm for DA3B-3 (compared to 0.9 mm recorded during the test) and 0.7 mm for DA5B-3 (compared to 1.3 mm recorded during the test). These deformations are considered inconsequential to overall connection performance.

6.3.7. Loading Arrangement

The proportion of vertical-to-horizontal load carried by the connection, which is largely controlled by the arrangement of the applied loads, is more significant to the performance of bolted–bolted angle connections than that of shear tab connections. The deformation-based failure criterion shown to replicate shear tab connection behaviour accurately is independent of load perpendicular to the tear-out direction (as discussed in Section 5.3.7). This is not the case for bolted–bolted angle connections because the force-controlled failure criterion in the model includes stresses induced by both vertical and horizontal loads. However, between the cases of an assumed central point load and a uniformly distributed

load, the effect is observed to be small. Figure 6.17 compares the vertical load development with rotation for two bolted–bolted single angle specimens tested under different loading arrangements. Both the physical tests and the mechanical model show that under a uniformly distributed load the connections fail at slightly lower rotations than similar specimens under a central point load, because of the increased rate of development of shear stress with rotation.

The moment developed in bolted–bolted angle connections is even smaller than for shear tab connections; consequently, including its contribution to the vertical load (i.e., including the second term in Equations 3.4 and 3.5 for the calculation of the vertical load at equilibrium) is even less significant. The dashed curves in Figure 6.17 show the predicted load development including the contribution of moment for specimens SA5B-1 and SA5B-3 (SA5B-1 had the most significant moment relative to the maximum vertical load of all the bolted–bolted angle specimens tested). The contribution of moment to the vertical load results in only a marginal increase in the maximum vertical load. The increase is more significant at low rotations than at failure, due to the relatively high moment that develops during compressive arching action. However, the eventual development of catenary tension dominates behaviour at failure. Neglecting the moment for the design and modelling of bolted–bolted angles under combined loading is a slightly-conservative simplifying assumption that produces reasonable results due to their high rotational flexibility.

6.4.   Combined Seat and Top Angle Connections

Six physical tests of bolted–bolted angle connections combined with seat and top angles were completed: two single angles with three bolts at the beam web (SA3C-1 and SA3C-2), two single angles with five bolts at the beam web (SA5C-1 and SA5C-2), and two double angles with three bolts at the beam web (DA3C-1 and DA3C-1). Details of the geometry of these specimens and individual test results are reported in Chapters 3 and 4, respectively.

The effects of adding seat and top angles to bolted–bolted angle connections are generally similar to those discussed in Section 5.4 for the case of shear tab connections. The rotational stiffness and moment capacity of bolted–bolted web angles with seat and top angles added were significantly increased as compared to otherwise-similar web-only connections, resulting in maximum moments that were approximately four to eight times greater than those recorded during tests of bolted–bolted web angles alone. Moment is predominantly developed by the seat and top angle because they act farthest from the neutral axis. Thus, the magnitude of the maximum moments achieved were similar for both shear tab and bolted–bolted angle connections combined with seat and top angles for connections that had the same overall depth (although total moments developed with shear tabs at the beam web were slightly greater because shear tabs have higher rotational stiffnesses than bolted–bolted angles). The large vertical eccentricity between the seat and top angles results in significant arching action at low rotations. The relatively high moments recorded during this stage of the tests suggest that, in some cases (particularly for deeper connections and shorter span lengths), the maximum static vertical load that was eventually achieved under catenary action may be approached during arching action if the contribution of moment to equilibrium is considered, although it is not likely to be exceeded by a substantial amount. As was discussed for shear tab connections combined with seat and top angles in Section 5.4, the loads developed during arching action in semi-rigid connections are more important to collapse resistance following column removal than those developed by rotationally-flexible shear connections (especially for considerations of energy absorption under dynamic loading) and should be included in column-removal analyses.

The performance of bolted–bolted single angles following column removal is generally improved by the addition of seat and top angles. Three-bolt single angle specimens displayed increases in the maximum vertical load capacity of 67 % (SA3C-1) and 73 % (SA3C-2); for five-bolt specimens, improvements of 27 % (SA5C-1) and 51 % (SA5C-2) were recorded. Similarly, for the three-bolt double angle specimens, the maximum vertical load capacity was increased by 24 %

170

(DA3C-1) and 59 % (DA3C-2). The benefit to the three-bolt single angle connections is greater (as a percentage) than for the five-bolt single angle and three-bolt double angle connections because the resistance added by the seat and top angles is larger in proportion to the capacity of the web connection alone. The improvements are greater for longer spans (the second specimen in each pair) because the increased rate of axial elongation corresponding to longer spans increases the extent to which the top angle is engaged in catenary tension prior to the failure of the web angle. The top angle is also more fully engaged in tension prior to failure of the web angle for bolted–bolted angles than for shear tab connections with similar overall geometries, because bolted–bolted angles generally endure greater axial deformations prior to failure; thus, bolted–bolted angles achieve a greater benefit from the addition of seat and top angles than do shear tabs.

6.5. Design Recommendations

6.5.1. Connection Detailing

Bolted–bolted angle connections have remarkable ductility, which is directly related to their ability to accommodate large axial deformations through the formation of plastic hinges in the angle(s). Favourable performance may also be achieved if failure is governed by ductile tear-out of the bolts at the beam web, as demonstrated for shear tab connections. In some cases, the flexibility of bolted–bolted angles may allow significant deformation even in connections governed by bolt failure, with the proviso that the extent of connection deformation from angle unfolding prior to bolt failure produces overall connection response that is sufficiently ductile. Although the use of slotted holes has been recommended for shear tab connections in Chapter 5, they would be less practical and less effective for use in bolted–bolted angle connection geometries similar to those included in the physical tests.

6.5.2. Retrofit Options

For angle connections that are bolted to both the beam and the column, retrofitting options are not typically as labour-intensive as for welded connections. As discussed in Section 6.3.4, 9.5 mm thick angles were observed to perform better than 6.4 mm thick angles, due to their improved strength and stiffness with comparable ductility prior to the initiation of tearing. Thus, connection performance under the effects of column removal could be improved by replacing existing angles with thicker ones; furthermore, the extent of the improvement achieved could be quantified using the approach outlined in Section 6.5.4. If bolt failure is predicted to govern connection strength and limit ductility, larger and/or higher-strength bolts could be installed. For existing single angle connections, the addition of a second angle on the opposite side of the beam web offers twice the strength of a single angle without sacrificing connection ductility (as discussed in Section 6.3.5), and eliminates the asymmetry that could cause detrimental effects in members that are not fully laterally-braced.

The potential benefit of adding seat and top angles to an existing bolted–bolted angle connection is demonstrated by the results reported in Chapter 4, and is discussed further in Section 6.4.

6.5.3. Tie Force Evaluation

This section evaluates the tie force requirements from the *International Building Code* (ICC, 2012) for bolted–bolted angle connections in a similar manner to the approach taken in Section 5.5.3 for shear tab connections. Table 6.3 lists the factored shear resistance, V_r (calculated according to CSA S16-09 (CSA, 2009), using specified minimum material strengths), and compares the factored horizontal resistance (H_r) and the maximum horizontal load measured during the test (H_{max}) to the *International Building Code* tie force resistance requirement of $2/3\ V_r$. The horizontal resistance of bolted–bolted angle connections under pure tension is calculated using Equation 6.11, as half its yield capacity in pure tension at the net section. This design equation was proposed by Owens and

172

Moore (1992) as a conservative approximation of the tie force resistance of double angles under pure tension, and has since been used in guidelines for tie force design (such as *Joints in Steel Construction: Simple Connections* (SCI, 2002)).

$$H_r = 0.5\, A_{nv}\, \sigma_y \qquad\qquad [6.11]$$

The horizontal resistance predicted by this equation slightly exceeds the tie force requirement for all connections shown in Table 6.3. In contrast, significant variation is present in the ratio of the measured maximum horizontal loads (in the presence of moment and vertical load) to the tie force requirement, as a consequence of the significant interaction effects of the combined loading.

The maximum vertical load under the column loss recorded in the physical tests (which is normalized in Table 6.3 as a function of factored shear resistance) varies between 0.08 and 0.29, even though all the specimens met the tie force requirement with similar adequacy. Figure 6.18 plots this ratio (representative of vertical load-carrying performance) against the normalized tie force resistance (i.e., the calculated factored tensile resistance) for both shear tab and bolted–bolted angle connections. Linear regression of the data shows that a positive correlation exists, although it is very weak (the coefficient of determination is equal to 0.32). While improving the horizontal resistance of shear connections may provide some benefit to connection performance under a column removal scenario, the scatter in the data suggests that the tie force approach does not adequately account for the effect of several other critical parameters that impact connection performance under combined loading. The small fraction of the design shear strength that was recorded during the bolted–bolted angle connection tests further suggests the limited ability of shear connections to prevent collapse following complete column removal without contributions from other structural components.

6.5.4. Simplified Connection Modelling for Column Removal Analysis

6.5.4.1. Moment–Rotation Relationship

The moment developed in bolted–bolted angle connections under the demands induced by column removal are not accurately modelled by the generalized curves provided in UFC 4-023-03 (DoD, 2009). Moment is typically largest at low rotations, as a result of high initial stiffness (and, in some cases, compressive arching action); at higher rotations, moment is heavily influenced by the presence of tensile catenary force. These characteristics are not included in the generalized curves provided in UFC 4-023-03, nor are adequate guidelines for the determination of the maximum moment under combined loading that is required to define the curves. The discrepancy between the modelling guidelines from UFC 4-023-03 and the test result for specimen DA3B-1 is illustrated in Figure 6.19. Two UFC 4-023-03 model curves are shown: the solid line represents the case where the maximum moment for the modelling curve is defined according to that measured during the test (thus including the limiting effects of axial tension on moment development), and the dashed line represents the case where the moment capacity is calculated in pure bending, which leads to the overestimation of the moment developed following column removal. The maximum rotation is given as a function of the bolt group depth in UFC 4-023-03; however, as demonstrated in the parametric study (Section 6.3), this value is significantly affected by several other parameters.

As discussed in Section 6.3.7, connection moment contributes little to collapse prevention following column loss—especially at large rotations, where any potential compressive arching action has ceased. Bolted–bolted angle connections are inherently flexible, and develop even lower moments than shear tab connections. Thus, modelling them as rotationally pinned is expected to result in reasonable approximations of collapse resistance. If a rotational spring is included to represent connection bending resistance in column removal analysis, it should include the effects of axial forces on moment development. The results of the bolted–bolted angle connection tests support the notion that the development of

174

catenary force is more important to shear connection resistance following column loss than the moment–rotation relationship. Thus, a simplified model of bolted–bolted angle connections that includes catenary force development under a column removal scenario is proposed in the following section.

6.5.4.2. Force–Deformation Relationship

The bilinear form of the proposed force versus deformation curve is illustrated schematically in Figure 6.20, which has the same form as the proposed curve for the simplified modelling of shear tab connections, as described in Section 5.5.4.2 (it is repeated here for convenience). The approach described in this section is a simplified adaptation of the more detailed mechanical model described in this chapter that eliminates the iterative process used in the computer program by identifying the critical parameters controlling connection behaviour and providing guidelines for defining them.

Because the force versus displacement curve of the dominant deformation mechanism (angle bending under tension) is bilinear, the overall connection force versus axial displacement is also approximately bilinear. This is different from shear tab connections, where the counteraction of the decreasing connection stiffness and increasing rate of axial deformation demand with beam rotation resulted in an approximately linear force versus rotation curve. However, for bolted–bolted angle connections within the range of rotations considered, similarly accurate predictions result from assuming that the resultant force develops linearly with respect to either rotation or axial displacement; thus, the former is adopted for consistency with the approach taken for shear tab connections.

The modelling parameters defined below apply to bolted–bolted angle connections where failure is governed by angle tearing. Selection of appropriate failure criteria is essential for the application of the procedure to connections that may be governed by other failure modes (for example, bolt failure or tear-out). Additionally, stiffness definitions must be adjusted for connection arrangements

where deformation is not dominated by angle bending under tension and beam rotation. The connection forces and rotations corresponding to the points that define the generalized bilinear curve in Figure 6.20 can be approximated using the following procedure:

1. Construct a bilinear force versus displacement curve of the form shown in Figure 6.2 for the segment of angle attributed to each bolt. This curve is defined by four parameters: $R_{y,angle}$ (Equation 6.1), K_1 (Equation 6.2), K_2 (Equation 6.3), and $R_{n,angle}$ (Equation 6.8). The maximum displacement, $\Delta_{max,angle}$, may be shifted to the right of the point determined by these equations to approximate the contribution of all other sources of deformation at the nominal resistance, $R_{n,angle}$, including bolt slippage, bolt shear deformation, and bolt bearing deformation. Shifting $\Delta_{max,angle}$ to the right by 3 mm plus the assumed bolt slippage (1.6 mm for standard holes) results in a force–displacement relationship that approximates the combined behaviour of all active deformation components for the bolted–bolted angle specimens tested and modelled in the current program.

2. Calculate rotation at initial failure, θ_u, by solving Equation 5.8 for θ_c, setting Δ_{spring} equal to $\Delta_{max,angle}$ and e equal to the vertical eccentricity between the connection centreline and the extreme bolt. If including ductile post-damage response in the model (as was observed when tearing occurred along the column bolt line), calculate the rotation at final failure, θ_{final}, by solving Equation 5.8 with e equal to the vertical eccentricity between the connection centreline and the last bolt to fail. If brittle failure of the gross section near the angle heel is assumed, take $\theta_{final} = \theta_u$.

3. Calculate the axial deformation at each bolt location in the connection at initial failure using Equation 5.8, setting θ_c equal to θ_u.

4. Determine the total resultant force at initial failure, $F_{R,max}$, by summing the component forces at θ_u, using the force versus displacement curve constructed in Step 1 and the deformations calculated in Step 3.

5. Plot the resultant force versus rotation curve as shown in Figure 6.20. The curve defines the behaviour of the connection as a single spring that acts

176

in the direction of the resultant force, γ (from horizontal). (As discussed in Section 5.1.1.2, $\gamma = \theta_c$ for point loads and $\gamma \approx 2\theta_c$ for uniformly distributed loads.) The curve can be manipulated to generate horizontal and vertical load versus rotation curves, and load versus displacement curves.

The load development curves generated using this approach for four representative bolted–bolted angle specimens are compared to the physical test results in Figure 6.21. (The results from the detailed mechanical model for the same four specimens are shown in Figures 6.6 through 6.9.) The curves show the results for an assumed ductile failure mode (i.e., stable vertical progression of the tear in the angle) as a solid blue line, and a vertical dashed blue line representing the post-damage response for an assumed brittle failure mode. The simplified model produces general agreement with the test results; however, the accuracy is limited by the same uncertainties as the detailed mechanical model (which are discussed in Section 6.2). In particular, the assumed net section failure mode provides a conservative capacity prediction for bolted–bolted angle connections that failed at the gross section near the angle heel (e.g., those depicted in Figure 6.21(c) and (d)).

The region of compressive arching action observed in the testing program and detailed modelling of some bolted–bolted angle connections is not included in the simplified model. If the effects of the compressive forces developed as a result of arching action are considered important to the objectives of a modelling effort, a mechanical model that can capture the phenomenon (similar to the one described in Section 6.1) should be used. However, in the bolted–bolted angle connections included in the current program, the forces developed during this stage are considered inconsequential to the ultimate response of the connection. Furthermore, the vertical loads at low rotations under the immediate development of catenary tension assumed in the simplified connection model—which are relatively small compared to forces developed at higher rotations—are similar to those expected from the contribution of connection moment to vertical load development during compressive arching action, as demonstrated in Figure 6.22

for specimen SA5B-1. While the simplified connection modelling procedure produces a disparity between the measured and predicted horizontal loads during arching action (as seen in Figure 6.21(a) for the same specimen as shown in Figure 6.22), the model results in reasonable predictions of vertical load response throughout the loading history, which is adequate for most practical column removal analysis applications.

Table 6.1. Comparison of mechanical model and physical test results for Series B specimens.

Specimen ID	Mechanical Model Results				Test-to-Predicted Ratio			
	M_{max} (kN·m)	H_{max} (kN)	V_{max} (kN)	θ_u (radians)	M_{max}	H_{max}	V_{max}	θ_u
SA3B-1	5.1	176.6	23.5	0.133	1.554	0.945	1.003	1.057
SA3B-2	6.0	162.1	49.8	0.153	1.131	0.809	0.947	0.997
SA3B-3	5.1	172.1	44.8	0.130	1.360	0.847	0.943	1.004
SA3B-4	6.0	168.0	26.7	0.158	1.362	0.911	0.997	1.060
SA3B-5	5.1	165.8	43.9	0.132	1.656	0.761	0.862	0.981
SA5B-1	30.3	240.4	29.5	0.122	0.985	1.073	1.119	1.090
SA5B-2	30.3	235.3	56.5	0.120	0.944	1.046	1.062	1.021
SA5B-3	19.0	252.8	52.3	0.103	1.355	0.950	1.024	1.049
SA5B-4	20.4	240.0	50.4	0.105	1.230	0.809	0.955	1.053
DA3B-1	10.7	324.2	99.7	0.153	0.979	1.064	0.991	0.977
DA3B-2	9.4	344.3	89.7	0.130	1.019	0.895	0.803	0.950
DA3B-3	9.4	342.3	89.5	0.130	1.103	1.030	0.918	0.923
DA5B-1	46.3	470.5	113.0	0.120	1.018	1.111	1.131	0.904
DA5B-2	29.0	505.7	104.5	0.103	1.249	1.083	1.040	0.942
DA5B-3	46.3	465.6	112.3	0.120	1.284	1.135	1.143	0.983
				Average	1.215	0.965	0.996	0.999
				Maximum	1.656	1.135	1.143	1.090
				Minimum	0.944	0.761	0.803	0.904
				Standard Deviation	0.217	0.122	0.096	0.055
				Coefficient of Variation	0.178	0.127	0.097	0.055

Table 6.2. Comparison of mechanical model and physical test results for Series A specimens.

Specimen ID	Mechanical Model Results				Test-to-Predicted Ratio			
	M_{max} (kN·m)	H_{max} (kN)	V_{max} (kN)	θ_u (radians)	M_{max}	H_{max}	V_{max}	θ_u
SA3A-1	7.3	232.1	30.0	0.129	1.706	1.416	1.837	1.292
SA3A-2	7.3	226.0	56.8	0.125	1.355	1.057	1.090	1.032
SA3A-3	6.6	239.2	51.1	0.107	1.571	1.459	1.856	1.268
SA3A-4	7.3	226.0	56.8	0.125	1.273	1.040	1.160	1.064
SA5A-1	39.0	322.1	61.7	0.096	1.075	1.605	2.267	1.393
SA5A-2	23.7	348.7	58.0	0.083	1.143	1.189	1.351	1.133
Average					1.354	1.294	1.594	1.197
Maximum					1.706	1.605	2.267	1.393
Minimum					1.075	1.040	1.090	1.032
Standard Deviation					0.245	0.232	0.465	0.142
Coefficient of Variation					0.181	0.180	0.292	0.119

Table 6.3. Tie force evaluation.

| Specimen ID | Factored Shear Resistance V_r (kN) | Horizontal-Resistance-to-Tie-Force-Requirement Ratio | | Measured-to-Factored Shear Resistance Ratio V_{max}/V_r |
		Factored $H_r/(2/3\ V_r)$	Measured $H_{max}/(2/3\ V_r)$	
SA3A-1	323	1.05	1.53	0.17[*]
SA3A-2	323	1.05	1.11	0.19
SA3A-3	323	1.05	1.62	0.29
SA3A-4	323	1.05	1.09	0.20
SA3B-1	237	1.02	1.06	0.10[*]
SA3B-2	237	1.02	0.83	0.20
SA3B-3	237	1.02	0.92	0.18
SA3B-4	237	1.02	0.97	0.11[*]
SA3B-5	237	1.02	0.80	0.16
SA5A-1	538	1.12	1.44	0.26
SA5A-2	538	1.12	1.16	0.15
SA5B-1	395	1.04	0.98	0.08[*]
SA5B-2	395	1.04	0.93	0.15
SA5B-3	395	1.04	0.91	0.14
SA5B-4	395	1.04	0.74	0.12
DA3B-1	474	1.02	1.09	0.21
DA3B-2	474	1.02	0.98	0.15
DA3B-3	474	1.02	1.12	0.17
DA5B-1	790	1.04	0.99	0.16
DA5B-2	790	1.04	1.04	0.14
DA5B-3	790	1.04	1.00	0.16

*Tests performed under central point load.
 (All other specimens tested under uniformly distributed load.)
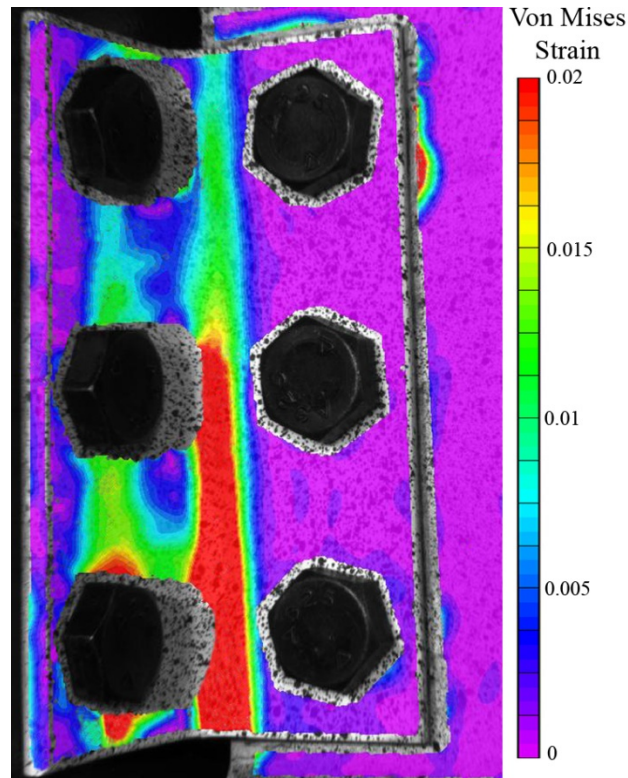
Figure 6.1. Von Mises strain showing plastic hinge formation along angle heel and column bolt line (at left).
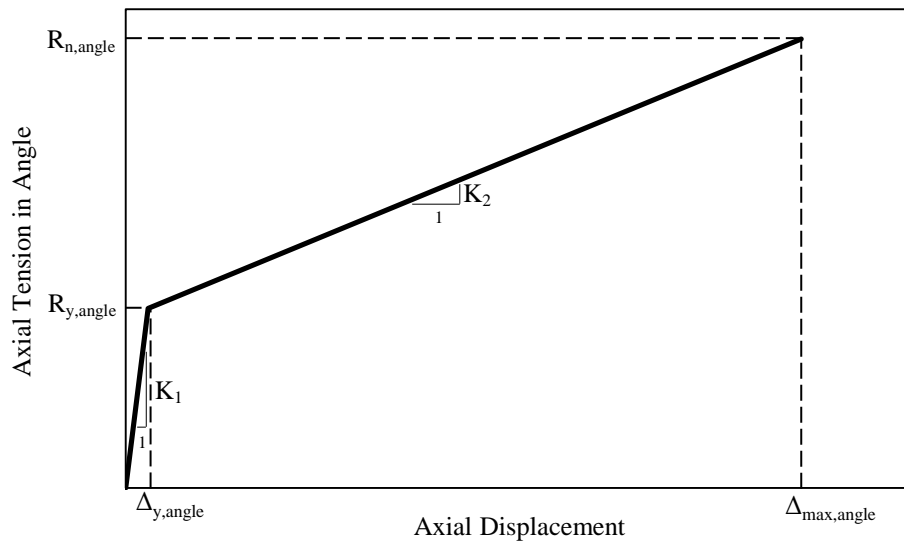
Figure 6.2. Force versus displacement for angle segments bending under tension.
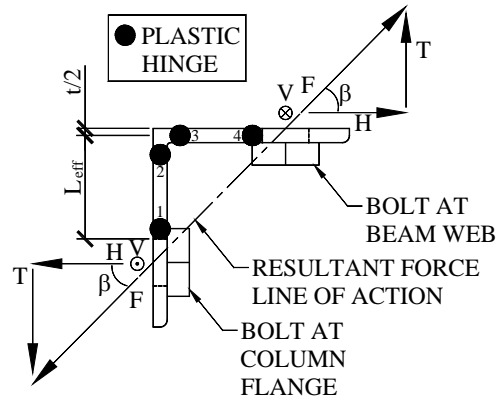
Figure 6.3. Plastic hinge formation in angle segments under tension.
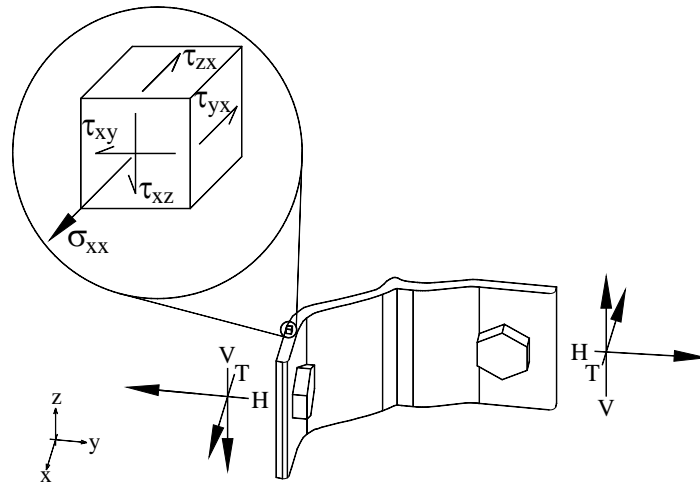
Figure 6.4. Stress state at plastic hinge near column bolt line.
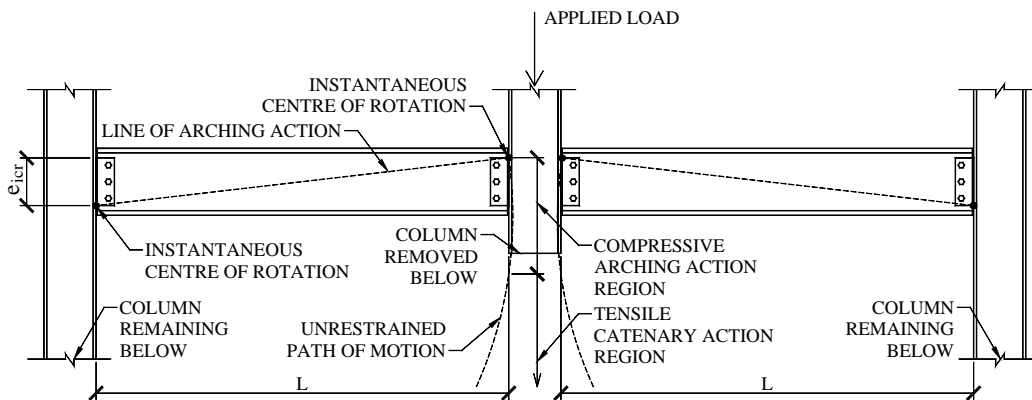
Figure 6.5. Development of compressive arching and tensile catenary action.

183
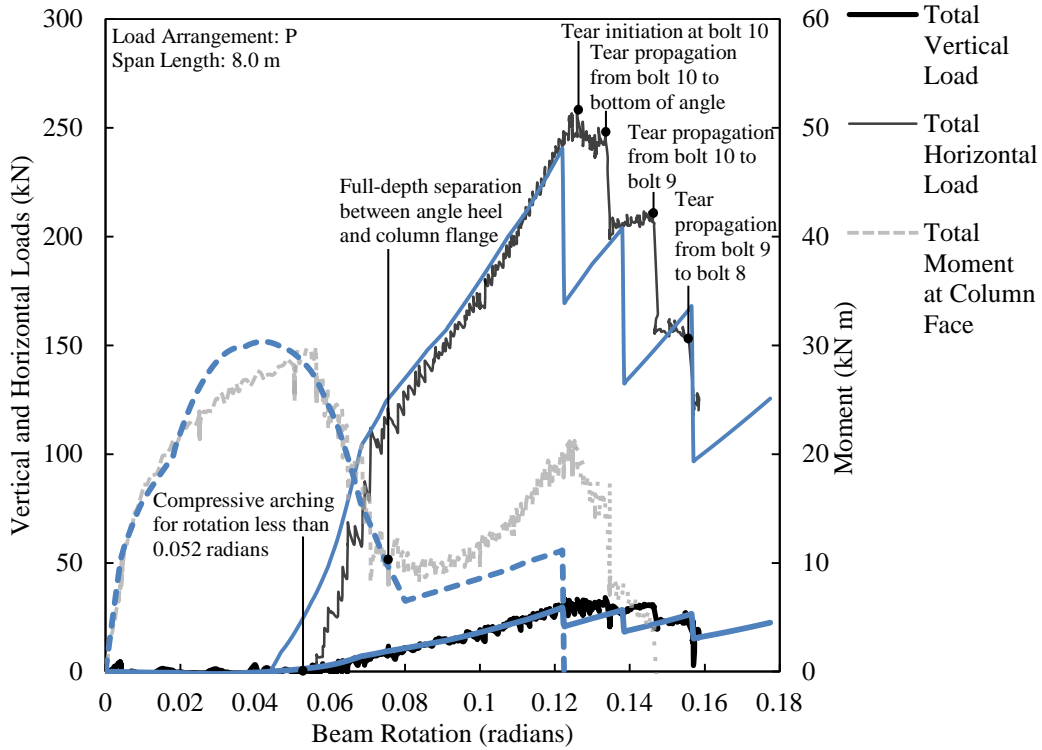
Figure 6.6. Comparison of mechanical model and test results for SA5B-1.
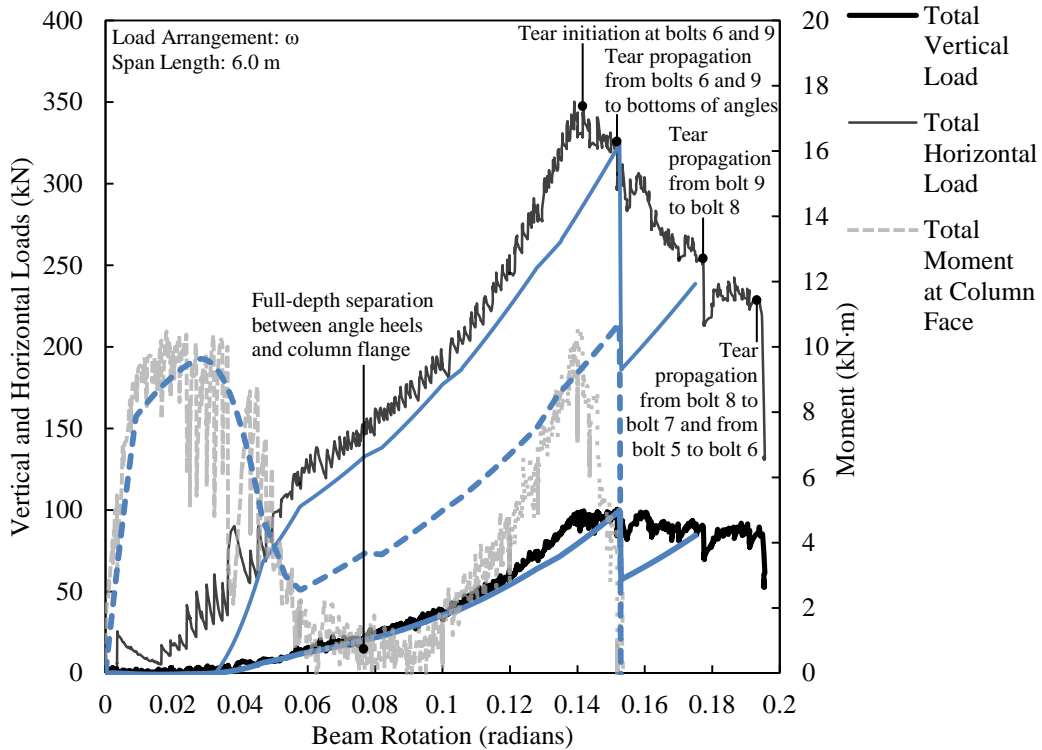
Figure 6.7. Comparison of mechanical model and test results for DA3B-1.

184
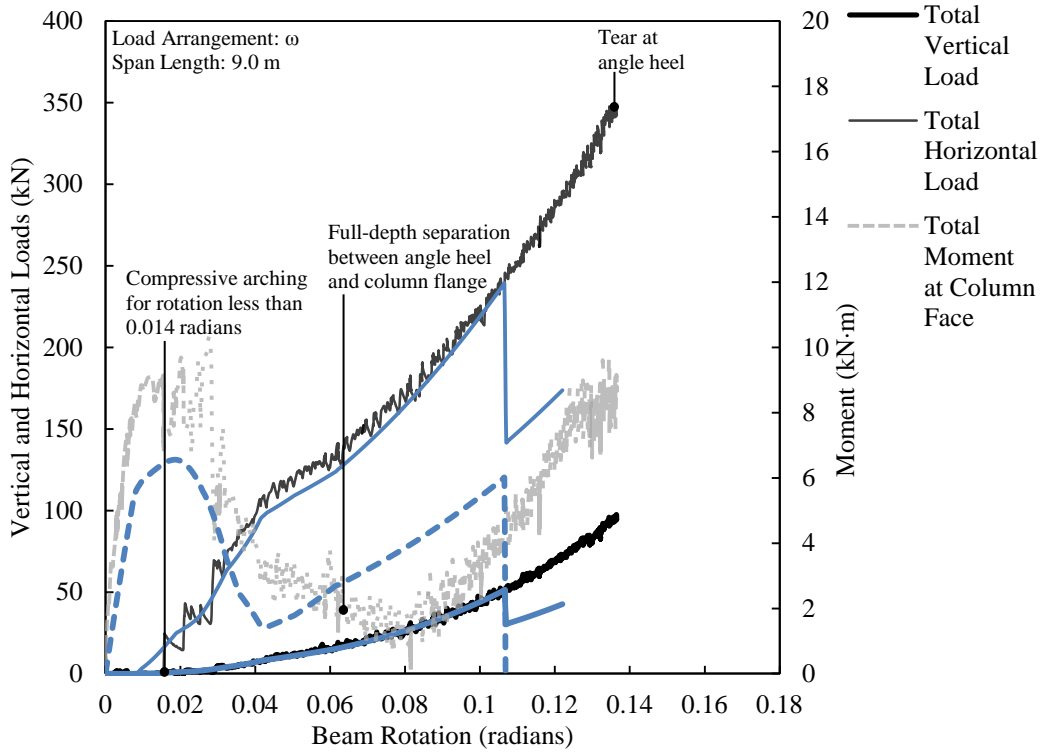
Figure 6.8. Comparison of mechanical model and test results for SA3A-3.
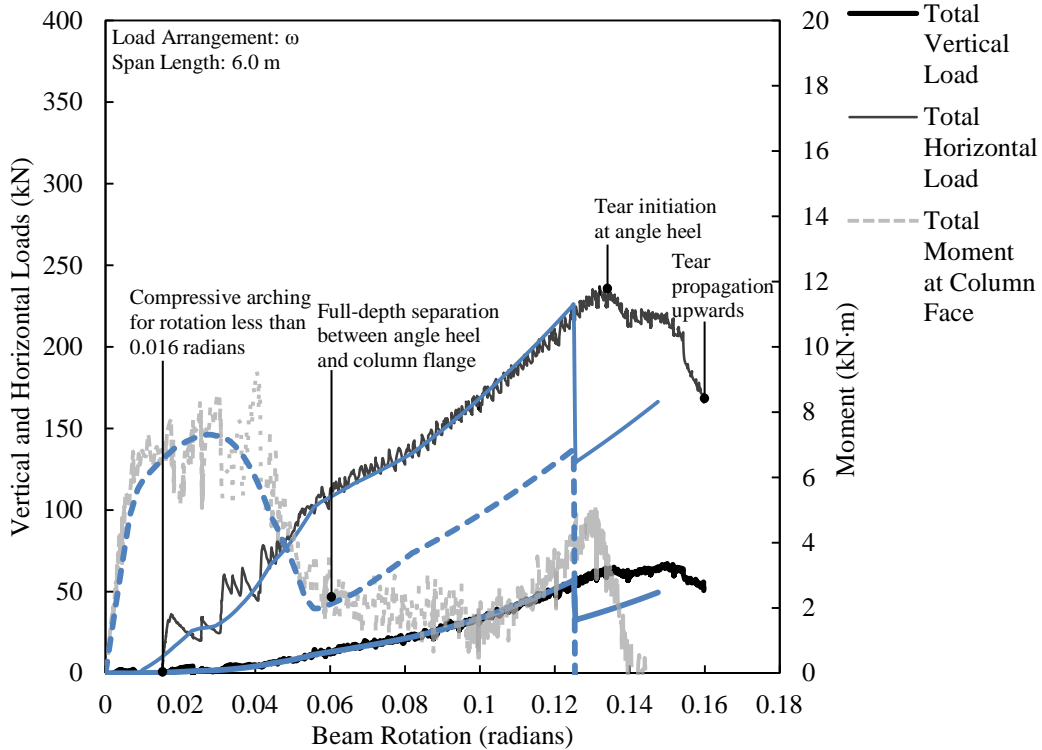
Figure 6.9. Comparison of mechanical model and test results for SA3A-4.

185
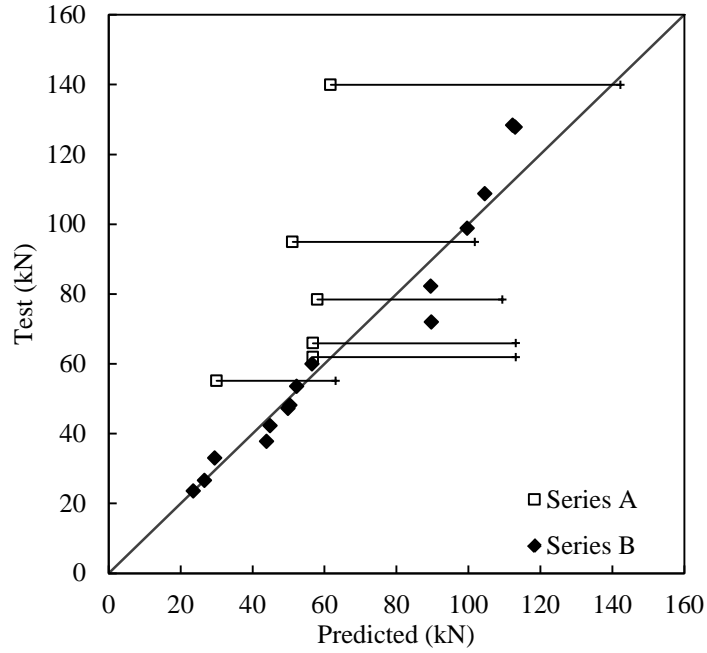
Figure 6.10. Comparison of mechanical model and test results for maximum vertical load.
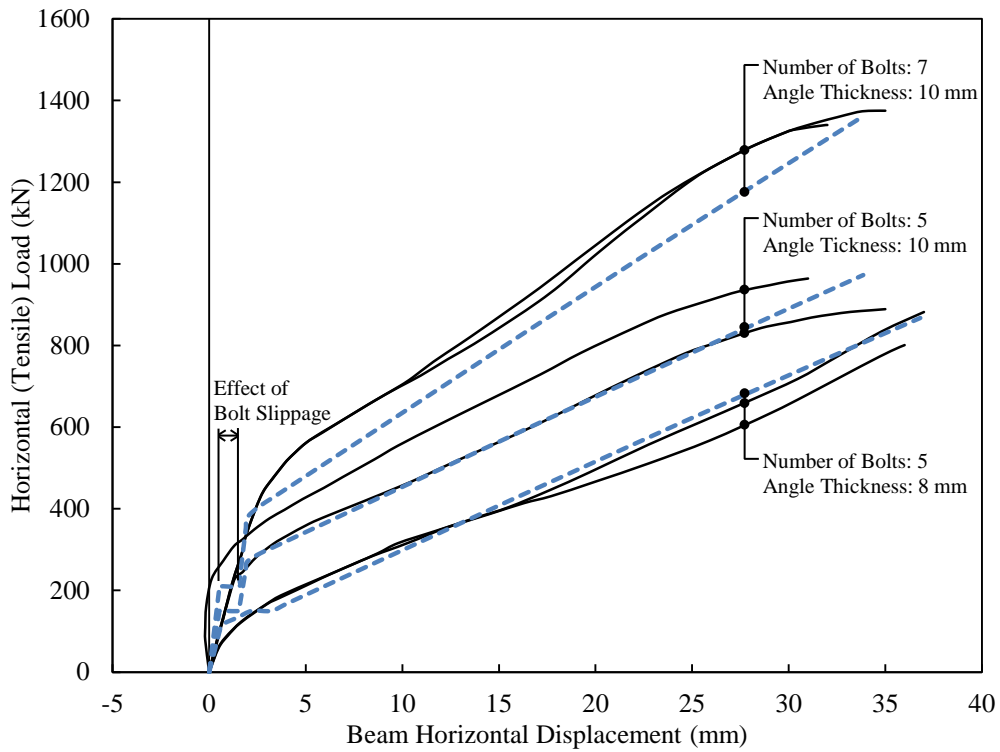
Figure 6.11. Comparison of mechanical model and test results for pure tension tests by Owens and Moore (1992).
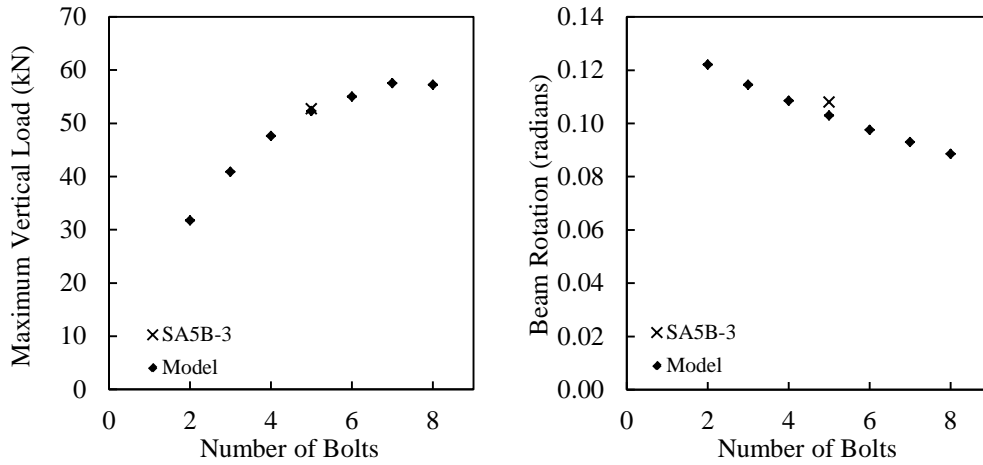
Figure 6.12. Parametric study: number of bolts.
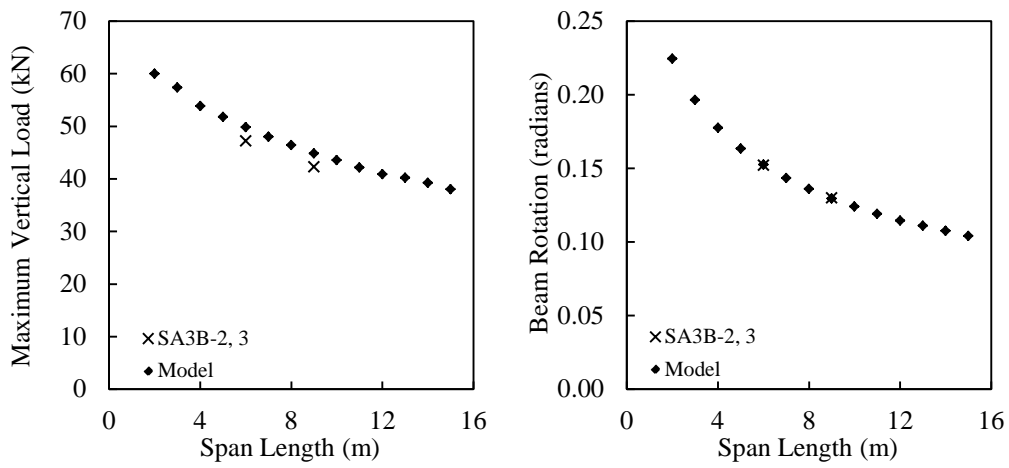
Figure 6.13. Parametric study: span length (three-bolt Series B connections).
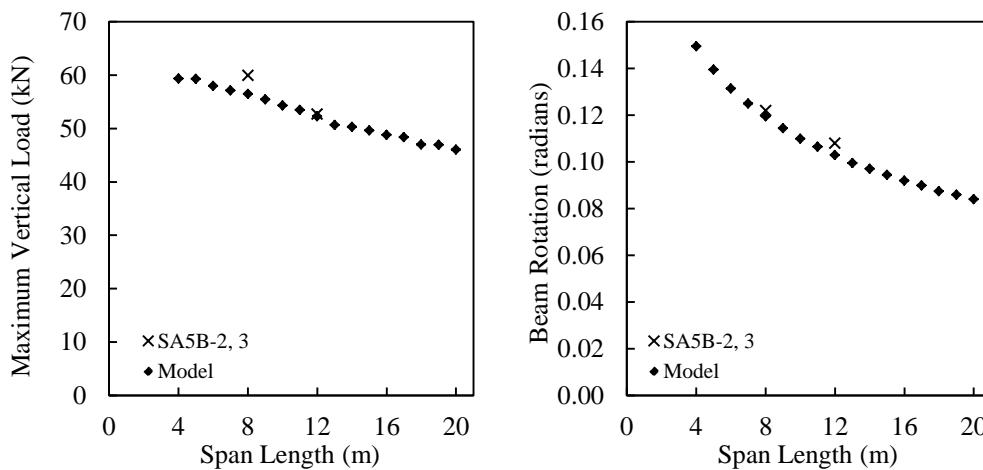
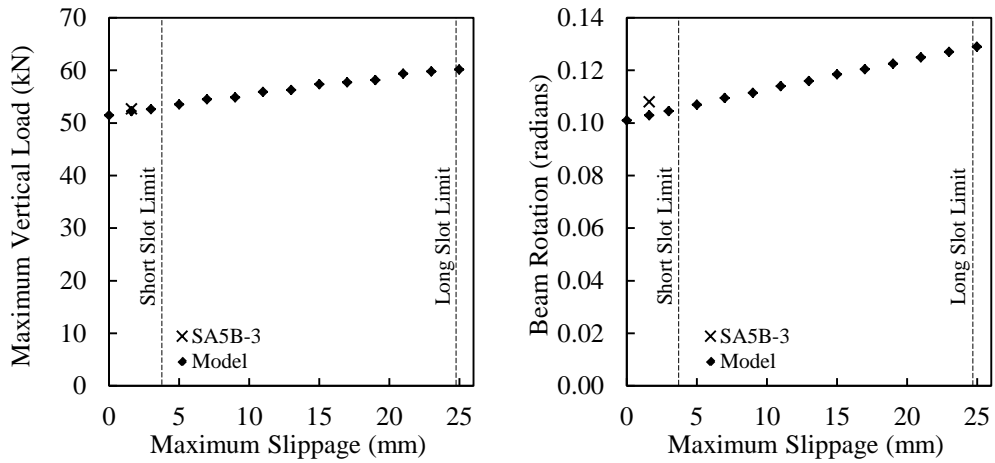**Figure 6.14. Parametric study: span length (five-bolt Series B connections).**

187
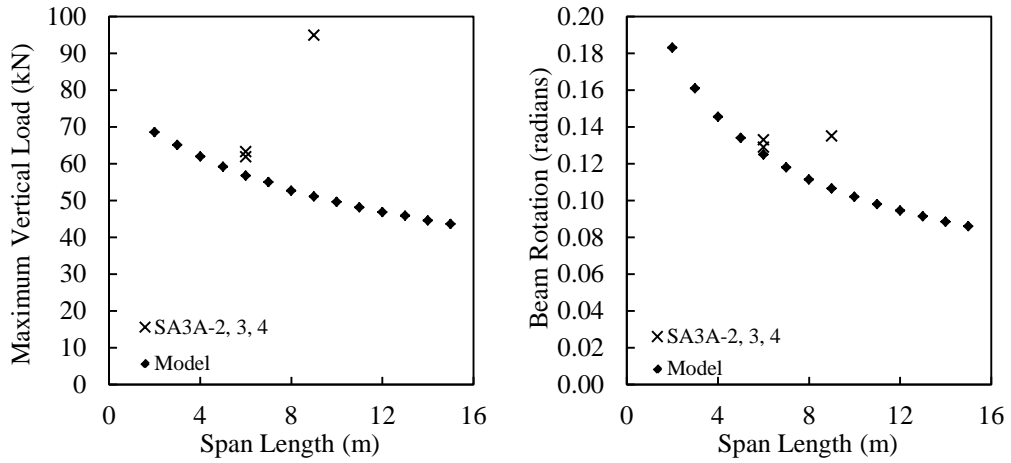
Figure 6.15. Parametric study: span length (three-bolt Series A connections).

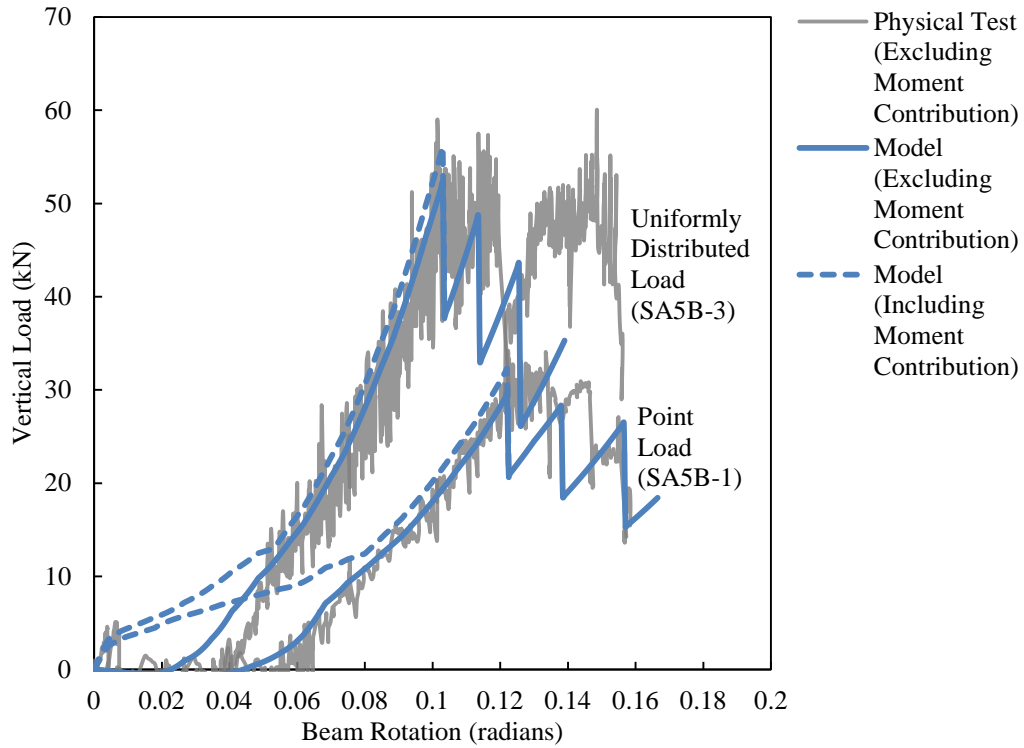**Figure 6.16. Parametric study: maximum bolt slippage.**

Figure 6.17. Parametric study: loading arrangement (proportion of vertical to horizontal load).
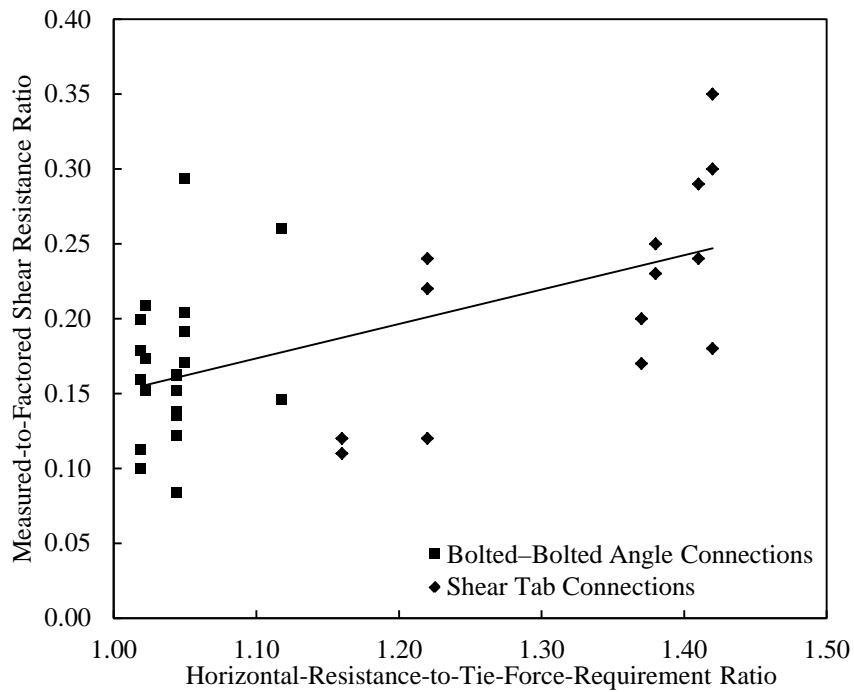

Figure 6.18. Comparison of tie force resistance and vertical load performance following column removal.
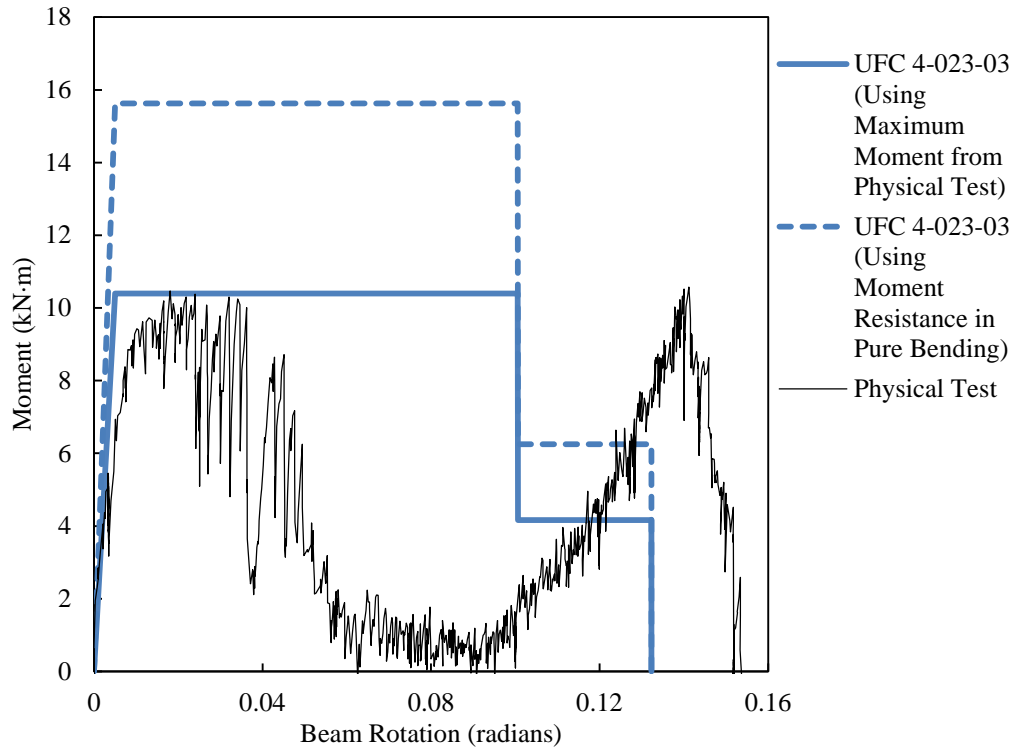
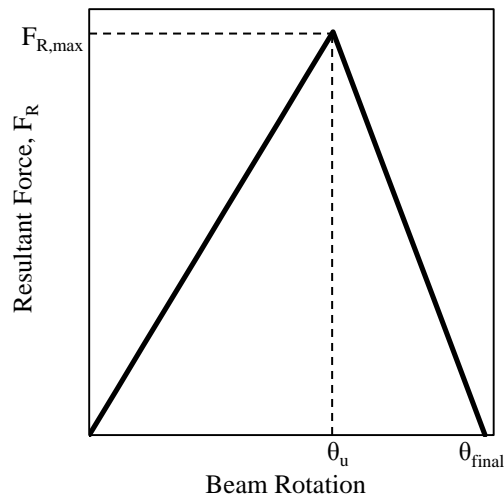**Figure 6.19. Comparison of moment versus rotation from UFC 4-023-03 (DoD, 2009) and test results for DA3B-1.**
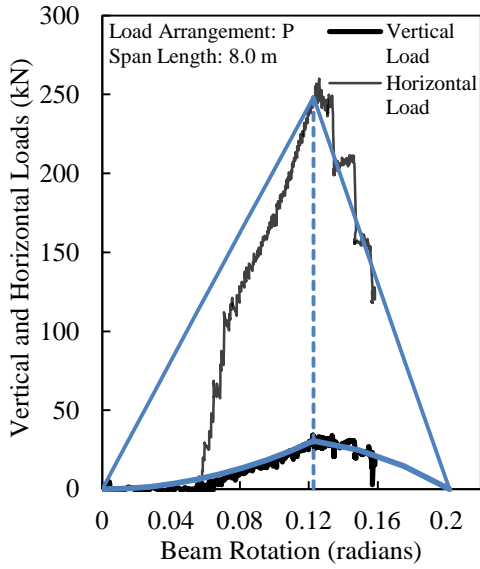

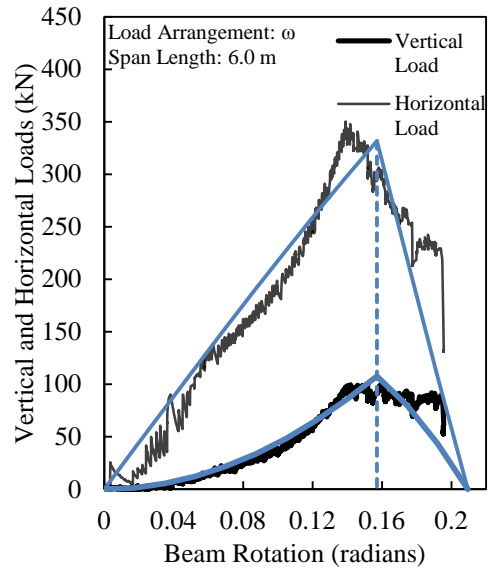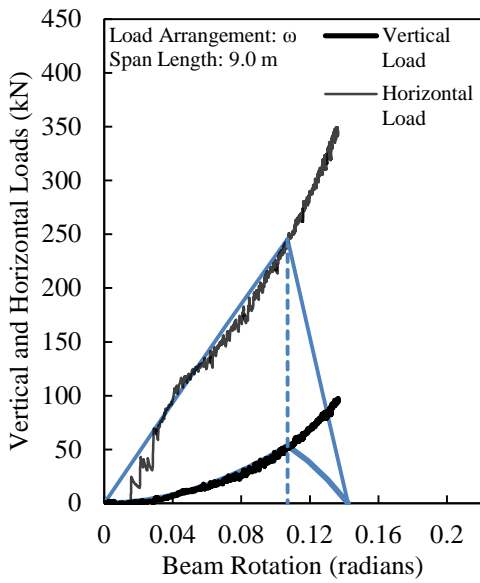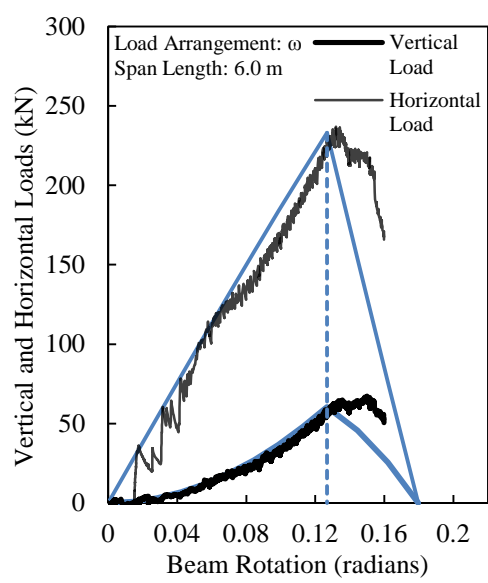**Figure 6.20. Generalized bilinear force versus rotation relationship.**

Figure 6.21. Simplified connection modelling results for: (a) SA5B-1, (b) DA3B-1, (c) SA3A-3, and (d) SA3A-4.
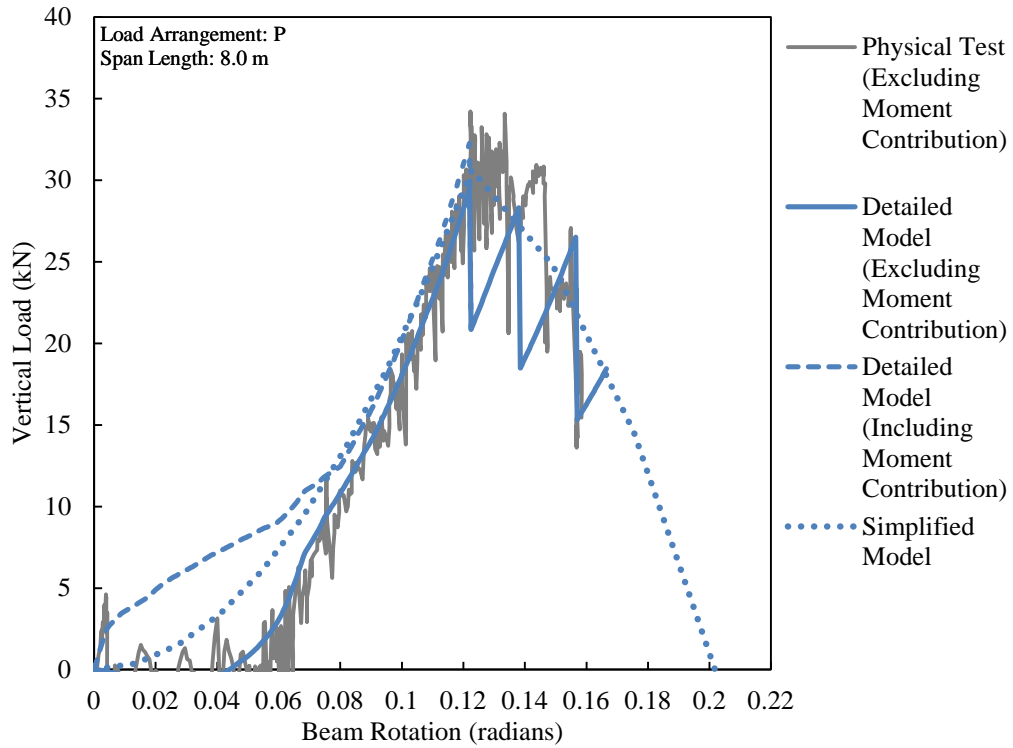
Figure 6.22. Prediction of vertical load by simplified connection model for specimen SA5B-1.

7.   SUMMARY AND CONCLUSIONS

7.1.   Summary

This study investigated the behaviour of commonly-used steel shear connections under extreme loading conditions relevant to the mitigation of disproportionate collapse, and has identified critical parameters that influence their strength and ductility under combined moment, shear, and tension through physical testing and analysis.

In order to obtain realistic characteristics of connection behaviour, which are necessary for the assessment of structural vulnerability to disproportionate collapse, 45 full-scale beam-to-column connections were tested to failure under demands representative of the effects of column removal scenarios, including large rotations and axial tension. Collapse resistance under column removal has been widely adopted as a metric for the quantification of structural integrity. Connection types that were tested include shear tab, welded–bolted single angle, bolted–bolted single angle, bolted–bolted double angle, and combined seat and top angle connections. Various geometric arrangements of each connection type were tested, and each arrangement was subjected to a range of loading histories representing different column removal scenarios. The test results improve the understanding of connection deformation mechanisms, axial and rotational stiffnesses, governing failure modes, and ultimate strength expected following column removal.

Mechanical models were developed that capture the important aspects of connection behaviour recorded in the physical tests. These models were used to expand the database of results and study the effects of critical parameters on performance, including: beam span length, various aspects of connection geometry, and loading arrangement. Design recommendations based on the physical tests and mechanical modelling are presented, addressing connection detailing considerations and an approach to simplified connection modelling for column removal analysis.

193

7.2. Conclusions

7.2.1. *Shear Tab and Welded–Bolted Angle Connections*

The main findings specific to shear tab and welded–bolted single angle connections are:

1. Welded–bolted single angle connections that are welded to the column along the angle heel exhibit deformation mechanisms and failure modes that are similar to those of shear tab connections; thus, they can be treated similarly for column removal analysis.

2. The physical tests demonstrate the ability of shear tab connections to resist vertical load following column removal through the development of catenary action. The maximum vertical loads developed were between 11 % and 35 % of the design shear strengths of the connections (although the expected shear demand may be considerably less than the design shear strength).

3. Connection ductility under axial tension is provided by the dominant deformation mechanism of localized plate bearing effects at bolt locations.

4. The failure of shear tab specimens governed by the bolt tear-out failure mode occurs gradually, beginning with tear-out of the extreme bolt and progressing in a stepwise manner to each successive bolt in the connection as beam rotation increases.

5. Significant levels of vertical load are sustained following initial failure at the extreme bolt, through the increasing efficiency of catenary forces with beam rotation.

6. Connection moment at the ultimate limit state approaches zero, being effectively supressed by interaction with large tensile forces.

7. Mechanical modelling using discrete component springs at bolt locations can accurately predict the behaviour of shear tab connections under the demands of column removal and provide excellent agreement with physical test results when using appropriate force–displacement relationships and failure criteria. Connection response is dominated by the

nonlinear bolt bearing force–displacement relationship and deformation-based failure criterion defined for individual spring elements.

8. The results of a parametric study reveal the relationship between several critical connection properties and performance under column removal scenarios:

    a. Increasing the number of bolts in a single vertical row (and concomitant connection depth) increases the vertical load-carrying capacity of a connection, but the benefit is limited for very deep connections due to their decreased rotational ductility.

    b. The vertical load-carrying capacity and ductility of connections decreases with increasing beam span length, as a consequence of the increased rate of axial deformation demand development with rotation. The extent of this effect has been quantified for a wide range of practical span lengths using mechanical modelling techniques.

    c. Although both the beam web and the shear tab are expected to undergo bearing deformation, assuming a balanced condition where both elements sustain large plastic deformations is likely to cause a gross overestimation of connection ductility.

    d. Horizontally slotted holes may improve performance by increasing rotational ductility, if their use does not compromise the horizontal edge distance at the bolt holes. Connection behaviour following contact of the bolts with the hole edges is expected to be governed by similar deformation mechanisms and failure modes to cases without slotted holes (such as those included in the experimental program).

    e. Shear tab connections that had a plate thickness of 9.5 mm displayed significant increases in both connection strength and ductility, compared to those with a 6.4 mm thick plate.

9. The bolt tear-out failure mode provides an overall ductile response that allows more extensive development of catenary action than is expected for

195

connections governed by more brittle failure modes, such as bolt failure, weld failure, or tearing of the net section.

10. While specified tie force requirements alone tend to improve the performance of shear tab connections under column removal, they are overly simplistic. They fail to account for several factors other than horizontal resistance that are critical to connection performance, including connection ductility, connection depth, beam span length, and loading arrangement on the beams. In some cases, increasing tie force resistance may lead to connection designs that decrease collapse resistance by reducing connection ductility.

11. The development of catenary forces through large deformations is the most important factor to include when modelling shear tab connections for column removal analysis. Simplified modelling of a shear tab connection as a single spring—with all parameters defined by connection geometry, material properties, failure criteria, beam span length, and loading arrangement—can be used to capture the development of catenary forces with acceptable accuracy.

12. The addition of seat and top angles to shear tab connections increases their resistance following column removal, and introduces significant resistance at low rotations through the development of compressive arching action. The angle under the greatest tensile demand (due to beam rotation) typically failed completely prior to the ultimate limit state, and thus did not contribute to the maximum vertical load carried by the connection assembly.

7.2.2.   *Bolted–Bolted Angle Connections*

The main findings specific to bolted–bolted single and double angle connections are:

1. In cases where the beam is laterally restrained, single and double angle connections have similar overall ductility and strength per connection angle under column removal demands.

2. Compressive arching action is expected at low rotations in bolted–bolted angle connections where the stiffness of bolts bearing in compression is significantly greater than the tensile stiffness of the angle. However, in all bolted–bolted angle tests without seat and top angles where it was observed, the compressive arching phase of behaviour is succeeded by the development of tensile catenary action at high rotations, which dominates the behaviour at the ultimate state and governs the maximum vertical load resisted by the connection following column removal. The maximum vertical loads developed were between 10 % and 29 % of the design shear strengths of the connections (although the expected shear demand may be considerably less than the design shear strength).

3. Bolted–bolted angle connections have lower stiffness and greater ductility under catenary tension than do shear tab or welded–bolted angle connections, due to the unfolding of the angle through the formation of plastic hinges near the bolt lines and angle heel.

4. The failure of bolted–bolted angle connections progresses gradually in cases where tearing of the net section occurs at the column bolt line (as the tear propagates in a stable, stepwise manner between successive bolt holes), but is sudden where failure occurs by tearing of the gross section near the angle heel. Thus, significant levels of vertical load are resisted following tear initiation only when tearing occurs at the column bolt line.

5. Connection moment throughout the load development history under the demands associated with column removal is negligible, due to the axial flexibility of bolted–bolted angles and the interaction between moment and tension.

6. Mechanical modelling using discrete component springs at bolt locations can accurately predict the behaviour of bolted–bolted connections under the demands of column removal and provide good agreement with physical test results when using appropriate force–displacement relationships and failure criteria. Connection response is dominated by the bilinear force–displacement relationship for angles unfolding under

tension and the stress-based failure criterion defined for individual spring elements.

7. The results of a parametric study reveal the relationship between several critical connection properties and performance under column removal scenarios. The general conclusions drawn from studies on the number of bolts and beam span length are generally similar to those listed above for shear tab connections; results unique to bolted–bolted angles include:

    a. Horizontally slotted holes improve performance slightly by increasing the rotational ductility of the connection; however, the benefit is not as extensive as for shear tab connections.

    b. The location of angle tearing is correlated to its thickness, with net section failure at the column bolt line tending to govern the behaviour of 6.4 mm thick angles, and failure of the gross section near the angle heel governing the failure of 9.5 mm thick angles. This shift in failure location is not captured by the failure criterion adopted for mechanical modelling.

8. Bolted–bolted angle connections that fail by angle tearing have lower horizontal tie force resistances than similarly-proportioned shear tab connections that fail by bolt tear-out. As was concluded for shear tab connections, tie force requirements alone tend to increase the collapse resistance of structures with bolted–bolted angle connections, but are too simplistic to provide consistent levels of improvement.

9. The development of catenary forces is the most important factor to include when modelling bolted–bolted angle connections for column removal analysis. Simplified modelling using a single spring—with all parameters defined by connection geometry, material properties, failure criteria, beam span length, and loading arrangement—can be used to capture the development of catenary forces with acceptable accuracy.

10. The addition of seat and top angles to bolted–bolted angle connections improves their resistance following column removal and increases the extent of compressive arching action developed at low rotations. The

angle under the greatest tensile demand (due to beam rotation) typically failed completely prior to the ultimate limit state, and thus did not contribute to the maximum vertical load carried by the connection assembly.

7.3.   Recommendations for Future Research

The research described in this report contributes to the current understanding of the robustness of steel shear connections by examining their performance under the effects of column removal both experimentally and analytically. However, the following subjects warrant additional research to further advance the current state of knowledge on this topic:

1. Similar physical testing programs that examine different arrangements of commonly-used steel shear connections would further expand the database of results available to assess the vulnerability of structures containing gravity frames to disproportionate collapse. Test specimens may include other connection types (such as extended shear tab or end plate connections), or different geometric arrangements of the connection types included in the current program (such as additional vertical rows of bolts or thicker connection elements).

2. The performance of shear connections under the effects of column removal scenarios not included in the current study, such as corner column removal or asymmetrical frames, should be studied to extend the range of analyses to which the methodologies developed in this research can be applied.

3. Further examination of the maximum total displacement for bolts bearing on a single plate prior to tear-out could result in a more generalized deformation-based failure criterion for shear tab and welded–bolted single angle connections that includes the effects of plate thickness, edge distance, bolt size, and material properties on ductility.

4. Additional research may be able to refine the stress-based failure criterion proposed for bolted–bolted angle modelling, including prediction of the

observed shift in tearing location (and its effects on connection capacity), which is apparently caused by changes in angle thickness and load proportions.

5. The nonlinear static test results reported herein should be applied to column removal analyses that account for dynamic effects, in order to study collapse resistance in the context of a larger structural framing system.

6. The effects of a concrete floor slab on the collapse resistance of a steel gravity frame should be studied. The physical test results from the current experimental program, in concert with the validated mechanical modelling approaches, can be applied as tools to facilitate a detailed study that includes the changes to connection demands and collapse resistance that are introduced by the presence of a slab.

REFERENCES

Aalberg, A., and Larsen, P.K., 2001. "Bearing Strength of Bolted Connections in High Strength Steel," *Proceedings, 9th Nordic Steel Construction Conference*, Helsinki, Finland: pp. 859–866.

AISC, 2002. *ANSI/AISC 341-02: Seismic Provisions for Structural Steel Buildings*, American Institute of Steel Construction Inc., Chicago, Illinois, USA.

AISC, 2010. *ANSI/AISC 360-10: Specification for Structural Steel Buildings*, American Institute for Steel Construction, Inc., Chicago, Illinois, USA.

AISC, 2011. *Steel Construction Manual,* 14th Edition, American Institute for Steel Construction, Inc., Chicago, Illinois, USA.

ASCE, 2007. *ASCE/SEI 41-06: Seismic Rehabilitation of Existing Buildings*, American Society of Civil Engineers, Reston, Virginia, USA.

ASCE, 2010. *ASCE/SEI 7-10: Minimum Design Loads for Buildings and Other Structures*, American Society of Civil Engineers, Reston, Virginia, USA.

Astaneh, A., 1989. "Demand and Supply of Ductility in Steel Shear Connections," *Journal of Constructional Steel Research*, Elsevier, 14(1): 1–19.

Astaneh, A., 2007. "Progressive Collapse Prevention of Steel Frames with Shear Connections," *Steel TIPS*, Structural Steel Educational Council, Berkeley, California, USA.

Astaneh, A., and Ho, I., 1993. "Behavior and Design of Angle Connections Subjected to Cyclic Axial Force and Shear," *Proceedings of the Symposium on Structural Engineering in Natural Hazards Mitigation*, American Society of Civil Engineers, Irvine, California, USA: 1232–1237.

Astaneh, A., Jones, B., Zhao, Y., and Hwa, R., 2002a. "Progressive Collapse Resistance of Steel Building Floors," *Rep. No. UCB/CEE-STEEL-2001/03*, University of California, Berkeley, California, USA.

Astaneh, A., Madsen, E.A., Noble, C., Jung, R., McCallen, D.B., Hoehler, M.S., Li, W., and Hwa, R., 2002b. "Use of Catenary Cables to Prevent Progressive Collapse of Buildings," *Rep. No. UCB/CEE-STEEL-2001/02*, University of California, Berkeley, California, USA.

ASTM, 2011. *ASTM A370-11: Standard Test Methods and Definitions for Mechanical Testing of Steel Products*, American Society for Testing and Materials, Easton, Pennsylvania, USA.

Baldassino, N., Bignardi, A., and Zandonini, R., 2010. "Response of End–plate Joints under Combined Forces," *SSDS 'Rio 2010,* Stability and Ductility of Steel Structures, Rio de Janeiro, Brazil: 183–190.

Burnett, E.F.P., 1975. "The Avoidance of Progressive Collapse: Regulatory Approaches to the Problem," *National Bureau of Standards Report NBS-GCR 75-48*, National Bureau of Standards, Washington, D.C., USA.

Byfield, M., and Paramasavim, S., 2007. "Catenary Action in Steel–framed Buildings," *Structures and Buildings*, Institution of Civil Engineers, 160(SB5): 247–257.

CEN, 2006. *EN 1991-1-7:2006: Eurocode 1: Actions on Structures*, European Committee for Standardization, Brussels, Belgium.

CSA, 2004. *CSA G40.21–04: General Requirements for Rolled or Welded Structural Quality Steel*, Canadian Standards Association, Toronto, Ontario, Canada.

CSA, 2009. *CSA S16-09: Limit States Design of Steel Structures*, Canadian Standards Association, Toronto, Ontario, Canada.

CSA, 2010. *Handbook of Steel Construction,* 10th Edition, Canadian Standards Association, Toronto, Ontario, Canada.

CSA, 2012. *CSA S850-12: Design and Assessment of Buildings Subjected to Blast Loads*, Canadian Standards Association, Toronto, Ontario, Canada.

De Stefano, M., and Astaneh, A., 1991. "Axial Force–Displacement Behavior of Steel Double Angles," *Journal of Constructional Steel Research*, Elsevier, 20(3): 161–181.

Demonceau, J., 2008. *Steel and Composite Building Frames: Sway Response under Conventional Loading and Development of Membrane Effects in Beams further to an Exceptional Action*, Ph.D. Thesis, University of Liège, Liège, Belgium.

DoD, 2009. *UFC 4-023-03: Unified Facilities Criteria: Design of Buildings to Resist Progressive Collapse*, U.S. Department of Defence, Washington, D.C., USA.

FEMA, 2000. *FEMA 355D: State of the Art Report on Connection Performance*, Federal Emergency Management Agency, Richmond, California, USA.

Foley, C.M., Martin, K., and Schneeman, C., 2007. "Robustness in Structural Steel Framing Systems," *Rep. No. MU-CEEN-SE-06-01*, Marquette University, Milwaukee, Wisconsin, USA.

Friedman, A., 2009. *Axial, Shear and Moment Interaction of WT Connections*, Master's Thesis, Milwaukee School of Engineering, Milwaukee, Wisconsin, USA.

Girhammar, U.A., 1980a. *Behaviour of Bolted Beam–Column Connections under Catenary Action in Damaged Steel Structures*, Swedish Council for Building Research, Stockholm, Sweden.

Girhammar, U.A., 1980b. *Dynamic Fall–Safe Behaviour of Steel Skeleton Structures Having Bolted Connections*, Swedish Council for Building Research, Stockholm, Sweden.

Gong, Y., 2010. "Analysis and Design for the Resilience of Shear Connections," *Canadian Journal of Civil Engineering*, NRC Research Press, 37: 1581–1589.

Gong, Y., 2013. "Re-examination of Double–angle Knife Shear Connections," *Journal of Constructional Steel Research*, Elsevier, 81(2): 44–51.

GSA, 2003. *Progressive Collapse Analysis and Design Guidelines for New Federal Office Buildings and Major Modernization Projects*, U.S. General Services Administration, Washington, D.C., USA.

Guravich, S.J., 2002. *Standard Beam Connections in Combined Shear and Tension*, Ph.D. Thesis, University of New Brunswick, Fredericton, New Brunswick, Canada.

Hong, K., Yang, J.G, and Lee, S.K., 2001. "Parametric Study of Double Angle Framing Connections Subjected to Shear and Tension," *Journal of Constructional Steel Research*, Elsevier, 57(9): 997–1013.

ICC, 2012. *International Building Code*, International Code Council, Country Club Hills, Illinois, USA.

Izzuddin, B.A., Vlassis, A.G., Elghazouli, A.Y., and Nethercot, D.A., 2008. "Progressive Collapse of Multi–storey Buildings Due to Sudden Column Loss, Part I: Simplified Assessment Framework," *Engineering Structures*, Elsevier, 30: 1308–1318.

Karns, J.E., Houghton, D.L., Hong, J., and Joonghwan, K., 2009. "Behavior of Varied Steel Frame Connection Types Subjected to Air Blast, Debris Impact, and/or Post–blast Progressive Collapse Load Conditions," *Structures Congress 2009*, American Society of Civil Engineers, Austin, Texas, USA: 1868–1877.

Kim, H.J., 1996. *The Effect of End Distance on the Bearing Strength of Bolted Connections.* Master's Thesis, University of Texas at Austin, Austin, Texas, USA.

Kulak, G.L., Fisher, J.W., and Struik, J.H.A., 2001. *Guide to Design Criteria for Bolted and Riveted Joints*, 2nd Edition, American Institute for Steel Construction, Inc., Chicago, Illinois, USA.

Lewis, B.E., and Zwerneman, F.J., 1996. *Edge Distance, Spacing, and Bearing in Bolted Connections*. Research Report, Department of Civil and Environmental Engineering, Oklahoma State University, Stillwater, Oklahoma, USA.

Liu, J.L., 2010a. "Preventing Progressive Collapse through Strengthening Beam-to-Column Connection, Part 1: Theoretical Analysis," *Journal of Constructional Steel Research*, Elsevier, 66(2): 229–237.

Liu, J.L., 2010b. "Preventing Progressive Collapse through Strengthening Beam-to-Column Connection, Part 2: Finite Element Analysis," *Journal of Constructional Steel Research*, Elsevier, 66(2): 238–247.

Main, J.A., and Sadek, F., 2012. "Robustness of Steel Gravity Frame Systems with Single-plate Shear Connections," *NIST Technical Note 1749*, National Institute of Standards and Technology, Gaithersburg, Maryland, USA.

Moore, A.M., Rassati, G.A., and Swanson, J.A., 2008. *Evaluation of the Current Resistance Factors for High-strength Bolts*, Research Council on Structural Connections.

NRC, 2010. *National Building Code of Canada,* Canadian Commission on Building and Fire Codes, National Research Council of Canada, Ottawa, Ontario, Canada.

Owens, G.W., and Moore, D.B., 1992. "The Robustness of Simple Connections," *The Structural Engineer*, The Institution of Structural Engineers, 70(3): 37–46.

Pucinotti, R., 2001. "Top–and–seat and Web Angle Connections: Prediction via Mechanical Model," *Journal of Constructional Steel Research*, Elsevier, 57(6): 661–694.

Raebel, C.H., 2011. *A Quantitative Study of Robustness Characteristics in Steel Framed Structures*, Ph.D. Thesis, Marquette University, Milwaukee, Wisconsin, USA.

Rex, C.O., 1996. *Behavior and Modeling of Partially Restrained Beam–girder Connections*, Ph.D. Thesis, Virginia Polytechnic Institute and State University, Blacksburg, Virginia, USA.

Rex, C.O., and Easterling, W.S., 2003. "Behavior and Modeling of a Bolt Bearing on a Single Plate," *Journal of Structural Engineering*, American Society of Civil Engineers, 129(6): 792–800.

Roddis, W.M.K., and Blass, D., 2012. "Finite Element Study of Single–angle Connection under Tensile Loading," *Structures Congress 2012*, American Society of Civil Engineers, Chicago, Illinois, USA: 1104–1110.

Sadek, F., El–Tawil, S., and Lew, H.S., 2008. "Robustness of Composite Floor Systems with Shear Connections: Modeling, Simulation, and Evaluation," *Journal of Structural Engineering*, American Society of Civil Engineers, 134(11): 1717–1724.

Sadek, F., Main, J.A., Lew, H.S., Robert, S.D., Chiarito, V.P., and El-Tawil, S., 2010. "An Experimental and Computational Study of Steel Moment Connections under a Column Removal Scenario," *NIST Technical Note 1669*, National Institute of Standards and Technology, Gaithersburg, Maryland, USA.

SCI, 2002. *Joints in Steel Construction: Simple Connections*, The Steel Construction Institute, London, UK.

Thompson, S., 2009. *Axial, Shear and Moment Interaction of Single Plate "Shear Tab" Connections*, Master's Thesis, Milwaukee School of Engineering, Milwaukee, Wisconsin, USA.

Thornton, W.A., 1997. "Strength and Ductility Requirements for Simple Shear Connections with Shear and Axial Load," *National Steel Construction Conference*, American Institute of Steel Construction, Inc., Chicago, Illinois, USA, 38: 1–17.

Tide, R.H.R., 2000. "Evaluation of Steel Properties and Cracking in "k"-area of W-shapes," *Engineering Structures*, Elsevier, 22: 128–134.

Timoshenko, S., 1955. *Strength of Materials, Part I – Elementary Theory and Problems*, D. Nostrand Company, Inc., Princeton, New Jersey, USA.

Weigand, J.M., Meissner, J.E., Francisco, T., Berman, J.W., Fahnestock, L.A., and Liu, J., 2012. "Overview of AISC/NSF Structural Integrity Research and Preliminary Results," *Structures Congress 2012*, American Society of Civil Engineers, Chicago, Illinois, USA: 135–145.

Yang, B., and Tan, K.H., 2012. "Numerical Analyses of Steel Beam–column Joints Subjected to Catenary Action," *Journal of Constructional Steel Research*, Elsevier, 70(3): 1–11.

Yang, B., and Tan, K.H., 2013a. "Behaviour of Composite Beam-column Joints under a Middle-column-removal Scenario: Experimental Tests," *Journal of Structural Engineering*, American Society of Civil Engineers. Posted ahead of print.

Yang, B., and Tan, K.H., 2013b. "Experimental Tests of Different Types of Bolted Steel Beam–column Joints under a Central-column-removal Scenario," *Engineering Structures*, Elsevier, 54: 112–130.

Yang, J.G., 1997. *Double Angle Framing Connections Subjected to Shear and Tension*, Ph.D. Thesis, Virginia Polytechnic Institute and State University, Blacksburg, Virginia, USA.

Yim, H.C., and Krauthammer, T., 2012. "Mechanical Properties of Single–plate Shear Connections under Monotonic, Cyclic, and Blast Loads," *Engineering Structures*, Elsevier, 37: 24–35.

APPENDIX A.   COMPUTATION OF TARGET LOAD HISTORY

The load application procedure used during testing required real-time measurements of the applied loads and deformed geometry of the system in order to compute the force and displacement demands representative of a column removal scenario to be applied to the connection. This appendix contains the details of the computational channels programmed in the data acquisition system.

A.1   Constants

Table A.1 lists the constants required for the real-time calculations performed, along with typical values for the tests. The assumed span length, L, represents the distance between column faces for a single beam in a two-bay frame where the central column has been removed. It affects the rate of development of axial elongation demand, Δ_3, and the vertical load required for equilibrium, V. All of the remaining constants are fixed or initial measured geometric quantities that are used in the calculations of the directions and locations of the forces applied by each of the three actuators. The initial angle of Actuator 3, $\theta_{3,i}$, was selected so that the actuator approached alignment with the beam axis in the range of beam rotation angles corresponding to the anticipated maximum axial forces.

A.2   Target Load History Computation Details

The total vertical load to be applied to the connection to satisfy the equilibrium condition shown in Equation 3.1 or 3.2 is a function of beam rotation, assumed span length, and applied horizontal load. Table A.2 shows the details of the resolution of each actuator force into its vertical and horizontal components, and the calculation of the moment arm for each resolved force. Horizontal tension and vertical (upward) force were taken as positive for all forces. The lengths shown as numbers (rather than variables) in the moment arm formulae are distances related to the geometry of the test set-up that were identical for all tests.

Table A.3 shows the axial displacement and total vertical load required for compatibility and equilibrium, respectively, of a two-bay frame following central

column removal. (Either V_1 or V_2 was used for the latter, depending on the loading arrangement.) Since both of these are functions of variables that change during testing, they were continuously updated using real-time measurements of applied forces and displacements. The calculated "target" values using the equations shown in the table were compared to the actual measured values of applied axial displacement (using cable transducer CT_4, mounted along the centreline of the beam web) and applied vertical load ($V_{applied}$, from Table A.2). Actuator forces were continuously adjusted to achieve convergence between the applied and target load histories, with beam rotation being continuously increased to drive the test forward.

A.3   Redundant Measurements

In order to confirm the accuracy of the critical parameters measured during the tests, as well as to provide an alternative source for measurements in the event of instrument failure, redundant measurements were taken wherever possible. In general, the more direct measurements were taken as primary and used in the reporting and analysis of the results. The calculations used to compute redundant values of beam rotation, axial displacement, and applied loads are shown in Table A.4. In all the tests performed, no primary instruments failed and redundant measurements proved consistent with the associated primary measurement, providing increased confidence in the primary measurements themselves. As a result, redundant measurements were not used in generating any of the reported test data.

Beam web rotation was measured directly using clinometer CL_4, which was mounted at the centreline of the beam web away from the connection. A redundant value of beam web rotation was calculated using the vertical displacements of Actuators 1 and 2. Axial displacement, Δ_3, was measured directly using cable transducer CT_4. A redundant measurement of axial displacement was calculated using the component of the displacements of Actuator 2 in the direction of the beam axis. A redundant measurement of applied load measured by each of the three load cells was achieved using a series of

208

pressure transducers in the hydraulic lines, and multiplying the applied hydraulic fluid pressure by the nominal area of the actuator piston head surface, as provided by the manufacturer.

In addition to these redundant measurements calculated using output from the electronic instruments, the optical strain imaging system also provides redundant measurements of beam rotation and axial displacement.

Table A.1. Load history constants.

Variable	Description	Typical Values
L	Assumed clear span length	6000 mm or 9000 mm for 3-bolt tests
		8000 mm or 12000 mm for 5-bolt tests
d_b	Beam depth	323 mm for 3-bolt tests
		546 mm for 5-bolt tests
d_{gap}	Initial gap distance between beam and column face	25 mm for shear tab connections
		10 mm for angle connections
$L_{1,i}$	Initial pin-to-pin length of	1250 mm to 1410 mm
$L_{2,i}$	Actuators 1 and 2	
$L_{3,i}$	Initial pin-to-pin length of Actuator 3	1825 mm to 1880 mm
$\theta_{1,i}$	Initial inclination of Actuator 1	Approximately zero (± 0.02 radians for specimen fit-up)
$\theta_{2,i}$	Initial inclination of Actuator 2	Approximately zero (± 0.02 radians for specimen fit-up)
$\theta_{3,i}$	Initial inclination of Actuator 3	0.1 to 0.2 radians

Table A.2. Applied force computations.

Variable	Description	Equation[†]
$P_{1\text{-}V}$	Resolved vertical force applied by Actuator 1	$[LC_1]\cos[CL_1]$
$P_{1\text{-}H}$	Resolved horizontal force applied by Actuator 1	$[LC_1]\sin[CL_1]$
$P_{2\text{-}V}$	Resolved vertical force applied by Actuator 2	$[LC_2]\cos[CL_2]$
$P_{2\text{-}H}$	Resolved horizontal force applied by Actuator 2	$[LC_2]\sin[CL_2]$
$P_{3\text{-}V}$	Resolved vertical force applied by Actuator 3	$[LC_3]\sin[CL_3]$
$P_{3\text{-}H}$	Resolved horizontal force applied by Actuator 3	$[LC_3]\cos[CL_3]$
$d_{1\text{-}H}$	Horizontal distance from column face to force applied by Actuator 1	$d_{gap}+375+\left(L_{1,i}+[CT_1]\right)\sin\left([CL_1]-\theta_{1,i}\right)$
$d_{1\text{-}V}$	Vertical distance from column face to force applied by Actuator 1	$\dfrac{d_b}{2}-\left(L_{1,i}+[CT_1]\right)\cos\left([CL_1]-\theta_{1,i}\right)+L_{1,i}$
$d_{2\text{-}H}$	Horizontal distance from column face to force applied by Actuator 2	$d_{gap}+1195+\left(L_{2,i}+[CT_2]\right)\sin\left([CL_2]-\theta_{2,i}\right)$
$d_{2\text{-}V}$	Vertical distance from column face to force applied by Actuator 2	$\dfrac{d_b}{2}-\left(L_{2,i}+[CT_2]\right)\cos\left([CL_2]-\theta_{2,i}\right)+L_{2,i}$
$d_{3\text{-}H}$	Horizontal distance from column face to force applied by Actuator 3	$d_{2\text{-}H}-\dfrac{d_b}{2}\sin[CL_4]+12.5\cos[CL_4]$
$d_{3\text{-}V}$	Vertical distance from column face to force applied by Actuator 3	$d_{2\text{-}V}-\dfrac{d_b}{2}\cos[CL_4]-12.5\sin[CL_4]$
$V_{applied}$	Total vertical load applied (upwards positive)	$\displaystyle\sum_{n=1}^{3}\left(P_{n\text{-}V}\right)$
$H_{applied}$	Total horizontal load applied (tension positive)	$\displaystyle\sum_{n=1}^{3}\left(P_{n\text{-}H}\right)$
$M_{applied}$	Total moment at column face applied	$\displaystyle\sum_{n=1}^{3}\left(P_{n\text{-}H}d_{n\text{-}V}+P_{n\text{-}V}d_{n\text{-}H}\right)$

†Instrument designations shown in [square brackets]; refer to Figure 3.3 for nomenclature.

Table A.3. Target load history computations.

Variable	Description	Equation[†]
Δ_3	Axial displacement demand required for compatibility, using Equation 3.7	$\dfrac{L}{2}\left(\dfrac{1}{\cos[CL_4]}-1\right)$
V_1	Total vertical load required for equilibrium under central point load, using Equation 3.1	$H_{applied}\tan[CL_4]$
V_2	Total vertical load required for equilibrium under uniformly distributed load, using Equation 3.2	$2\,H_{applied}\tan[CL_4]$

†Instrument designations in [square brackets]. Refer to Figure 3.3 for nomenclature.

Table A.4. Redundant measurement computations.

Variable	Description	Equation[†]
$\theta_{c,redundant}$	Redundant measurement of beam rotation using position of Actuators 1 and 2	$\arcsin\left(\dfrac{[CT_2]\cos[CL_2]-[CT_1]\cos[CL_1]}{820}\right)$
$\Delta_{3,redundant}$	Redundant measurement of axial displacement using position of Actuator 2	$(L_{A2,i}+[CT_2])\sin([CL_2]-\theta_{2,i})\cos\theta_c$ $+\Big[(L_{A2,i}+[CT_2])\cos([CL_2]-\theta_{2,i})-L_{A2,i}\Big]\sin\theta_c$
$P_{1-3,redundant}$	Redundant measurement of loads applied using pressure transducers	$\Big[PT_{1,2,or3}\Big]*\text{Area}_{actuator\,piston}$

†Instrument designations in [square brackets]. Refer to Figure 3.3 for nomenclature.

APPENDIX B.   FABRICATION DRAWINGS

This appendix contains the drawing set used to fabricate the test specimens and select loading fixtures and elements of the reaction frame used in the experimental program. Drawing scales shown have been adjusted to reflect the 50 % scaling factor applied to the original drawing set to accommodate the 8.5"x11" page size of this document.

LIST OF DRAWINGS:

SHEET NUMBER	SHEET NAME
01	GENERAL NOTES
02	OVERALL TEST SET-UP
03	3-BOLT SHEAR TABS AND WELDED ANGLES
04	5-BOLT SHEAR TABS AND WELDED ANGLES
05	REUSABLE BEAMS
06	REUSABLE COLUMNS
07	BOLTED ANGLE COLUMNS
08	BOLTED ANGLES

ABBREVIATIONS:

℄ – CENTRE LINE
CJP – COMPLETE JOINT PENETRATION
ø – DIAMETER
IN. – INCHES
MIN. – MINIMUM
N.T.S. – NOT TO SCALE
PL – PLATE
PTFE – POLYTETRAFLUOROETHYLENE
QTY – QUANTITY TO BE SUPPLIED
SIM. – SIMILAR
TYP. – TYPICAL
U.N.O. – UNLESS NOTED OTHERWISE

SPECIMEN NAMING CONVENTION:

GEOMETRY CLASSIFICATION:
A – 7/8"ø BOLTS
B – 3/4"ø BOLTS
C – COMBINED SEAT AND TOP ANGLE, 3/4"ø BOLTS

NUMBER OF ROWS OF BOLTS

ST3A-1

SERIES NUMBER

CONNECTION TYPE:
ST – SHEAR TAB
WA – WELDED-BOLTED SINGLE ANGLE
SA – BOLTED-BOLTED SINGLE ANGLE
DA – BOLTED-BOLTED DOUBLE ANGLE

BOLT SCHEDULE:

BOLT DIAMETER (IN.)	BOLT LENGTH (IN.)	GRADE	QUANTITY
3/4	2	A325	152
3/4	2 1/4	A325	94
3/4	2 1/2	A325	70
7/8	2 1/4	A325	68
1	3 1/4	A490	32
1	4	A490	16

MATERIAL GRADE:

1. W-SHAPES:
   CAN/CSA-G40.20/G40.21-04
   GRADE 350W

2. ANGLES AND PLATES:
   CAN/CSA-G40.20/G40.21-04
   GRADE 300W

3. BOLTS:
   ASTM A325 OR ASTM A490,
   AS NOTED IN BOLT SCHEDULE

WELDING:

1. WELDING SHALL CONFORM TO
   CSA W59-03.

2. WELDING SHALL BE DONE USING
   MATCHING ELECTRODES.

GENERAL NOTES:

1. ALL DIMENSIONS ARE IN MILLIMETRES
   UNLESS NOTED OTHERWISE.

2. DRAWING LAYOUTS ARE TO BE PLOTTED
   ON 11"x17" SHEETS.

3. DO NOT SCALE DRAWINGS. IF
   CLARIFICATION IS REQUIRED, PLEASE
   CONTACT:
   ROBERT DRIVER: 780-492-0091
   STEVEN OOSTERHOF: 780-452-3510

4. SHOP DRAWINGS SHALL BE SUBMITTED
   FOR REVIEW PRIOR TO FABRICATION.

5. ALL BOLT HOLES SHALL BE DRILLED.

6. PROVIDE ALL BOLTS COMPLETE WITH
   NUTS AND FLAT WASHERS.

7. SUPPLY A COPY OF MILL TEST REPORTS
   FOR ALL STRUCTURAL STEEL USED.

8. ALL PLATE OF SAME THICKNESS SHALL
   BE CUT FROM ONE PIECE. ALL
   W-SHAPES AND ANGLES OF SAME SIZE
   SHALL BE CUT FROM ONE PIECE.

9. PROVIDE THE FOLLOWING FOR MATERIAL
   TESTING CUT FROM THE SAME PIECE
   USED FOR SPECIMENS SHOWN IN
   SHEETS 03-10:
   1-PL500x500x6.4
   1-PL500x500x9.5
   1-L89x89x6.4 (MIN. 1500 LONG)
   1-L89x89x9.5 (MIN. 1500 LONG)
   1-L102x102x6.4 (MIN. 1500 LONG)
   1-W250x89 (MIN. 1000 LONG)

10. SOME PIECES REQUIRE PAINTING. USE
    NO PAINT UNLESS NOTED OTHERWISE
    ON DRAWINGS.

DEPARTMENT OF CIVIL AND
ENVIRONMENTAL ENGINEERING
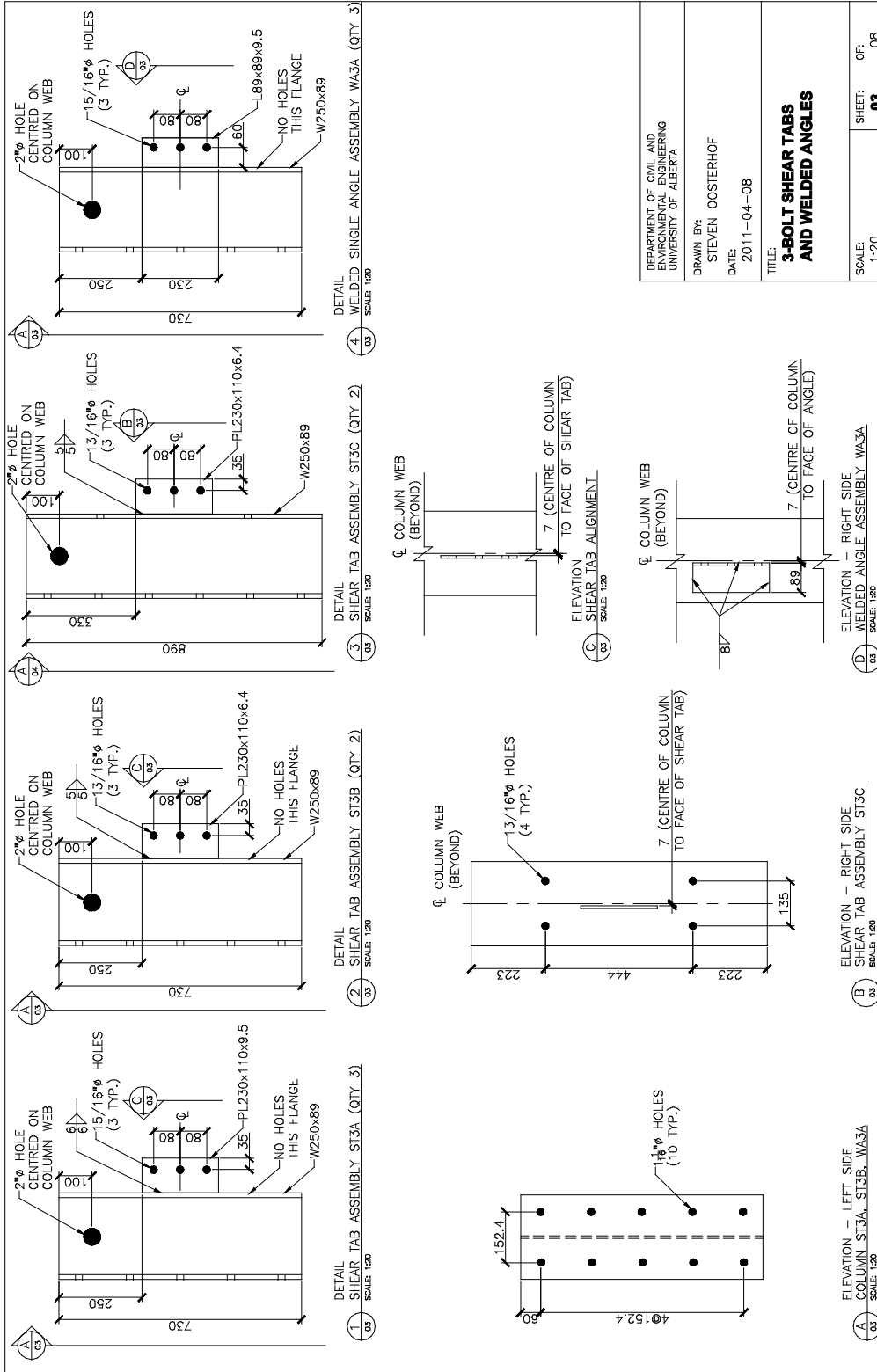UNIVERSITY OF ALBERTA

DRAWN BY:
STEVEN OOSTERHOF

DATE:
2011-04-08
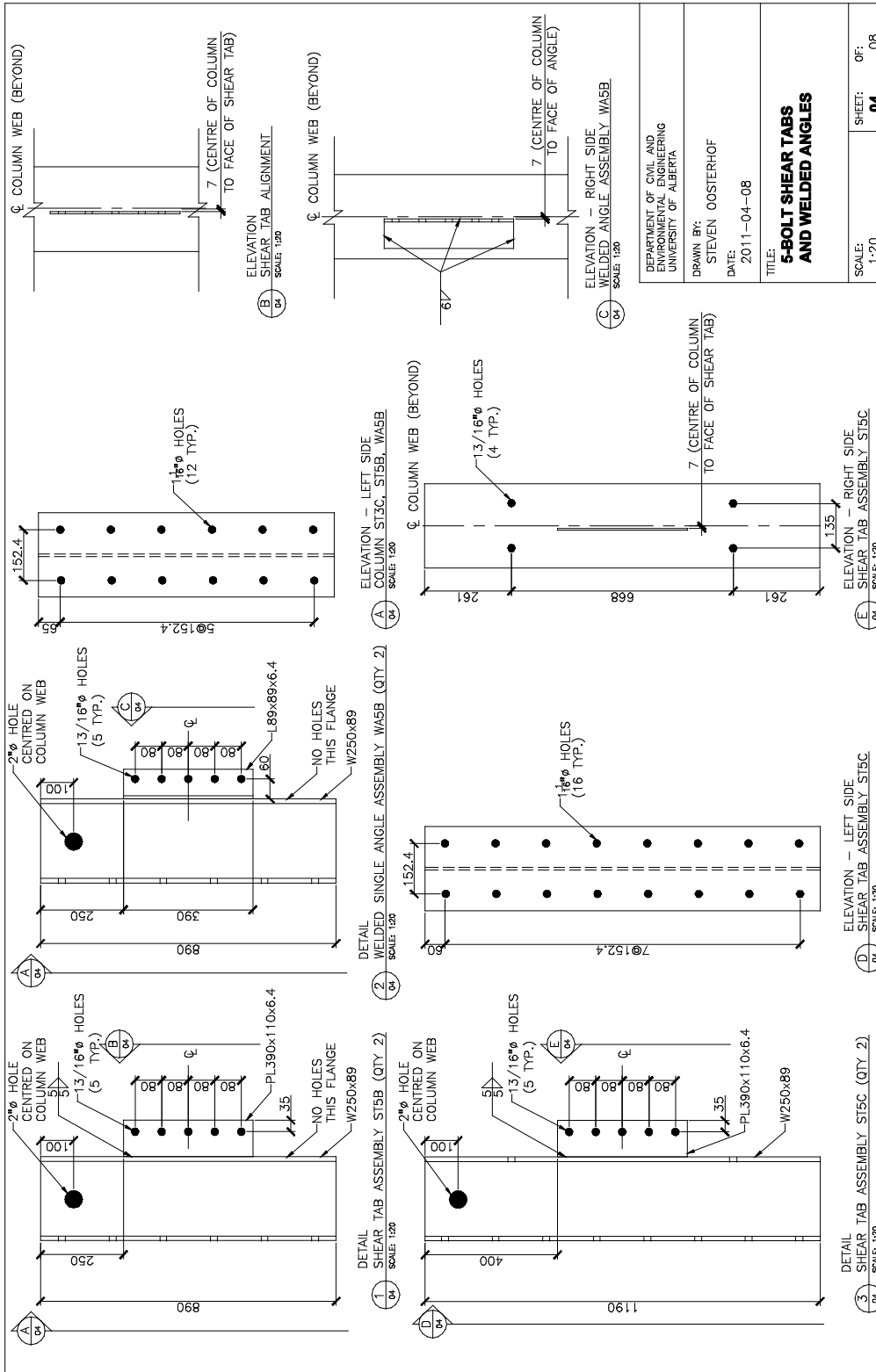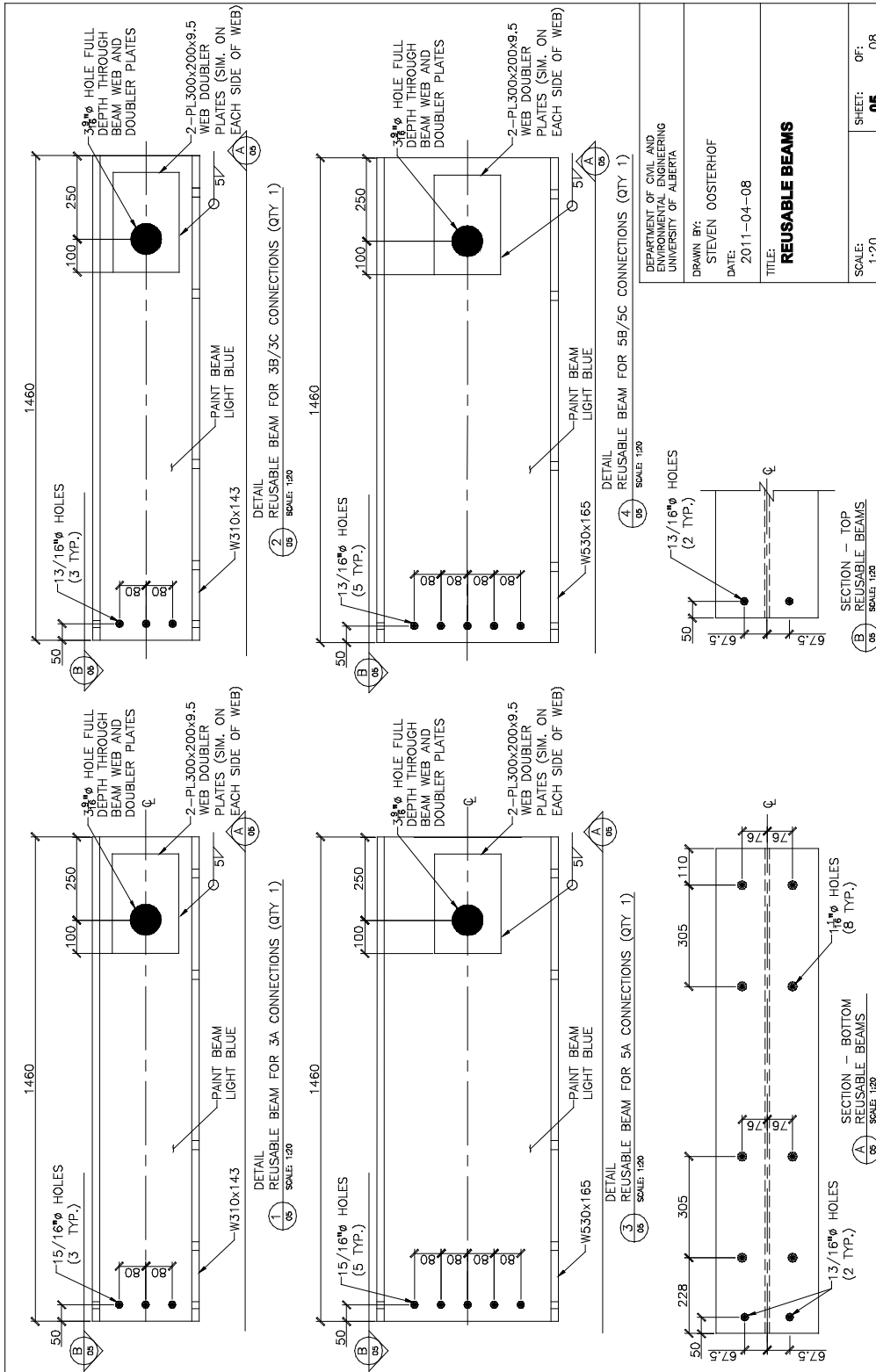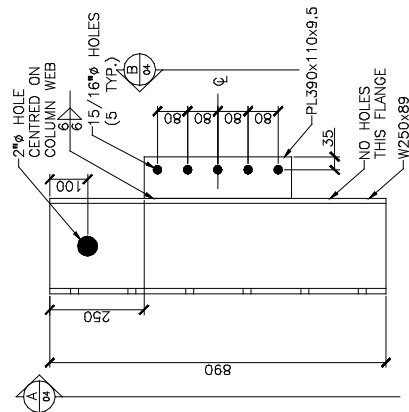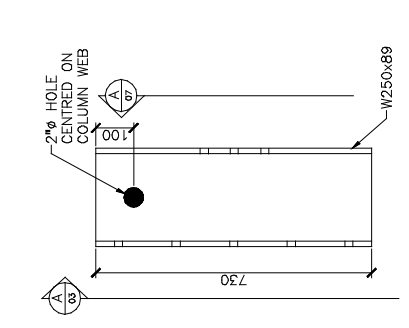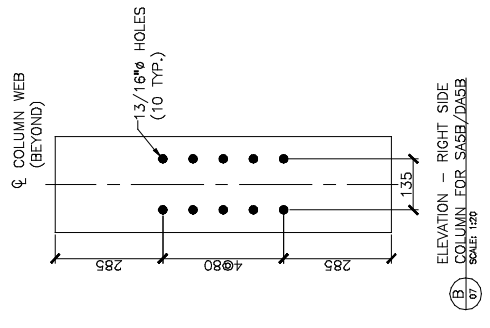
TITLE:
GENERAL NOTES

SCALE:
N.T.S.

SHEET: 01   OF: 08

This is a full-page engineering drawing titled "OVERALL TEST SET-UP".

DETAIL
SLIDE PLATE (QTY 4)
SCALE: 1:20
4/02

L51x51x6.4 (550 LONG) ON BACK SIDE OF STEEL BACKER PLATE
STEEL BACKER PLATE PL650x400x10
PTFE SLIDE PLATE PL550x300x5 CENTRED ON STEEL BACKER PLATE. ATTACH USING ADHESIVE OR COUNTERSUNK SCREWS.

SECTION
SLIDE PLATE
SCALE: 1:10
B/02

STEEL BACKER PLATE
PTFE
4 V 50-175

NOTES:
1. ITEMS SHOWN IN GREY ARE EXISTING STRUCTURE AND ARE NOT TO BE SUPPLIED AS PART OF THIS CONTRACT.

DEPARTMENT OF CIVIL AND ENVIRONMENTAL ENGINEERING
UNIVERSITY OF ALBERTA
DRAWN BY: STEVEN OOSTERHOF
DATE: 2011-04-08
TITLE: OVERALL TEST SET-UP
SCALE: VARIOUS
SHEET: 02
OF: 08

DETAIL
ACTUATOR BASEPLATE (QTY 2)
SCALE: 1:20
3/02

PL305x305x51
TAPPED HOLES THREADED FULL DEPTH TO MATCH 1"ϕx3¼" LONG A490 BOLTS FROM BOLT SCHEDULE (4 TYP.)
38 229 38
76 153 76

SHEAR WALL

ACTUATOR 3
ACTUATOR 2
ACTUATOR 1

TEST SPECIMEN – REFER TO SHEETS 03-10
REFER TO DETAIL 2/02
SLIDE PLATE EACH SIDE REFER TO DETAIL 4/02
REFER TO DETAIL 3/02
STEEL BASEPLATE AND STRONG FLOOR

ELEVATION
OVERALL TEST SET-UP
SCALE: 1:40
1/02

REACTION BEAMS
SUPPORTING BEAM BEYOND
REACTION COLUMN

SECTION
ACTUATOR 3 CONNECTION PLATE A3
SCALE: 1:20
A/02

45 230 260 35 230 45
95 130 95
PL810x320x51
CJP
1⅛"ϕ HOLES (8 TYP.)

DETAIL
ACTUATOR 3 CONNECTION ASSEMBLY A3 (QTY 1)
SCALE: 1:20
2/02

PL810x320x51 LOAD TRANSFER PLATE
PAINT ASSEMBLY LIGHT BLUE
2-PL 38 THICK
290
TANGENT
R105
3⅛"ϕ HOLE

215

2"∅ HOLE CENTRED ON COLUMN WEB

15/16"∅ HOLES (3 TYP.)

L89x89x9.5

NO HOLES THIS FLANGE

W250x89

DETAIL
WELDED SINGLE ANGLE ASSEMBLY WA3A (QTY 3)
SCALE: 1:20

2"∅ HOLE CENTRED ON COLUMN WEB

13/16"∅ HOLES (3 TYP.)

PL230x110x6.4

W250x89

DETAIL
SHEAR TAB ASSEMBLY ST3C (QTY 2)
SCALE: 1:20

2"∅ HOLE CENTRED ON COLUMN WEB

13/16"∅ HOLES (3 TYP.)

PL230x110x6.4

NO HOLES THIS FLANGE

W250x89

DETAIL
SHEAR TAB ASSEMBLY ST3B (QTY 2)
SCALE: 1:20

2"∅ HOLE CENTRED ON COLUMN WEB

15/16"∅ HOLES (3 TYP.)

PL230x110x9.5

NO HOLES THIS FLANGE

W250x89

DETAIL
SHEAR TAB ASSEMBLY ST3A (QTY 3)
SCALE: 1:20

₵ COLUMN WEB (BEYOND)

7 (CENTRE OF COLUMN TO FACE OF SHEAR TAB)

ELEVATION
SHEAR TAB ALIGNMENT
SCALE: 1:20

₵ COLUMN WEB (BEYOND)

7 (CENTRE OF COLUMN TO FACE OF ANGLE)

ELEVATION - RIGHT SIDE
WELDED ANGLE ASSEMBLY WA3A
SCALE: 1:20

₵ COLUMN WEB (BEYOND)

13/16"∅ HOLES (4 TYP.)

7 (CENTRE OF COLUMN TO FACE OF SHEAR TAB)

ELEVATION - RIGHT SIDE
SHEAR TAB ASSEMBLY ST3C
SCALE: 1:20

1"∅ HOLES (10 TYP.)

ELEVATION - LEFT SIDE
COLUMN ST3A, ST3B, WA3A
SCALE: 1:20

℄ COLUMN WEB (BEYOND)

7 (CENTRE OF COLUMN TO FACE OF SHEAR TAB)

ELEVATION
SHEAR TAB ALIGNMENT
SCALE: 1:20

B / D4

℄ COLUMN WEB (BEYOND)

7 (CENTRE OF COLUMN TO FACE OF ANGLE)

ELEVATION – RIGHT SIDE
WELDED ANGLE ASSEMBLY WA5B
SCALE: 1:20

C / D4

19

$\frac{13}{16}"\phi$ HOLES (12 TYP.)

152.4

5@152.4

55

ELEVATION – LEFT SIDE
COLUMN ST3C, ST5B, WA5B
SCALE: 1:20

A / D4

℄ COLUMN WEB (BEYOND)

13/16"φ HOLES (4 TYP.)

7 (CENTRE OF COLUMN TO FACE OF SHEAR TAB)

135

261   899   261

ELEVATION – RIGHT SIDE
SHEAR TAB ASSEMBLY ST5C
SCALE: 1:20

E / D4

2"φ HOLE CENTRED ON COLUMN WEB

13/16"φ HOLES (5 TYP.)

℄

L89x89x6.4

NO HOLES THIS FLANGE

W250x89

100

80 80 80 80

60

250   390

890

DETAIL
WELDED SINGLE ANGLE ASSEMBLY WA5B (QTY 2)
SCALE: 1:20

2 / D4

C / D4

13/16"φ HOLES (16 TYP.)

152.4

7@152.4

60

ELEVATION – LEFT SIDE
SHEAR TAB ASSEMBLY ST5C
SCALE: 1:20

D / D4

2"φ HOLE CENTRED ON COLUMN WEB

13/16"φ HOLES (5 TYP.)

℄

PL390x110x6.4

NO HOLES THIS FLANGE

W250x89

100

80 80 80 80

35

250

890

DETAIL
SHEAR TAB ASSEMBLY ST5B (QTY 2)
SCALE: 1:20

1 / D4

A / D4

B / D4

2"φ HOLE CENTRED ON COLUMN WEB

13/16"φ HOLES (5 TYP.)

℄

PL390x110x6.4

W250x89

100

80 80 80 80

35

400

1190

DETAIL
SHEAR TAB ASSEMBLY ST5C (QTY 2)
SCALE: 1:20

3 / D4

D / D4

E / D4

DETAIL 1 REUSABLE BEAM FOR 3A CONNECTIONS (QTY 1) SCALE: 1:20

DETAIL 2 REUSABLE BEAM FOR 3B/3C CONNECTIONS (QTY 1) SCALE: 1:20

DETAIL 3 REUSABLE BEAM FOR 5A CONNECTIONS (QTY 1) SCALE: 1:20

DETAIL 4 REUSABLE BEAM FOR 5B/5C CONNECTIONS (QTY 1) SCALE: 1:20

SECTION - TOP REUSABLE BEAMS SCALE: 1:20

SECTION - BOTTOM REUSABLE BEAMS SCALE: 1:20

3 9/16"Ø HOLE FULL DEPTH THROUGH BEAM WEB AND DOUBLER PLATES

2-PL300x200x9.5 WEB DOUBLER PLATES (SIM. ON EACH SIDE OF WEB)

15/16"Ø HOLES (3 TYP.)
13/16"Ø HOLES (3 TYP.)
15/16"Ø HOLES (5 TYP.)
13/16"Ø HOLES (5 TYP.)
13/16"Ø HOLES (2 TYP.)
1 1/16"Ø HOLES (8 TYP.)

PAINT BEAM LIGHT BLUE

W310x143
W530x165

1460
250
100
50
80
228
305
110
305
76
76
67.5

DEPARTMENT OF CIVIL AND ENVIRONMENTAL ENGINEERING UNIVERSITY OF ALBERTA

DRAWN BY: STEVEN OOSTERHOF
DATE: 2011-04-08
TITLE: REUSABLE BEAMS
SCALE: 1:20
SHEET: 05   OF: 08

ELEVATION – RIGHT SIDE
REUSABLE COLUMN FOR 3B/5B
SCALE: 1:20
13/16"⌀ HOLES
(18 TYP.)
Ç BEAM WEB (BEYOND)
135
281 112 62 80 80 80 80 62 112

ELEVATION – RIGHT SIDE
REUSABLE COLUMN FOR 3A/5A
SCALE: 1:20
15/16"⌀ HOLES
(10 TYP.)
Ç BEAM WEB (BEYOND)
135
455 80 80 80 80

ELEVATION – LEFT SIDE
REUSABLE COLUMNS
SCALE: 1:20
11/16"⌀ HOLES
(16 TYP.)
Ç BEAM WEB (BEYOND)
152.4
60 7@152.4

DETAIL
REUSABLE COLUMN FOR 3B/5B (QTY 1)
SCALE: 1:20
2"⌀ HOLE
CENTRED ON
COLUMN WEB
100
PAINT COLUMN
LIGHT BLUE
W250x89
1190
316 251 161 286

DETAIL
REUSABLE COLUMN FOR 3A/5A (QTY 1)
SCALE: 1:20
2"⌀ HOLE
CENTRED ON
COLUMN WEB
100
PAINT COLUMN
LIGHT BLUE
W250x89
1190
405 160 447

SECTION
COLUMN STIFFENER
SCALE: 1:20
STIFFENER
PL(FITTED)x110x16
EACH SIDE
TYP.

DEPARTMENT OF CIVIL AND
ENVIRONMENTAL ENGINEERING
UNIVERSITY OF ALBERTA

DRAWN BY:
STEVEN OOSTERHOF
DATE:
2011-04-08

TITLE:
REUSABLE COLUMNS

SCALE:
1:20

SHEET: OF:
06   08

219

DEPARTMENT OF CIVIL AND
ENVIRONMENTAL ENGINEERING
UNIVERSITY OF ALBERTA

DRAWN BY:
STEVEN OOSTERHOF

DATE:
2011-04-08

TITLE:
BOLTED ANGLE COLUMNS

SCALE:
1:20

SHEET: **07** OF: 08

Detail 3 — SHEAR TAB ASSEMBLY ST5A (QTY 2)

2"∅ HOLE CENTRED ON COLUMN WEB
15/16"∅ HOLES (5 TYP.)
PL390x110x9.5
NO HOLES THIS FLANGE
W250x89
100
35
80 80 80 80
250
890

Detail 2 — COLUMN FOR SA5B/DA5B (QTY 2)

2"∅ HOLE CENTRED ON COLUMN WEB
W250x89
100
890

Detail 1 — COLUMN FOR SA3B/DA3B (QTY 2)

2"∅ HOLE CENTRED ON COLUMN WEB
W250x89
100
730

Elevation B — RIGHT SIDE COLUMN FOR SA5B/DA5B

13/16"∅ HOLES (10 TYP.)
℄ COLUMN WEB (BEYOND)
135
285 4@80 285

Elevation A — RIGHT SIDE COLUMN FOR SA3B/DA3B

13/16"∅ HOLES (6 TYP.)
℄ COLUMN WEB (BEYOND)
135
285 2@80 285

89
60
35 80 80 80 80 35
390
13/16"∅ HOLES
(10 TYP.)
L89x89x6.4

DETAIL
4 / 08   5B/5C ANGLE CONNECTION (QTY 12)
SCALE: 1:10

89
60
35 80 80 80 80 35
390
15/16"∅ HOLES
(10 TYP.)
L89x89x9.5

DETAIL
3 / 08   5A ANGLE CONNECTION (QTY 2)
SCALE: 1:10

89
60
35 80 80 35
230
13/16"∅ HOLES
(6 TYP.)
L89x89x6.4

DETAIL
2 / 08   3B/3C ANGLE CONNECTION (QTY 17)
SCALE: 1:10

89
60
35 35 35
13/16"∅ HOLES
(4 TYP.)
L89x89x6.4
205

TYPICAL DETAIL
6 / 08   SEAT ANGLE FOR ANGLE CONNECTIONS (QTY 12)
SCALE: 1:10

89
60
35 80 80 35
230
15/16"∅ HOLES
(6 TYP.)
L89x89x9.5

DETAIL
1 / 08   3A ANGLE CONNECTION (QTY 4)
SCALE: 1:10

102
60
35 35 35
75
13/16"∅ HOLES
(4 TYP.)
L102x102x6.4
205

TYPICAL DETAIL
5 / 08   SEAT ANGLE FOR SHEAR TAB CONNECTIONS (QTY 8)
SCALE: 1:10

221

APPENDIX C.   MATERIAL DATA

This appendix contains the stress-strain plots from each of the tension coupon tests performed, shown in Figures C.1 through C.7. Curves for multiple tension coupons extracted from the same specimen are plotted together. Table C.1 summarizes the results of all tension coupon tests conducted. Coupons were not extracted from the reusable beam segments, since these elements remained elastic during testing.

Table C.1. Coupon test results.

Section	Coupon Number	Young's Modulus E (MPa)	Static Yield Strength σ_y (MPa)	Static Ultimate Strength σ_u (MPa)
PL9.5	i	201380	350	436
	ii	190850	356	439
	iii	195240	351	430
	iv	191550	356	429
	Mean	**194755**	**353**	**433**
Coefficient of Variation		**0.025**	**0.009**	**0.010**
PL6.4	i	195350	339	465
	ii	200430	330	455
	iii	191180	311	457
	iv	195300	312	456
	Mean	**195565**	**323**	**458**
Coefficient of Variation		**0.019**	**0.043**	**0.010**
L89×89×9.5	i	191280	359	499
	ii	198280	350	508
	iii	190920	365	507
	iv	181040	331	491
	Mean	**190380**	**351**	**501**
Coefficient of Variation		**0.037**	**0.042**	**0.016**
L89×89×6.4	i	200490	343	495
	ii	195800	343	498
	iii	190630	345	502
	Mean	**195640**	**344**	**499**
Coefficient of Variation		**0.025**	**0.002**	**0.007**
L102×102×6.4	i	201380	350	436
	ii	190850	356	439
	iii	195240	351	430
	iv	191550	356	429
	Mean	**194755**	**353**	**433**
Coefficient of Variation		**0.025**	**0.009**	**0.010**
W250×89 (flange)	i	201080	351	475
	ii	198210	355	472
	iii	193620	351	468
	iv	203530	350	471
	Mean	**199110**	**352**	**472**
Coefficient of Variation		**0.021**	**0.006**	**0.006**
W250×89 (web)	i	195830	382	475
	ii	192350	388	487
	Mean	**194090**	**385**	**481**
Coefficient of Variation		**0.013**	**0.011**	**0.017**
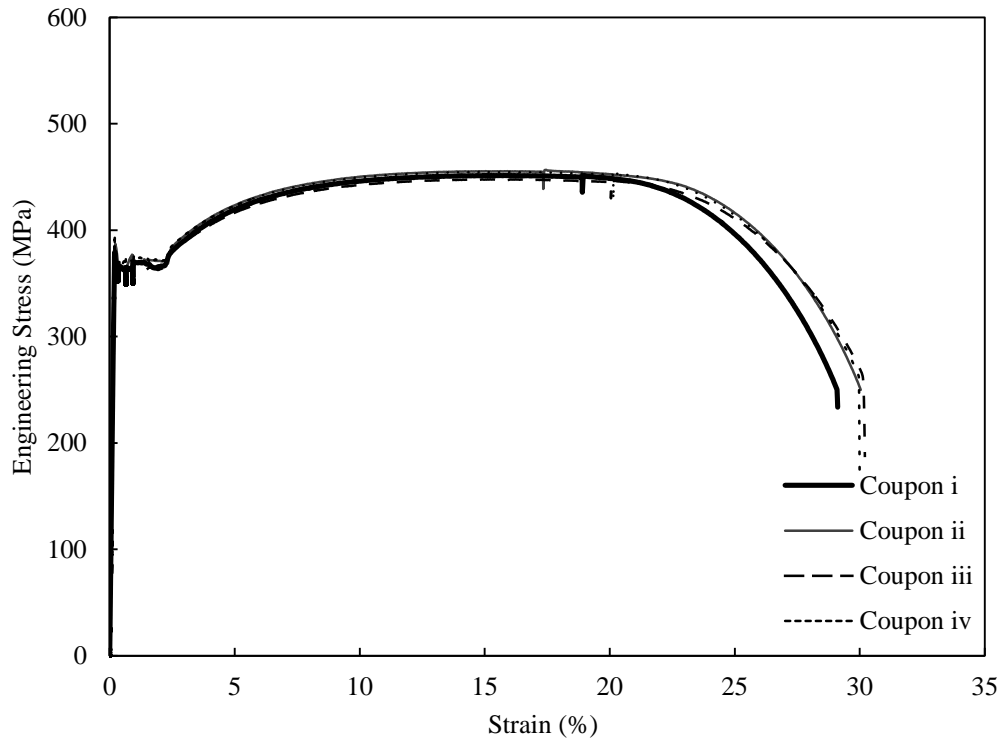
Figure C.1. Stress–strain curves for 9.5 mm plate.
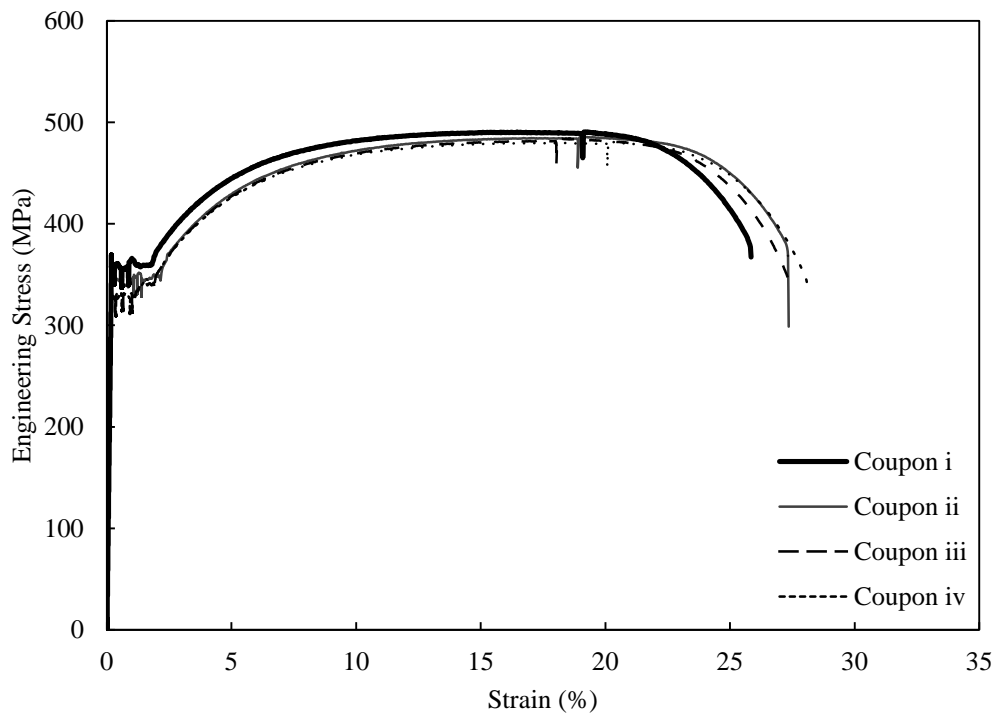
Figure C.2. Stress–strain curves for 6.4 mm plate.

224
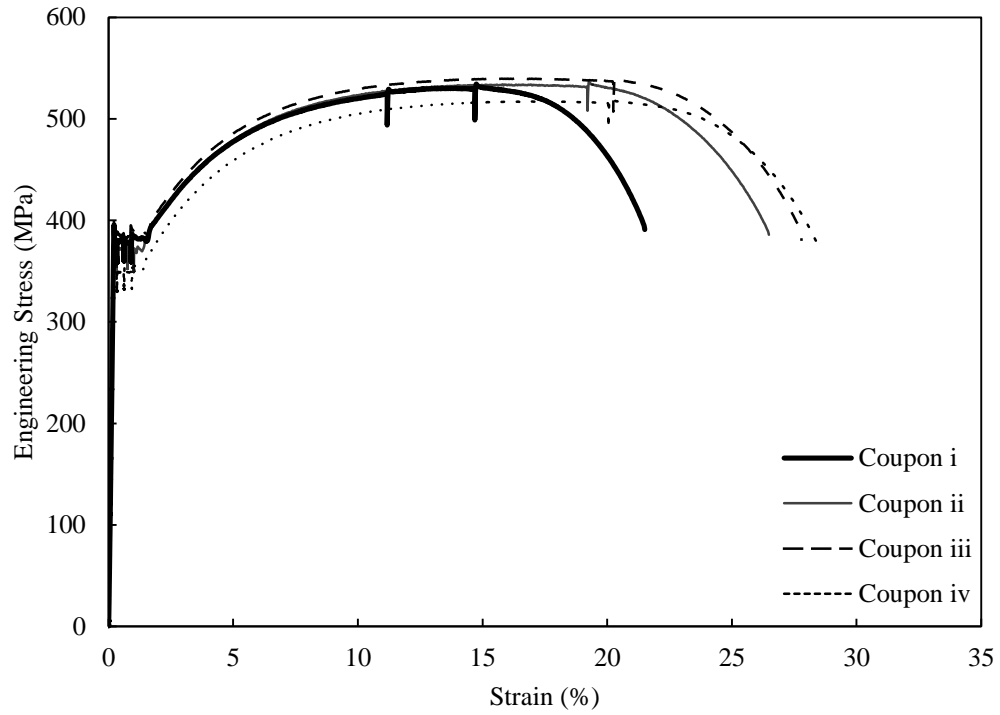
Figure C.3. Stress–strain curves for L89×89×9.5.

Premature rupture of
Coupon i at initial
imperfection (notch in the
reduced cross section).
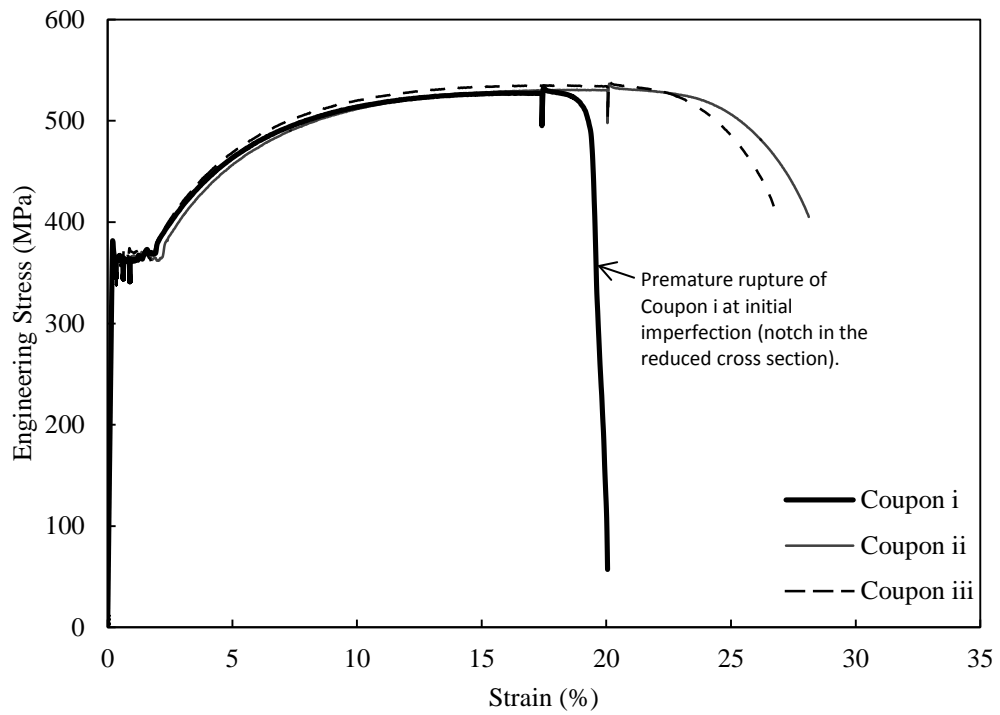
Figure C.4. Stress–strain curves for L89×89×6.4.

225
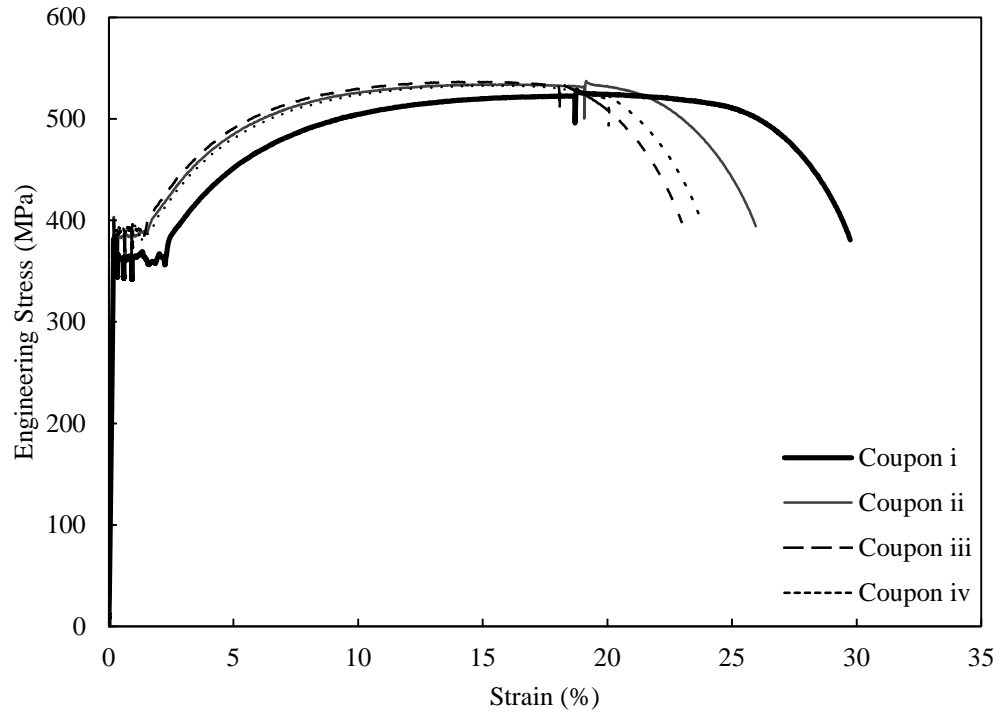
Figure C.5. Stress–strain curves for L102×102×6.4.
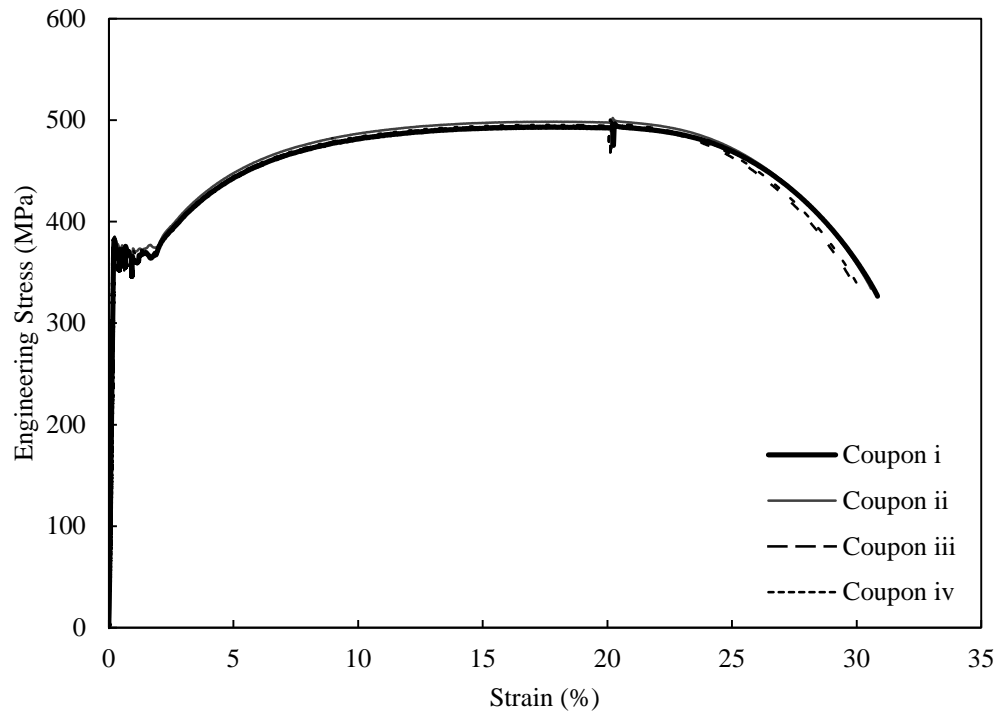
Figure C.6. Stress–strain curves for W250×89 flanges.

226
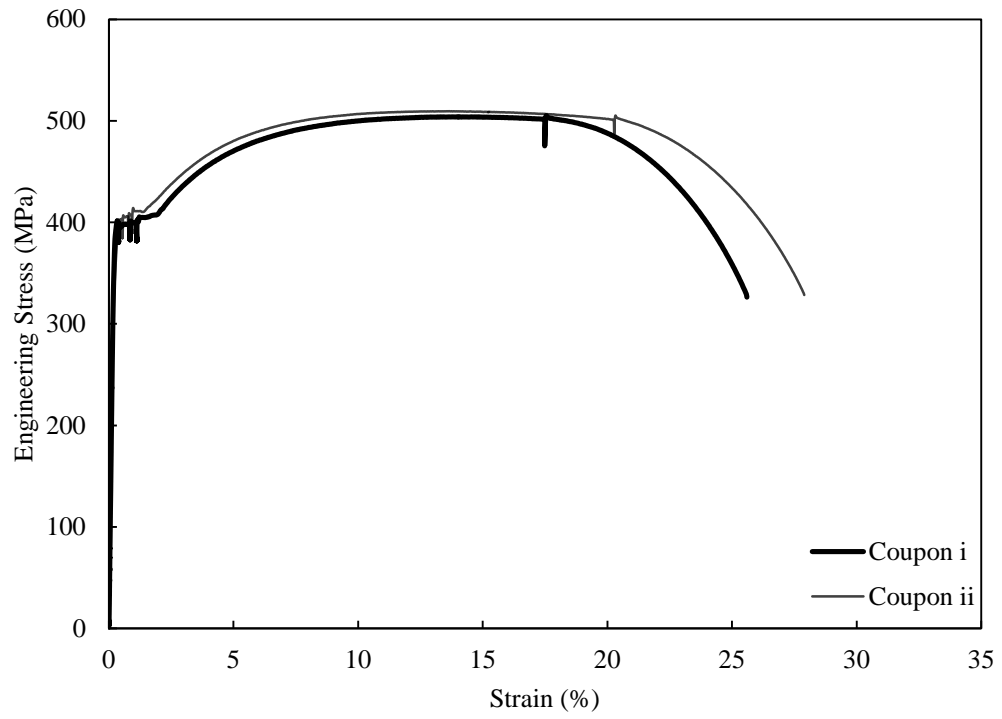
Figure C.7. Stress–strain curves for W250×89 web.

APPENDIX D.   LOAD VERSUS ROTATION CURVES

This appendix contains the load versus rotation curves for all of the 45 specimens tested in the experimental program. The curves are annotated with observations of events that had significant effects on the applied load history. Bolt locations are numbered sequentially from the top to the bottom of the connection, beginning with the line of bolts on the beam web. For cases where the connection was also bolted to the column flange, the numbering is continued from the top to the bottom of the left side of the column flange (when facing the column from the test beam side), followed by the bolts on the right side of the column flange (where present). Specimens with the same nominal geometry are plotted with equal scales on the x- and y-axes.
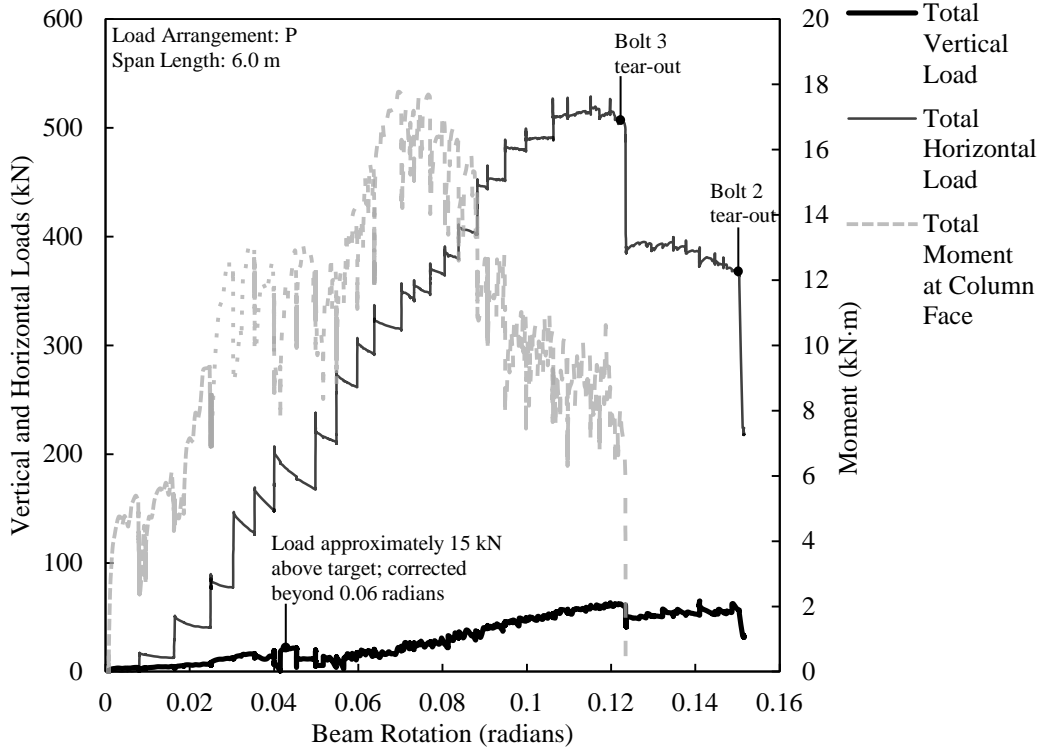
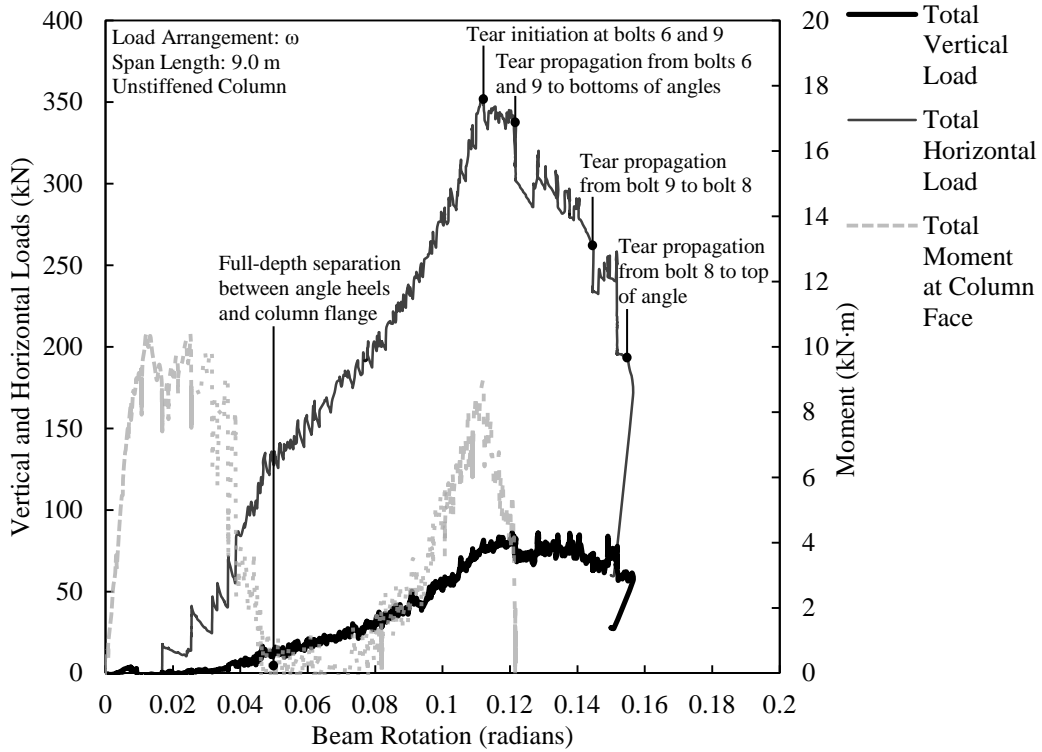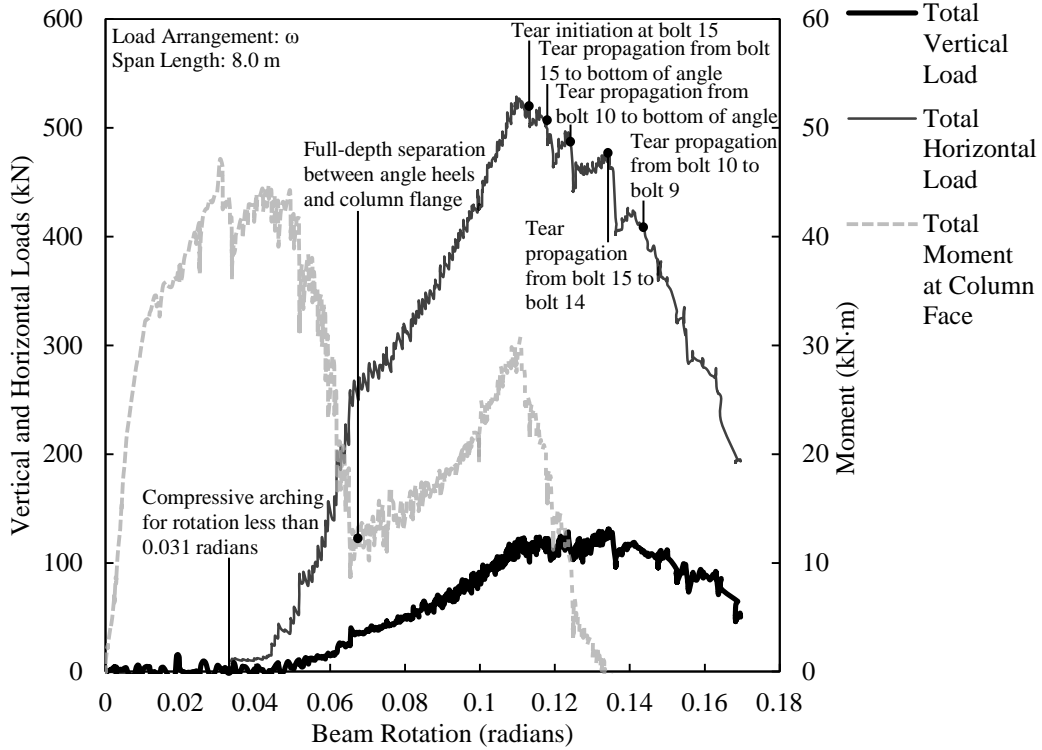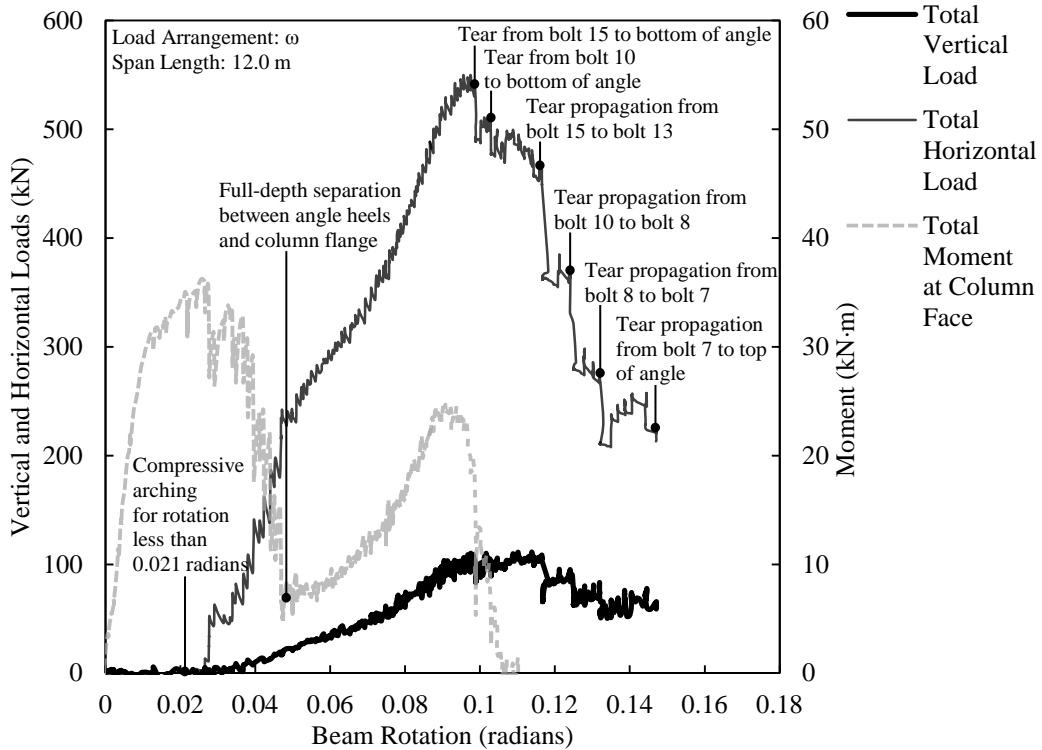**Figure D.1. Load versus rotation for ST3A-1.**
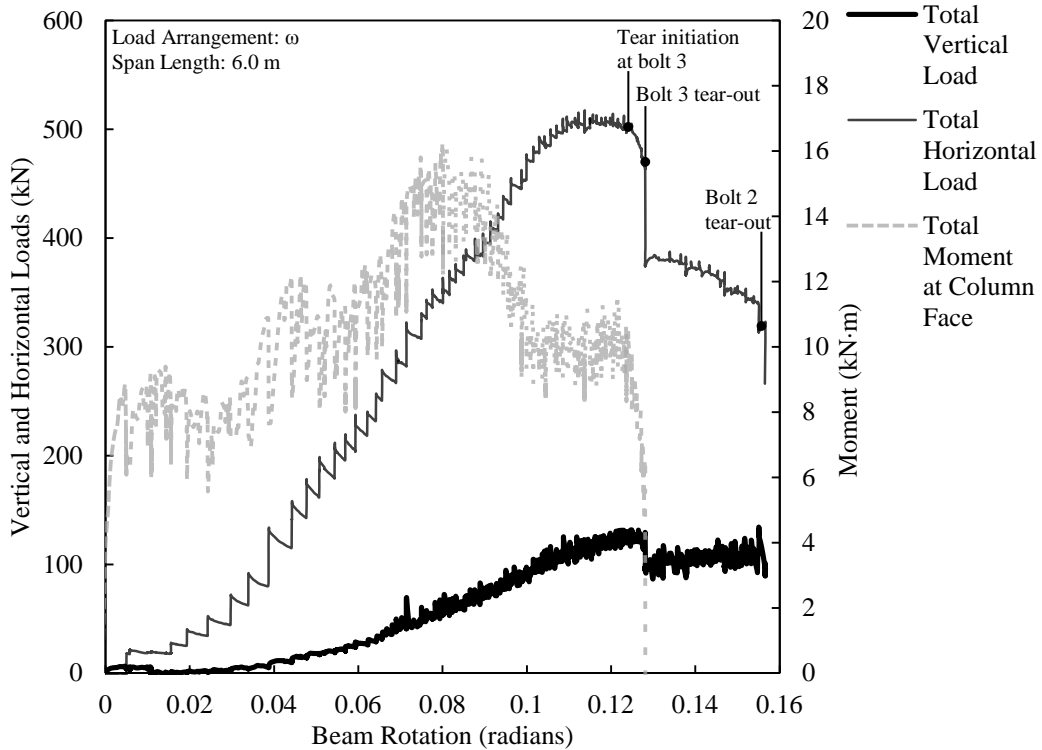
Figure D.2. Load versus rotation for ST3A-2.
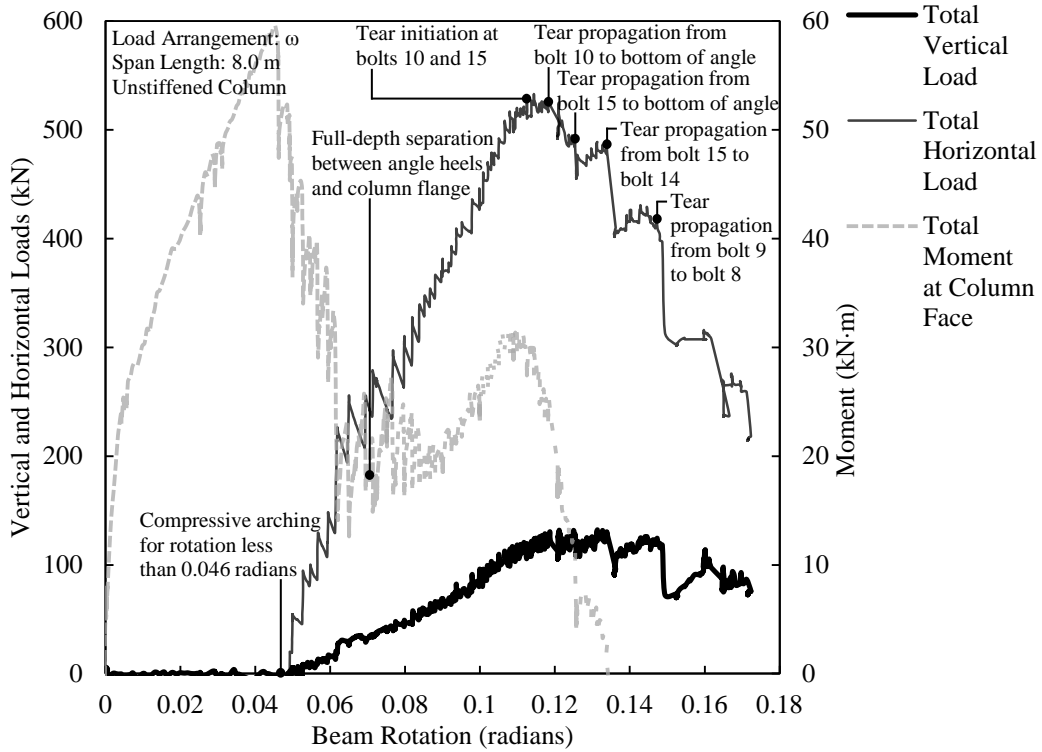
229
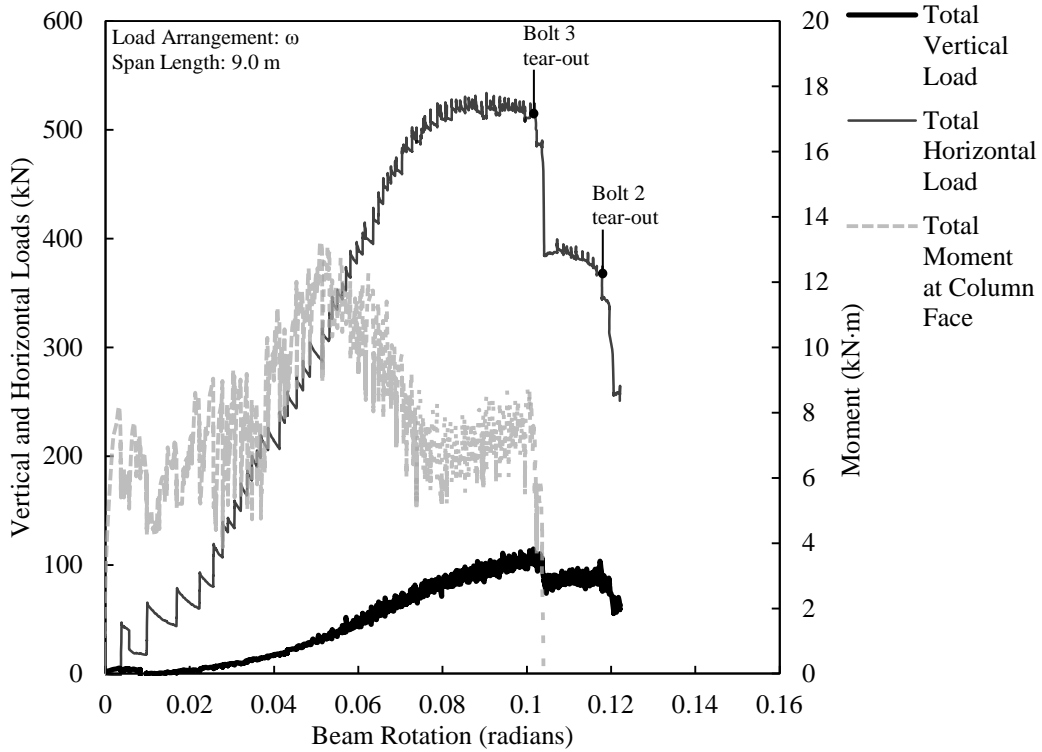
Figure D.3. Load versus rotation for ST3A-3.
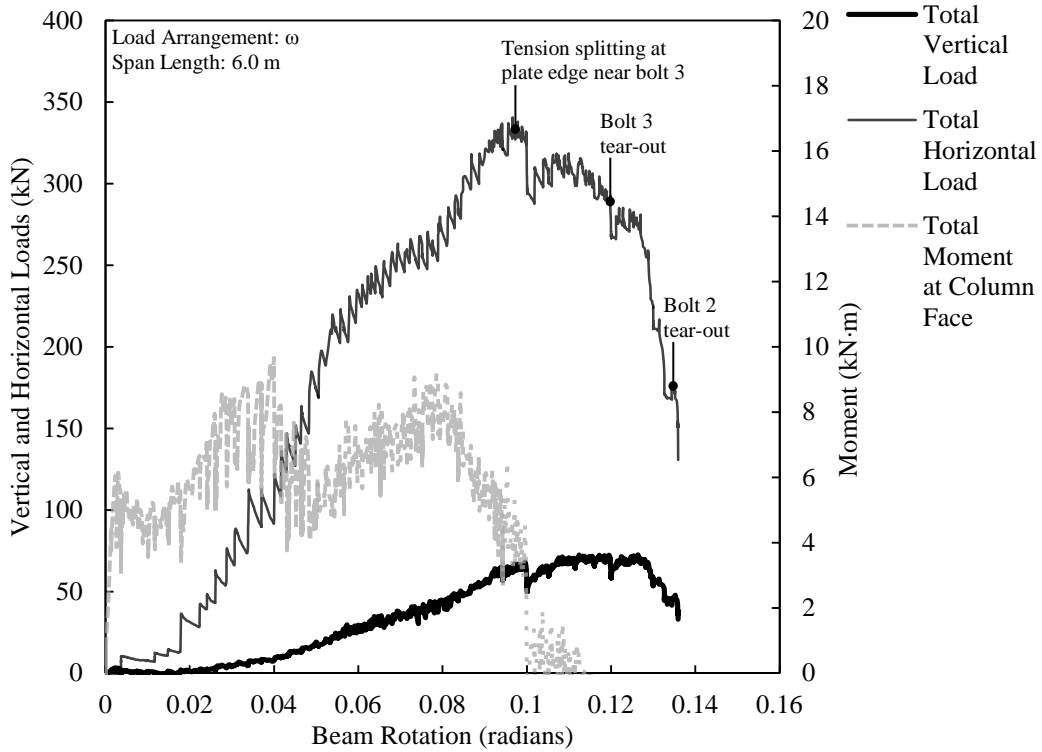
Figure D.4. Load versus rotation for ST3B-1.

230
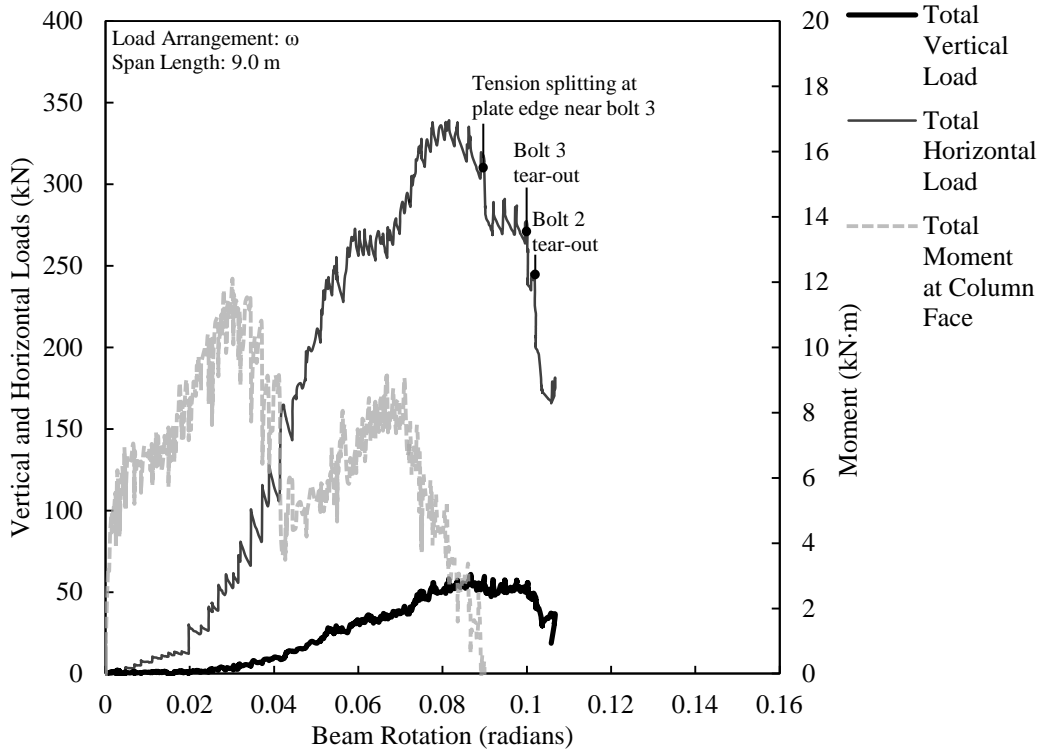
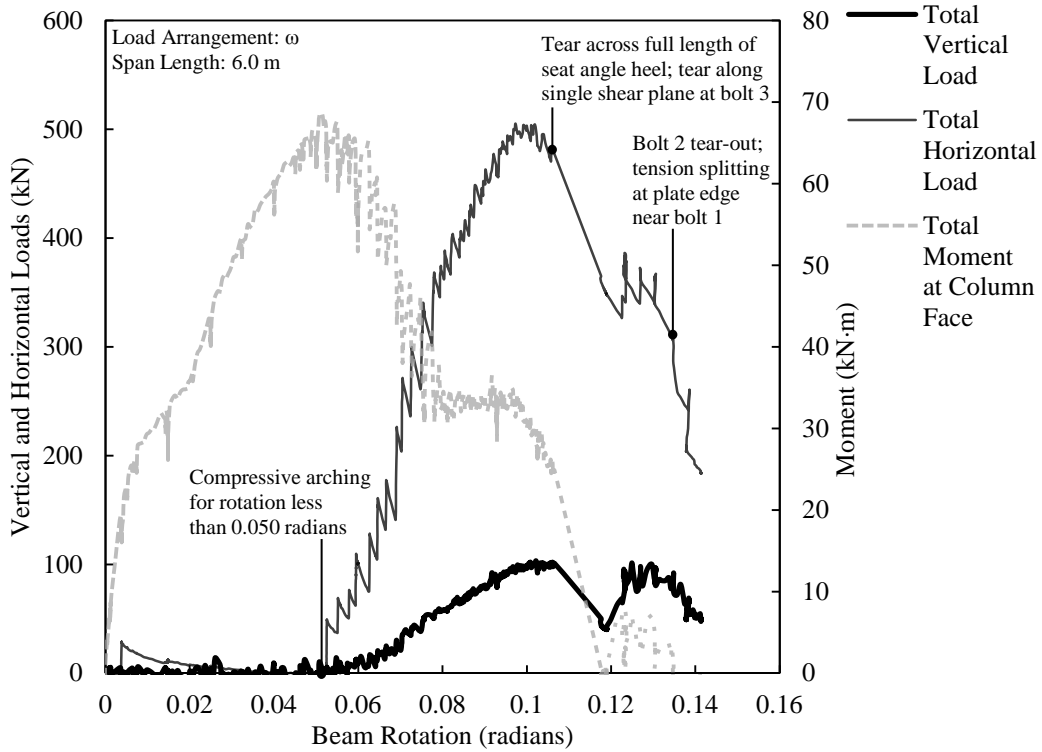**Figure D.5. Load versus rotation for ST3B-2.**
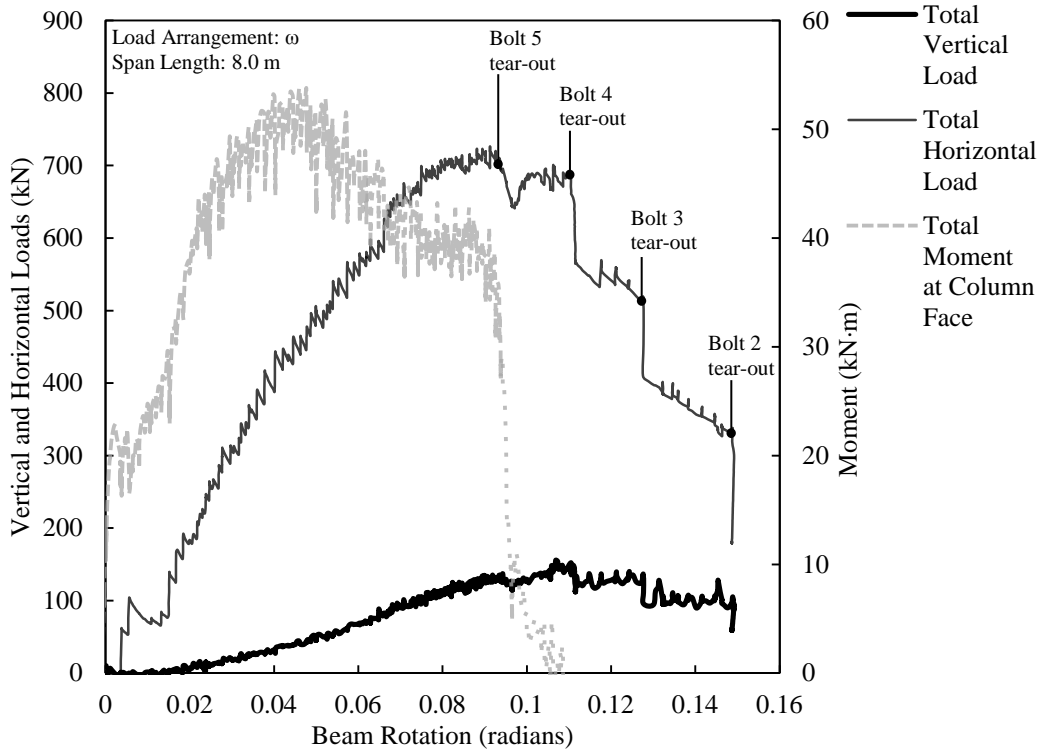
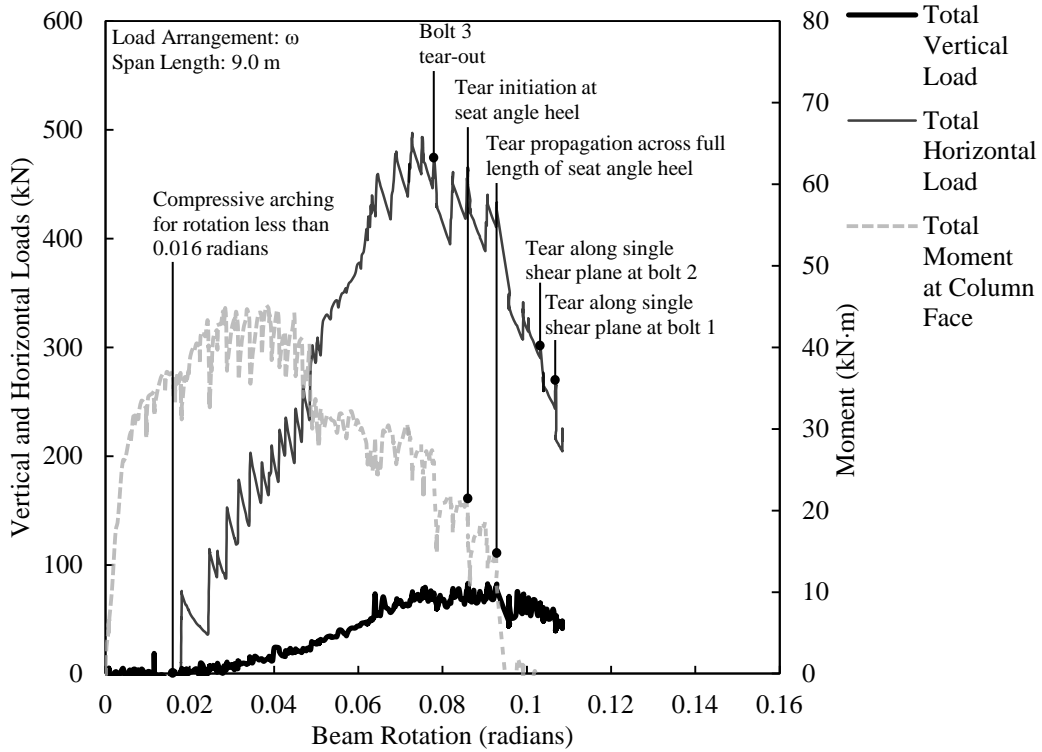**Figure D.6. Load versus rotation for ST5A-1.**

231
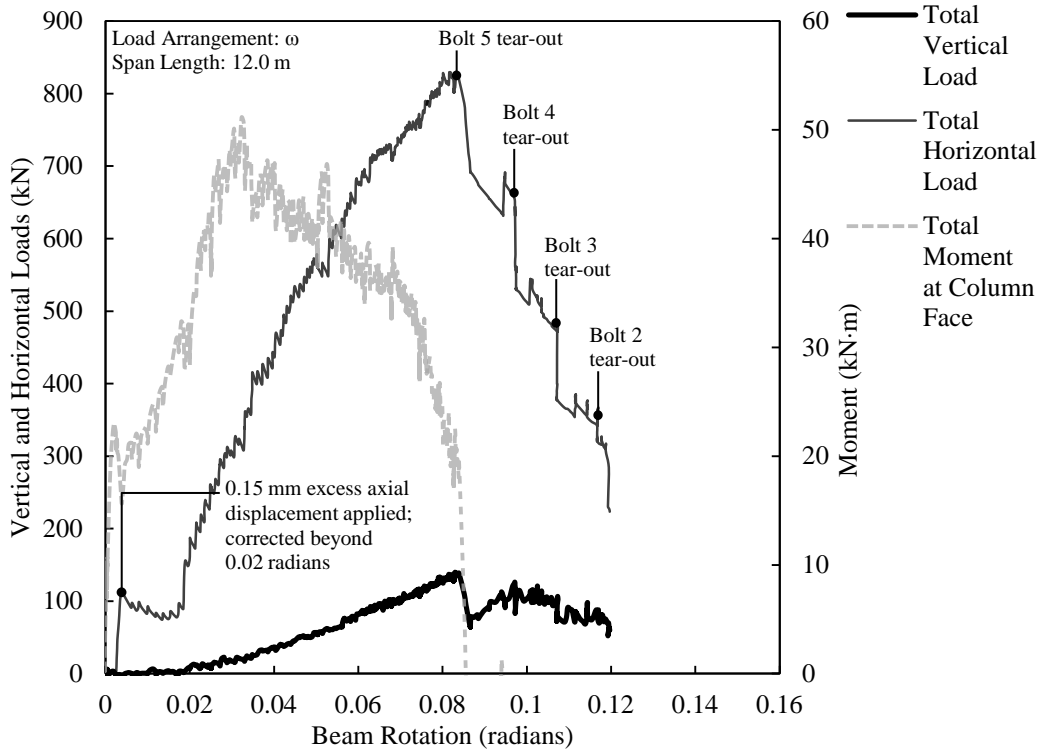
Figure D.7. Load versus rotation for ST5A-2.
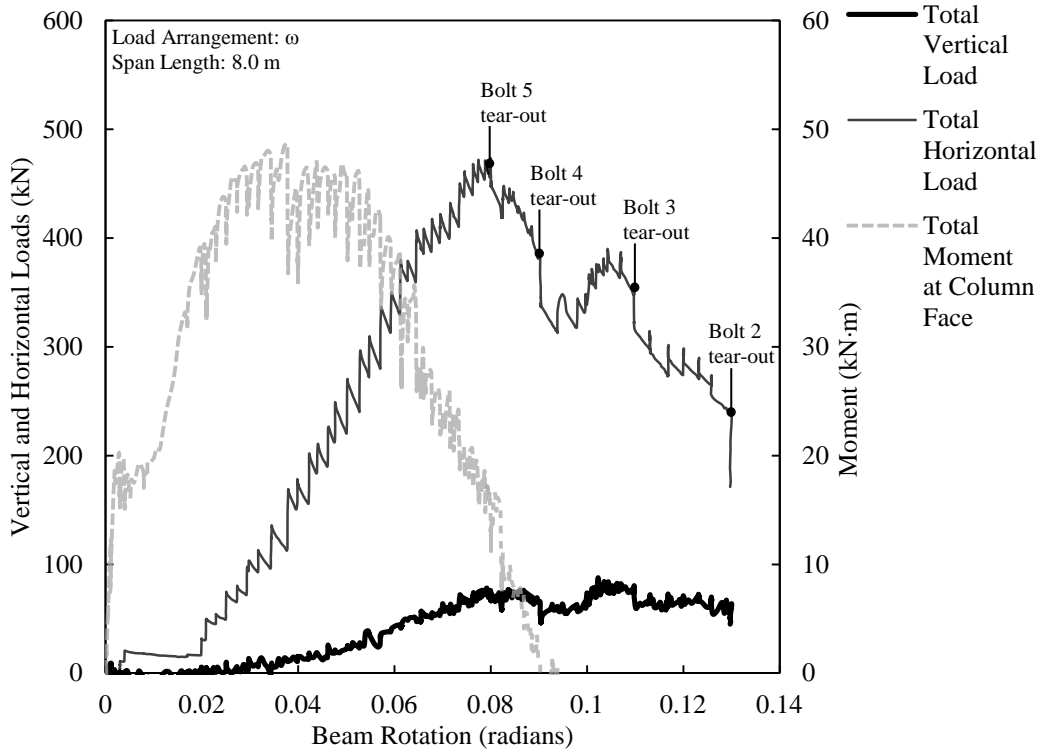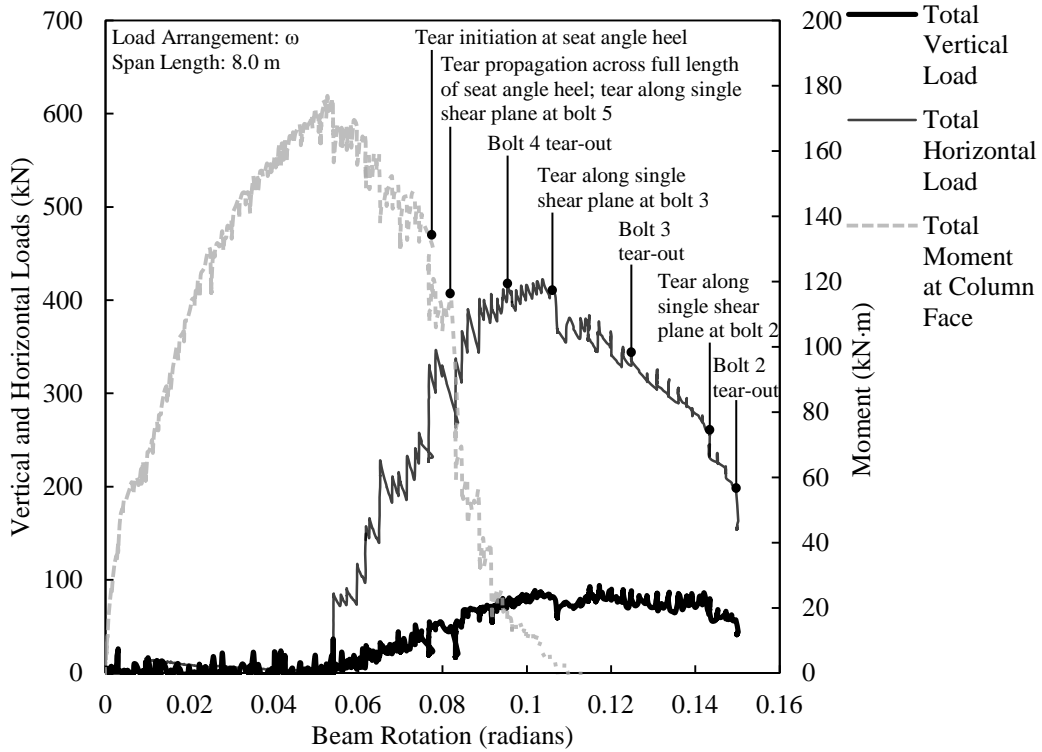

Figure D.8. Load versus rotation for ST5B-1.

232
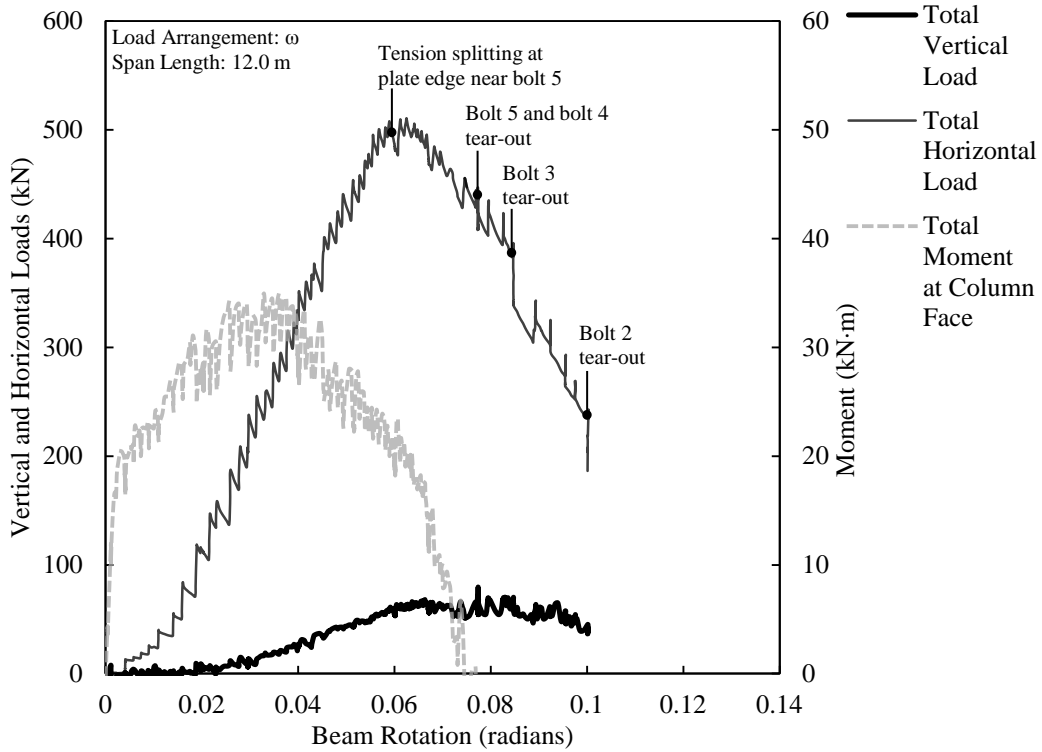
Figure D.9. Load versus rotation for ST5B-2.
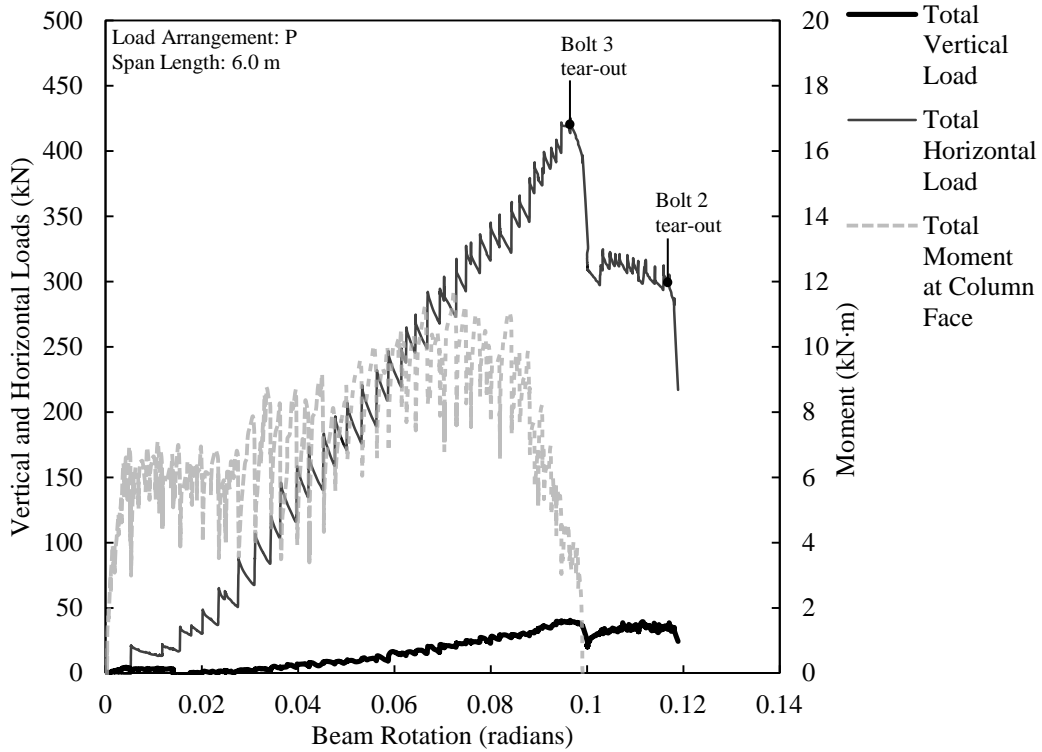
Figure D.10. Load versus rotation for WA3A-1.

233
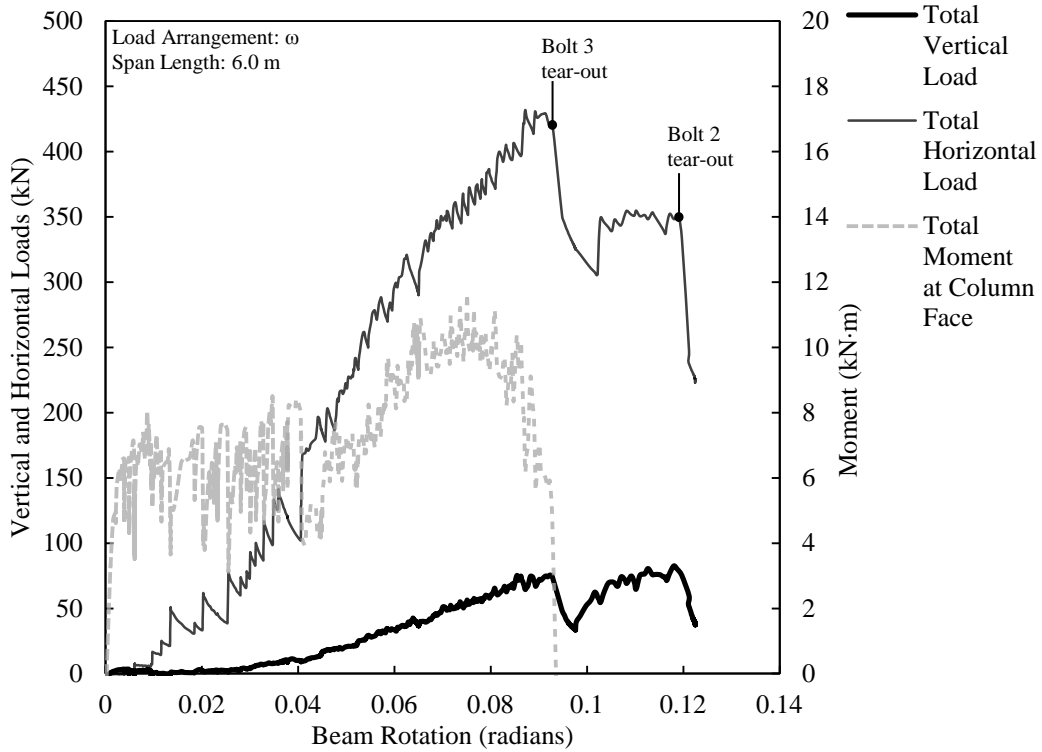
Figure D.11. Load versus rotation for WA3A-2.
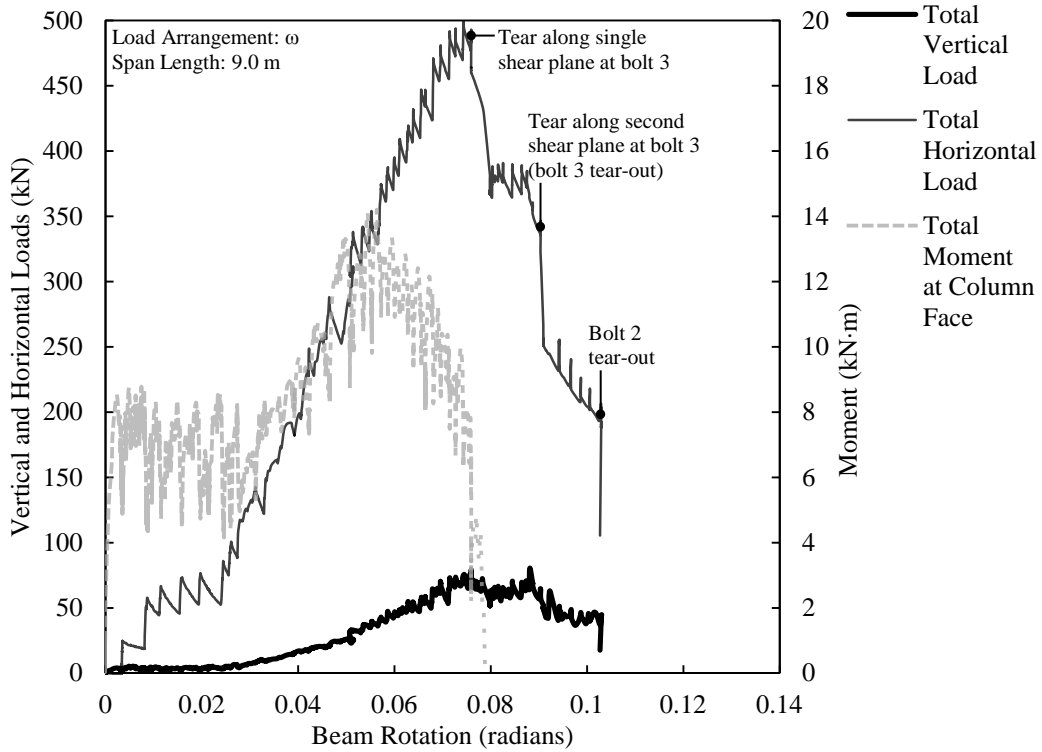
Figure D.12. Load versus rotation for WA3A-3.

234
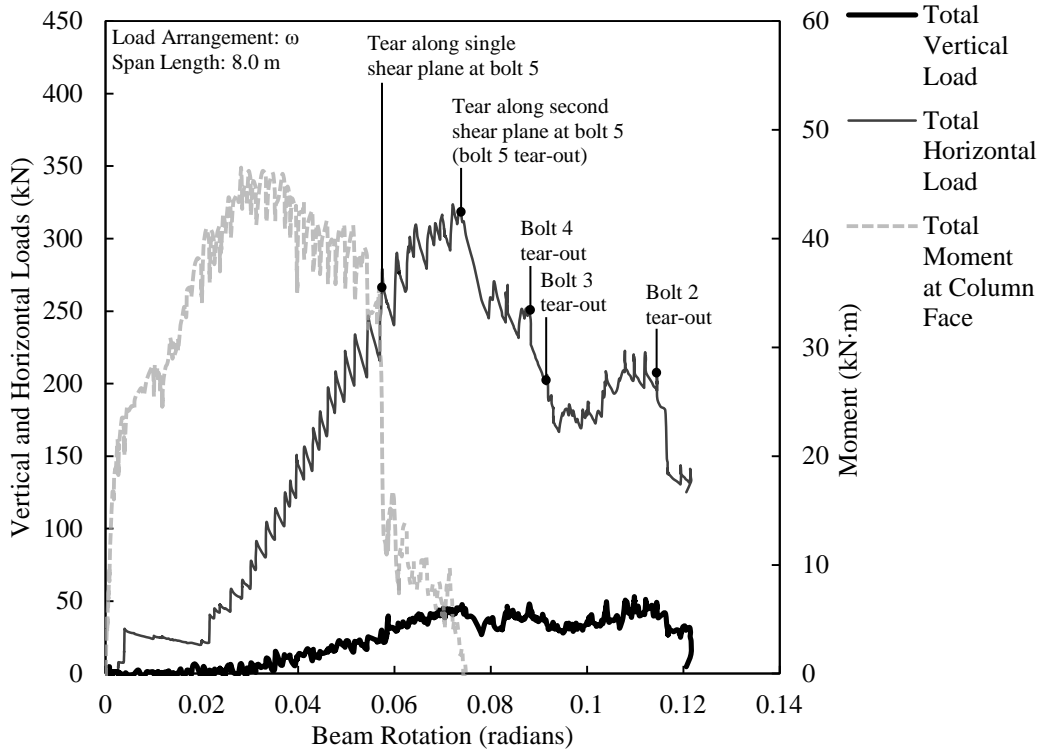
Figure D.13. Load versus rotation for WA5B-1.
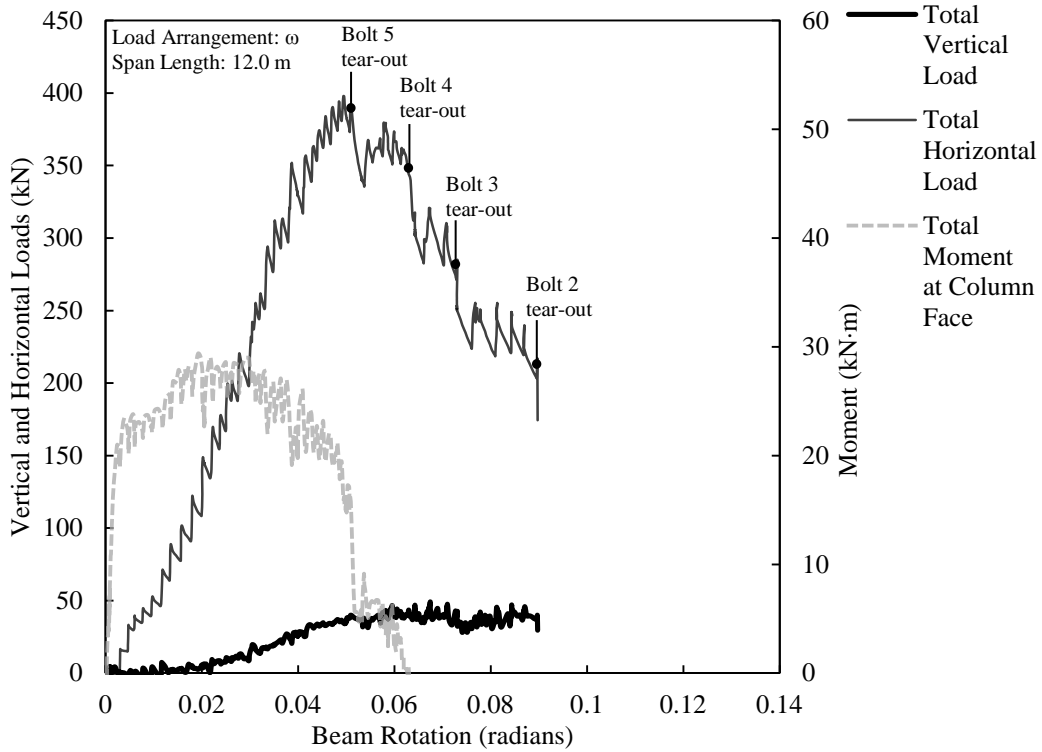
Figure D.14. Load versus rotation for WA5B-2.

235
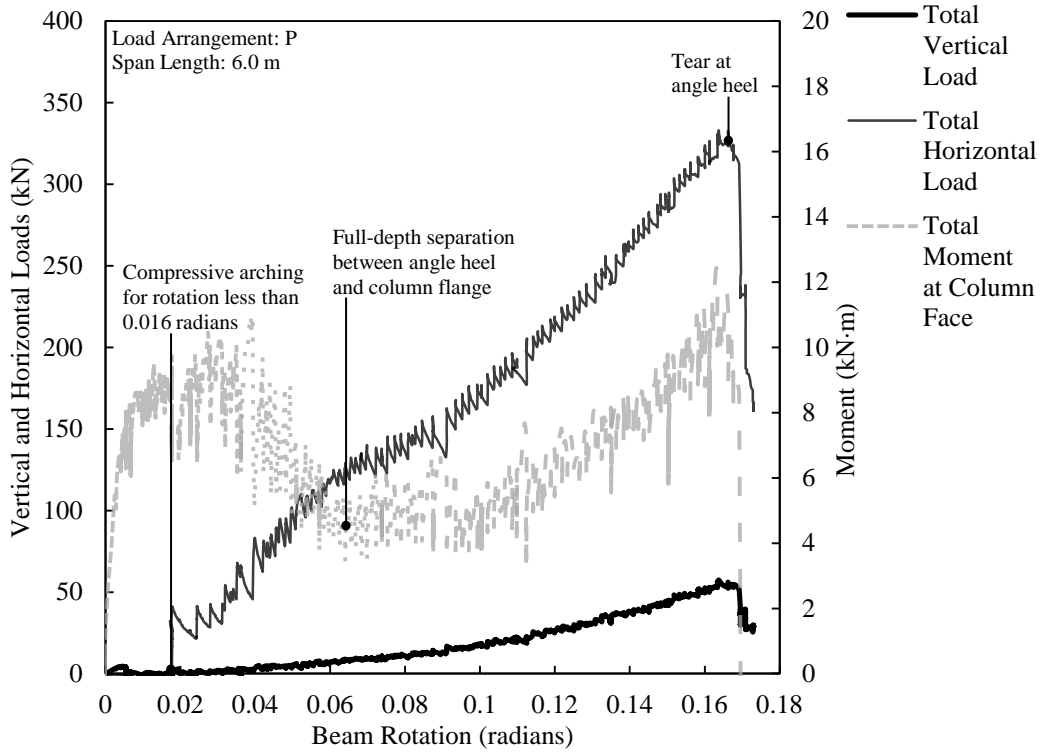
Figure D.15. Load versus rotation for SA3A-1.
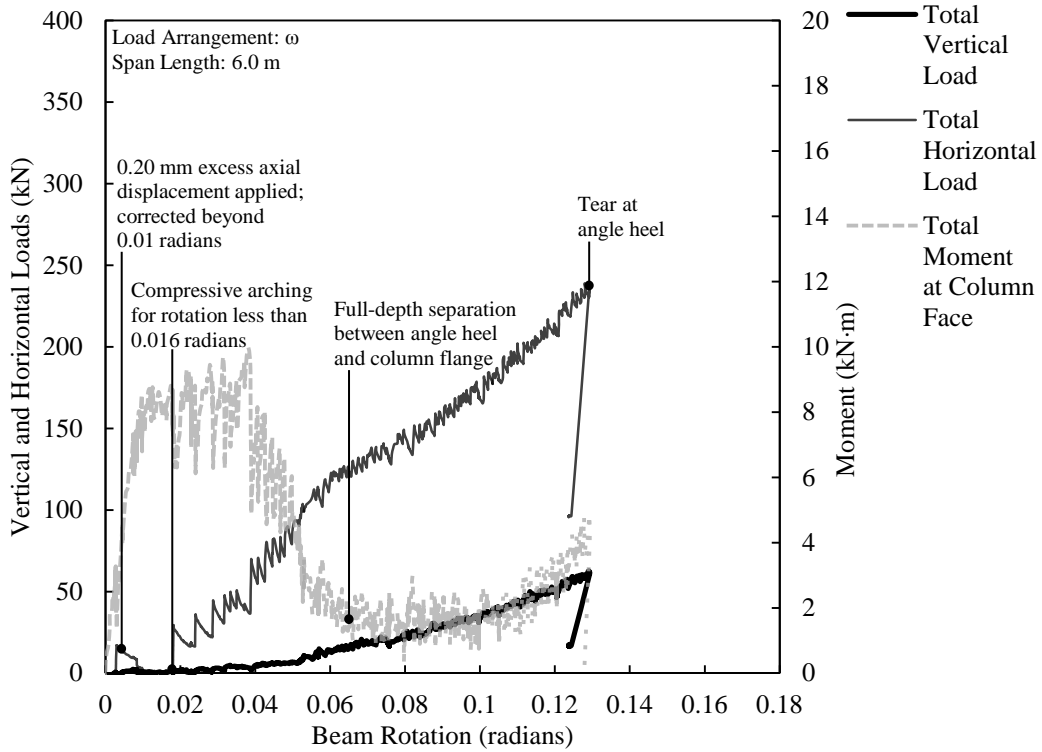
Figure D.16. Load versus rotation for SA3A-2.

236
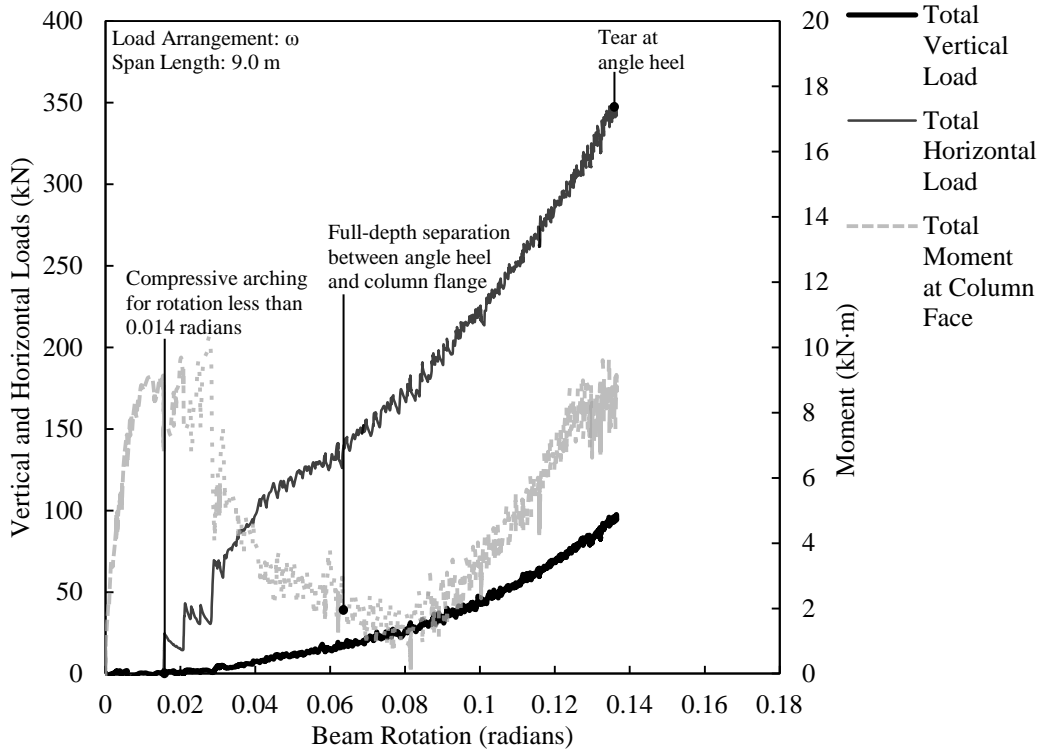
Figure D.17. Load versus rotation for SA3A-3.
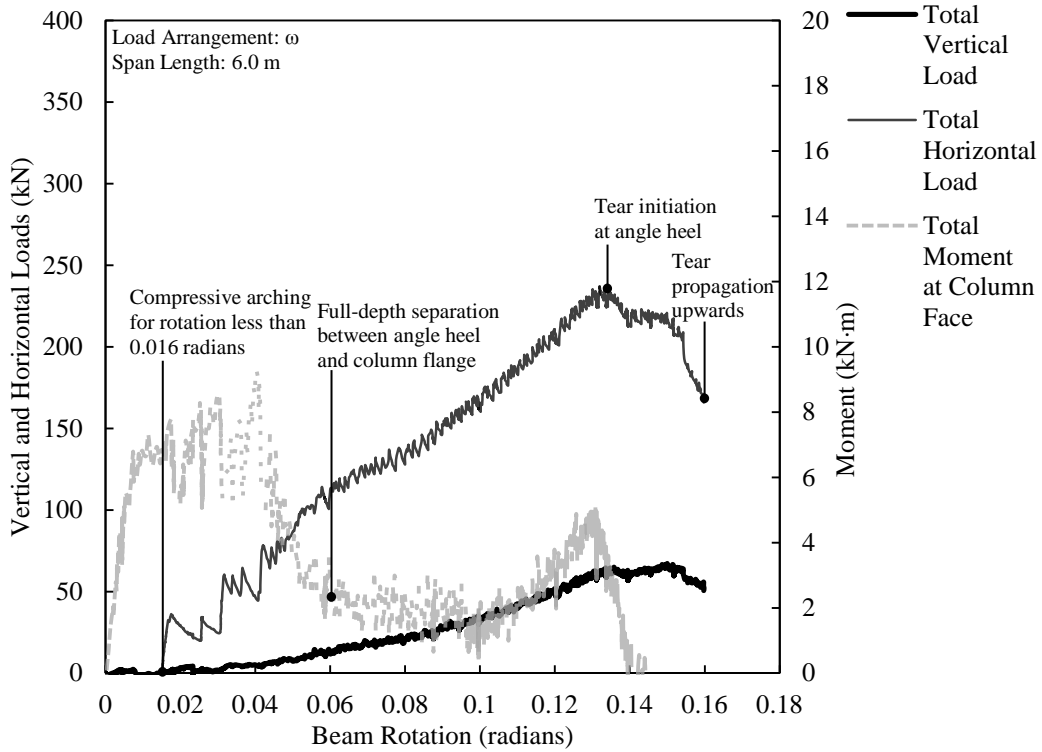
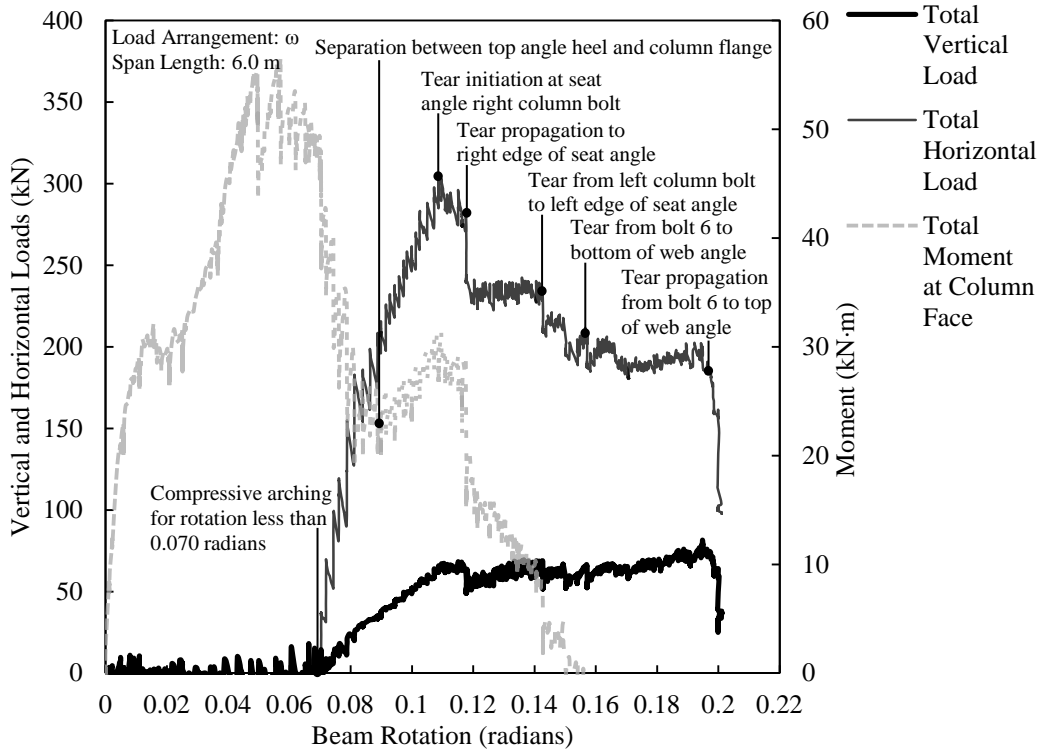**Figure D.18. Load versus rotation for SA3A-4.**

237
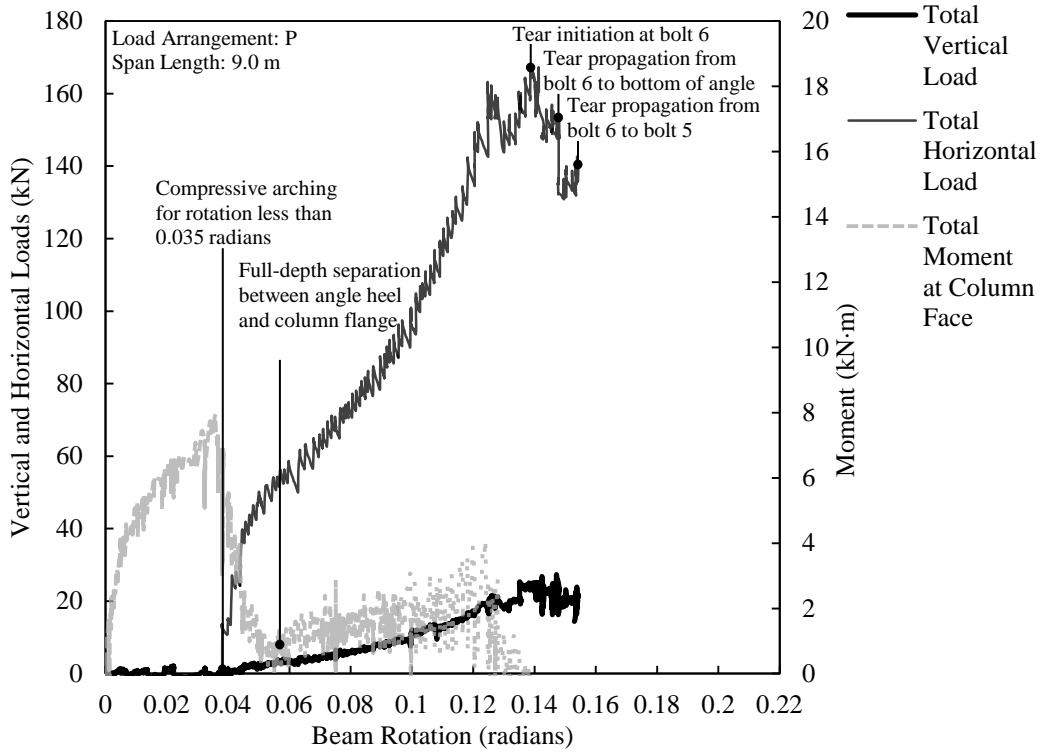
Figure D.19. Load versus rotation for SA3B-1.
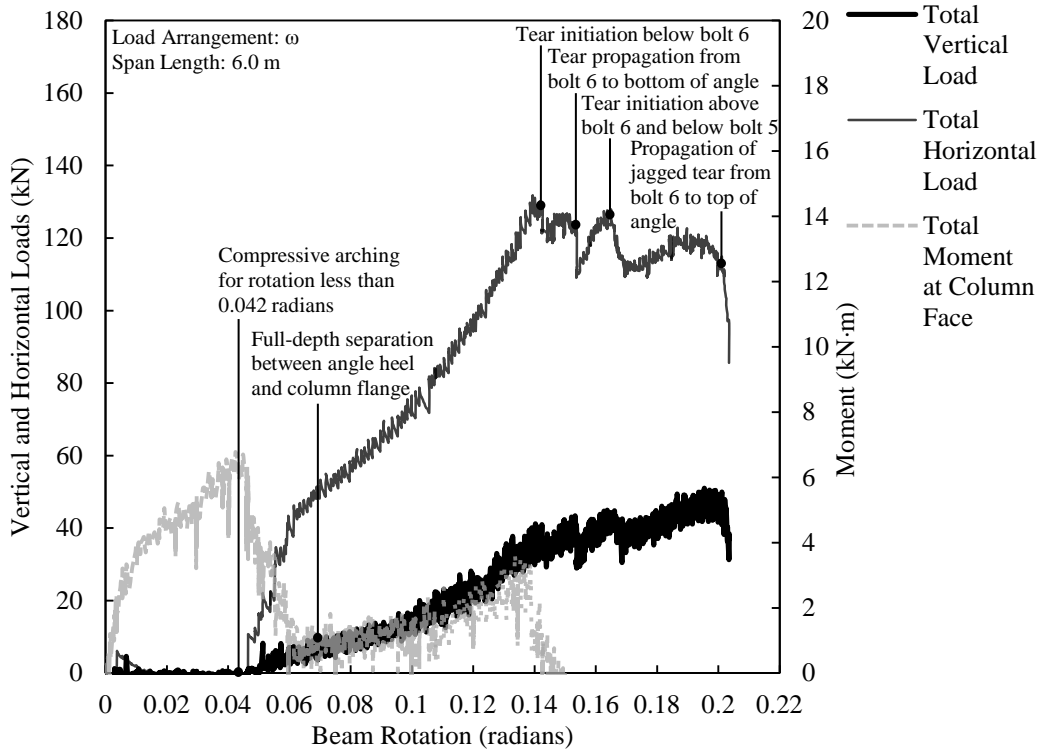
Figure D.20. Load versus rotation for SA3B-2.

238
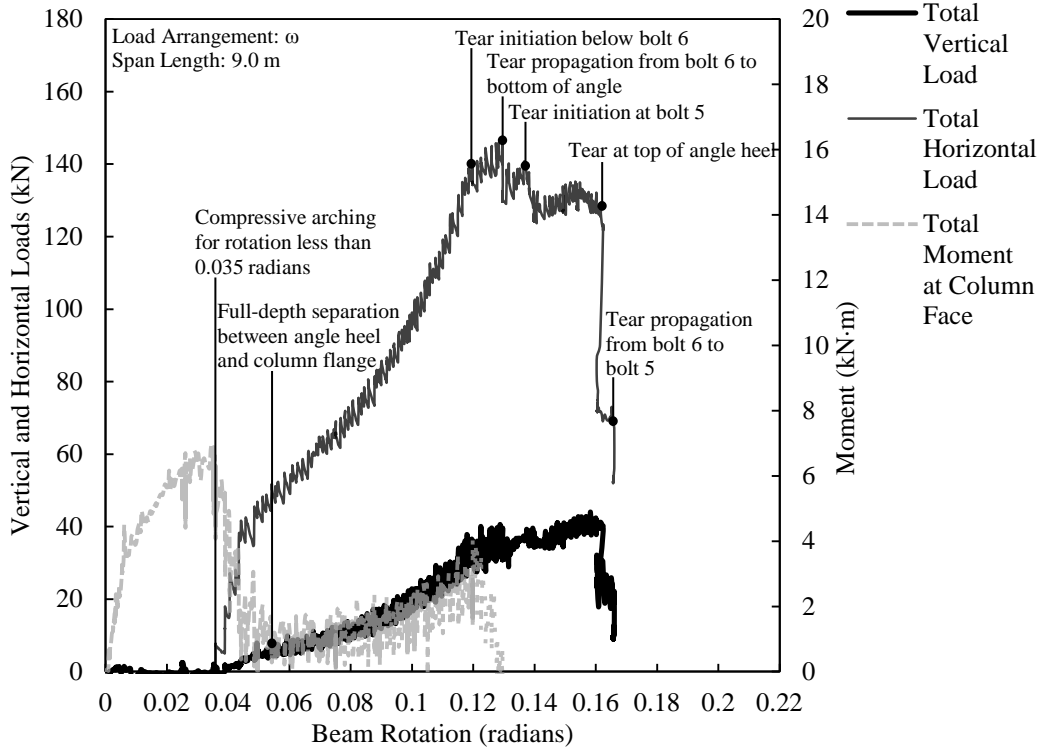
Figure D.21. Load versus rotation for SA3B-3.
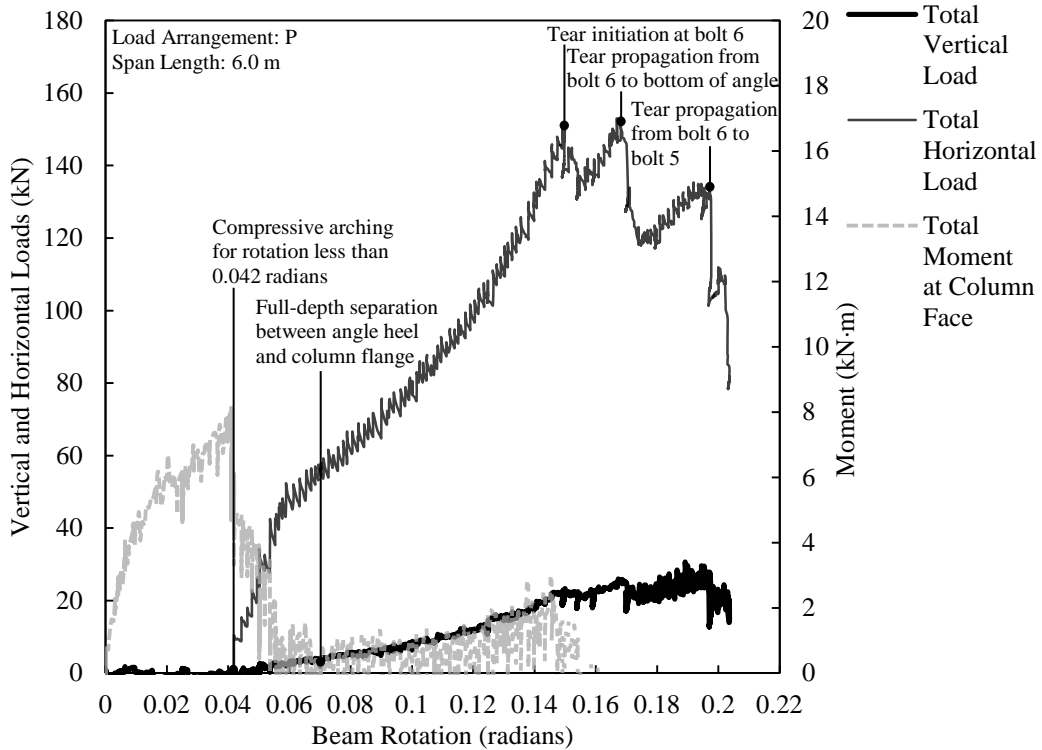
Figure D.22. Load versus rotation for SA3B-4.

239
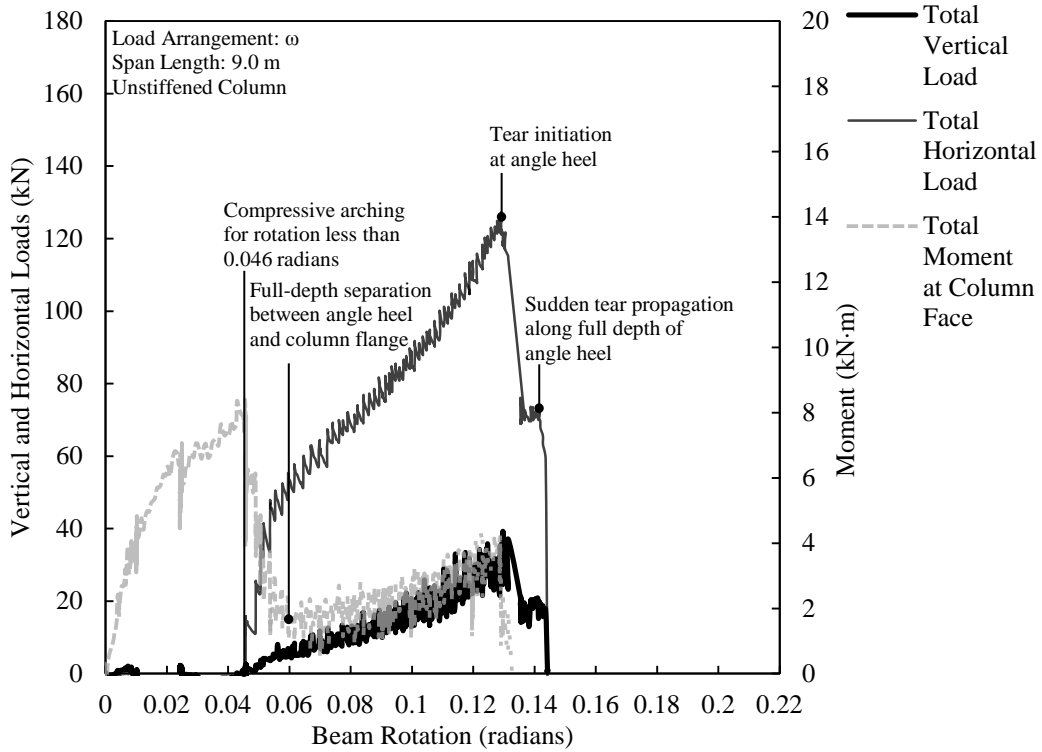
Figure D.23. Load versus rotation for SA3B-5.
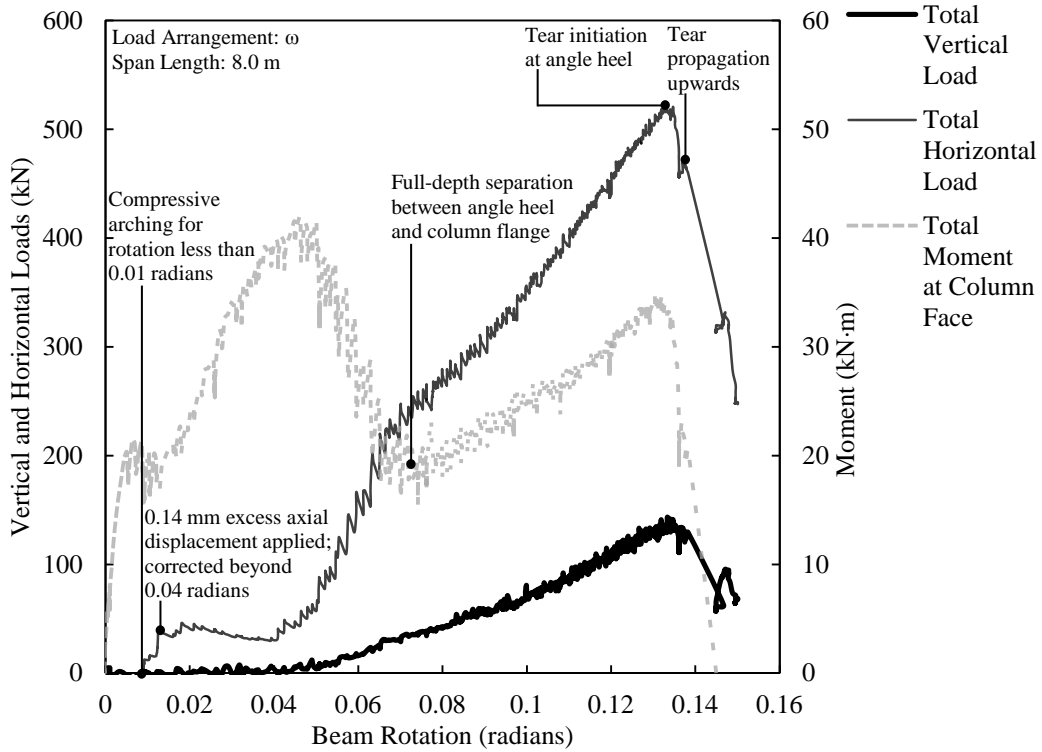
Figure D.24. Load versus rotation for SA5A-1.
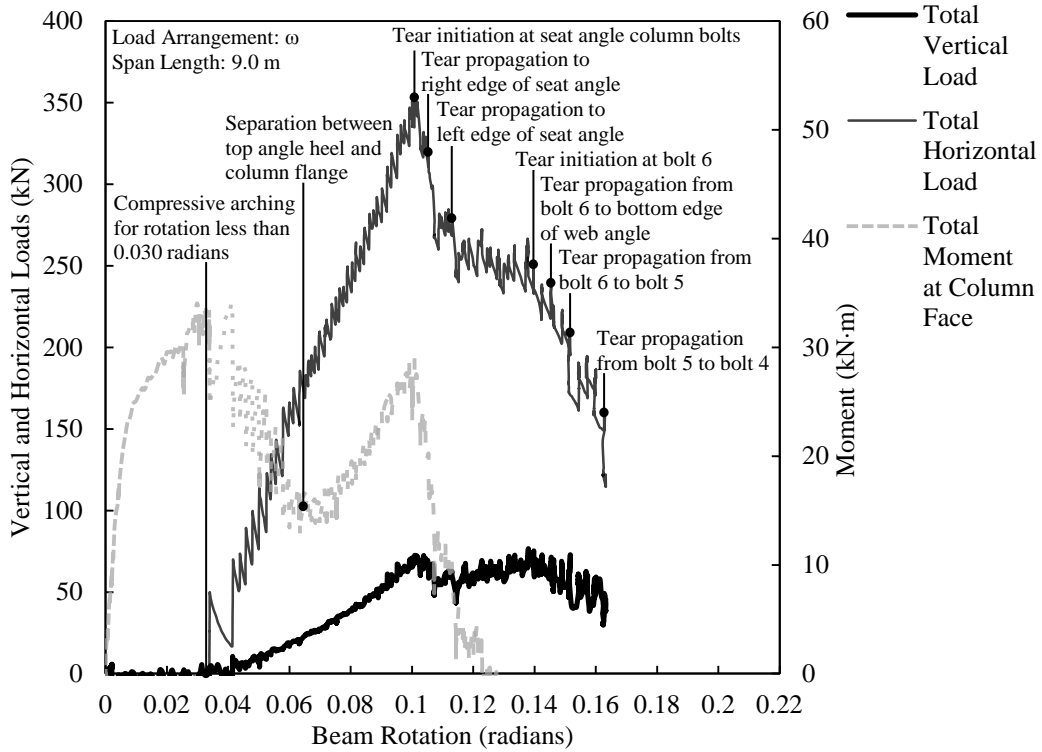
240
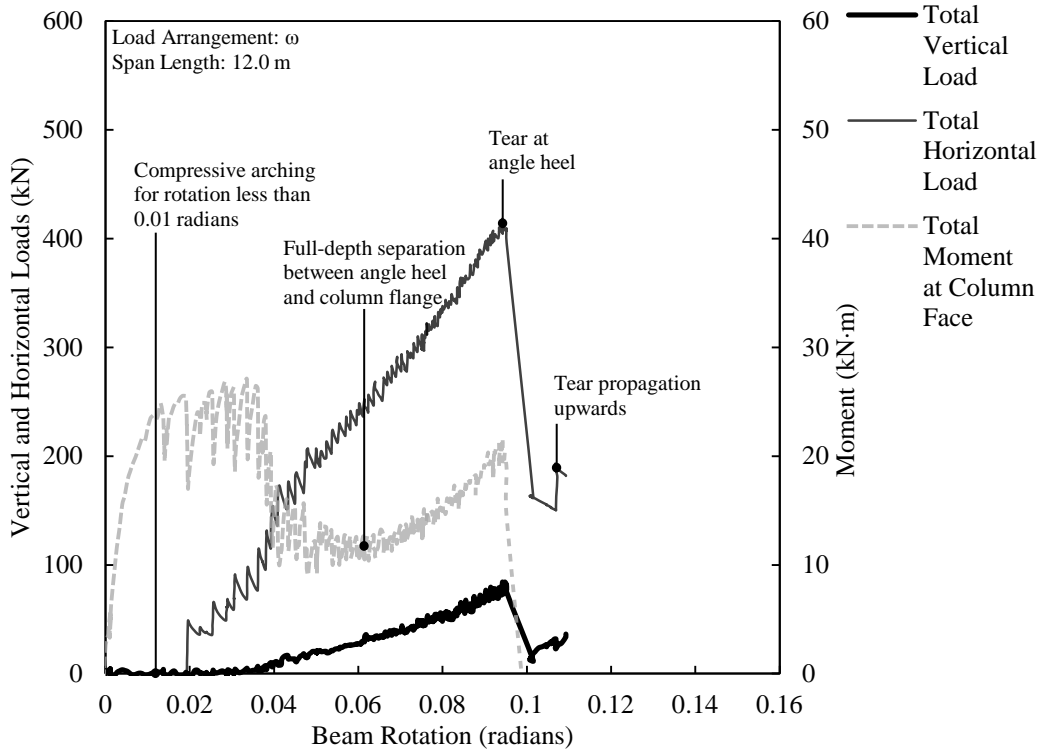
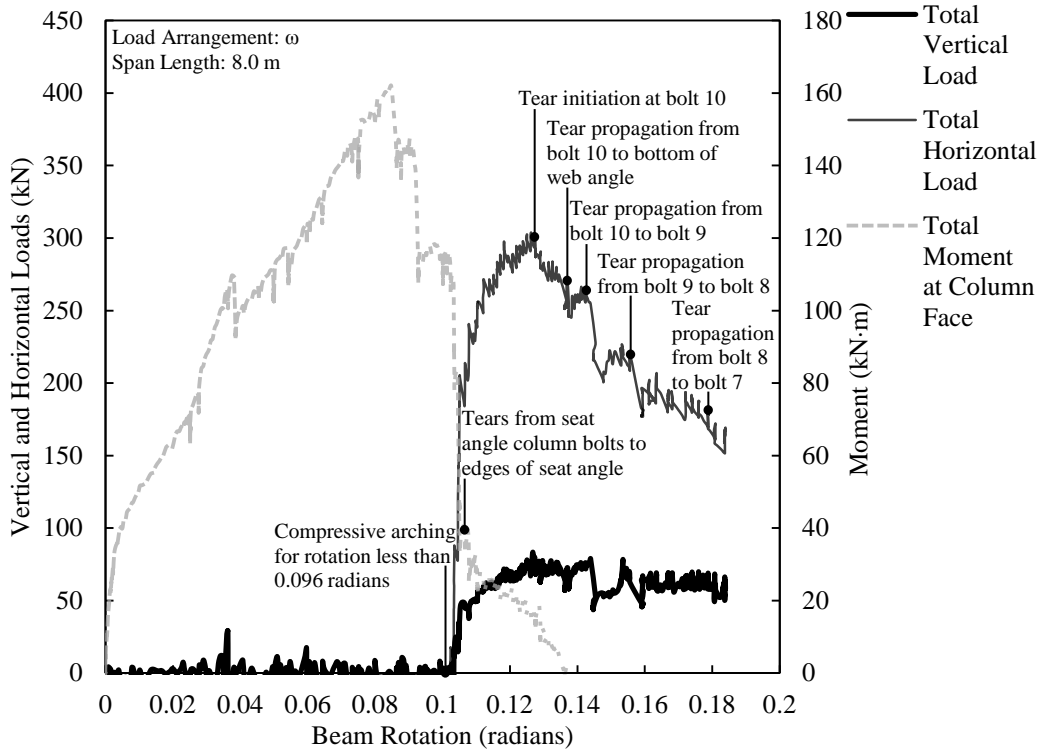**Figure D.25. Load versus rotation for SA5A-2.**
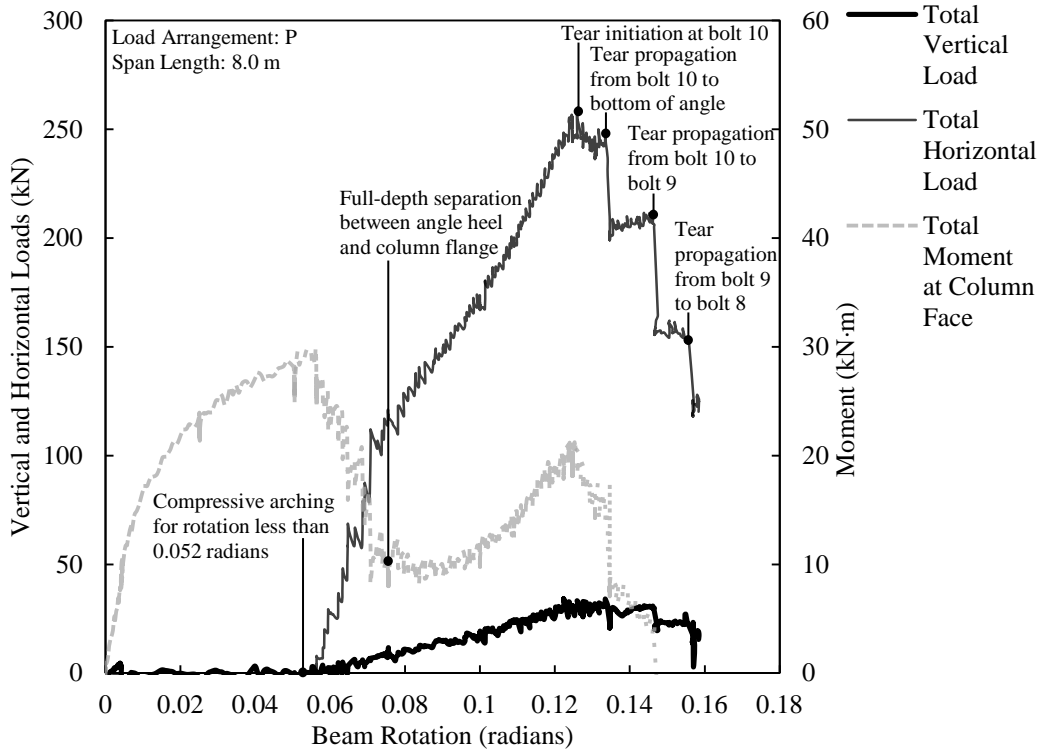
Figure D.26. Load versus rotation for SA5B-1.
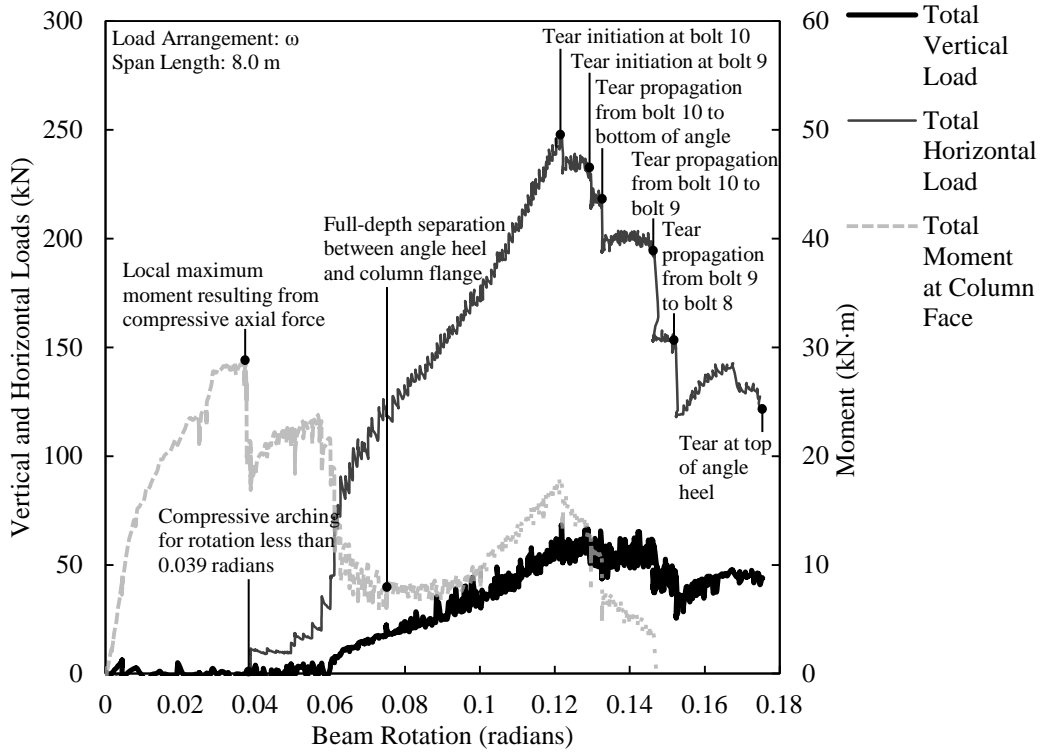
Figure D.27. Load versus rotation for SA5B-2.
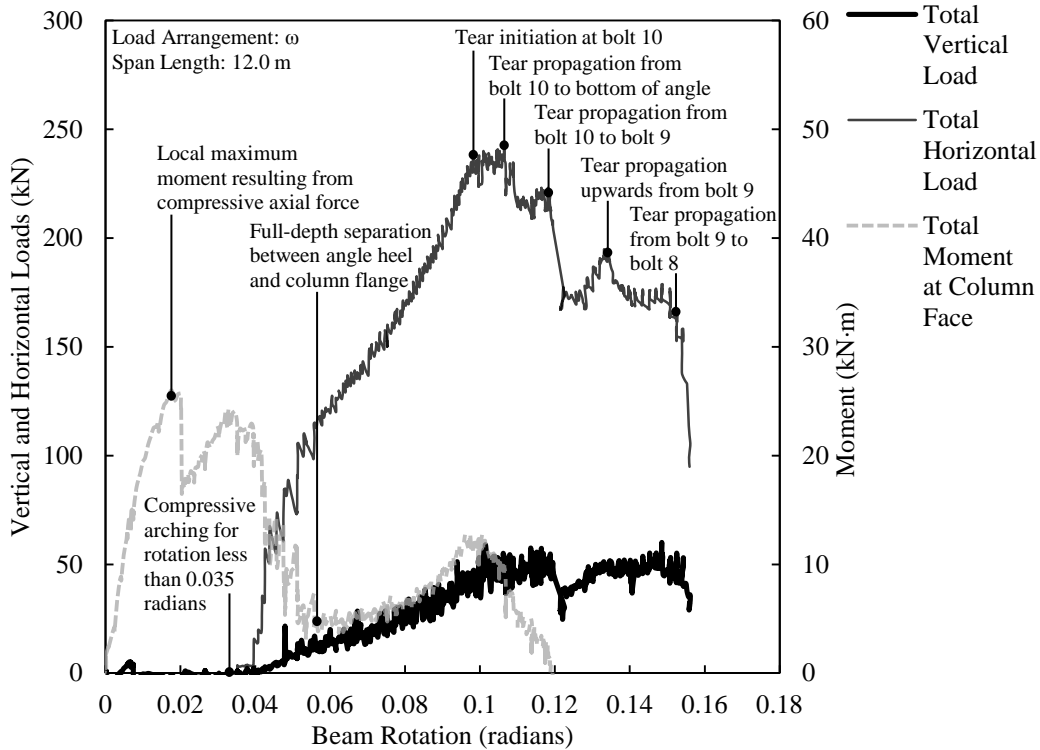
Figure D.28. Load versus rotation for SA5B-3.

242
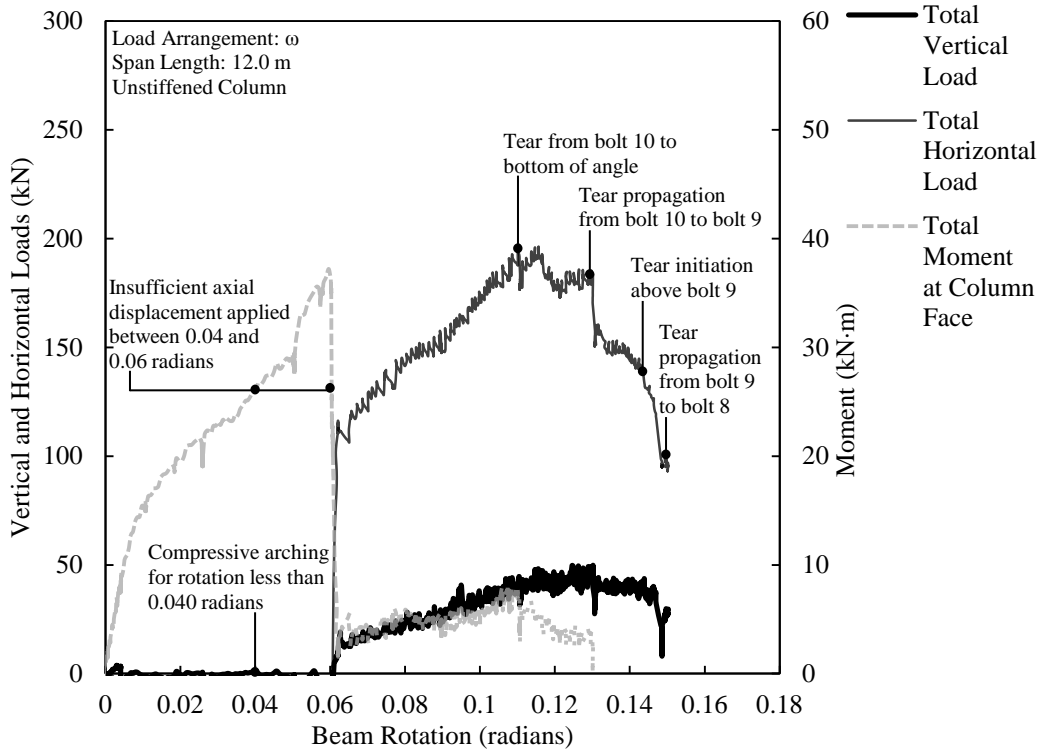
Figure D.29. Load versus rotation for SA5B-4.
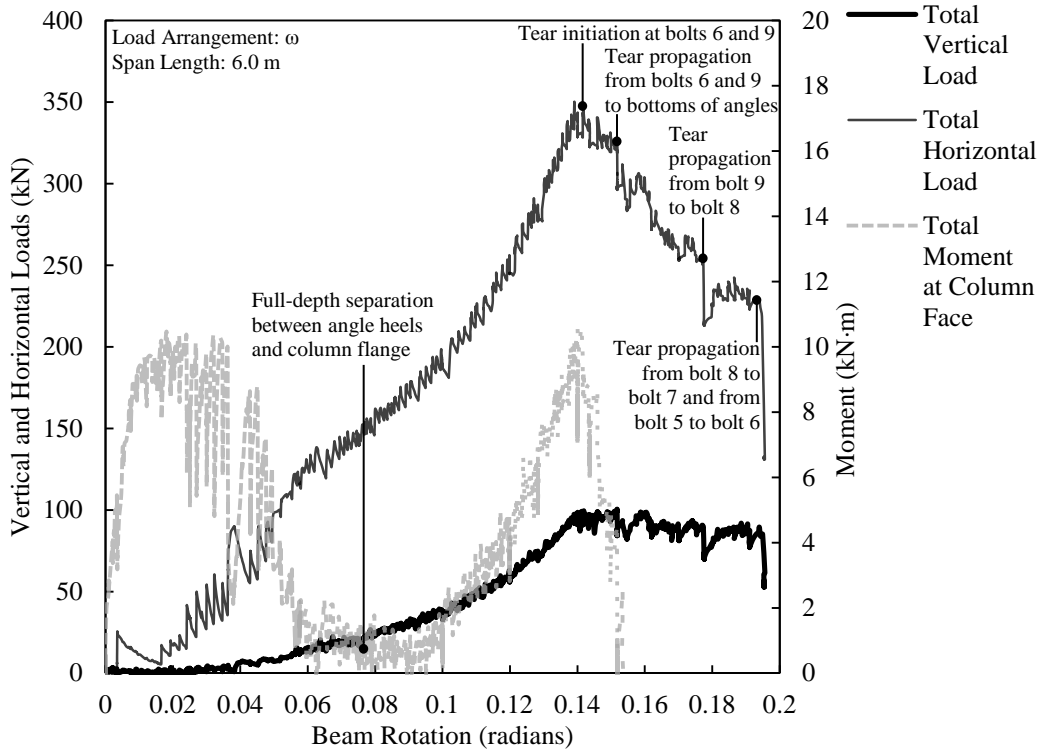
Figure D.30. Load versus rotation for DA3B-1.

243
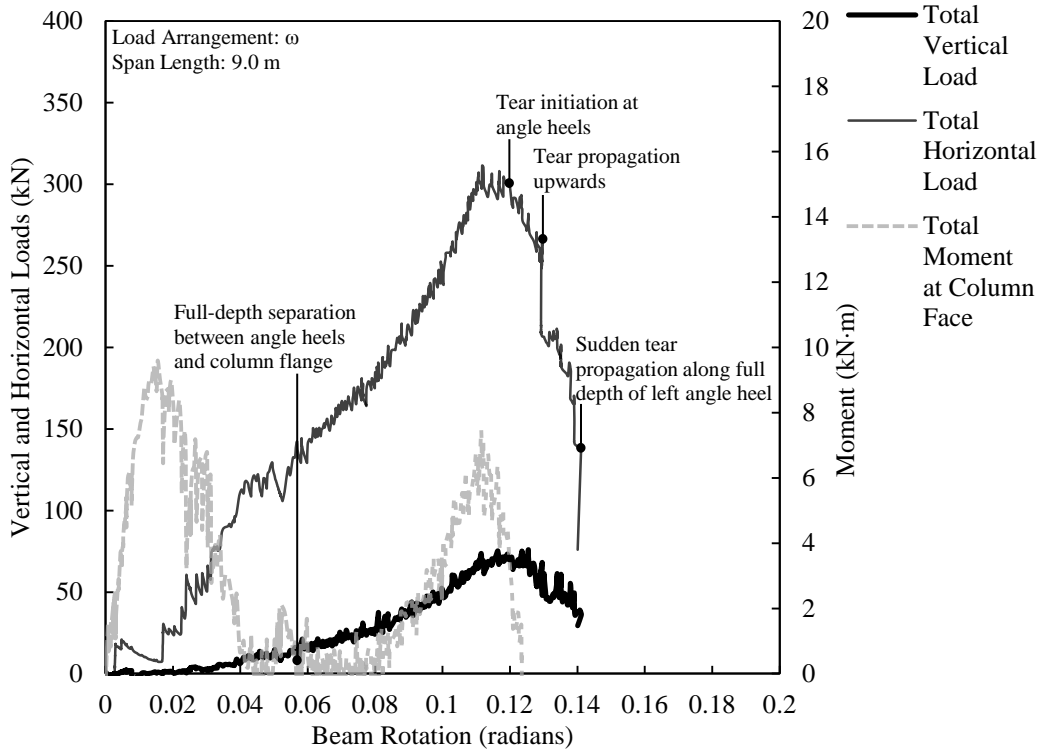
Figure D.31. Load versus rotation for DA3B-2.

Figure D.32. Load versus rotation for DA3B-3.

244

Figure D.33. Load versus rotation for DA5B-1.

Figure D.34. Load versus rotation for DA5B-2.

245

Figure D.35. Load versus rotation for DA5B-3.

Figure D.36. Load versus rotation for ST3C-1.

246

Figure D.37. Load versus rotation for ST3C-2.

Figure D.38. Load versus rotation for ST5C-1.

247
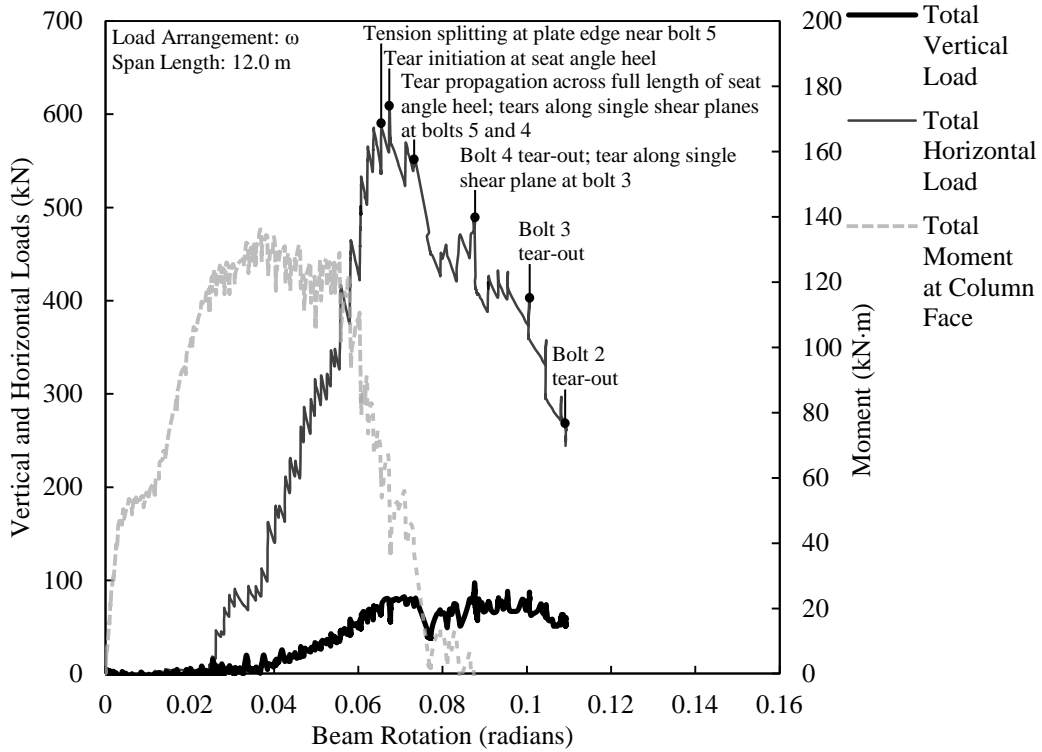
Figure D.39. Load versus rotation for ST5C-2.

Figure D.40. Load versus rotation for SA3C-1.

248

Figure D.41. Load versus rotation for SA3C-2.

Figure D.42. Load versus rotation for SA5C-1.
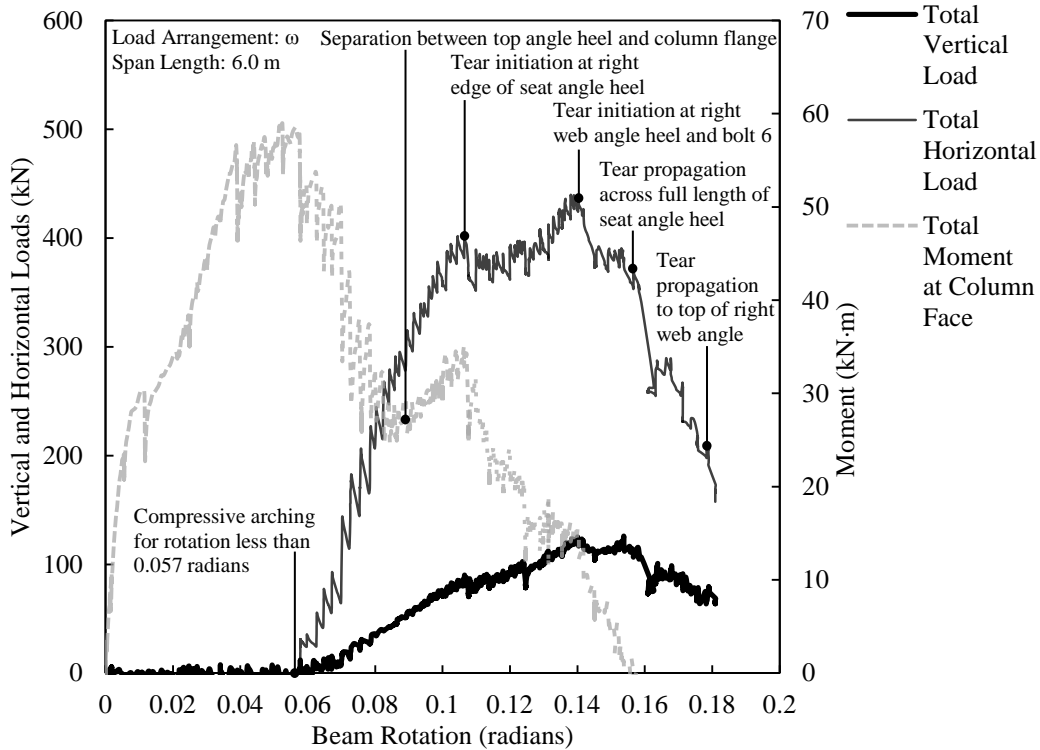
249
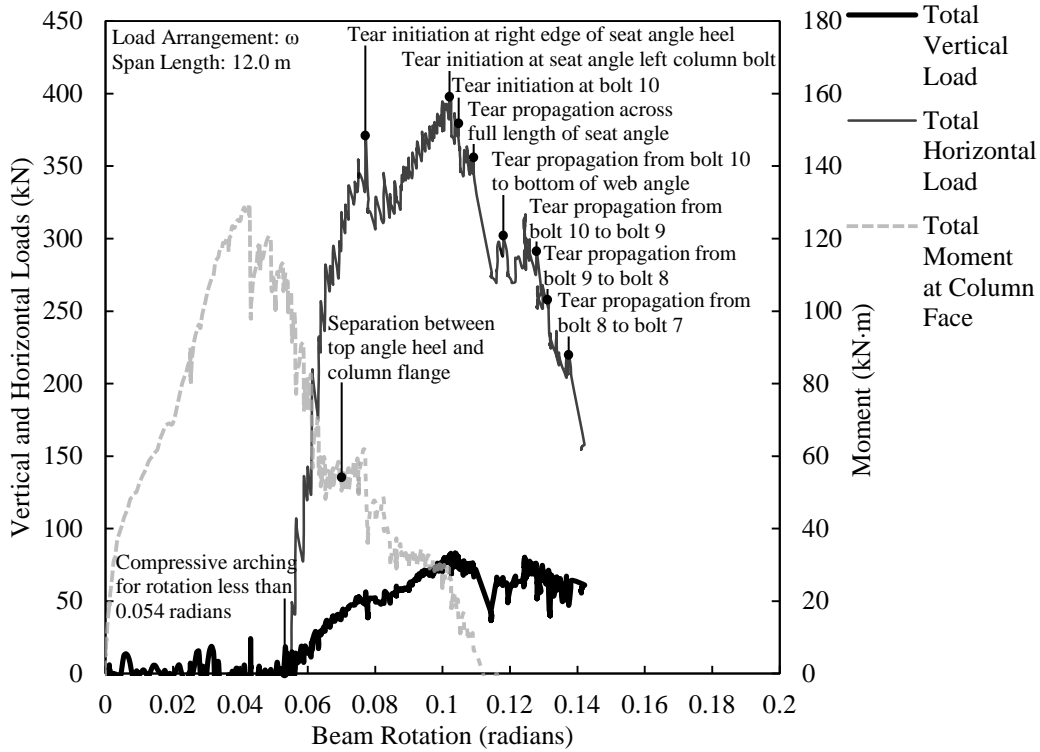
Figure D.43. Load versus rotation for SA5C-2.

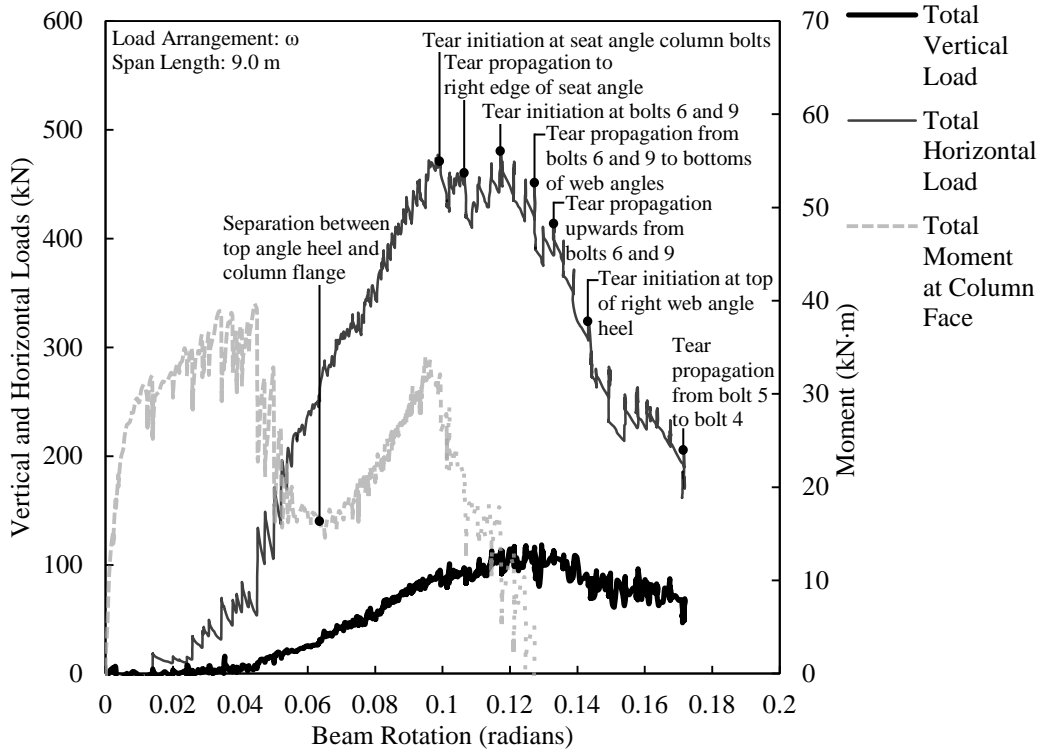**Figure D.44. Load versus rotation for DA3C-1.**

250

Figure D.45. Load versus rotation for DA3C-2.

APPENDIX E. APPLICATION OF SIMPLIFIED MODELLING PROCEDURE FOR SHEAR TAB CONNECTIONS

This appendix contains a worked example of the simplified approach to modelling shear tab connections under the demands imposed by column removal as a single bilinear spring for specimen ST5B-2. The example is organized according to the steps listed in Section 5.5.4.

Specimen Parameters

Specimen ID: ST5B-2; Load Arrangement: ω; $L = 12.0$ m; $n = 5$; $s = 80$ mm; $L_e = 35$ mm; $t = 6.4$ mm; $L_e = 35$ mm; $\sigma_y = 300$ MPa; $\sigma_u = 450$ MPa

STEP 1: Estimate Δ_{max}

Take $\Delta_{max} = 27$ mm (from Table 5.1).

(Alternatively, Δ_{max} could be estimated as $0.7L_e = 24.5$ mm.)

STEP 2: Determine θ_u and θ_{final}

Using Equation 5.8 to find θ_u:

$$\Delta_{max} = \frac{L}{2}\left(\frac{1}{\cos\theta_u} - 1\right) + e_{extreme\ bolt}\ \tan\theta_u$$

$$27 = \frac{12000}{2}\left(\frac{1}{\cos\theta_u} - 1\right) + 160\tan\theta_u$$

Solving gives:

$$\theta_u = 0.072 \text{ radians}$$

Similarly, for θ_{final}:

$$27 = \frac{12000}{2}\left(\frac{1}{\cos\theta_{final}} - 1\right) - 160\tan\theta_{final}$$

$$\theta_{final} = 0.125 \text{ radians}$$

STEP 3: Calculate deformation at individual bolt locations at θ_u

Using Equation 5.8:

$$\Delta_{bolt} = \frac{L}{2}\left(\frac{1}{\cos\theta_u} - 1\right) + e_{bolt}\,\tan\theta_u$$

$$\Delta_{bolt\,1} = \frac{12000}{2}\left(\frac{1}{\cos 0.072} - 1\right) - 160\tan 0.072$$

$$= 4.0\,\text{mm}$$

Similarly, for the remaining bolts:

$$\Delta_{bolt\,2} = 9.7\,\text{mm}; \Delta_{bolt\,3} = 15.5\,\text{mm}; \Delta_{bolt\,4} = 21.2\,\text{mm}; \Delta_{bolt\,5} = 27.0\,\text{mm};$$

STEP 4: Determine n_{eff}

The force–deformation curve at each bolt is assumed elastic–perfectly plastic, with the yield point defined at 5 mm plus expected slippage of 1.6 mm, which gives $\Delta_{\text{yield point}} = 6.6$ mm. Using the deformations calculated in Step 3 and Equation 5.9 gives:

$$\frac{F_{br}}{R_n} = \frac{\Delta_{bolt}}{\Delta_{\text{yield point}}} \leq 1.0$$

$$n_{eff} = \sum\frac{F_{br}}{R_n} = \frac{4.0}{6.6} + 1 + 1 + 1 + 1 = 4.61$$

STEP 5: Determine R_n and Maximum Resultant Force

For this connection, resistance in the horizontal direction is governed by bolt tear-out.

$$R_n = 0.6\,A_{gv}\frac{\sigma_y + \sigma_u}{2} \leq 3\,t\,d\,\sigma_u$$

$$= (0.6)\big[(2)(35)(6.4)\big]\left(\frac{300+450}{2}\right) \leq (3)(6.4)(19.1)(450)$$

$$= 100.8\,\text{kN}$$

For the sake of comparison to physical test results, the expected value of $R_n = 114$ kN (calculated using $\sigma_y = 323$ MPa, $\sigma_u = 458$ MPa, and multiplying by the average test-to-predicted ratio from previous tear-out tests of 1.086, as

discussed in Section 5.1.1) is applied below in place of the nominal factored value recommended for design.
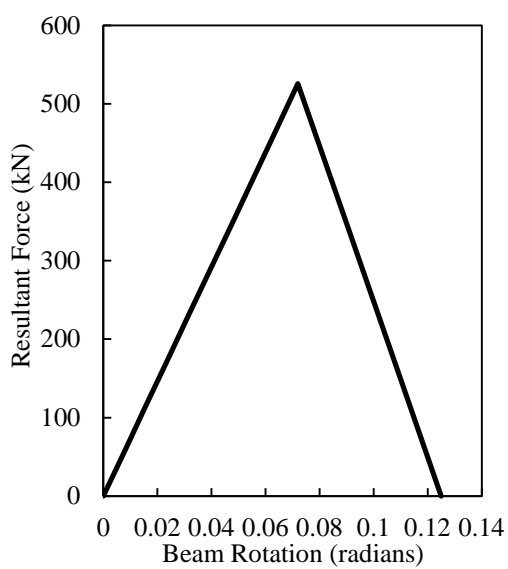
The maximum (expected) resultant force, which occurs at θ_u, is:

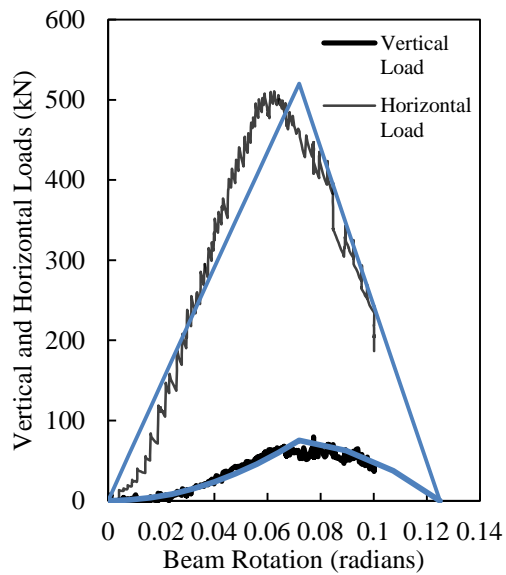$$n_{eff} R_n = (4.61)(114) = 526 \text{ kN}$$

STEP 6: Plot force versus rotation

The resulting bilinear curve for modelling connection behaviour is defined by the points (0, 0), (θ_u, $n_{eff}R_n$), and (θ_{final}, 0), as shown in Figure E.1(a).

Under a uniformly distributed load, the vertical load at the remaining column is found by multiplying the resultant force by $\sin(2\theta_c)$, and is equal to zero at the removed column. The horizontal force versus rotation curve (at either column) is found by multiplying the resultant force by $\cos(2\theta_c)$. The predicted forces at the remaining column are compared to those measured during the physical test in Figure E.1(b).

Figure E.1. Simplified force versus rotation relationship for ST5B-2:
(a) bilinear resultant force curve, and (b) comparison to test results.